Ollscoil na hÉireann, Corcaigh

National University of Ireland, Cork

The Design, Synthesis and Characterization of Chitosan-Based Interpenetrating Polymer Networks and Thin Film Systems

Thesis presented by

Catherine Claire Ryan

for the degree of

Doctorate of Chemistry

University College Cork

School of Chemistry

Head of School: Prof Justin Holmes

Supervisors: Prof Martyn Pemble and Dr Maria Bardosova

March 2018

Contents

Declaration

This is to certify that the work I am submitting is my own and has not been submitted for another degree, either at University College Cork or elsewhere. All external references and sources are clearly acknowledged and identified within the contents. I have read and understood the regulations of University College Cork concerning plagiarism.

_____

Catherine Ryan

Dedication

Dedicated to the memory of my father, Joseph Ryan (1949-2015).

"Happiness is often the result of being too busy to be miserable"

– Paul Frank Baer

Acknowledgements

Firstly, I would like to sincerely thank Professor Martyn Pemble, Dr Maria Bardosova, Professor Osvaldo Oliveira, Dr Hiroshi Fudouzi, Dr Simon Elliott, Dr David Clarke, Professor Colm O'Dwyer and Dr Martyn McLachlan and all associated research staff, postdocs and students who I have worked alongside.

Secondly, I would like to thank my family and friends whose support and encouragement has been outstanding throughout the course of my studies. Especially my mother, Kathleen, and fiancée John, for knowing when a wide berth was best required!

The work was supported by Science Foundation Ireland (PI Grant No. 11/PI/1117 and ISCA Grant No. 12/ISCA/2494 & 2846), the European Union's Seventh Framework Programme (FP7/2007-2013) under grant agreement number FP7-IRSES-295182.

Abstract

Chitosan is a polymer derived from naturally-abundant sources of chitin and can be seen referred to in the literature for a wide variety of applications. However, it has its limitations due to lack of strength and stability as a single polymer structure. This problem can be overcome by cross-linking the polymer with other natural or synthetic polymers, in the hope of providing the 'back-bone' structure it is missing. This PhD thesis describes the study of a range of organic-inorganic composites which were synthesised by combining chitosan with a tetra ethyl orthosilicate (TEOS) cross-linker to form an interpenetrating polymer network (IPN). In combination with a variety of ordered and disordered polymer and metal nanoparticles, the composites formed were studied with respect to their optical, mechanical and antimicrobial properties.

The IPNs made from chitosan and TEOS were prepared in an aqueous-acid environment to form a hydrogel which could then be drop-cast onto a substrate of choice to dry and form a thin film structure. It could also be drop-cast onto pre-existing structures such as photonic crystals, in order to study the resulting optical properties or infused with particles such as gold and silver nanoparticles in order to form composites with enhanced mechanical and antimicrobial properties. The properties of all individual materials have been studied, while the novel composites described above have been studied in-depth the results of which have been published. For this reason, the following thesis has been prepared using a publication format with the main results chapters presented in their published form.

Briefly, the main findings of the work are as follows: the pH-sensitivity of chitosan carries forward to the Chi-TEOS IPN and that by combining this feature with the optical properties of a SiO_2 photonic crystal provides a pH-sensitive composite which elicits an optical response as an indicator of pH conditions. The mechanical properties of chitosan are found to be enhanced by cross-linking, even though it is occurring by weak bonding interactions. The ideal chitosan: TEOS ratio was determined as 1:1 as this ratio results in a mechanically strong thin film which retains chitosan's inherent flexibility. This is then further enhanced by the addition of polymer particle structure enhancers in the form of colloidal silica and polystyrene particles. While the addition of Ag and Au NPs did not contribute

towards enhanced tensile strength these films were also investigated with respect to their antimicrobial abilities. Here it was concluded that the NPs weren't being released when pH is neutral and so they effectively couldn't contribute towards antimicrobial activities. In contrast the metal NPs were released under more acidic conditions, potentially providing some possibilities in terms of their use in *in-vivo* drug release materials. While embedding particles/ drugs for release in neutral conditions isn't suitable, the Chi-TEOS IPN is an ideal candidate as a stand-alone antimicrobial wound-dressing or for drug release in acidic conditions.

1. Introduction

1.1 Introduction to Chitosan and the Chitosan-Based Composites Studied

Chitosan, a polymer derived from natural sources, was the central material studied during the course of this PhD. A range of organic-inorganic composites were synthesised by combining chitosan with a tetraethyl orthosilicate cross-linker to form an interpenetrating polymer network (IPN) and also in combination with various ordered and disordered polymer and metal nanoparticles. The composite structures formed were studied with respect to their optical, mechanical and antimicrobial properties; all of which will be described and discussed in individual sub-chapters of this introductory chapter, which also serves to introduce the main individual topics – chitosan, interpenetrating polymer networks and SiO_2 photonic crystals along with their properties which have been studied. Subsequent chapters describe the synthesis and analysis of the application-focussed composites based on their optical, mechanical and antimicrobial properties, respectively. The diagram in figure 1.1 displays an overall schematic of the work carried out. A brief description of each of the entities along with how they are connected is also given here.

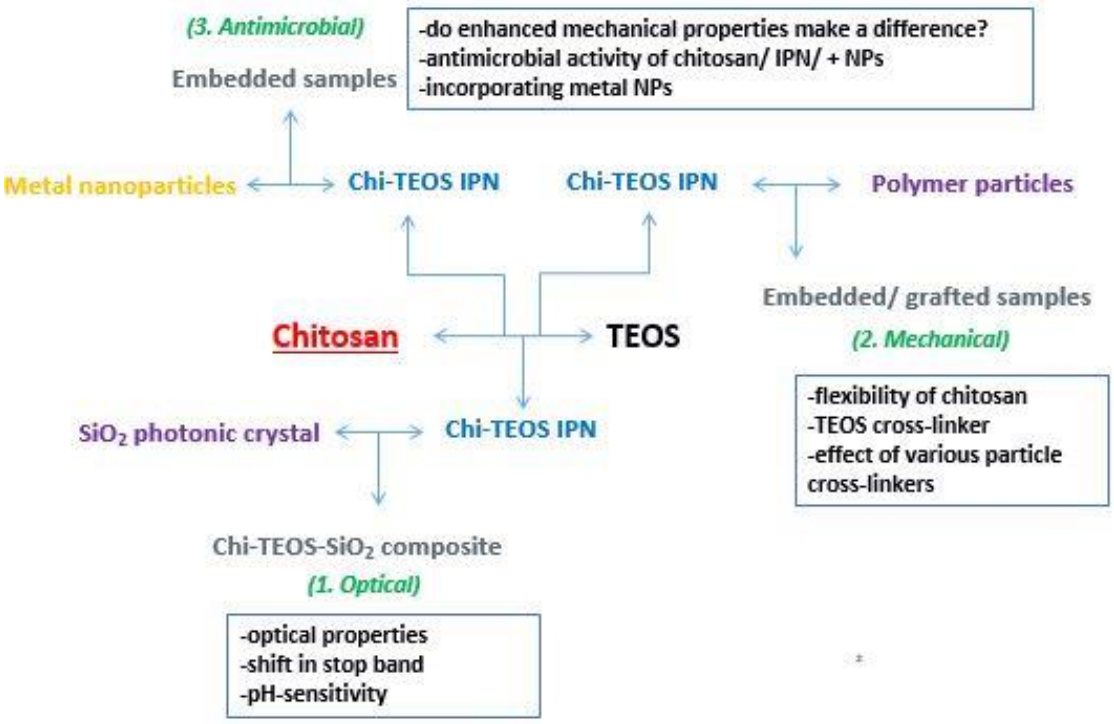

Figure 1.1. A schematic representation of the work described in this thesis which displays all individual components of the research and shows the connectivity which exists between topics while also indicating the main research questions addressed

1.2 Chitosan

1.2.1 Chitin and chitosan

Chitin is a naturally occurring polysaccharide which serves as the structural 'backbone' to crustacean exoskeletons and fungal cell walls. Its structure is analogous to the chemical structure of cellulose with the hydroxyl groups in the C2 position replaced by acetamido groups. Figure 1.2 below displays the regularly repeating chemical structures of cellulose and chitin. The chemical and physical properties of cellulose have been extensively researched and many materials and applications have been derived from this polysaccharide e.g. celluloid, rayon and cellophane. Chitin has also been greatly studied in the medical and biomedical fields due to its biocompatibility. However, there are some drawbacks associated with chitin, the most prominent of which is its insolubility in most solvents. This is due to the presence of acetamido groups which form very strong intersheet hydrogen bonds in the chitin structure[1].

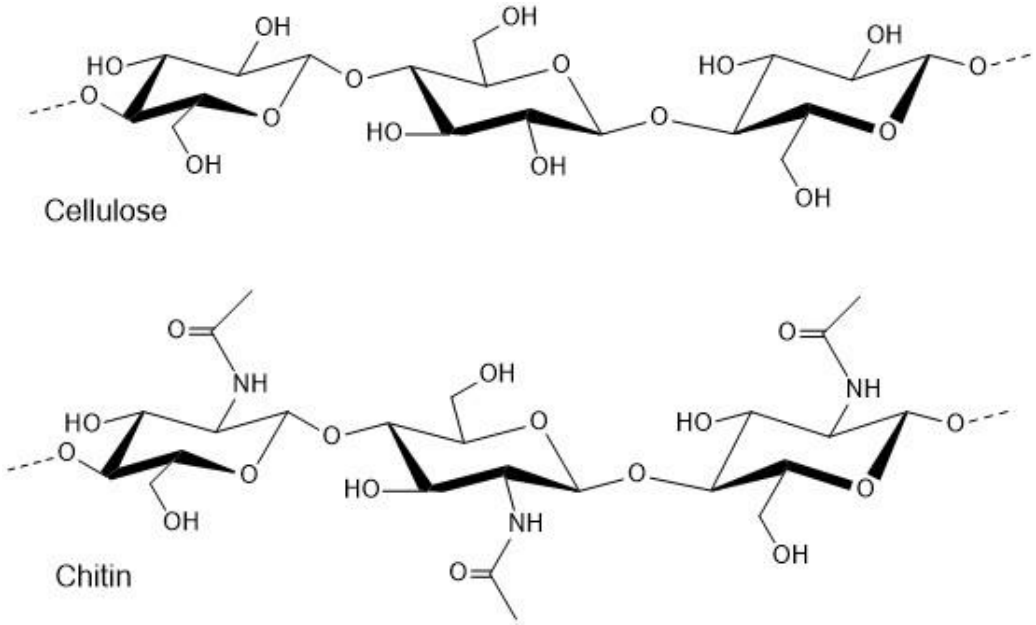

Figure 1.2. Repeating D-glucose units make up the structure of cellulose and repeating N-acetyl glucosamine units make up the structure of chitin.

Due to solubility problems an acid-soluble derivative of chitin, chitosan, has come to the forefront as a valuable substitute for the more insoluble polysaccharide, chitin. Chitosan is formed by the deacetylation of chitin in the presence of alkali hydroxides such as sodium hydroxide. The conversion process does not result in 100 % deacetylation. Generally, once the degree of deacetylation exceeds 50 % the polysaccharide structure is referred to as chitosan[2, 3]. With the majority of acetamido groups replaced by amino groups chitosan, with less hydrogen-bonding sites available, becomes more susceptible to protonation and so it becomes acid-soluble. Figure 1.3 shows the chemical structure of chitosan.

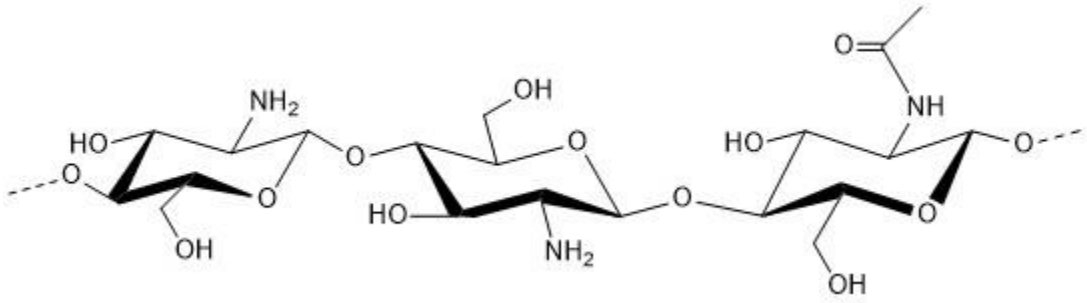

Figure 1.3. The chemical structure of chitosan, the deacetylated derivative of chitin.

Chitin is found in three forms; namely α-chitin, β-chitin and γ-chitin. α-chitin strands are arranged in an antiparallel fashion while β-chitin strands are arranged in a parallel

fashion. The cross-linked form, α-chitin, is the most common form and is found in crustacean exoskeletons[4] and fungi[5]. β-chitin is commonly derived from squid pens[6] and γ-chitin is a mixture of α-chitin and β-chitin. Research into the structures of chitin and chitosan suggests that the chitosan structure bears the most resemblance to α-chitin[7].

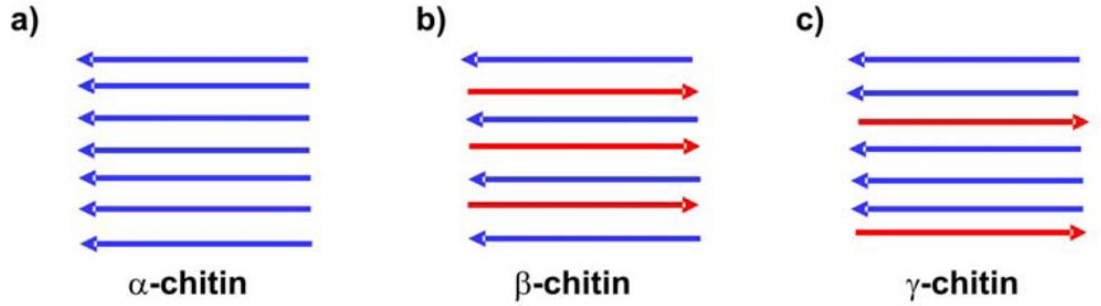

Figure 1.4. Arrows representing the alternating directions of folded chains in a) α-chitin b) β-chitin and c) γ-chitin[8].

A very important feature of chitosan is its cationic polyelectrolyte structure. Unlike other naturally charged polysaccharides the structure of chitosan contains many positive charges rather than many negative charges, unlike alginates for example which are composed of alginic acid and consequently are anionic polyelectrolytes[9]. Due to its cationic structure chitosan is a good candidate for selective complexation with negatively charged ligands[10] and chelation to macromolecules such as proteins[11].

The alkaline hydrolysis of chitin is the primary method for processing chitosan and it has been well studied. The method generally involves the dissolution of chitin in concentrated potassium hydroxide or sodium hydroxide by heating the solution. This is followed by neutralization, filtration, washing and drying of the chitosan product. Tolaimate *et al.* describe the process in their study of the preparation of chitin and chitosan[2]. An overall outline of the process is as follows: in the presence of strong base the depolymerisation of chitin leads to the formation of monomeric N-acetyl glucosamine units; strong base also causes the deacetylation of the N-acetyl glucosamine monomers leading to the formation of monomeric glucosamine units. The subsequent polymerisation of the monomeric glucosamine units and remaining N-acetyl glucosamine units leads to the formation of polymeric chitosan. The first depolymerisation step can also be caused by a hydrolytic enzyme named chitinase as this enzyme is a catalyst in the degradation of glycosidic bonds. Chitinases occur

widely in nature and have been isolated from living organisms such as plants (barley seed chitinase)[12], bacteria[13] and fungi[14].

As can be concluded from the brief structure and processing descriptions above, the resulting degree of deacetylation of chitosan is a highly important chemical characteristic. This characteristic gives an indication of the number of amino groups present, thereby giving an indication of the capabilities of the polysaccharide as a cationic polyelectrolyte. When the degree of deacetylation of chitosan exceeds 70 % the solid polysaccharide becomes soluble in aqueous acid solution[15], and it is this dissolution of chitosan which allows for the fabrication of polymer membranes. The degree of deacetylation can be determined by employing such methods as infrared spectroscopy, titrimetric analysis, NMR spectroscopy and gas chromatography. The molecular weight of chitosan can be categorized into three groups; low, medium and high. These are simply categorized by the overall molecular weight of the polymer; low molecular weight refers to a polymer having molecular weight in the range 50,000-190,000 $gmol^{-1}$, medium molecular weight refers to a polymer having molecular weight in the range 190,000-310,000 $gmol^{-1}$ and high molecular weight refers to a polymer having molecular weight in the range 310,000- >375,000 $gmol^{-1}$. The dispersity (formerly known as polydispersity index) is a variable in polymers which gives an indication of the distribution of molecular weight in the overall polymer structure. It is a calculation of the weight average molecular (M_w) mass divided by the number average molecular mass (M_n)[16], equation 1.1:

Equation 1.1: $Đ_M = M_w/M_n$

As this value increases from unity it is an indication of a decrease in uniformity of the structure[17]. Determination of molecular weight can be carried out employing chromatography, light scattering and viscometry. It has been reported that the viscosity of chitosan in solution is affected by molecular weight, degree of deacetylation, concentration, ionic strength, pH and temperature[18]. An increase in viscosity is observed with increasing molecular weight and degree of deacetylation[19]. However, with an increase in ionic strength, pH or temperature a decrease in molecular weight is observed[20]. For a polymer system the intrinsic viscosity can be determined using the Mark-Houwink equation, equation 1.2 below, which relates intrinsic viscosity η to molecular weight M[21]. K and α are the Mark-Houwink parameters,

unitless values which vary depending on the nature of the polymer system i.e. how flexible or rigid the polymer system may be.

Equation 1.2: $[\eta]=KM^{\alpha}$

Being naturally abundant, non-toxic and biocompatible chitosan is a valuable commodity in many research fields such as chemistry, biochemistry and biomedicine. Nanoparticles, microparticles, hydrogels and composites are reported in the literature[22]. Chitosan nanoparticles and microparticles are being developed for *in vivo* drug and gene delivery and the ionic gelation technique is commonly employed for their fabrication[22,23,8]. High surface area and improved mechanical properties are among the attributes of chitosan micro- and nanoparticles. Chitosan hydrogels are often reported in medical and biomedical journals due to their antimicrobial and antifungal activity[23]. This is largely due to the positive charge density of chitosan hydrogels which can chelate to negatively charged ligands, such as those on the surface of bacteria[24]. pH-sensitivity is a feature of chitosan which is present due to the amino groups available for protonation, hence the greater the degree of deacetylation the greater the pH-sensitivity. This phenomenon has been extensively researched for nano- and microparticles along with hydrogels as part of drug-release systems[25]. Chitosan membranes, which are generally prepared by drop-casting of hydrogels, are pH-sensitive but tend to be lacking in mechanical strength. This can be improved upon by the introduction of cross-linking agents[26]. A cross-link in a polymer structure is a bond that links one chain to another. Cross-linkers such as tetraethyl orthosilicate (TEOS) used by Park *et al.* and genipin (a naturally-occurring, water-soluble, cross-linking aglycone[27]) used by Lien *et al.*[28], serve to enhance the mechanical stability of chitosan membranes[29]. Glutaraldehyde is also commonly used as a cross-linker in hydrogel systems. Rohindra *et al*. conducted a study on chitosan hydrogels cross-linked with glutaraldehyde and reported how the hydrogel structure becomes increasingly "compacted" with increasing cross-linker concentration; the swelling ability, percentage free water and glass transition temperature (Tg) decreased[30].

1.2.2 Properties of chitosan films

The chemical and physical properties of chitosan vary massively depending on the source, structure, degree of deacetylation, molecular weight and cross-linking character. The number of variables in such systems is quite extensive. The most

commonly studied properties of chitosan are their chemical, physical, mechanical and antimicrobial properties

Chemical properties such as degree of deacetylation and molecular weight, described in section 1.2.1, contribute to the physical properties. The pH-sensitivity of chitosan depends on the degree of deacetylation, molecular weight and cross-linker density. As the degree of deacetylation increases intersheet hydrogen-bonding decreases resulting in more freedom for separation of sheets which in turn allows access to amino groups for protonation. Electrostatic repulsion between protonated amino groups causes intersheet and intrasheet (chain) expansion resulting in system swelling[25]. Molecular weight also contributes to swelling ability; with increasing molecular weight the average chain length elongates, therefore an accumulation of longer chain lengths dispersed in aqueous media leads to greater swelling in the polymer system. The temperature-sensitivity of chitosan films has also been extensively researched. The degree of deacetylation and water content are important factors with respect to thermal analysis[31]. Thermogravimetric analysis carried out by Nieto *et al*. showed a mass loss of 10 % at 60 °C which corresponded to the loss of water and a maximum mass loss of 41.4 % at 380 °C which corresponded to the thermal and oxidative decomposition of chitosan. It was suggested by Nieto *et al.* that the decomposition is increased by the split of glycosidic linkages in the intersheet hydrogen structure[32].

The mechanical properties of chitosan vary depending on whether the structure is enhanced by incorporation of cross-linkers and / or further additives. Studies on various systems have been carried out e.g. Wang *et al.* incorporated montmorillonite particles in a chitosan structure to improve its mechanical properties[33]. The aim of cross-linking is often to provide an enhanced structural 'backbone' for chitosan's flexible chemical structure. Analysis of the improvement in strength is carried out using mechanical tests. Aryaei *et al*. applied a method of determining the elastic modulus to show that films of chitosan cross-linked with tripolyphosphate have improved hardness and mechanical properties, while they also report that cross-linked films become more brittle than chitosan films[34]. The optical properties of chitin and chitosan also depend on the system studied because naturally occurring chitin often displays structural colour due to the ordered micro-fibrils which make up its structure[35]. Azofeifa *et al.* carried out an extensive study on the optical properties of chitin and chitosan in both particulate and thin film form. With regard to optical

analysis on a chitosan thin film in the visible range of the spectrum the average refractive index, n, is about 1.52[36]. This can be modified e.g. an increase to n=1.69 has been observed by the inclusion of silver nanoparticles in the polymeric system[37].

1.2.3 Chi-TEOS IPN

An interpenetrating polymer network (IPN) is defined as a 'combination of two polymers in network form, at least one of which is synthesized and /or cross-linked in the immediate presence of the other'[38]. IPN synthesis is basically a reaction between a monomer and a cross-linker to form a polymer network, where the monomer could be a protein, a natural monomer or a synthetic monomer. A cross-link is formed by a chemical reaction with any species which successfully bonds two polymer chains together, either covalently or ionically[39]. The chitosan – tetraethyl orthosilicate (TEOS) IPN contains two main components; chitosan is a monomer which forms individual polymer chains, TEOS is also a monomer which undergoes hydrolysis followed by condensation to form a siloxane polymer chain. These two chains subsequently cross-link to form a chitosan-TEOS interpenetrating polymer network (Chi-TEOS IPN). This material can be successfully formed into membranes.

In order to exploit the pH-sensitive characteristics of chitosan such membranes must be stable in solution. For this reason, IPNs comprising chitosan and TEOS have been studied previously. The synthesis of such IPNs was first described by Park *et al.*[29]. The experimental method employed involved the preparation of hydrogels comprised of chitosan in aqueous acid solution and TEOS in the presence of concentrated acid. The chitosan dissolved in the aqueous acid and the TEOS formed so-called 'strands' of linear molecules in the presence of the acid[40], figure 1.5. When formed, the IPN displayed two particularly interesting characteristics; flexibility due to the presence of chitin and mechanical strength due to the presence of the TEOS-contributed siloxane 'backbone'. The study conducted by Park *et al.* involved swelling studies on IPNs of varying chitosan: TEOS ratio, namely 1:1, 1:2 and 1:3. It was observed that the degree of swelling decreased with increasing TEOS concentration.

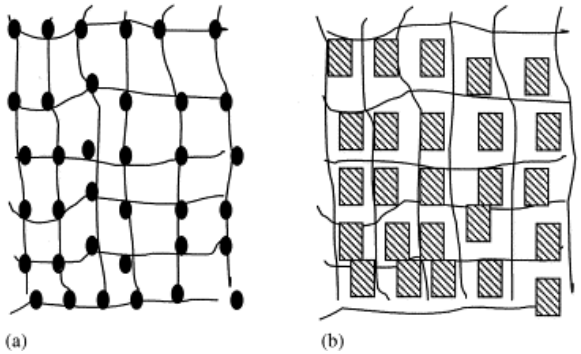

Figure 1.5. Schematic of IPN proposed by Park *et al*.(a) TEOS IPN (b) Chitosan-TEOS IPN[41].

TEOS has been previously reported as a cross-linker; Jena *et al.* cross-linked TEOS with hyper-branched polyurethane as an organic-inorganic hybrid material[42] and Pinto *et al*. cross-linked TEOS with polydimethyl siloxane (PDMS) in the presence sodium dodecyl sulphate (SDS) in a study on conduction mechanisms in the membrane with varying concentration of SDS[43].

1.2.4 Experimental Methods for Chitosan: TEOS IPN Formation

Chi-TEOS IPN formation initially involves the synthesis of two separate networks; a chitosan hydrogel in the presence of aqueous acetic acid and a TEOS solution in the presence of concentrated hydrochloric acid. The two separate networks are then combined to form the IPN hydrogel. According to the polymeric composition the Chi-TEOS IPN is in the class of hydrogels known as multi-polymer interpenetrating polymer hydrogels. This class of hydrogels consists of two independent cross-linked synthetic and/or natural polymer component(s), contained in a network form[39]. Hydrogels are also classified according to the nature of the cross-linking mechanism; being either chemically or physically cross-linked depending on whether the cross-linking interaction is irreversible or reversible, respectively. The TEOS network undergoes hydrolysis and condensation in the formation of a polymer chain linked by siloxane groups and the remaining hydroxyl groups are then available for interaction with the cationic chitosan polymeric structure, see figure 1.6. It is proposed that the cross-linking occurs physically by H-bonding interactions in the polymer chain entanglements between the polar hydroxyl groups of the TEOS network and the polar hydroxyl and amino groups of the chitosan polymer network. The amino groups on

the chitosan polymer network are then still available for protonation, hence retaining the pH-sensitive properties of the IPN. See figure 1.7.

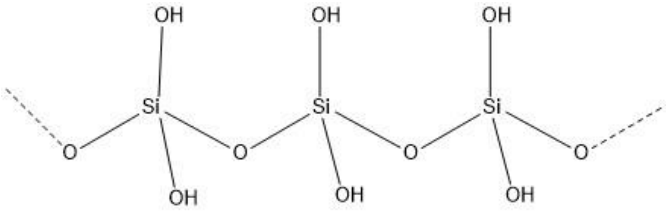

Figure 1.6. The chemical structure of the of the polymer chains formed by the hydrolysis and condensation of TEOS, showing both the bridging siloxane groups and the hydroxyl groups.

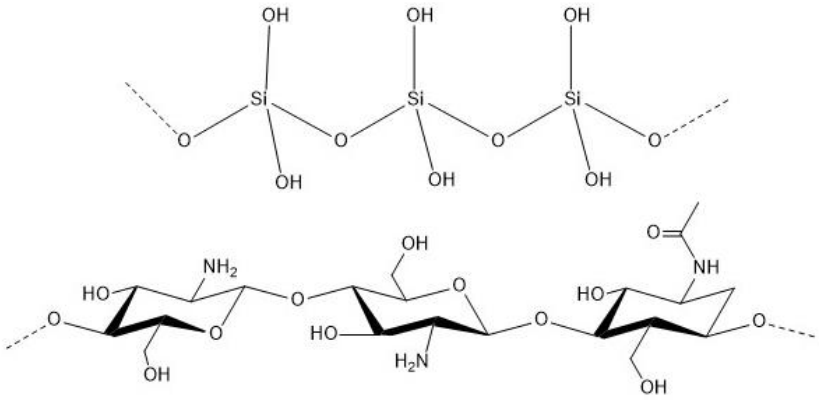

Figure 1.7. Adjacent siloxane and chitosan networks, illustrating how physical polymer chain entanglements may form via H-bonding between amino, hydroxyl and carbonyl groups.

The viscosity of the resulting hydrogel depends on the quantity of TEOS in the IPN and increases with increasing quantity of TEOS. This is attributed to the increasing degree of cross-linker density in the IPN which is caused by H-bonding and hydrophobic interactions[44]. IPN membranes are formed by casting hydrogels and allowing the evaporation of water under controlled conditions. The dimensions and thickness of the membranes are controlled by varying volume of hydrogel and substrate dimensions. Thermogravimetric studies on chitosan report thermal stability up to ≥300 °C with initial thermal degradation observed at 326.8 °C[45] suggesting that thin film membranes can be formed at temperatures ≤ 300 °C. Membrane formation can be carried out under ambient atmosphere or under vacuum[46,47].

1.2.5 Applications of pH Sensitive Chitosan-based Membranes

Currently, the majority of the applications for pH-sensitive chitosan membranes are related to *in vivo* controlled release of biologically active agents or substances, wound dressings and other biomedical applications. In 2013 Chen *et al*. profiled the controlled release of gastro-retentive drug delivery systems with respect to time employing chitosan as a pH-sensitive medium under conditions similar to those found in the digestive system[48]. Also, in 2013, Mukhopadhyay *et al*. successfully demonstrated the possibility of oral insulin delivery via self-assembled chitosan-insulin nanoparticles with insulin release occurring under the acidic pH conditions inherent to the gastric system[49]. Several other applications of chitosan membranes have been described; for example, Barros *et al.* studied the swelling behaviour of chitosan-cellulose hydrogel films with aqueous solutions mimicking human sweat[50]. Such materials could find application is various skin patch drug delivery systems for example. See chapter 3 for further development on this topic[51].

1.3 Colloidal SiO_2 Photonic Crystals

1.3.1 What are colloidal photonic crystals?

Photonic crystals are periodic optical materials that occur in nature in the form of opals, butterfly wings, beetle shells and peacock feathers. The change in colour seen when examining any of the above naturally occurring photonic crystals is the most obvious feature observed by the human eye but there are several other scientifically-applicable features which occur due to the internal structure of the crystals. Such materials are termed 'periodic' in that they have a crystal-like lattice structure and 'photonic' as photons, light energy, propagate throughout and can possibly be confined within the crystal lattice structure. The geometry present has been described as a "suitable environment for the guiding or trapping of photons"[52].

Considering the term 'colloidal', a material is said to be colloidal when it contains a specific substance dispersed throughout another separate substance e.g. spherical silica nanoparticles in water/air. Silica nanoparticles are prepared in situ using the well-known Stöber method[53]; this is discussed to a greater extent in section 1.3.2. Photonic crystals constructed of silica particles are known as 'artificial opals' as they bear the same chemical and physical structure as naturally occurring opals.

1.3.2 Fundamentals of crystal lattice structure

As mentioned above the silica (SiO_2) particles are prepared via the Stöber method[53]. This is a base-catalysed reaction which involves the hydrolysis and condensation of tetra-alkyl silicates in the presence of a low molecular weight alcohol and/or water. Owing to the basic conditions mono-disperse, uniform silica spheres (of 0.05-2 μm diameter) are formed while under acidic conditions a sol-gel form is adopted due to the formation of linear molecules[40]. An increase in ammonia concentration leads to the formation of larger spheres, it acts as a catalyst by providing OH^- ions which are necessary for the hydrolysis of tetra-alkyl silicates[54]. The kinetics of the Stöber synthesis were under speculation for many years with much research put into whether hydrolysis or condensation was the rate-limiting step and what optimum reaction conditions were. A study was carried out based on the structures present at the various stages using ^{29}Si NMR[55]. This study provided great insight revealing that (1), a higher reactive temperature was beneficial, (2), the rate-limiting step is the first step, hydrolysis of the tetra-alkyl silicate and (3), the key intermediate is the silanol $Si(OH)_4$ species formed during hydrolysis. The silica particles formed via the Stöber synthesis undergo self-assembly when in a colloidal suspension and form a distinct face-centred cubic (fcc) close-packed crystal lattice[56], the most energetically favourable array. Self-assembly occurs via a natural, gravitational sedimentation process. It is apparent in all self-assembly processes as it is here that "weak forces usually ignored in macroscopic processes, such as entropic, electrostatic and capillary forces, become the essential driving forces for the self-assembly of colloidal particles"[57]. Much research has been undertaken in providing evidence that the crystal lattice structure of SiO_2 is face-centred cubic. The majority of this evidence is based on the statistical study of SEM imagery of artificial opals. The ordering is believed to be due to the successive adsorption/desorption processes that the particles undergo which allow for them to organise into this minimum energy structure[56,58]. There are three low-index planes present in a face-centred cubic structure which can be described and labelled using Miller indices notation. These are the (100), (110) and (111) planes. The natural formation of this ordered internal structure is a major advantage in SiO_2 synthesis and provides for many of the distinct properties of photonic crystals.

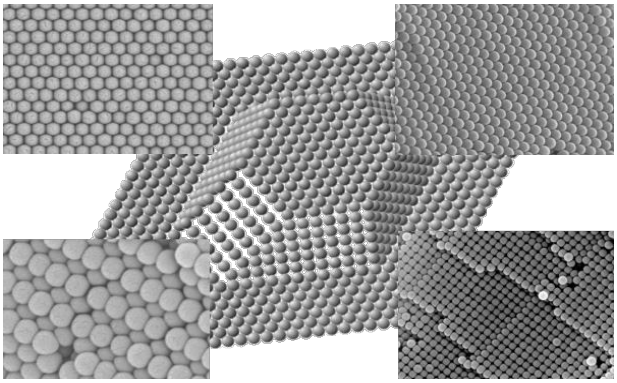

Figure 1.8. SEM images of the faces of an fcc photonic crystal. Upper left and upper right (111), bottom left (110) and bottom right (100)[59].

1.3.3 Optical Properties of Photonic Crystals and their Applications

A key feature of photonic crystals is that the regularly repeating crystal lattice that constitutes their structure is of the same order as the wavelength of light in a particular part of the electromagnetic spectrum; this is a key concept as it is very important to understand light energy (photons) as wave vectors in relation to photonic crystals. Essentially, photons exhibit wave-particle duality and should be thought as neither wave nor particle alone. The photon behaves as a wave as it transmits (propagates) through the crystal lattice, of comparable wavelength, without scattering. Whereas it behaves as a particle when it interacts with an impurity or defect and is reflected in another direction, scattered within the crystal lattice[60]. The photon that enters the photonic crystal may be transmitted (light propagating through the crystal), reflected (reflection off external surface or within internal structure), refracted/diffracted (interaction with internal structure causing the light to scatter or bend in another direction) or absorbed (light transformed to internal energy of absorbing medium). In addition, there can also be scattering effects which generally contribute to the losses observed when considering propagation in specific directions. Considering these various interactions should make it easier to visualise the so-called "guiding and trapping of photons"[52] within the crystal. Unlike most materials which generate their colour from the absorption of light, photonic crystals generate their colour by a combination of light interactions. So-called 'structural colour' arises from this phenomenon; upon observing a photonic crystal green light may appear due to reflection and red light may appear due to transmission. It is for this reason that it is

essential to carry out both reflection and transmission optical analysis on photonic samples. This is discussed to a greater extent later in this chapter.

The feature that affects electromagnetic wave propagation in a photonic crystal is the regularly repeating regions of high and low dielectric constant within the crystal lattice. "If the dielectric constants (refractive indices) of the materials in the crystal are sufficiently different, and if the absorption of light by the materials is minimal, then the refractions and reflections of light from all of the various interfaces can produce many of the same phenomena for photons (light modes) that the atomic potential produces for electrons"[60]. The dielectric constant (k) is related to permittivity; a measure of a material's ability to be polarized by an electric field. It is the ratio of the permittivity of a substance to the permittivity of free space. Silica has a permittivity of ca 3.8-3.9, while air has a permittivity of 1.05, yielding a dielectric constant of ca 3.66 for a SiO_2 photonic crystal. Refractive index (n) describes how light propagates through a medium and represents the ratio of the velocity of light in a vacuum to its velocity in a specified medium with a dimensionless, numerical value. The refractive index of silica prepared by the Stöber method is about 1.45[61], while the refractive index of air is 1. A lot of interest lies in increasing the refractive index contrast in photonic crystals by introducing high refractive index materials within the voids of the crystal[62] for applications in advanced optoelectronics. Much research has been carried out on the efficiency of various colloidal structures as photonic crystals and it has been concluded that "if they possess enough refractive index contrast and proper packing order and density" fabricating colloidal crystals is an effective route in the development of photonic crystals[63]. Depending on the periodic structure involved, photonic crystals may have a 1D, 2D or 3D framework. The dimensionality is based on how the differing refractive index materials align within the crystal, figure 1.9 (a) provides a conceptual view of this phenomenon using a simple cubic example. In a 1D photonic crystal the refractive index varies along one direction only, while in 2D and 3D photonic crystals the refractive index varies along two and three axes respectively. Summarising the optical and dimensionality requirements; "this can be realised in three dimensions in arrays of mono-disperse nanoparticles which are embedded in a medium that has a diffraction (or refraction) index sufficiently different (by ca. 2 units) from that of the particles in order to generate diffraction (or refraction) effects"[64].

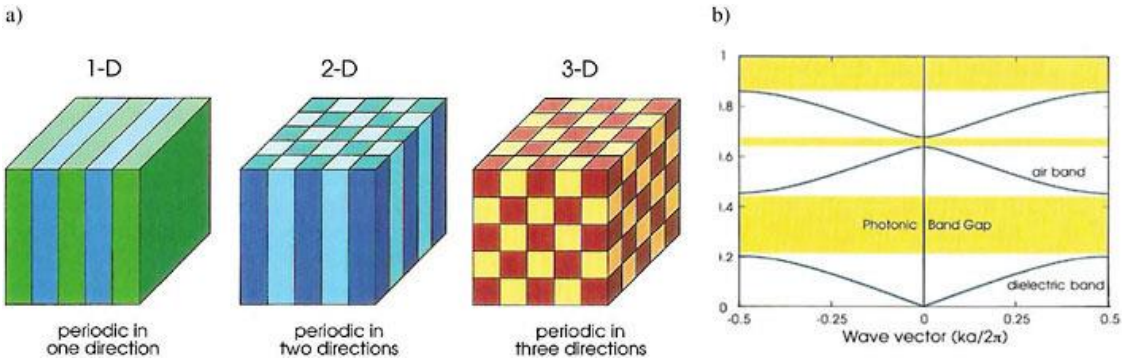

Figure 1.9. (a) The 1D, 2D and 3D cubes above illustrate the varying refractive indices in the various structures. (b) A diagram similar to that of an electronic band gap corresponds to a photonic band gap. Excitation from the dielectric band (high dielectric constant) to the air band (low dielectric constant) provides optical energy in the photonic material[60].

When describing the light interactions within a photonic crystal lattice the presence of the so-called 'photonic band gap' emerges as a concept. There is a familiarity here with the electronic band gap which arises due to the band structure in semiconductor materials where electrons are forbidden from having certain energies (and hence wave vectors), due to the lack of available states within photonic band gaps photons possessing specific energies and moving in specific directions are forbidden[60]. This phenomenon arises due to the destructive interference of the associated waves. Figure 1.9 (b) is an example of a photonic band diagram in which the photonic band gap can be seen. The band below a band gap is referred to as the dielectric band and the band above the band gap as the air band, a promotion in optical energy is required for photon promotion from the dielectric band to the air band[65]. Consideration of the light as a wave vector is of key importance when relating to photonic band gaps. Photons are forbidden to propagate with certain energies and certain wavelengths in certain directions[60], becoming rejected wavelengths. This means that a change in direction would correspond to a change in the wave vector. The rejected wavelengths, if within the visible part of the spectrum, correspond to colour, hence the reflected (rejected) wavelengths are the colours observed from the photonic crystals. The peak wavelength corresponding to the rejected photons is referred to as the 'stop band' In transmission it appears as a dip while in reflectance it appears as a peak, figure 1.10.

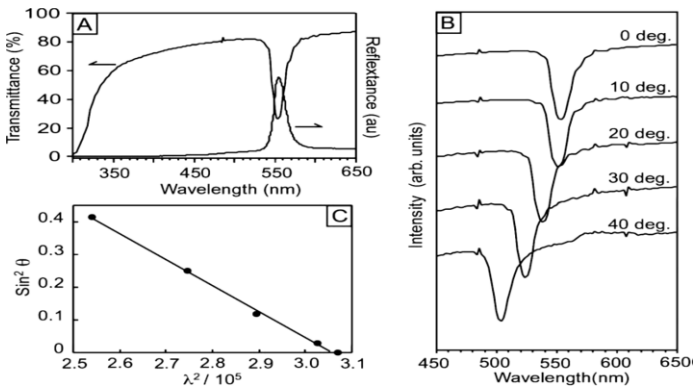

Figure 1.10. (a) Transmittance dip and reflectance peak at ca. 554nm. (b) Transmittance shift with change in incident angle. (c) Graph of incident angle versus dip wavelength (stop band)[66].

Transmittance and reflectance spectra play a very important role in the analysis of photonic crystals. As already mentioned the reflectance peak and transmittance dip overlap at the same wavelength corresponding to the viewed colour of the photonic crystal. An example of this can be seen in Figure 1.10 (a); in this case 560 nm corresponds to green structural colour. Figure 1.10 (b) shows the shift in transmittance as the incident angle of the beam of light is varied from 0-40 degrees as measured from normal. This demonstrates the change in structural colour as the incident angle is changed. Figure 1.10 (c) is a graph of tilting angle (y-axis) versus dip wavelength (x-axis)[66]. Application of these properties to Bragg's law of diffraction and Snell's law which relates to refraction led to development of the modified Bragg-Snell law, which is accurate for calculating the effective refractive index:

Equation 1.3: $\lambda=2D\sqrt{(n_{eff}^2 - sin^2\theta)}$

Here D is the interplanar spacing, λ is the wavelength at the stop band, n_{eff} is the effective refractive index and θ is the incident angle[67]. Upon calculating the effective refractive index of the photonic crystal sample, the refractive indices of the contrasting materials can be calculated separately via the following equation:

Equation 1.4: $n_{eff}=\sqrt{(n_1^2V_1 + n_2^2V_2)}$

Here n is the refractive index of the respective materials and V is the volume fraction of the respective materials.

1.3.4 Fabrication of Photonic Crystal Structures

There are various types of three-dimensional photonic crystals which can be made using particular fabrication techniques. The range includes 'woodpile' stacked structures, Yablonovite structures, opals and inverse opals.[60]. 'Woodpile' photonic crystals are fabricated by a top-down technique which involves etching by lithography and the synthesis of perpendicular stacks of dielectric materials and the name 'woodpile' arises to the similarity of the photonic crystal to a crossed-stack of wooden logs[68]. The Yablonovite structure is named after its proposer Prof Eli Yablonovitch-a pioneering photonic crystals researcher. The original Yablonovite structure was fabricated by drilling holes in a dielectric material simulating (110) faces in the diamond-like structure[69]. Opals themselves, being fcc arrangements of colloidal silica particles, can be made by controlled evaporation[70], under-oil crystallisation[66] and Langmuir-Blodgett (LB) crystallisation[71]. Inverse opals are constructed from opal crystal lattice templates that are initially infilled with a different material, such as a metal[72], a semiconductor[73] or a polymeric material[74]. The crystal lattice template can subsequently be etched or removed with a suitable organic solvent leaving the inverse opal, bearing the varying dielectric of the infill material/air[75]. The formation of inverse opals generally leads to greater refractive index contrast, which leads to a more complete photonic bandgap. SEM images of some of the photonic crystal structures described above are shown in Figure 1.11

This present work focuses on synthetic opal crystal lattice structures fabricated by the bottom-up self-assembly of silica particles by capillary-enhanced, under-oil and controlled evaporation techniques. A detailed description of the various experimental methods employed is presented in sections 1.3.5, 1.3.6 and 1.3.7.

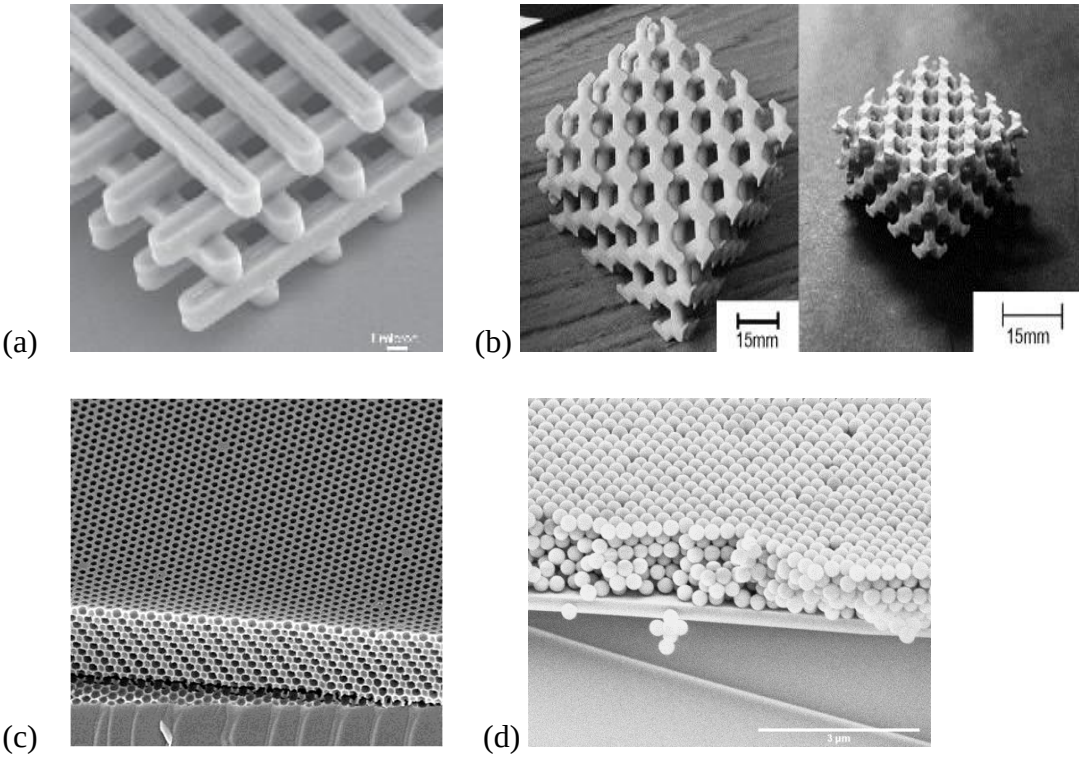

Figure 1.11. SEM images of (a) a 'woodpile' structure (b) a Yablonovite structure (c) an inverse opal and (d) a 3D fcc opal crystal lattice of silica particles.

1.3.5 Fabrication of Colloidal Photonic Crystals

1.3.5.1 The Capillary-Enhanced Method

One of the most commonly used methods to grow colloidal photonic crystals is the so-called capillary-enhanced method[76]. This method involves the primary and secondary capillary forces which occur at different stages of the solvent evaporation process during the horizontal sedimentation of dilute particles onto a substrate of choice. The primary capillary force is a gathering force which begins as the bulk solvent evaporates from a position close to the surface of the substrate; the particles are attracted to the substrate surface by capillary forces and arrange in a poorly packed fashion. Secondary capillary forces begin when the liquid interface is below the substrate. It is via the evaporation of solvent remaining between the particles that further capillary action takes place; this inverse force arranges the particles in an ordered structure. It is important to note that a humid environment is essential in this experimental setup. Figure 1.12 shows a schematic

of the primary and secondary capillary forces taking place at different stages of the evaporation process.

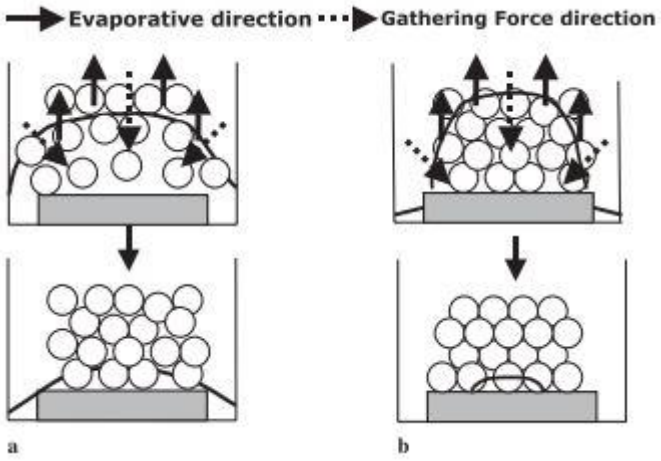

Figure 1.12. (a) Primary capillary forces and the resultant poorly ordered structure of the colloidal particles and (b) secondary capillary forces and the resultant highly ordered structure of the colloidal particles[76].

1.3.5.2 The 'Under Oil' Approach

Very similar to the capillary enhanced setup described above is a method known as 'under-oil', developed by Fudouzi *et al.*[66]. This method overcomes some problems encountered during the capillary enhanced method. Due to the fact that the rate of evaporation is faster at the edge than at the centre of the colloidal suspension the capillary flow occurs from the centre to the edge. As a result, a thicker ring of particles deposits at the edge of the hydrophilic substrate, reducing the uniformity of the film. Employing an 'under-oil' setup reduces this effect. It involves covering the colloidal suspension with high viscosity hydrophobic silicone oil; this enhances uniform evaporation throughout the film as evaporation at the edge of the suspension has been reduced significantly due to the presence of excess oil on the surface[66,77]. Upon completion the colloidal film can be rinsed with low viscosity silicone oil to remove any excess high viscosity oil. The diagram in Figure 1.13 below represents a comparison of the capillary enhanced method and the 'under-oil' method, highlighting the areas of solvent evaporation in both.

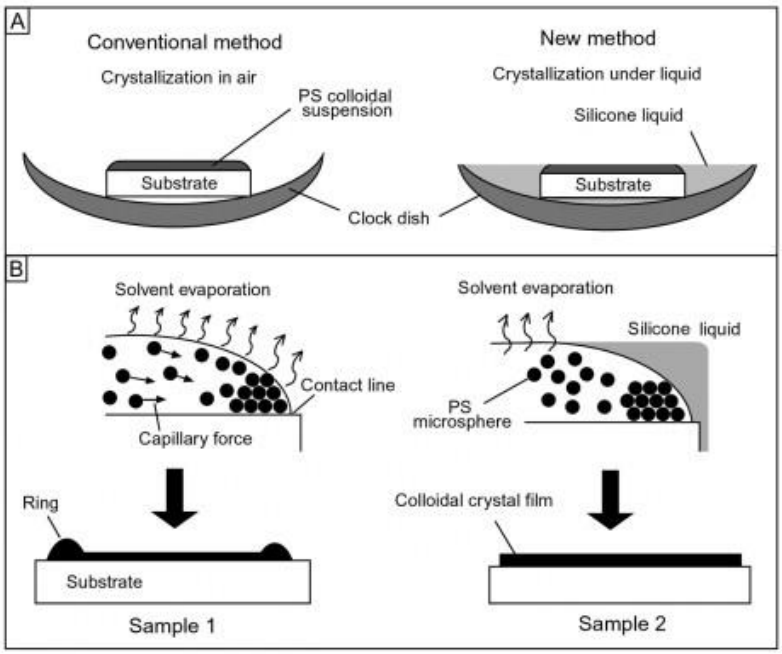

Figure 1.13. (a) Represents the experimental setup of the capillary enhanced method and the 'under-oil' method. (b) Demonstrating the different areas of solvent evaporation in both methods[66].

1.3.5.3 The Controlled Evaporation Method

This final method is a controlled evaporation technique for fabricating high quality colloidal films on hydrophilic substrates. It also depends on capillary forces but the experimental setup differs in comparison to the two methods previously discussed, in that it is said to be a vertical deposition technique[70]. It differs in that the hydrophilic substrate of choice is placed vertically in a prepared dilute silica particle suspension solution and as the solvent evaporates the colloidal particles deposit onto the substrate in an ordered fashion. A major advantage of this technique is the ability to control the thickness of the colloidal film when the concentration of the original colloidal suspension is known. Due to the fact that larger volume solutions must be prepared for the vertical deposition method there is a certain degree of freedom when it comes to the solvent system that may be used. Generally, ethanol and water mixtures are employed, while the ratios of EtOH: H_2O can be varied according to the desired results.

This present work focuses on the use of Capillary-Enhanced Growth, Under Oil Growth and Controlled Evaporation Growth for the production of the photonic crystals described.

1.3.6 Substrates Employed in Colloidal Photonic Crystal Fabrication

In general researchers working in this area have not discussed the possible 'substrates of choice' for the deposition of colloidal suspensions and growth of colloidal photonic crystal films. Necessarily many types of substrate can and have been employed, including both flexible and rigid substrates.

Flexibility allows for stretching, compressing, bending and flexing of the crystal lattice all of which in turn can result in the alteration of the crystal lattice causing a change in the structural colour of the photonic crystal, which sometimes can be observed by the naked eye. Many photonic crystals have been successfully deposited on glass with a resulting highly ordered structure[66,77,70,78]. Subsequently various plastics and minerals have been used, including; PMMA (polymethyl methacrylate), PET (polyethylene terephthalate), Kapton and mica. In all cases, it is essential that the substrates are suitably cleaned to ensure that their surfaces are hydrophilic prior to deposition; this is required in order to ensure that the first monolayer adheres to the surface due to hydrophilic interactions between the prepared surface and the colloidal particles. The cleaning technique employed varies with the nature of the substrate material. Glass and mica can be cleaned by soaking in a corrosive solution and drying with an inert gas such as N_2, while in general plastics must be plasma cleaned; both methods are successful in removing contaminating organic material and providing a hydrophilic surface. A more detailed description of the specific substrate preparation methods used in this work is provided in the experimental methods section.

1.3.7 Analysis of Colloidal Photonic Crystal Thin Films

Without doubt the most important parameter that is always discussed in relation to a particular colloidal photonic crystal thin film is the degree of ordering, since it is this order that results in the interesting optical properties of the materials concerned. The order of a colloidal photonic crystal can be assessed using two main approaches, these being electron microscopy and optical analysis.

Scanning electron microscopy (SEM) is an analytical technique which reveals spatial heterogeneities of a microstructure with dimensions of nm to mm. The sample is scanned with a high energy electron beam, which results in backscattered electrons and secondary electrons, it is these electrons which are detected and provide information on the composition and structural properties of the sample. SEM analysis

generally provides vital information associated with the size of the particles, the order and uniformity of the structure, the thickness of the sample, the structure of the substrate and the presence of impurities or defects; it is an excellent visual aid. Show some examples with references, taken from both your work and from the literature.

As described in section 1.3.3 optical analysis of the photonic crystal film is very important in revealing information associated with the quality and structure. The types of optical analysis employed are transmission and reflectivity, these being of the four fundamental light interactions that can occur between the photons and the crystal structure, the others being absorption and scattering. Figure 1.10 displays some examples of transmittance and reflectance spectra of colloidal photonic crystals taken from some highly cited papers in the literature. It is important to observe that the spectra display Bragg peaks or stop bands (see section 1.3.3) in the visible region of the electromagnetic spectrum due to the presence of particles of appropriate diameters; this visual information has been found to be a very helpful diagnostic tool as it gives an idea of the film quality prior to SEM analysis[79]. It is also important to observe that in general transmittance/reflectance is measured as a percentage and the greater the percentage the better the quality of the crystal. Such optical set ups are usually calibrated against a very high performance, control reflector such as a silver mirror, such that dimensionless 'percentages' may be used rather than some other unit system. The sample spectra selected also reveal other features- namely the presence of Fabry-Pérot fringes at either side of the Bragg/stop band feature. These fringes occur due to light interference within the crystal which is maximised when the crystal is viewed to be a slab having parallel top and bottom faces, such that the individual layers are also parallel to each other. The Fabry-Perot fringes occur at different wavelengths[80]. The wavelengths of the Fabry-Pérot fringes can be used to calculate the number of layers in the sample prior to SEM analysis.

As mentioned previously the dip/peak of the transmission/reflection spectrum is also referred to as the Bragg peak or stop band. The wavelength of the stop band allows for calculating the effective refractive index of the crystal film using the Bragg-Snell law, see equation (1.3). The effective refractive index, which is a combination of the refractive index of the colloidal crystal and the medium within which it is suspended, can then be used to determine the refractive index of the colloidal crystal film, see equation (1.4). Thus, as may be easily appreciated, the optical spectrometer is an

essential tool in the analysis of colloidal photonic crystals and the associated substrates.

1.4 Chitosan-based composite materials

1.4.1 Introduction

The work presented under the heading of composite materials in this thesis revolves around the following scientific hypothesis: for a SiO_2 photonic crystal embedded in a Chi-TEOS IPN it should hold true that as the IPN swells in aqueous environment of particular pH the photonic crystal lattice should also swell, while retaining its order and therefore its optical properties.

With this in mind this section presents information designed to demonstrate to the reader exactly what the composite materials are and how an experiment was designed in order to test our basic hypothesis, which is illustrated schematically in figure 1.14 below:

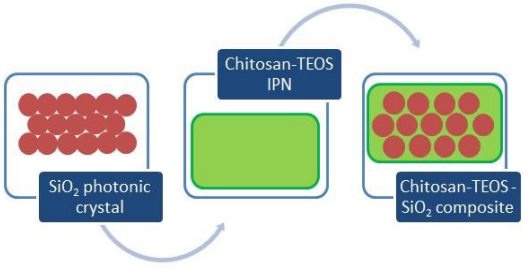

Figure 1.14. Schematic representation of the 3-step formation of a Chi-TEOS-SiO_2 photonic crystal composite.

1.4.2 Composite Materials

The IUPAC definition of a composite is a "multicomponent material comprising multiple, different (non-gaseous) phase domains in which at least one type of phase domain is a continuous phase". There are many types of composite depending on the individual component materials. According to the IUPAC definition, the Chi-TEOS-SiO_2 composite proposed in section 1.4.1 is considered as a polymer composite; "a composite in which at least one component is a polymer", with the polymer component being chitosan. However, it may also be considered as a nanocomposite; "a composite in which at least one of the phase domains has at least one dimension on the order of

nanometres", due to the presence of the SiO_2 nanoparticles. For the purpose of our research we may refer to the material as a 'polymer nano-composite', bearing in mind that this is not an official IUPAC definition. Composites are made up of phase domains; "a region of a material that is uniform in chemical composition and physical state". The proposed Chi-TEOS-SiO_2 composite is made up of three so-called 'phase domains' – chitosan polymer, siloxane polymer derived from TEOS and SiO_2 nanoparticles. We refer to these 'phase domains' as networks.

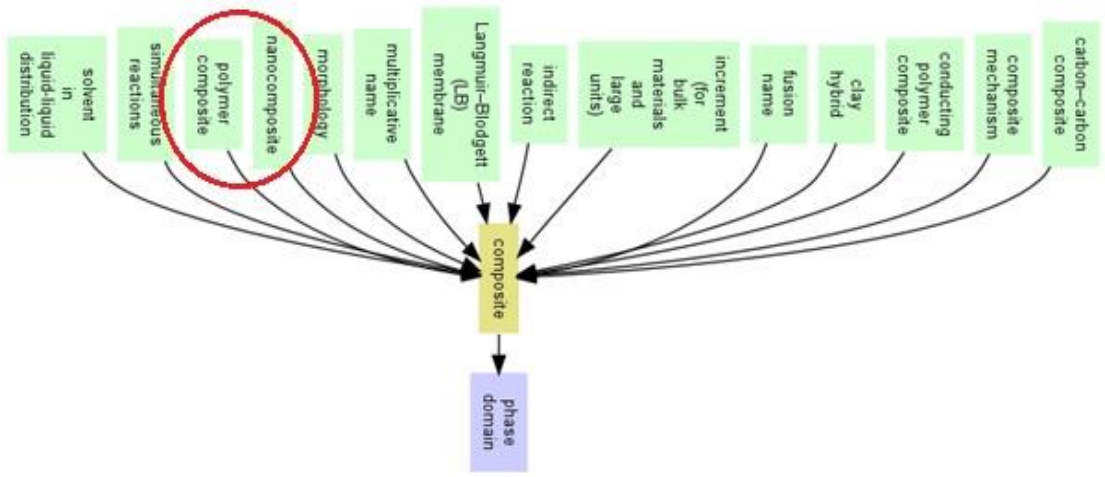

Figure 1.15. Concept map diagram depicting the connection between phase domains, composites and the resulting types of composites. Both polymer composites and nanocomposites are highlighted as they both apply to the Chi-TEOS IPN suggested in section 1.4.1. Resulting in a 'polymer nano-composite'.

The IUPAC definitions in the above text and the concept map diagram in figure 1.15 are available from the following reference[81].

A wide range of polymer composites bearing chitosan as the polymer chain have been researched. Wang *et al.* report the synthesis of chitosan/ multi-walled carbon nanotube composites prepared by a solution evaporation method, where the presence of carbon nanotubes at low concentration significantly improves the mechanical strength of the chitosan films[82]. Venkatesan *et al.* also report on incorporating carbon nanotubes into chitosan polymer composites for enhanced mechanical properties; this is present in a review on chitosan/ hydroxyapatite polymer composites for bone tissue engineering, due to the biocompatibility of both chitosan and hydroxyapatite[83]. This topic has been extensively studied with a variety of methods reported; including electrospinning[84], solvent casting[85] and electrochemical deposition[86]. The biocompatibility of chitosan

is one of its most widely researched attributes, because bio-reactive entities are easily introduced into the polymer, such as hydroxyapatite for bone engineering already described. Chitosan polymer composites have also been proposed as antibacterial dressings for wound-healing. Sezer *et al*. prepared chitosan/ fucoidan polymer composites of varying concentration to study wound-healing on burns[87]. Fucoidan is a naturally-occurring sulphated polysaccharide. Results indicated that the chitosan/ fucoidan composite had enhanced healing properties compared to either chitosan or fucoidan on its own. Nanocomposite films with antibacterial activity have also been reported; many referring to the inclusion of biocompatible polysaccharides such as chitosan and cellulose. For example, zinc oxide/ cellulose nanocrystal composites were synthesised by Azizi *et al*. with antibacterial activity enhanced with decreasing particle size against gram-positive and gram-negative bacteria[88]. A variety of nanoparticle/ chitosan nanocomposite films were prepared by Rhim *et al.* by a solvent-casting technique with both quantitative and qualitative studies carried out by the cell count method and the inhibition zone method, respectively. Results indicated high antibacterial activity with the inclusion of silver nanoparticles[89].

1.4.3 Stimuli-sensitive composites

Stimuli-sensitive composites are composites which react to external stimulus in a way that reflects the physical properties of the composite. It may be a reflection on one or more networks in the composite structure, again depending on the physical properties present. External stimuli include heat, light, pH, ionic strength, magnetic field and solvent, among others. A simple example is the dissolution of a polymer in a heated solution: when the upper critical solution temperature is reached, the physical properties of the polymer react to heat and a phase change to hydrogel/ solution occurs. If this is a reversible reaction, then the polymer will phase change back to solid upon a decrease of temperature below the upper critical solution temperature. A vast amount of colorimetric sensors have been reported in the literature with their development based on the methods outlined above[90]. The basic principle is that of a polycrystalline colloidal array (PCCA) where the tuneable and detectable structural colour of a colloidal crystalline network embedded in an external network responds to external stimulus such as solvent, temperature, pH or strain. In a review article by Stuart *et al.* the diverse range of stimuli-responsive polymers is referred to as a ‘galaxy’ of stimuli-responsive materials, aptly describing the vast range of materials that have been

studied[91]. Stimuli-sensitive polymers react to specific stimuli in a specific manner; this can then be detected depending on the response action and applications derived.

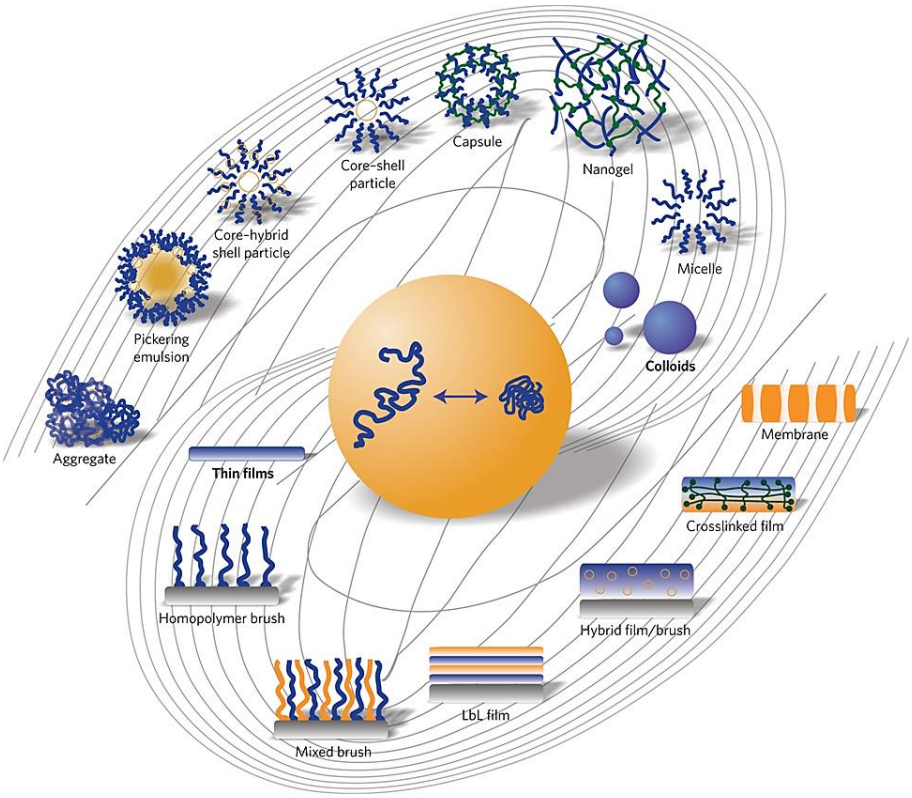

Figure 1.16. The 'galaxy' of stimuli-responsive materials, illustrated by Stuart *et al.*[91].

A variety of pH-responsive polymer systems have been reported in the literature, together with associated targeted applications. One example is the development of pH-sensitive polymeric micelles for the controlled delivery of doxorubicin by Hruby *et al.*[92]. The polymeric micelles are composed of two biocompatible block copolymers; polyethylene oxide and a doxorubicin antibiotic block. The pH-sensitivity arises from the formation of hydrazine bonds between the drug and the carrier. Cleavage of the hydrazine bonds occurs in mildly acidic conditions; this was confirmed by results as more than double the concentration of doxorubicin is released in aqueous conditions of pH 5, as compared to aqueous conditions of pH 7.

The Asher research group are prominent in the study of both colloidal photonic crystals and polymeric composites[93]. As part of this group Lee *et al.* have done extensive research on so-called polymeric crystalline arrays (PCCAs) which are composite materials constructed of acrylamide hydrogel and colloidal polystyrene nanoparticles[94]. The PCCA is sensitive to pH and ionic strength due to the presence of

carboxylated acrylamide. The polymer system swells between pH 5 and 11 and with this the crystalline colloidal array swells. The swelling can then be detected by a red-shift in the Bragg peak – see figure 1.17. The mechanism of action is similar to that proposed for the Chi-TEOS-SiO_2 composite described in this present work.

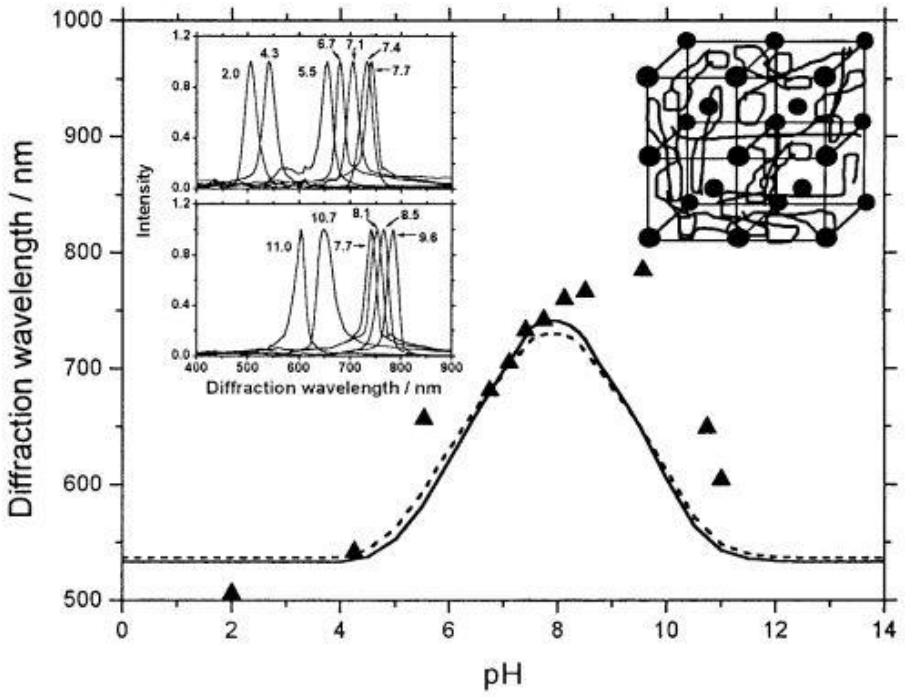

Figure 1.17. Optical data collected by Lee *et al.*[94] from a polymerized crystalline colloidal array made up of acrylamide and colloidal polystyrene. The ordered colloidal polystyrene swells with the acrylamide in aqueous conditions of pH 5-11. Here the Bragg diffracted wavelength is monitored as a function of pH.

In more recent work carried out by the Asher research group application-specific development of such PCCAs was researched. As before, the PCCA was made up of polystyrene nanoparticles surrounded by an acrylamide polymer network. Glucose sensing abilities were introduced to the system by the inclusion of boronic acid derivatives which are available for glucose-binding[95]. In this case the swelling phenomenon was different in that the polymer network shrinks upon binding glucose causing a blue-shift in the Bragg diffracted wavelength of the colloidal crystal structure, see figure 1.18. This is due to contraction of the photonic crystal lattice. Blood-glucose level sensing is the proposed application of such a PCCA.

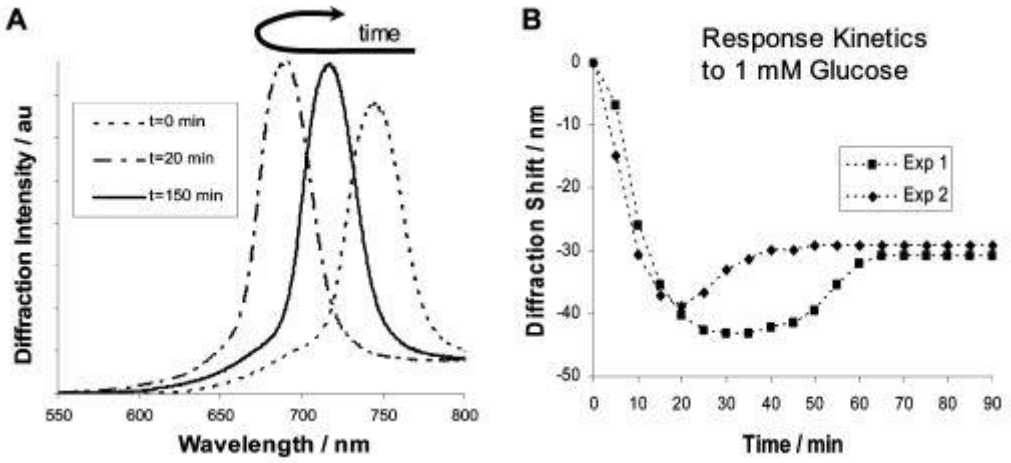

Figure 1.18. Data collected by Ward *et al.*[95] in the development of a polymer composite glucose sensor known as a polymerized crystalline colloidal array (PCCA). Boronic acid derivative in the array binds with glucose causing the network to shrink and as the photonic crystal component of the array shrinks a blue-shift in Bragg diffracted wavelength is observed.

The Chi-TEOS-SiO_2 composite introduced in section 1.4.1 is very similar to the PCCAs produced by the Asher research group; therefore, an in-depth understanding of the previous work cited here is very important in terms of the discussions regarding the development of a Chi-TEOS-SiO_2 composite presented in this thesis. The underlying rationale here is that by successfully introducing colloidal particles into a stimuli-sensitive framework, such as a chitosan-TEOS interpenetrating polymer network (Chi-TEOS IPN) it should be possible to manipulate the lattice structure as the crystal lattice would be expected to swell and shrink as the framework reacts to external changes in pH. Chitin/chitosan-silica composites have been reported in the past but without the ordered crystal structure[96,97]. In order to exploit the optical properties of a photonic crystal embedded in an IPN the colloidal silica particles which make up the photonic crystal must be ordered in an fcc orientation. This is one of the issues that is addressed in this thesis.

There are three key variables in the formation and study of composite membranes such as those described above; hydrogel material, colloidal suspension and external stimulus. For example, Asher *et al.* prepared their PCCA's employing acrylamide as hydrogel material, polystyrene as colloidal material and pH and ionic strength as external stimuli[94]. Wu *et al.* prepared a chitosan composite with polystyrene

nanoparticles incorporated, using water as external stimulus and varying particle size allow for a tuneable stop band and observable colour[98]. In 2013, Wang *et al*. developed a pH-sensitive nanocomposite constructed of colloidal polystyrene nanoparticles embedded in a PVA/ acrylamide IPN[99]. They successfully demonstrated how the embedded polystyrene photonic crystal swells with the IPN as a function of pH. In this case the IPN swells in transition from acidic to neutral conditions.

1.4.4 Experimental Methods for the Synthesis of the Chi-TEOS-SiO_2 Composite

Logically, a three-step formation mechanism may be suggested for the synthesis of a Chi-TEOS-SiO_2 composite. The first two steps would be the separate synthesis of the two basic elements of the composite; the SiO_2 photonic crystal and the Chi-TEOS IPN. The third step would then involve combination of the two separate elements to form a composite membrane.

SiO_2 photonic crystal synthesis could be performed using any of the methods described earlier. As will be discussed, in this work the vertical controlled evaporation method described in section 1.3.5 was employed. Similarly, there are several possible routes to the production of the Chi-TEOS IPN hydrogel. In our case the method described in section 1.2.4 was employed. Combining the two separate entities to form the composite may then be achieved using a simple casting technique, which involves casting the hydrogel onto the SiO_2 photonic crystal film and with the aid of capillary action and at constant temperature the IPN should infill the film, surrounding the SiO_2 particles.

Considering this process in more detail, capillary action is the phenomenon by which liquid travels in narrow spaces without the aid of external forces. It is due to intermolecular forces between the liquid and the solid - or hydrogel and photonic crystal structure. In an fcc structure the packing factor is known to be 0.74:0.26 i.e. in a fcc SiO_2 photonic crystal the SiO_2 particles account for 74 % of the total volume and air takes up the remaining 26 %. It is this 26 % void area that can be filled with hydrogel by the capillary action described. Chen *et al*. describe the fabrication of a two-dimensional nano-patterned surface by capillary action at the interface between a hydrophilic substrate and a 3D photonic crystal structure[100]. In this case the polymer array pattern (octadecyltrichlororsilicane) is limited to the surface through a

phenomenon described by the authors as "colloidal crystal-assisted capillary nanofabrication". Galusha *et al.* utilize capillary forces to infill a naturally-occurring photonic crystal structure in the formation of a 3D inverse opal framework[101]. The naturally-occurring crystal structure chosen was the scale of a biopolymeric beetle; *L. augustus*, which was infilled with a mesoporous silica sol-gel by capillary action. The beetle scales were subsequently removed via acid etch to yield an inverse opal photonic crystal structure. The inverse opal was then infilled with a titania sol-gel by capillary forces and acid-etched to yield the final titania structure. This method successfully describes how 'simple' capillary action is utilized in the manipulation of photonic crystal structures. See figure 1.19 for an overview.

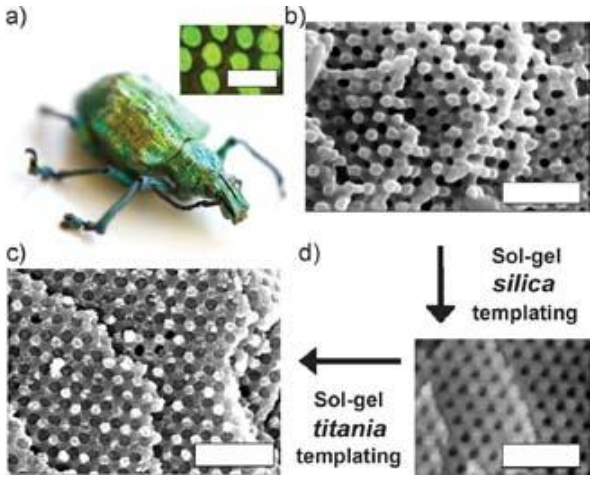

Figure 1.19. Galusha *et al.* synthesised a titania mimic of *L. augustus* beetle scales by formation of a silica inverse opal structure and subsequent titania templating; templating method in both steps is attributed to the phenomenon of capillary action[101].

In another study, Cho *et al*. prepared inverse opal structures suitable for force sensing via changes in optical response since the application of force on impact alters the inverse opal structure[102]. Their initial SiO_2 photonic crystal structure was fabricated by a dip-coating method and subsequently infilled with a thermoplastic polymer by capillary forces. This reference is important in portraying how capillary action driven experiments are relevant in modern research and also how the resulting structures and their associated mechanisms are suitable for a wide array of applications. See figure 1.20 for the associated schematic.

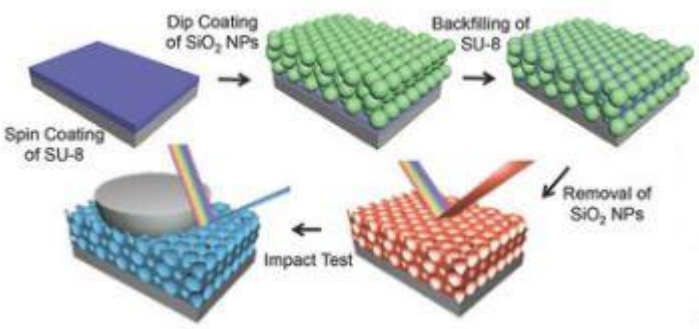

Figure 1.20. Schematic of the synthesis of a thermoplastic inverse opal structure by Cho *et al.*[102]. Backfilling is carried out by capillary action of the porous structure. Upon impact the structure behaves as a pressure sensor due to changes in optical response.

The capillary infilling methods described illustrate how the thermoplastic polymer can be added so as to surround the porous structures in question, facilitating further manipulation of the structure and the development of various applications. The capillary infilling method described has been used in this present work, in order to surround the SiO_2 photonic crystal with the Chi-TEOS IPN during the formation of the Chi-TEOS-SiO_2 composites described here, see Chapter 5.

1.4.5 Analysis of Composite Thin Films

As with the colloidal photonic crystals research in the area of composite thin films containing said photonic crystals also requires that optical analysis must be carried out both prior to and after infilling PhCs to compare Bragg diffraction peaks before and after infilling samples with Chi-TEOS IPN. Such analysis is also necessary in order to be able to quantify changes in refractive index contrast. The refractive index of cross-linked chitosan thin films has been reported in the range of 1.54 to 1.59; Yap *et al.* reported a stable refractive index of n= 1.54 for chitosan films with a range of chitosan concentrations and glutaraldehyde as a cross-linker[103], while Ligler *et al.* reported a refractive index of n=1.59 for a chitosan thin film cross-linked with tetra ethylene glycol[104]. Where the composite contains a photonic crystal then swelling will alter the optical properties of the composite which can be measured using the optical approaches described earlier, see section 1.3.7. As described further in Chapter 5, when exposed to an acidic environment the composite should swell to a greater extent

than when exposed to a neutral or basic environment and therefore the Bragg diffracted wavelength should shift accordingly.

The structure and morphology of most composite can be examined using electron microscopy. In the case of the materials described in this thesis, SEM analysis can be used as a visual tool to observe the degree to which the IPN hydrogel has infilled the SiO_2 photonic crystal structure upon composite formation. Backscattered electron imaging can also be used for imaging samples with areas of contrasting molecular weight due to the fact that heavier atomic constituents backscatter electrons more intensively than lighter atomic constituents. The differing compositions can be identified according their brightness; areas of heavier atomic constituents appear brighter. The thickness and packing quality of the crystals can also be observed. In this present work secondary electron SEM imaging has been used in order to analyse of the structural properties of the Chi-TEOS IPNs. Secondary electrons are inelastically scattered from the surface of the sample hence providing surface information with the same overall energy distribution, whereas backscattered electrons are elastically scattered from deeper in the sample yielding overall constituent analysis with relative energies. Figure 1.21 displays the difference in interaction of secondary electrons (SE) and backscattered electrons (BSE)[105].

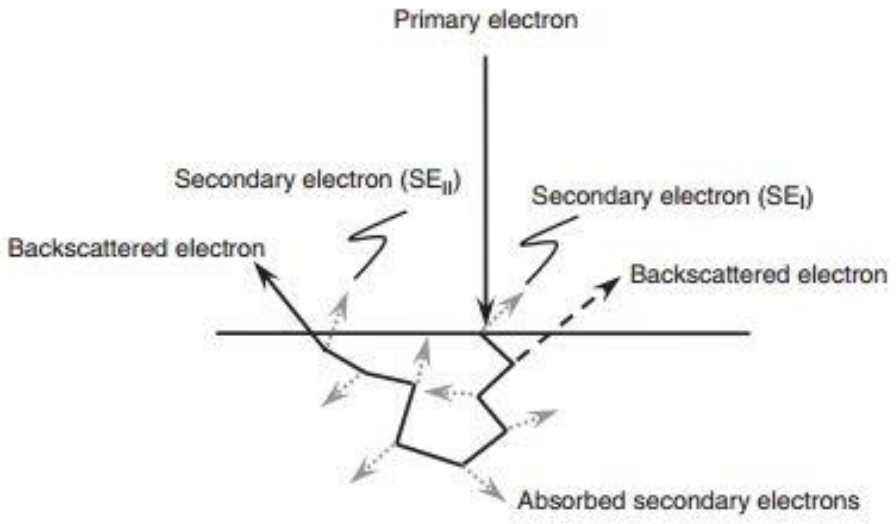

Figure 1.21. Diagram displaying the path of a primary electron whether emitted from the sample surface as a secondary electron or as a backscattered electron from a certain depth of the sample[105].

1.4.6 Proposed Applications of Inorganic- Organic Composites

The primary applications of an inorganic-organic composite such as the Chi-TEOS-SiO_2 composites described in this thesis are in the area of environmental, chemical and biological sensing. Due to the pH-sensitivity of the IPN the composite would be an ideal proton detection system in aqueous conditions, since the SiO_2 photonic crystal lattice would then be expected to swell and shrink with the IPN providing a colour change or shift in Bragg wavelength as an indicator for particular pH conditions. The pH range of aqueous, biological and environmental systems is quite broad depending on the particular system, ranging from neutralization and protection in the body[106] to animal or plant growth and survival in bodies of water[107,108] In addition materials that alter their shape under the influence of a particular external stimulus (such as pH), may also find application is areas such as drug delivery and wound dressings refs.

1.5 The Mechanical Properties of Chitosan-Based Composites

1.5.1 The Need to Understand the Mechanical Properties of Chitosan-Based Composites

In order to contribute to the development of applications such as the drug delivery or wound dressings mentioned above, it was apparent that an understanding of the mechanical properties of chitosan-based membranes was required. In particular, one of the aims of the work presented in this thesis was to understand how the incorporation of nanoparticles into chitosan-based membranes influences their mechanical properties -specifically to study whether the presence of nanoparticles will improve the tensile strength properties of the IPNs. The variables to consider include the type and diameter of the nanoparticles. In addition, the method of incorporation of nanoparticles also needed to be investigated. The proposal that was investigated was whether or not the nanoparticles act as structure enhancers when included in the polymer structure. The nanoparticles were introduced by two means;

1. Grafting separate Chi-TEOS IPN membranes.

2. Introducing nanoparticles to the Chi-TEOS IPN hydrogel prior to membrane formation, so that the nanoparticles were essentially ‘embedded’ in the Chi-TEOS IPN membrane.

Both methods of nanoparticle incorporation have been studied. The nanoparticles employed this work include SiO_2 nanoparticles of varying diameter, polystyrene (PS) nanoparticles of varying diameter, Ag nanoparticles and Au nanoparticles. The SiO_2 and PS nanoparticles were studied since they were available in a range of diameters, meaning the influence of the size of the nanoparticle could be studied. The Ag and Au nanoparticles were of interest due to their antimicrobial properties, which are frequently mentioned in the literature in conjunction with the antimicrobial properties of chitosan.

Indeed, there is currently a great demand for the use of natural and biocompatible sources in the biomedical industry; therefore, providing that ways can be found to incorporate a significant antimicrobial function without compromising mechanical robustness, this may facilitate the development of a range of functional dressings. With this in mind the focus of these present studies has been on mechanical properties, in the presence of the added nanoparticles.

1.5.2 The Mechanical Properties of Chitosan

Before conducting research into the properties of any composite material it is important to have an understanding of the properties of the individual components, as this allows for direct comparison of results and true insight into whether the properties of the individual components are enhanced following combination. First of all, it is important that the mechanical properties of the chitosan component of the composite are investigated. Chitosan is the original polymer structure which has been altered in this work, initially by introduction of TEOS to form an IPN (see section 1.2.3) and then by altering the Chi-TEOS IPN further by the incorporation of various nanoparticles. The mechanical properties of chitosan and chitosan composites have been researched extensively in the past. However, factors such as quantity of chitosan, sample dimensions and environmental conditions are likely to influence the resulting properties; therefore, it is important to consider the differing synthetic procedures employed when comparing results from different studies.

Zhang *et al.* carried out a study on the mechanical properties of chitosan films modified by the presence of varying concentration of vanillin[109]. They performed tests on a pure chitosan control film with a concentration of 3 % (w/v) and a thickness of 77 ± 2.3 μm with a yielding tensile strength of 6.64 ± 0.77 MPa (1 MPa = 1 Nmm^{-2}).

In another study Qin *et al*. examined chitosan films modified by the presence of montmorillonite and natural antioxidants from pomegranate rind, their analysis including a study of the mechanical properties[110]. In this case the chitosan control film had a concentration of 1.5 % (w/v) and a thickness of 65 ± 2.3 μm and yielded tensile strength results of 20.8 ± 1.20 MPa. Despite minor differences between the experimental arrangements employed by Zhang et al. And Qin et al., it is apparent that the results obtained vary considerably. This is perhaps surprising considering that the samples concentrations and thickness values don't vary to the same degree. This sort of variance in results highlights the importance in understanding that there will be differences from study to study and that the main comparisons should be drawn from variables within the individual studies. The most prominent variables are pore size, swelling index, thickness, charging effect, synthesis conditions, casting method, molecular weight and chain flexibility[111].

It is for this reason that in the work described in this thesis, tests were carried out on chitosan films with the same concentration of chitosan as in the Chi-TEOS IPNs from the original study in section 1.2.3 and also the IPNs which were grafted with nanoparticles.

The properties of chitosan which contribute most to the mechanical properties are poly dispersity index (PDI) and average molecular weight. A lower PDI value is expected to result in a lower distribution in molecular weight i.e. the uniformity of the polysaccharide chain structure. It is also expected that the mechanical properties should be enhanced with increasing average molecular weight. Huei *et al.* conducted a study on how varying molecular weight affects the tensile strength, tensile elongation and enthalpy of high purity chitosan samples with degree of deacetylation of 90 %[111]. Their results showed that the mechanical properties and enthalpy increase with increasing molecular weight of chitosan. Their results were attributed to two factors; more molecular entanglement with longer chain length and a higher degree of crystallinity in the higher molecular weight samples, which is suggested by the increase in enthalpy values.

More recently, Leceta *et al.* carried out a study on how varying glycerol concentration influences the functional properties of both low molecular weight and high molecular weight films[112]. The study included analysis of both low molecular weight and high

molecular weight films, in order that the functional properties of the materials with contrasting molecular weights could also be compared. As expected, their results revealed that the high molecular weight chitosan films have greater tensile strength properties than the low molecular weight films; 61.82 ± 4.43 MPa and 55.83 ± 2.96 MPa, respectively. Here the enhanced mechanical properties were attributed to the distribution and density of inter- and intramolecular interactions in the chitosan network, which was interpreted as a greater degree of possible interactions by chain overlap with increasing chain length.

A study on the effects of solvent acid and molecular weight of chitosan on the barrier and mechanical properties of chitosan films was carried out by Park *et al.* [113]. Tensile strength tests revealed that acetic acid is the best solvent acid for the preparation of mechanically strong films with tensile strength results increasing accordingly from low to medium to high molecular weight chitosan. The lowest tensile strength results were obtained from chitosan films prepared with citric acid solvent. Interestingly the opposite behaviour was seen in the percentage elongation tests: here chitosan films prepared with acetic acid showed the lowest results while those prepared with citric acid showed the greatest percentage elongation as a function of increasing molecular weight. This inverse relationship between tensile strength and percentage elongation is generally expected for such polymer films. These results are a good reflection on the influence of chain length and chain overlap on mechanical properties.

With respect to the research carried out on chitosan entities up to the time of writing (as described in sections 1.3 and 1.4) there have been no mechanical tests on chitosan membranes prior to IPN formation. As previously noted the main reason for considering IPN formation is to prevent the chitosan membrane from degrading when in solution as the TEOS IPN provides a mechanical 'backbone' for the chitosan polymer network. Cross-linking is therefore paramount and without it the IPNs and composites described in sections 1.4 would not be long-lasting or reusable. However, what is apparent is that prior to the studies presented here, there was a knowledge gap in that the tensile strength of the chitosan composite described was unknown.

1.5.3 The Mechanical Properties of Chitosan-Based IPNs

As previously described in section 1.3.3 - an interpenetrating polymer network (IPN) is defined as a 'combination of two polymers in network form, at least one of which

is synthesized and /or cross-linked in the immediate presence of the other'[38]. It is expected that the mechanical properties of the individual components of the IPN would be altered when cross-linking of the individual components occurs. The mechanical properties might be expected to change depending on the physical and/or chemical changes which occur upon IPN formation.

Aryaei *et al.* carried out a study on the mechanical properties of both non-cross-linked and cross-linked chitosan films, with the aim of enhancing the mechanical properties of chitosan for applications in the biomedical field[34]. Results from both elastic modulus and hardness tests show that the cross-linked chitosan sample had enhanced properties; however, the cross-linked chitosan sample was described as brittle compared to the non-cross-linked chitosan sample which was described as ductile. This provides evidence for modification properties due to cross-linking and although the cross-linked sample was stronger the brittle characteristic may not be desirable.

The changes in the physical properties of chitosan cross-linked with starch and varying glutaraldehyde concentration were studied by Li *et al*.[114]. This was an extensive study with analysis methods ranging from thickness measurements, FTIR, Raman, SEM, light transmission, mechanical, swelling studies, moisture uptake and water vapour transmission rate. Spectroscopic methods provided evidence for the reaction of glutaraldehyde with the polymer composite due to the loss of the characteristic aldehyde peak in the FTIR spectrum and a decrease in light transmittance in the UV-Vis spectrum with increasing glutaraldehyde concentration. This was attributed to phase separation within the composite as the glutaraldehyde was interfering with the integrity of the composite structure. Evidence of phase separation with increasing glutaraldehyde concentration was also seen in the results from the mechanical studies. The tensile strength and elongation at break values decreased with increasing glutaraldehyde concentration. According to the authors this was a contradiction to the other studies which appeared to show that the mechanical strength increased with increasing cross-linker concentration. However, it could be suggested that glutaraldehyde was not acting as a cross-linker as such but rather it was interfering with the chitosan-starch composite, inducing phase separation and weakening the cross-links between the chitosan and starch entities. Results from the elongation at break and tensile strength tests performed in this study are shown in figure 1.22.

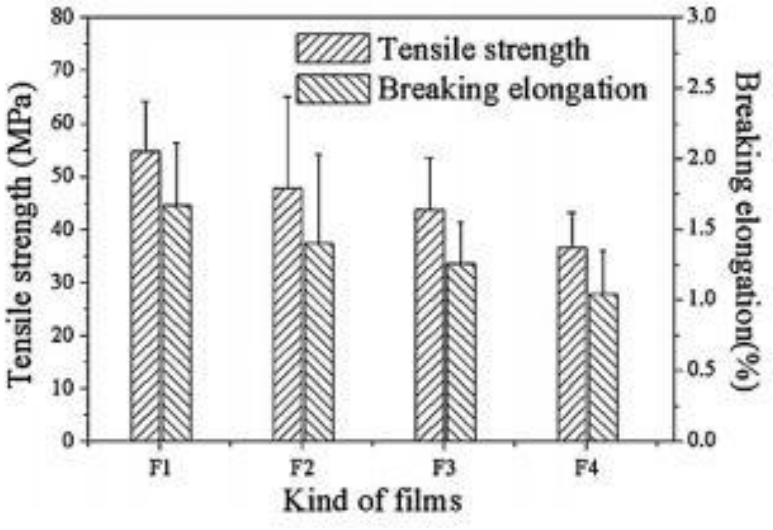

Figure 1.22. Results obtained by Li *et al.* for mechanical tests carried out on chitosan-starch composites with varying concentration of glutaraldehyde cross-linker incorporated (F1-no glutaraldehyde, F2, F3, F4 - 3, 6, 12 x 10^{-6} $molg^{-1}$, respectively). These results were said by the authors to be contradictory to the data produced in other studies. However, the results may be interpreted in a different way – perhaps increasing the concentration of the 'cross-linker, glutaraldehyde, actually induced phase separation which then interferes with the chitosan-starch bonds thereby reducing the mechanical properties of the structure[114].

1.5.4 The Incorporation of Nanoparticles into Chitosan-Based IPNs

There has been an abundance of research carried out on chitosan-cross-linker networks with respect to their mechanical and other properties. Typically, the same general trends are described and it can be concluded that the mechanical properties of chitosan are enhanced with increasing cross-linker concentration, as the cross-linker acts as a so-called 'backbone' when introduced to the chitosan polymer structure. The increase in mechanical strength generally causes a reduction in swelling ability as the flexibility and freedom for polymer chains to elongate is inhibited by the presence of a cross-linker 'backbone'. Moving on from this the question now is whether the mechanical properties of chitosan can be further enhanced while retaining the 'backbone' characteristic of the cross-linker; which should be maintained to prevent solubilisation of chitosan in aqueous solutions and a range of solvents. The overall aim of this section is therefore to review the previous work pertinent to this question and by doing so

provide some background to the studies described in this thesis, involving the introduction of nanoparticles into the composite structures.

In general, the properties and applications of nanoparticles seem endless due to the vast array of nanoparticles that exist together with their shared and individual characteristics. One invaluable property and common denominator for all nanoparticles is the high surface area associated with a minute quantity of nanoparticle material. This property is highly exploitable in catalytic chemical and physical reactions as only a minute quantity of nanoparticle material is required to significantly decrease the activation energy, compared to the quantity that would be required at the macro level. The phenomenon behind the large surface area of nanoparticles is neatly illustrated in figure 1.23.

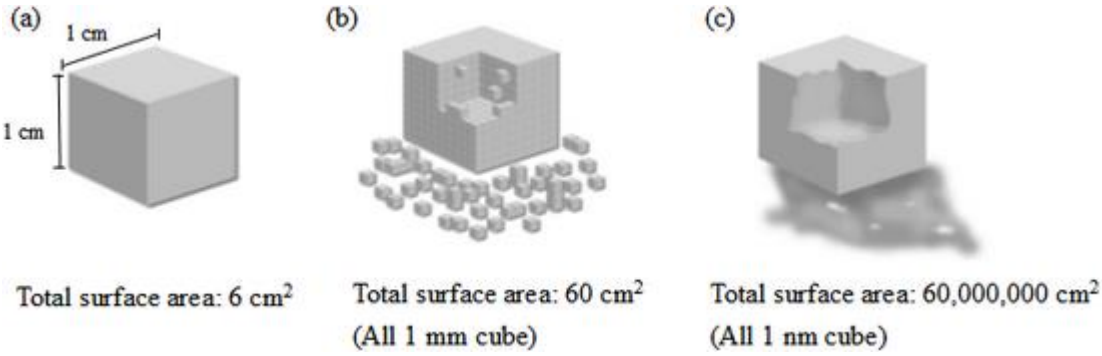

Figure 1.23. A simple illustration to demonstrate the phenomenon behind the large surface area of nanoparticles[115].

A recent study by Mathesan *et al*. on the mechanical properties of modified chitosan samples included incorporating nanoparticles into the chitosan network[116]. The stress-strain behaviour of three different chitosan networks was analysed; chitosan polymer, chitosan-hydroxyapatite (HAP) network and chitosan cross-linked with glutaraldehyde. It was determined that the Young's modulus and maximum stress increased in both the presence of HAP and glutaraldehyde; with the latter showing the greater increase. Radial distribution function analysis was carried out and provided evidence that hydrogen bonding and electrostatic interactions were the primary bonding interactions leading to the enhanced mechanical properties. These results are concise and novel, however there is room for further study as to how a network with the three combined entities would behave; chitosan, cross-linker and nanoparticle. Such a network has been investigated here.

The size of nanoparticles employed is a fundamental variable when considering the fabrication of a polymer network into which nanoparticles are to be incorporated, because it is expected that as the size of the nanoparticles varies that the bond strength between the nanoparticle and the polymer would also vary. An inverse relationship might be expected between particle size and bond strength as the increasing surface area should allow for more interactions. However, the opposite result was observed by Rose *et al.* as they performed tensile strength tests on various materials, including animal tissue, grafted with various nanoparticles of varying size[117], including SiO_2 nanoparticles. In their work they describe how the nanoparticle size (needs to be?) is comparable to the dimensions of the network into which it is being grafted. The results obtained were outstanding from a biomedical viewpoint as the nanoparticles employed have been suggested as wound-healing entities due to their ability to graft human tissue. Figure 1.24 displays a schematic of nanoparticle and a polymer network as illustrated by Rose *et al.*

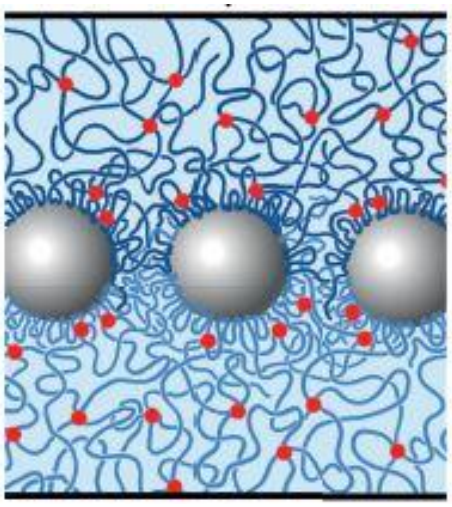

Figure 1.24. Nanoparticle surrounded by and interacting with a polymer network put reference here also.

1.5.5 Experimental Methods for the Preparation of Nanoparticle-Loaded Chitosan-Based IPNs

In general, the work described has involved the use of three types of chitosan; namely LMWChi, MMWChi and HMWChi. However, in relation to the work presented in the part of the thesis that describes the incorporation of nanoparticles into the chitosan: TEOS IPNs, only LMWChi is relevant (See Chapter 6).

This material was chosen due to the nature of the results obtained from other studies presented here and in particular the fact that it has the lowest degree of swelling. This is advantageous because elsewhere in this thesis we describe the exposure of LMWChi samples to aqueous conditions after the incorporation of nanoparticles and as such a lower degree of swelling was desirable in order to control the experimental conditions. The same experimental conditions as described in section 1.2.3 were employed for IPN synthesis. For tests on non-cross-linked chitosan the chitosan hydrogel was synthesised in aqueous acid conditions, see Chapter 3.

Silica (SiO_2), polystyrene (PS), silver (Ag) and gold (Au) nanoparticles have all been used in this work as part of the embedding/ grafting studies using LMWChi-TEOS IPNs. The main aim of using Ag nanoparticles was to compare the abilities of metal nanoparticles versus polymer nanoparticles in relation to antimicrobial activity and mechanical strength. Ag is renowned for its antimicrobial activity and as such it was of interest to combine this with the antimicrobial activity of chitosan. SiO_2 nanoparticles were prepared by the modified Stöber method first described in section 1.3.2; PS particles were prepared by Fudouzi *et al.* in the National Institute of Materials Science by the polymerisation of styrene monomers. Varying sizes of both SiO_2 and PS nanoparticles were used. Using similar concentrations for the SiO_2 and PS solutions allowed for direct comparison of the respective nanoparticles abilities as cross-linkers for embedding/ grafting. Also, comparison of the results from the Ag nanoparticles and the PS/SiO_2 nanoparticles allowed for a comparison of metal nanoparticles versus polymer nanoparticles in terms of their ability to act as structure enhancers.

The first method used in this work for testing the interactions of the nanoparticles with the Chi-TEOS IPN is referred to as ‘embedding’. In this method the nanoparticles are introduced to the polymer network when it is in hydrogel form and the IPN membranes are subsequently formed with nanoparticles ‘embedded’ in the polymer network. Using this approach, it is expected that there would be more of the bonding interactions, such as H-bonding and van der Waals forces already discussed, taking place, as the nanoparticles would be present throughout the polymer network rather than only at the surface as would be the expected situation for the alternative approach known as ‘grafting’, discussed below.

The second method described for testing the interactions of the nanoparticles with Chi-TEOS IPNs is referred to as 'grafting'. In this case two of the same polymeric networks (LMWChi-TEOS IPNs) are joined when a layer of nanoparticle solution is spread onto the surface of a LMWChi-TEOS IPN membrane and then another LMWChi-TEOS IPN membrane is placed on top. In this case the bonding interactions are expected to form between the surfaces of the membranes and the nanoparticles in between. H-bonding would be expected to occur between amine and alcohol groups of chitosan, siloxane/ alcohol groups of TEOS and surface siloxane/ alcohol groups of SiO_2. Bonding between PS and the Chi-TEOS IPN would be expected due to interactions such as van der Waals forces, which are significantly weaker than hydrogen bonds and occur in the presence of non-polar groups on PS. However, an induced dipole due to the presence of electronegative atoms in the IPN may enhance the intermolecular bonding. These types of interactions are generally expected of polymers as part of the so-called supramolecular chemistry that they facilitate[118]. The exact bonding interactions between silver nanoparticles and differing organic entities are not fully understood. Sun *et al*. proposed coordination bonding between silver nanoparticles and O and N atoms of a polyvinylpyrrolidone polymer network[119]. Obviously, a similar mechanism of bonding may be proposed for silver nanoparticles and a Chi-TEOS IPN.

This strategy was adopted in an attempt to determine if, as proposed, the IPN-nanoparticle interactions are primarily at the surface for grafted membranes and throughout the membranes for membranes with nanoparticles embedded. Tensile strength tests were carried out on chitosan membranes for comparison with results from tests on various Chi-TEOS IPNs, see Chapter 6. The main thrust of the experiments described in this thesis concerns the tensile strength testing of the various membranes although other mechanical testing as well as electron microscopy morphology studies were also performed. Following results from these further mechanical tests such as elongation at break and hardness tests may provide more insight. SEM analysis should also be carried out on the various IPNs with nanoparticles introduced.

1.5.6 Potential Applications of the NP-Containing Membranes?

The grafted/ embedded membranes described above have considerable potential on the development of various mechanical, antimicrobial and biomedical applications of chitosan membranes enhanced by cross-linking of the polymer network. The mechanical properties of chitosan have been widely discussed and reported but in general these previous reports have focused on modifying the chitosan membrane with one cross-linking entity[109,112]. In contrast this thesis looks at the effects of cross-linking with TEOS and also the possibility of further enhancing the mechanical properties by introducing nanoparticles as a third cross-linking entity.

Cross-linked chitosan networks have many potential applications in the biomedical industry. One proposed application which would benefit from increased cross-linker density and tensile strength is the use of chitosan membranes as wound-dressings. Chitosan provides a breathable, biocompatible layer which is well-suited for biomedical applications such as wound protection[26]. However, currently the lifetime of such wound dressings is questionable and so the concept addressed here concerns the possibility of improving the durability of the dressings via an increase in tensile strength. In addition, surface wound-healing membranes as described are ideal candidates for the controlled release of drugs at the epidermis[120] or at the surface of bone tissue[121]. The other underlying driver to the research described here concerns enhancement of the anti-microbial activity of the membranes. This is discussed in more detail in the following section.

1.6 Antimicrobial Activity of Chitosan Composites

1.6.1 Rationale Behind the Antimicrobial Studies

In addition to studying the optical and mechanical properties of chitosan and its various composites the aims of this work include a study of the possible antimicrobial properties of the materials prepared. The overall aim was to compare the antimicrobial activity of chitosan, Chi-TEOS IPN and a range of chitosan samples with metal nanoparticles embedded. This has been done with respect to gram-positive and gram-negative bacteria in both quantitative and qualitative tests. A specific area of interest was to study whether membranes with enhanced mechanical properties will display good antimicrobial activity. Such a material would be desirable as the mechanically

strong chitosan membranes would be ideal candidates for long-term use wound dressings or antibacterial coatings.

The pH-sensitivity of chitosan can be attributed to the presence of cationic (protonated) amino groups on the polyelectrolyte structure which have the ability to interact with charged cell walls leading to cell proliferation. As mentioned previously, upon cross-linking the mechanical properties of chitosan are enhanced, depending on the chemical make-up of the cross-linker and the degree of cross-linking, which may affect the antimicrobial activity both positively or negatively [122,123,124]. As part of this study additional functionalization in the form of metal and metal oxide nanoparticles were introduced into the materials since it is well documented in the literature that metal nanoparticles such as silver and gold possess antimicrobial properties [89,125]. This activity is attributed to the ability of metal nanoparticles to chelate to negatively charged bacterial cell walls and modify bacterial DNA which essentially leads to bacterial cell death [126,127,128].

1.6.2 The Antimicrobial Properties of Chitosan

A description of the chemical structure and properties of chitosan has already been given in section 1.2 while the antimicrobial properties of chitosan have also been referred to previously in this thesis. The purpose of this section is to review the literature pertaining to the antimicrobial properties of chitosan in an attempt to understand the phenomenon in greater detail (and the same can be said for sections 1.6.3 and 1.6.4).

The antimicrobial activity of chitosan is said to stem from four main mechanisms of action[129]. The first proposed mechanism is that positively charged chitosan reacts with negatively charged bacterial cell walls. This increases membrane permeability and cell lysis. The cationic character of the structure is also behind the second mechanism of action which involves chelation to nutrients and essential metals which inhibit bacterial cell growth. A third mode of action is based on the proposal that the chitosan membrane essentially ‘smothers’ the bacterial cell by encapsulating it and preventing oxygen and other essential nutrients from entering the cell. Finally, it is also proposed that diffused hydrolysis products interact with microbial DNA, leading to inhibition of mRNA and protein synthesis.

Theoretically, the overall mode of action of chitosan in relation to the killing of micro-organisms may involve a combination of the mechanisms described which mainly arise due to the presence of the cationic charge and the dense polymer structure[24]. Of course, this could then also be enhanced by the addition of antimicrobial cross-linkers[26], to be discussed in section 1.6.3. In addition, there are also a range of experimental factors which are proven to affect the antimicrobial activity of chitosan; these include pH, molecular weight, concentration, complexation, derivatives, type of microorganism, degree of deacetylation and chitosan source[129].

The pH sensitivity of chitosan is mainly due to the presence of amino groups in the polymer structure which are readily available for protonation. Chitosan hydrogel which is the precursor to thin film membranes is formed in aqueous acid solution and so a residual cationic charge is expected to remain in the thin film membrane state. The release of protons is therefore possible in aqueous conditions such as those often found in microbial samples.

It was revealed in a study by Liu *et al*. that chitosan essentially breaks down the bacterial cell membranes allowing the cell contents to permeate through the cell wall and causing cell death[130]. This is proposed to occur due to electrostatic interactions between the NH_3^+ groups of the chitosan and the phosphoryl groups of phospholipids in the bacterial cell membrane[131].

According to TEM analysis the treatment of gram-negative and gram-positive bacteria appeared to invoke different mechanisms of antimicrobial action. For *Escherichia coli* (*E. coli)*, a gram-negative, bacterium the outer membrane of the bacterial cell was damaged while the inner membrane remained intact. For *Staphylococcus aureus* (*S. aureus)*, a gram-positive bacterium, the dividing cells were affected resulting in irregular newly formed cells; however non-dividing *S. aureus* cells were not affected. In general, the antimicrobial activity of chitosan is more effective against gram-negative bacteria[132]. Molecular weight also holds significance with results suggesting that low molecular weight chitosan displays the best antimicrobial activity[133,134], presumably due to the ability for low molecular weight samples to penetrate the outer cell wall and inhibit the DNA and mRNA transcription processes[135]. The permeability of chitosan, which is essentially its ability to penetrate cell walls, has been reported as decreasing with increasing molecular weight, as might be expected. Rong-Huei *et al.*

carried out a study on the effect of molecular weight on a variety of properties including the thermal, mechanical and permeability properties of the material[111]. Results showed that with increasing molecular weight the crystallinity and enthalpy of the membrane also increased however there was also a decrease in permeability. This suggests that permeability is supported by shorter chain length and the presence of amorphous regions in the structure. The same effect was observed by Trung *et al*. in a study aimed at varying the degree of deacetylation while keeping constant the molecular weight where the percentage crystallinity increased from 28.1±2.1 % to 37.9±1.9 % with increasing degree of deacetylation; 75 % to 96 %[136]. Following on from this their permeation studies revealed greater percentage permeability with decreasing percentage degree of deacetylation.

In 2014 Younes *et al*. conducted an in-depth study involving a wide range of chitosan samples of varying molecular weight and degree of acetylation[3]. The materials were tested against four gram-negative and four gram-positive bacterial samples. Their results showed overall greater efficiency with lower molecular weight and lower degree of acetylation. The fact that chitosan with a lower degree of acetylation is purer, containing more proton-sensitive amino groups, means that there is a higher positive charge density on the sample. This coincides with the theory that the cationic polyelectrolyte structure of chitosan is one of the main contributors towards its antimicrobial activity [137,138]. Interestingly, greater antimicrobial activity was observed when testing gram-negative bacteria with low molecular weight chitosan and when testing gram-positive bacteria with higher molecular weight chitosan[3]. Contrasting results were observed in a study by Takahashi *et al*. where chitosan was observed to have a greater inhibitory effect on the growth of *S. aureus* than on the growth of *E. coli* (gram-positive and gram-negative, respectively)[139]. Similar results were observed in a study by No *et al*. in a series of antimicrobial tests carried out on four gram-negative and seven gram-positive bacterial samples[140]. Better antimicrobial activity was generally observed against gram-positive samples while the antimicrobial activity against gram-negative bacteria increased with decreasing molecular weight, as previously seen by Younes *et al.*[3]. Better antimicrobial activity was displayed against gram-negative bacteria in study by Fernandez-Saiz *et al*., again due to the chelation and migration of chitosan through gram-negative cell membranes[141]. These workers also accounted for the mechanism of antimicrobial activity towards gram-positive

bacteria, explaining how cationic chitosan reacts with the gram-positive cell walls without being repelled. They suggested that the gram-positive cell walls should be more susceptible to interactions with chitosan due to the make-up of the cell wall – it is constructed of negatively charged phosphate groups in the techoic acid building blocks of peptidoglycans.

To summarise, it appears that previous studies have resulted in a degree of variability in terms of results, which may be attributable to the variability in experimental conditions. Whatever the fundamental reason(s) behind the behaviour observed it seems that the antimicrobial activity occurs through ionic interactions at the bacterial cell wall.

1.6.3 The Antimicrobial Properties of Cross-Linked Chitosan

The inherent variability in chitosan and its associated complexes and derivatives contribute to the observed variability of activity towards micro-organisms[129]. Li *et al*. carried out an extensive study on the synthesis, characterization and antimicrobial activity of chitosan cross-linked with glutaraldehyde[142]. The aim of the study was to compare the antimicrobial activity of chitosan to chitosan cross-linked with glutaraldehyde with respect to the gram-negative *Burkholderia cepacia* bacteria. Results from inhibition zone tests showed negative results for chitosan in that there was no inhibition of bacterial growth, whereas for cross-linked chitosan the inhibition zone ranged from 15-20 mm for a range of *Burkholderia cepacia* bacterial samples. The non-inhibitory effect of chitosan had been previously noted by Tripathi *et al*. and put down to the inability of the solid chitosan membrane to diffuse through the solid agar[143]. Structural analysis revealed varying morphological and bonding properties before and after cross-linking. SEM analysis revealed a smooth morphology for chitosan whereas the cross-linked sample had a rougher, porous surface – yielding a larger surface area which was more favourable for further reactions. FTIR analysis displayed the appearance of a new peak at 1559 cm^{-1} for the cross-linked chitosan film which was attributed to the quaternary amino groups present for the positively charged species, which is said to be responsible for the antimicrobial ability of cross-linked chitosan samples[144]. XRD analysis also showed a significant change in structure in that the crystallinity decreased following cross-linking. This was due to the disruption to the main interlacing functional groups, such as hydroxyl and amino groups, when

the cross-linker was interlaced in the chitosan structure. Overall the study confirmed the structural changes which accompany increasing antimicrobial activity upon cross-linking chitosan, in this case with glutaraldehyde.

Mohamed *et al*. carried out a similar study by cross-linking chitosan with varying concentrations of oxalyl bis 4-(2,5-dioxo-2H-pyrrol-1(5H)-yl) benzamide and performed FTIR, SEM, XRD and antifungal and antibacterial analysis[145]. FTIR analysis confirmed that the amino and hydroxyl groups react with the cross-linker due to the disappearance of bands associated with both. Again, the cross-linked hydrogels displayed a porous structure during SEM analysis. XRD also yielded similar results to Li *et al*. where a clear reduction in crystallinity was observed suggesting that the network was becoming more disordered upon cross-linking[142]. In terms of the antimicrobial activity it was observed that both chitosan and the cross-linked hydrogels displayed better antimicrobial activity against gram-positive bacteria than gram-negative bacteria, with a marked increase in antimicrobial activity when the chitosan was cross-linked. However, as the degree of cross-linking increased the antimicrobial activity reduced. This was due to the fact that the network cannot swell to the same extent with greater degree of cross-linker, and with reduced swelling ability there is a reduced surface area and hence reduced chance of surface interactions.

Zhang *et al*. recently developed a carboxyl-modified poly (vinyl alcohol)-cross-linked chitosan hydrogel as a proposed network for wound-dressing applications[146]. See figure 1.25 for a schematic of the associated cross-linked system.

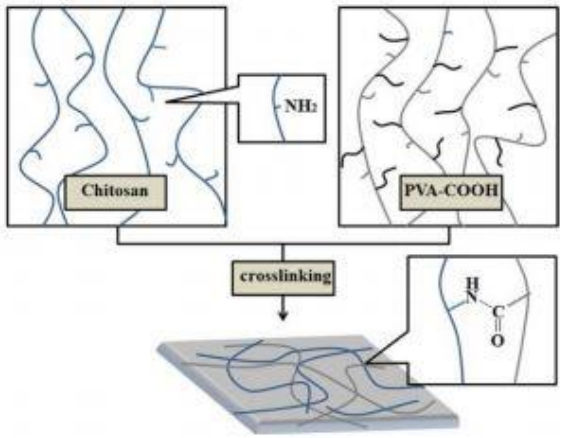

Figure 1.25. Schematic of chitosan cross-linked with PVA-COOH[146].

Mechanical studies, as well as water and oxygen permeability properties were performed, leading up to biocompatibility tests. Results from the water and oxygen permeability tests proved that the cross-linked films were suitable for use under *in vivo* conditions that required controlling the moisture conditions and allowing for sufficient oxygen permeation in order to replicate a range of biological functions. Interestingly, the membranes were studied for both antibacterial properties and antibiotic drug release ability by loading with gentamicin sulphate, an antimicrobial agent, in cross-linked networks of varying chitosan: PVA-COOH ratios. In this study, the best results were observed from the chitosan: PVA-COOH ratio of 70:30 with up to 85 % drug release in under an hour. In antibacterial tests carried out on both gram-negative and gram-positive bacteria *E. coli* and *S. aureus* good results were obtained in that bacterial growth was inhibited after six hours with continued growth in both the control and the sulphate-free cross-linked membrane. Overall the gentamicin-sulphate loaded chitosan-PVA-COOH cross-linked network provided an ideal system for sufficient wound hydration, tissue repair and sustained drug release.

1.6.4 The Antimicrobial Properties of Ag and Au Nanoparticles

In recent years, silver and gold nanoparticles have been extensively researched with respect to their antibacterial properties. There is a large-scale difference between the two entities- the bacteria and the nanoparticles- with nanoparticles on the scale of 1-100 nm[147] and bacteria typically on the scale of 1-5 μm[148]. This contrasting size is one of the main contributing factors towards the mechanism of antibacterial action. See figure 1.26 for an illustration of comparable biological and technological scales[149].

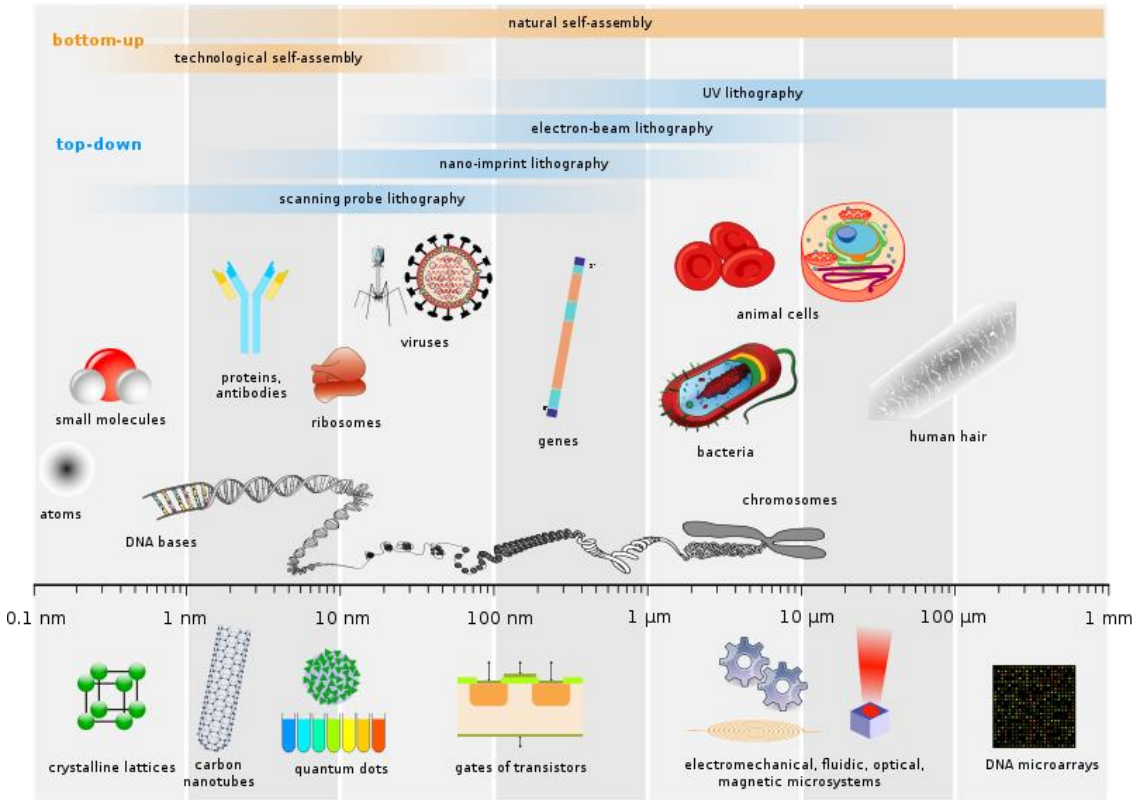

Figure 1.26. The illustration by Paumier *et al.* from Wikimedia Commons depicts the comparable biological and technological scales, including the nanoscale and bacterial scale[149].

A number of mechanisms of antimicrobial action have been proposed with respect to silver nanoparticles, as outlined in a review by Prabhu *et al.*[150]. A frequently proposed mechanism is that the Ag nanoparticles attach to bacterial cell walls (affecting various functions such as respiratory ability) and gradually permeate the cell wall, leading to cell death. This is said to be particle-size dependant with greater penetration observed for smaller particle diameters and more surface interactions with greater surface area[151]. It has also been suggested that the formation of free radicals from the Ag nanoparticles provides reactive entities with the ability to greatly damage the cell structure and it is likely that these two mechanisms go hand in hand[126,152]. Similar to the release of free radicals the release of reactive ions from the Ag nanoparticle is also proposed. These ions have the ability to penetrate the bacterial cell wall - reacting with the thiol groups of enzymes and leading to the inactivation of enzymatic processes, disturbing bacterial cells functions[153].

An interesting study by Morones *et al*. proposes that the hard-soft acid base (HSAB) theory plays a role in the reaction mechanism between Ag nanoparticles and

bacteria[154]. They propose that silver, being a soft acid, reacts with sulphur and phosphorous groups on the cell membrane, which can be considered as soft bases. Cell DNA is largely made up of sulphur and phosphorous groups and the interaction of Ag nanoparticles in this instance leads to problems in DNA replication and hence cell growth. Jin *et al.* describe a different method of antimicrobial activity through reaction with RNA and DNA[155]. They propose that reactive oxygen species are formed due to the redox reactive properties of metals. These reactive oxygen species are fatal to bacterial cells as they influence the role of RNA and DNA strands in cell apoptosis i.e. controlled cell death. This was confirmed in a concentration-time based study as the increasing level of reactive oxygen species in cells coincided with increased cytotoxicity[156].

Au nanoparticles, on the other hand, have a limited toxicity to bacteria. This is said to be due to the inert nature of the elemental gold nanoparticles in biological environments[155]. In a study on the antibacterial activities of gold and silver nanoparticles against *Bacillus Calmette-Guérin* (BCG) and *E. coli* by Zhou *et al*. the gold nanoparticles were capped with polyallylamine hydrochloride (PAH) and citrate functional groups while the silver nanoparticles were left uncapped[157]. While significant antimicrobial activity was observed on the samples treated with Ag nanoparticles there were contrasting results observed for the samples with both types of capped Au nanoparticles. Interestingly, the PAH capped Au nanoparticles were successful in inhibiting bacterial cell growth. It was also concluded from the study that better antimicrobial activity was observed with lower levels of aggregation of nanoparticles. The most important characteristic which contributes towards antibacterial ability is the strength with which the capping agents are bound to the surface of the nanoparticle: PAH is strongly bound while the citrate is only weakly bound resulting in increased aggregation. The explanation behind this is related to surface area. Increased aggregation means reduced surface area and hence less surface interactions which are essential for bacterial inhibition.

In their review article Zhang *et al.* described a variety of applications for gold nanostructures in the biomedical field[158]. The main variables contributing to efficiency are particle size, shape, surface functionalities and state of aggregation; this has previously been touched on briefly. The point of interaction between the bacterial cell and the nanoparticle is known as the ‘bio-nano interface’ and the nanoparticles ability

to interact here and subsequently cross the bacterial cell membrane greatly influences their toxicity to bacteria. With the development of medical applications including antimicrobial activity[157], cancer therapy[159,160] and vaccines[161,162] there are still stigmas related to the overall biological toxicity of Au nanoparticles, and Ag nanoparticles. This has resulted in a degree of reluctance towards investment in research and development based on the use of nanoparticles in the biomedical field.What is generally agreed is that the consequences of introducing nanoparticles into the body are far from understood and hence caution must always be applied. In general, it must always be assumed that nanoparticles are hazardous and this will continue to be the case unless it is proved to be inaccurate at some point in the future.

A possible alternative strategy would involve the specific targeting of cells or perhaps immobilization of nanoparticles in composite structures which would prevent their release and free travel around the body.

1.6.5 Experimental Methods for the Study of Antimicrobial Activity

For the purpose of this research the microbiological method employed is the crystal violet attachment assay- a qualitative test which comparatively measures the attachment of bacteria to surfaces by allowing the formation of a biofilm and subsequently staining this film with crystal violet. Live cells will attach to the biofilm while dead cells will detach and therefore be exempt from staining[163]. This method is an effective visual tool for comparing the antimicrobial abilities of solid samples. To a certain extent it can be considered both a qualitative and quantitative analysis tool as the quality of staining gives an idea of the attachment ability while the analysis of multiple varying samples can be quantitatively compared according to relative absorbance values despite the fact that this does not definitively measure the quantity of bacteria. According to an informative video article by O'Toole *et al.* 'biofilms are communities of microbes attached to surfaces' [164]. The crystal violet attachment assay is carried out under static, batch-growth conditions with the chitosan thin films immobilized on hydrophilic substrates. The thin film provides an extracellular matrix for the growth of the biofilm which may or may not be hindered depending on the properties of the thin film. One of the main advantages of the crystal violet attachment assay is the flexibility of experimental conditions; including sample type and bacterial

source, as well as the concentrations and incubation periods which can be adjusted to suit the experimental requirements. It is also a cheap, low-cost and reliable method.

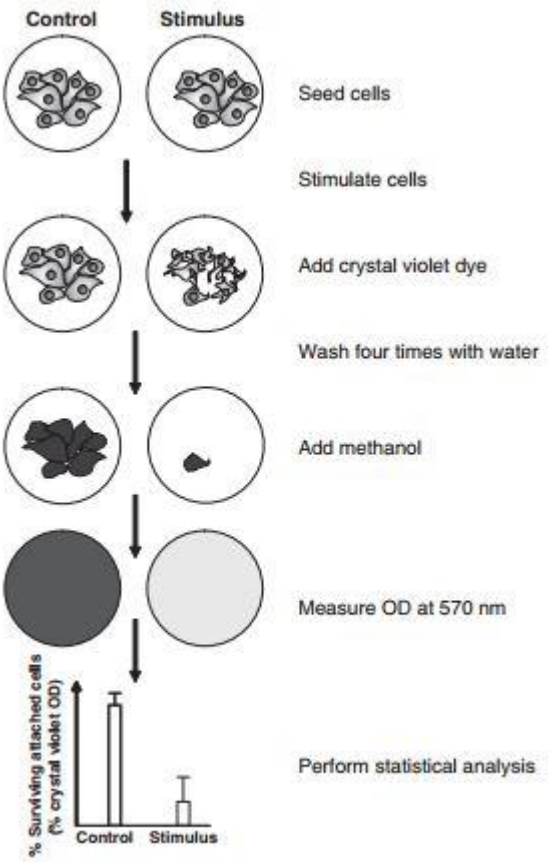

Figure 1.27. A typical work-flow of a crystal violet attachment assay, presented by Feoktistova *et al*. [163].

It is typical in microbiological analysis techniques to carry out all tests with a certain number of biological replicates, meaning using replicates of bacterial samples i.e. multiple samples with the same conditions and the same host[165]. Employing this method increases the precision of results due to statistical significance[166]. This approach can be adopted in microbiological analysis techniques, including the crystal violet attachment assay which has been employed here. For the purpose of our tests we have employed two biological replicates along with blank controls in each test.

1.6.6 Emerging Applications of Chitosan

As part of the work described here a review article describing the applications of chitosan has been prepared[51]. This article is included in this thesis as Chapter 2.

As is clearly demonstrated by this article, in recent years, there has been an increase in the number of reported chitosan-based biomedical studies and applications. Ease of processing and diversity of possible applications are among the attributes of the polysaccharide structure and its derivatives. In a review by Anitha *et al.* the ease of processing is referenced to as an advantage. A variety of forms are mentioned including "membranes, sponges, gels, scaffolds, microparticles, nanoparticles and nanofibers", with applications directed towards "drug delivery, gene therapy, tissue engineering and wound healing"[167]. A chitosan sponge network suitable for controlled drug release was developed by Noel *et al.*, amikacin and vancomycin are the two antibiotics which were loaded into the chitosan scaffold[168]. Zone of inhibition tests were carried out against *P. aeruginosa* and *S. Aureus*. The concentration of drug was measured as a function of time to determine the rate of elution of both drugs. Results were positive, showing sustained release of > 40 µg/mL of vancomycin and > 13 µg/mL of amikacin after 72 hours. These values are considered to be high levels of release of both drugs and are proposed as a treatment of early-stage infection. The degradation of chitosan in aqueous conditions was taken advantage of in that the sponges were designed to break down within 72 hours after sufficient drug release. The chitosan sponges break down to biocompatible, simple sugars and so are considered safe *in vivo*.

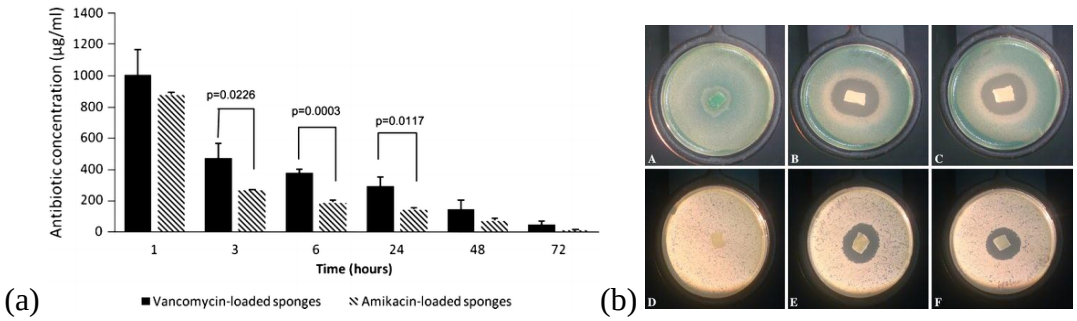

Figure 1.28. (a) Graph of results displaying the concentration of drug release as a function of time, showing that the satisfactory elution of both drugs was reached within 72 hours. (b) Images displaying the clear zones of inhibition of bacterial growth when comparing the abilities of amikacin (B-C) and vancomycin (E-F) against *P. aeruginosa* and *S. aureus*, respectively. (A) and (D) are saline-loaded control samples[168].

Chitosan has been referred to in the literature as a wound-healing agent[169,170]. Pang *et al*. developed a chitosan composite consisting of a layered structure of chitosan, PVA and carboxymethyl chitosan[171]. It was shown that the membrane, referred to as C-P-C, had a range of good capabilities including its mechanical properties, light transparency, vapour permeability and wound skin "adherence". It was found that *E. coli* did not grow on the multilayer structure and cell culture tests revealed the inhibition of keloid fibroblast growth and promotion of human skin fibroblasts – these conditions combined with the biocompatibility suggest an ideal network for development of a wound-healing membrane.

According to market research, the compound annual growth rate of the wound-dressing market is set to rise by 6 % in the five-year period from 2016 to 2021-that is an increase from $6.31 billion to $8.46 billion[172]. This coincides with an expected continued growth in incidences of obesity-related diseases. Diabetic foot ulcers, pressure ulcers, venous ulcers and surgical wounds are the types of obesity-related wounds which require attention. The fact that the aging population is increasing contributes significantly, with an increase of 11-22 % aged over 60 years by 2050. This is the age group most likely to suffer from surface skin wounds, such as those mentioned above. According to the World Health Organisation 13 % of adults worldwide were considered obese in 2014[173], whereas an Irish survey from 2015 revealed that 23 % of Irish adults were considered obese[174]. Obesity-related illnesses, such as surface wound infections, are considered acute up to a point. Treatment at this acute stage is vital and so the development of cheap, effective wound-dressings is a primary goal in both national and global and healthcare initiatives – reducing the number of short-term hospital visits and revisits for patients with obesity-related illnesses. This could provide further contribution to the steadily-declining acute hospital care costs in Ireland; for example, a reduction in annual costs of €60 million was achieved from 2006 to 2015[175].

The aim of the current study was to develop a chitosan composite membrane utilising cross-linkers and nanoparticles. It is suggested that the results presented in this thesis may contribute to the realisation of this aim and provide the means to enhance both the antimicrobial properties and the mechanical properties of the membranes and by so doing enhance their durability and lifetime.

References

1. Pillai, C.; Paul, W.; Sharma, C. P., Chitin and chitosan polymers: Chemistry, solubility and fiber formation. *Progress in Polymer Science* **2009,** *34* (7), 641-678.

2. Tolaimate, A.; Desbrieres, J.; Rhazi, M.; Alagui, A., Contribution to the preparation of chitins and chitosans with controlled physico-chemical properties. *Polymer* **2003,** *44* (26), 7939-7952.

3. Younes, I.; Sellimi, S.; Rinaudo, M.; Jellouli, K.; Nasri, M., Influence of acetylation degree and molecular weight of homogeneous chitosans on antibacterial and antifungal activities. *International Journal of Food Microbiology* **2014,** *185*, 57-63.

4. Inoue, H.; Ozaki, N.; Nagasawa, H., Purification and structural determination of a phosphorylated peptide with anti-calcification and chitin-binding activities in the exoskeleton of the crayfish, Procambarus clarkii. *Bioscience, biotechnology, and biochemistry* **2001,** *65* (8), 1840-1848.

5. Blumenthal, H. J.; Roseman, S., Quantitative estimation of chitin in fungi. *Journal of bacteriology* **1957,** *74* (2), 222.

6. Falini, G.; Fermani, S.; Ripamonti, A., Crystallization of calcium carbonate salts into beta-chitin scaffold. *Journal of inorganic biochemistry* **2002,** *91* (3), 475-480.

7. Averbach, B. L. *Report MITSG*; 75-17; National Infromation Service, U.S. Department of Commerce: NOAA 75102204, 1975.

8. Kumirska, J.; Weinhold, M. X.; Thöming, J.; Stepnowski, P., Biomedical Activity of Chitin/Chitosan Based Materials—Influence of Physicochemical Properties Apart from Molecular Weight and Degree of N-Acetylation. *Polymers* **2011,** *3* (4), 1875.

9. George, M.; Abraham, T. E., Polyionic hydrocolloids for the intestinal delivery of protein drugs: Alginate and chitosan — a review. *Journal of Controlled Release* **2006,** *114* (1), 1-14.

10. Chassary, P.; Vincent, T.; Guibal, E., Metal anion sorption on chitosan and derivative materials: a strategy for polymer modification and optimum use. *Reactive and Functional Polymers* **2004,** *60*, 137-149.

11. Chen, Z.; Mo, X.; He, C.; Wang, H., Intermolecular interactions in electrospun collagen–chitosan complex nanofibers. *Carbohydrate Polymers* **2008,** *72* (3), 410-418.

12. Gomez, L.; Allona, I.; Casado, R.; Aragoncillo, C., Seed chitinases. *Seed Science Research* **2002,** *12* (4), 217-230.

13. Xiao, X.; Yin, X.; Lin, J.; Sun, L.; You, Z.; Wang, P.; Wang, F., Chitinase genes in lake sediments of Ardley Island, Antarctica. *Applied and environmental microbiology* **2005,** *71* (12), 7904-7909.

14. Salzer, P.; Bonanomi, A.; Beyer, K.; Vögeli-Lange, R.; Aeschbacher, R. A.; Lange, J.; Wiemken, A.; Kim, D.; Cook, D. R.; Boller, T., Differential expression of eight chitinase genes in Medicago truncatula roots during mycorrhiza formation, nodulation, and pathogen infection. *Molecular Plant-Microbe Interactions* **2000,** *13* (7), 763-777.

15. Rege, P. R.; Block, L. H., Chitosan processing: influence of process parameters during acidic and alkaline hydrolysis and effect of the processing sequence on the resultant chitosan's properties. *Carbohydrate Research* **1999,** *321* (3–4), 235-245.

16. Gilbert, R.; Hess, M.; Jenkins, A.; Jones, R.; Kratochvil, P.; Stepto, R., Dispersity in Polymer Science (IUPAC Recommendations 2009). *Pure and Applied Chemistry* **2009,** *81* (2), 351-353.

17. Stepto, R. F., Dispersity in polymer science (IUPAC Recommendations 2009). *Pure and Applied Chemistry* **2009,** *81* (2), 351-353.

18. Muzzarelli, R. A., *Chitin*. Pergamon Press Oxford: 1977.

19. Bough, W.; Salter, W.; Wu, A.; Perkins, B., Influence of manufacturing variables on the characteristics and effectiveness of chitosan products. I. Chemical composition, viscosity, and molecular-weight distribution of chitosan products. *Biotechnology and Bioengineering* **1978,** *20* (12), 1931-1943.

20. Zikakis, J., *Chitin, chitosan, and related enzymes*. Elsevier: 1984.

21. Wang, W.; Bo, S.; Li, S.; Qin, W., Determination of the Mark-Houwink equation for chitosans with different degrees of deacetylation. *International Journal of Biological Macromolecules* **1991,** *13* (5), 281-285.

22. Shukla, S. K.; Mishra, A. K.; Arotiba, O. A.; Mamba, B. B., Chitosan-based nanomaterials: A state-of-the-art review. *International journal of biological macromolecules* **2013,** *59*, 46-58.

23. Qian, T. S., Haijia; Tan, Tianwei., The bactericidal and mildew-proof activity of a TiO_2-chitosan composite. *Journal of Photochemistry and Photobiology A: Chemistry* **2011,** (218), 130-136.

24. Kong, M.; Chen, X. G.; Xing, K.; Park, H. J., Antimicrobial properties of chitosan and mode of action: a state of the art review. *International journal of food microbiology* **2010,** *144* (1), 51-63.

25. Qu, X.; Wirsen, A.; Albertsson, A.-C., Novel pH-sensitive chitosan hydrogels: swelling behavior and states of water. *Polymer* **2000,** *41* (12), 4589-4598.

26. Dash, M.; Chiellini, F.; Ottenbrite, R.; Chiellini, E., Chitosan—A versatile semi-synthetic polymer in biomedical applications. *Progress in Polymer Science* **2011,** *36* (8), 981-1014.

27. Manickam, B.; Sreedharan, R.; Elumalai, M., 'Genipin' - the natural water soluble cross-linking agent and its importance in the modified drug delivery systems: an overview. *Curr Drug Deliv* **2014,** *11* (1), 139-45.

28. Lien, S.-M.; Li, W.-T.; Huang, T.-J., Genipin-crosslinked gelatin scaffolds for articular cartilage tissue engineering with a novel crosslinking method. *Materials Science and Engineering: C* **2008,** *28* (1), 36-43.

29. Park, S.-B.; You, J.-O.; Park, H.-Y.; Haam, S. J.; Kim, W.-S., A novel pH-sensitive membrane from chitosan—TEOS IPN; preparation and its drug permeation characteristics. *Biomaterials* **2001,** *22* (4), 323-330.

30. Rohindra, D. R.; Nand, A. V.; Khurma, J. R., Swelling properties of chitosan hydrogels. *The South Pacific Journal of Natural and Applied Sciences* **2004,** *22* (1), 32-35.

31. Mucha, M.; Pawlak, A., Thermal analysis of chitosan and its blends. *Thermochimica Acta* **2005,** *427* (1–2), 69-76.

32. Nieto, J.; Peniche-Covas, C., Characterization of chitosan by pyrolysis-mass spectrometry, thermal analysis and differential scanning calorimetry. *Thermochimica acta* **1991,** *176*, 63-68.

33. Wang, S.; Shen, L.; Tong, Y.; Chen, L.; Phang, I.; Lim, P.; Liu, T., Biopolymer chitosan/montmorillonite nanocomposites: preparation and characterization. *Polymer Degradation and Stability* **2005,** *90* (1), 123-131.

34. Aryaei, A.; Jayatissa, A. H.; Jayasuriya, A. C., Nano and micro mechanical properties of uncross-linked and cross-linked chitosan films. *Journal of the Mechanical Behavior of Biomedical Materials* **2012,** *5* (1), 82-89.

35. Vukusic, P.; Sambles, J. R., Photonic structures in biology. *Nature* **2003,** *424* (6950), 852-855.

36. Azofeifa, D. E.; Arguedas, H. J.; Vargas, W. E., Optical properties of chitin and chitosan biopolymers with application to structural color analysis. *Optical Materials* **2012**.

37. Mironenko, A.; Modin, E.; Sergeev, A.; Voznesenskiy, S.; Bratskaya, S., Fabrication and optical properties of chitosan/Ag nanoparticles thin film composites. *Chemical Engineering Journal* **2014,** *244*, 457-463.

38. Sperling, L. H., *Interpenetrating polymer networks and related materials*. Springer Science & Business Media: 2012.

39. Ahmed, E. M., Hydrogel: Preparation, characterization, and applications: A review. *Journal of Advanced Research* **2015,** *6* (2), 105-121.

40. Buckley, A.; Greenblatt, M., The sol-gel preparation of silica gels. *Journal of chemical education* **1994,** *71* (7), 599.

41. Park, S.-B.; You, J.-O.; Park, H.-Y.; Haam, S. J.; Kim, W.-S., A novel pH-sensitive membrane from chitosan — TEOS IPN; preparation and its drug permeation characteristics. *Biomaterials* **2001,** *22* (4), 323-330.

42. Jena, K. K.; Raju, K. V. S. N., Synthesis and Characterization of Hyperbranched Polyurethane Hybrids Using Tetraethoxysilane (TEOS) As Cross-Linker. *Industrial & Engineering Chemistry Research* **2008,** *47* (23), 9214-9224.

43. Pinto, R. C. d. F.; de Araujo Paschoal, C. W.; Paraguassu, W.; Castro, M. C.; Tanaka, A. A.; Filho, J. S. B.; José, N. M., Ionic properties of an organic–inorganic sol–gel hybrid based on polydimethylsiloxane and tetraethoxysilane doped with sodium dodecyl sulfate. *Journal of Applied Polymer Science* **2010,** *115* (2), 851-854.

44. Montembault, A.; Viton, C.; Domard, A., Rheometric Study of the Gelation of Chitosan in Aqueous Solution without Cross-Linking Agent. *Biomacromolecules* **2005,** *6* (2), 653-662.

45. Hong, P.-Z.; Li, S.-D.; Ou, C.-Y.; Li, C.-P.; Yang, L.; Zhang, C.-H., Thermogravimetric analysis of chitosan. *Journal of Applied Polymer Science* **2007,** *105* (2), 547-551.

46. Pierog, M.; Gierszewska-Drużyńska, M.; Ostrowska-Czubenko, J., Effect of ionic crosslinking agents on swelling behavior of chitosan hydrogel membranes. *Progress on Chemistry and Application of Chitin and its Derivatives. Polish Chitin Society, Łódź* **2009,** *75*, 82.

47. Cardea, S.; Pisanti, P.; Reverchon, E., Generation of chitosan nanoporous structures for tissue engineering applications using a supercritical fluid assisted process. *The Journal of Supercritical Fluids* **2010,** *54* (3), 290-295.

48. Chen, Y.-C.; Ho, H.-O.; Lee, T.-Y.; Sheu, M.-T., Physical characterizations and sustained release profiling of gastroretentive drug delivery systems with improved floating and swelling capabilities. *International Journal of Pharmaceutics* **2013,** *441* (1–2), 162-169.

49. Mukhopadhyay, P.; Sarkar, K.; Chakraborty, M.; Bhattacharya, S.; Mishra, R.; Kundu, P. P., Oral insulin delivery by self-assembled chitosan nanoparticles: In vitro and in vivo studies in diabetic animal model. *Materials Science and Engineering: C* **2013,** *33* (1), 376-382.

50. Barros, S.; da Silva, A.; Costa, D.; Cesarino, I.; Costa, C.; Lanceros-Méndez, S.; Pawlicka, A.; Silva, M., Thermo-sensitive chitosan–cellulose derivative hydrogels: swelling behaviour and morphologic studies. *Cellulose* **2014,** *21* (6), 4531-4544.

51. Ryan, C.; Pemble, M.; Bardosova, M., *Current Trends in Chitosan-Related Research in the Biomedical Feld: A short review*. Natural Product Communications, 2017; Vol. 12, p 855-861.

52. Andrews, D. L., *Structured light and its applications: An introduction to phase-structured beams and nanoscale optical forces*. Academic Press: 2011.

53. Stober, W., Fink, A., Bohn, E., Controlled growth of mono-disperse silica spheres in the micron size range. *Journal of Colloid and Interface Science* **1968,** *26,* 62-69.

54. Bagwe, R. P.; Yang, C.; Hilliard, L. R.; Tan, W., Optimization of dye-doped silica nanoparticles prepared using a reverse microemulsion method. *Langmuir* **2004,** *20* (19), 8336-8342.

55. Xu, Y.; Wu, D.; Sun, Y.; Gao, H.; Yuan, H.; Deng, F., A new study on the kinetics of Stöber synthesis by *in-situ* liquid 29Si NMR. *Journal of sol-gel science and technology* **2007,** *42* (1), 13-20.

56. Miguez, H.; Meseguer, F.; Lopez, C.; Mifsud, A.; Moya, J.; Vazquez, L., Evidence of FCC crystallization of SiO2 nanospheres. *Langmuir* **1997,** *13* (23), 6009-6011.

57. Zhou, Q.; Dong, P.; Liu, L.; Cheng, B., Study on the sedimentation self-assembly of colloidal SiO_2 particles under gravitational field. *Colloids and Surfaces A: Physicochemical and Engineering Aspects* **2005,** *253* (1), 169-174.

58. Cheng, B.; Ni, P.; Jin, C.; Li, Z.; Zhang, D.; Dong, P.; Guo, X., More direct evidence of the fcc arrangement for artificial opal. *Optics communications* **1999,** *170* (1), 41-46.

59. López, C., Materials aspects of photonic crystals. *Advanced Materials* **2003,** *15* (20), 1679-1704.

60. Joannopoulos, J. D.; Johnson, S. G.; Winn, J. N.; Meade, R. D., *Photonic Crystals: Molding the Flow of Light*. Princeton University Press: Princeton, 1995.

61. van Blaaderen, A.; Vrij, A., Synthesis and Characterization of Monodisperse Colloidal Organo-silica Spheres. *Journal of Colloid and Interface Science* **1993,** *156* (1), 1-18.

62. Miguez, H.; Blanco, A.; Lopez, C.; Meseguer, F.; Yates, H. M.; Pemble, M. E.; Lopez-Tejeira, F.; Garcia-Vidal, F. J.; Sanchez-Dehesa, J., Face centered cubic photonic bandgap materials based on opal-semiconductor composites. *Journal of Lightwave Technology* **1999,** *17* (11), 1975-1981.

63. Zhang, J.; Sun, Z.; Yang, B., Self-assembly of photonic crystals from polymer colloids. *Current Opinion in Colloid and Interface Science* **2009,** *14* (2), 103-114.

64. Roduner, E., *Nanoscopic materials: size-dependent phenomena*. Royal Society of Chemistry: 2006.

65. Novotny, L.; Hecht, B., *Principles of nano-optics*. Cambridge university press: 2012.

66. Fudouzi, H., Fabricating high-quality opal films with uniform structure over a large area. *Journal of colloid and interface science* **2004,** *275* (1), 277-283.

67. Fudouzi, H., Optical properties caused by periodical array structure with colloidal particles and their applications. *Advanced Powder Technology* **2009,** *20* (5), 502-508.

68. Maldovan, M.; Thomas, E. L., Diamond-structured photonic crystals. *Nature materials* **2004,** *3* (9), 593-600.

69. Berger, V., Photonic crystals and photonic structures. *Current Opinion in Solid State and Materials Science* **1999,** *4* (2), 209-216.

70. Jiang, P.; Bertone, J.; Hwang, K.; Colvin, V., Single-crystal colloidal multilayers of controlled thickness. *Chemistry of Materials* **1999,** *11* (8), 2132-2140.

71. Bardosova, M.; Dillon, F. C.; Pemble, M. E.; Povey, I. M.; Tredgold, R. H., Langmuir–Blodgett assembly of colloidal photonic crystals using silica particles prepared without the use of surfactant molecules. *Journal of Colloid and Interface Science* **2009,** *333* (2), 816-819.

72. Barako, M. T.; Sood, A.; Zhang, C.; Wang, J.; Kodama, T.; Asheghi, M.; Zheng, X.; Braun, P. V.; Goodson, K. E., Quasi-ballistic Electronic Thermal Conduction in Metal Inverse Opals. *Nano Letters* **2016,** *16* (4), 2754-2761.

73. Yang, P.; Yang, Y.; Wang, Y.; Gao, J.; Sui, N.; Chi, X.; Zou, L.; Zhang, H. Z., Spontaneous emission of semiconductor quantum dots in inverse opal SiO2 photonic crystals at different temperatures. *Luminescence* **2016,** *31* (1), 4-7.

74. Zhao, H.; Gao, J.; Pan, Z.; Huang, G.; Xu, X.; Song, Y.; Xue, R.; Hong, W.; Qiu, H., Chemically Responsive Polymer Inverse-Opal Photonic Crystal Films Created by a Self-Assembly Method. *The Journal of Physical Chemistry C* **2016,** *120* (22), 11938-11946.

75. Meseguer, F.; Blanco, A.; Mıguez, H.; Garcıa-Santamarıa, F.; Ibisate, M.; Lopez, C., Synthesis of inverse opals. *Colloids and Surfaces A: Physicochemical and Engineering Aspects* **2002,** *202* (2), 281-290.

76. Chung, Y.-W.; Leu, I.-C.; Lee, J.-H.; Hon, M.-H., Fabrication of high-quality colloidal crystals by a capillary-enhanced method. *Applied Physics A* **2004,** *79* (8), 2089-2092.

77. Fudouzi, H., Novel coating method for artificial opal films and its process analysis. *Colloids and Surfaces A: Physicochemical and Engineering Aspects* **2007,** *311* (1), 11-15.

78. Deng, T.-S.; Zhang, J.-Y.; Zhu, K.-T.; Zhang, Q.-F.; Wu, J.-L., Highly monodisperse vinyl functionalized silica spheres and their self-assembled three-dimensional colloidal photonic crystals. *Colloids and Surfaces A: Physicochemical and Engineering Aspects* **2010,** *356* (1), 104-111.

79. Shen, J.; Yu, B.; Xu, Y.; Xu, F.; Shen, J., Particle sizing by spectral analysis on transmission fluctuations. *Powder technology* **2006,** *166* (2), 91-99.

80. Yang, S.; Tan, S.; Zhang, Y.; Xu, J.; Zhang, X., Fabry–Pérot fringes of hydrogen-bonded assembly films. *Thin Solid Films* **2008,** *516* (12), 4018-4024.

81. Work, W. J.; Horie, K.; Hess, M.; Stepto, R. F. T., Definition of terms related to polymer blends, composites, and multiphase polymeric materials (IUPAC Recommendations 2004). *Pure and applied chemistry* **2004,** *76* (11), 1985-2007.

82. Wang, S.-F.; Shen, L.; Zhang, W.-D.; Tong, Y.-J., Preparation and Mechanical Properties of Chitosan/Carbon Nanotubes Composites. *Biomacromolecules* **2005,** *6* (6), 3067-3072.

83. Venkatesan, J.; Kim, S. K., Chitosan composites for bone tissue engineering--an overview. *Marine drugs* **2010,** *8* (8), 2252-66.

84. Teng, S.-H.; Lee, E.-J.; Yoon, B.-H.; Shin, D.-S.; Kim, H.-E.; Oh, J.-S., Chitosan/nanohydroxyapatite composite membranes via dynamic filtration for guided bone regeneration. *Journal of Biomedical Materials Research Part A* **2009,** *88A* (3), 569-580.

85. Xianmiao, C.; Yubao, L.; Yi, Z.; Li, Z.; Jidong, L.; Huanan, W., Properties and in vitro biological evaluation of nano-hydroxyapatite/chitosan membranes for bone guided regeneration. *Materials Science and Engineering: C* **2009,** *29* (1), 29-35.

86. Redepenning, J.; Venkataraman, G.; Chen, J.; Stafford, N., Electrochemical preparation of chitosan/hydroxyapatite composite coatings on titanium substrates. *Journal of Biomedical Materials Research Part A* **2003,** *66A* (2), 411-416.

87. Sezer, A.; Hatipoglu, F.; Cevher, E.; Oğurtan, Z.; Bas, A.; Akbuğa, J., Chitosan film containing fucoidan as a wound dressing for dermal burn healing: Preparation and in vitro/in vivo evaluation. *AAPS PharmSciTech* **2007,** *8* (2), E94-E101.

88. Azizi, S.; Ahmad, M.; Mahdavi, M.; Abdolmohammadi, S., Preparation, Characterization, and Antimicrobial Activities of ZnO Nanoparticles/Cellulose Nanocrystal Nanocomposites. *BioResources; Vol 8, No 2 (2013)* **2013**.

89. Rhim, J.-W.; Hong, S.-I.; Park, H.-M.; Ng, P. K. W., Preparation and Characterization of Chitosan-Based Nanocomposite Films with Antimicrobial Activity. *Journal of Agricultural and Food Chemistry* **2006,** *54* (16), 5814-5822.

90. Wang, H.; Zhang, K.-Q., Photonic Crystal Structures with Tunable Structure Color as Colorimetric Sensors. *Sensors (Basel, Switzerland)* **2013,** *13* (4), 4192-4213.

91. Stuart, M. A. C.; Huck, W. T. S.; Genzer, J.; Muller, M.; Ober, C.; Stamm, M.; Sukhorukov, G. B.; Szleifer, I.; Tsukruk, V. V.; Urban, M.; Winnik, F.; Zauscher, S.; Luzinov, I.; Minko, S., Emerging applications of stimuli-responsive polymer materials. *Nat Mater* **2010,** *9* (2), 101-113.

92. Hrubý, M.; Koňák, Č.; Ulbrich, K., Polymeric micellar pH-sensitive drug delivery system for doxorubicin. *Journal of Controlled Release* **2005,** *103* (1), 137-148.

93. Group, Asher Research Colloid Group. http://www.pitt.edu/~asher/homepage/colgrp.html (accessed 22/4/2014).

94. Lee, K.; Asher, S. A., Photonic crystal chemical sensors: pH and ionic strength. *Journal of the American Chemical Society* **2000,** *122* (39), 9534-9537.

95. Ward Muscatello, M. M.; Stunja, L. E.; Asher, S. A., Polymerized crystalline colloidal array sensing of high glucose concentrations. *Analytical chemistry* **2009,** *81* (12), 4978-4986.

96. Wysokowski, M.; Behm, T.; Born, R.; Bazhenov, V. V.; Meissner, H.; Richter, G.; Szwarc-Rzepka, K.; Makarova, A.; Vyalikh, D.; Schupp, P.; Jesionowski, T.; Ehrlich, H., Preparation of chitin-silica composites by in vitro silicification of two-dimensional Ianthella basta demosponge chitinous scaffolds under modified Stober conditions. *Mater Sci Eng C Mater Biol Appl.* **2013,** *33* (7), 3935-41.

97. Oliveira, F. C.; Barros-Timmons, A.; Lopes-da-Silva, J. A., Preparation and characterization of chitosan/SiO2 composite films. *J Nanosci Nanotechnol.* **2010,** *10* (4), 2816-25.

98. Du, X.; Li, T.; Li, L.; Zhang, Z.; Wu, T., Water as a colorful ink: transparent, rewritable photonic coatings based on colloidal crystals embedded in chitosan hydrogel. *Journal of Materials Chemistry C* **2015,** *3* (15), 3542-3546.

99. Cui, Q.; Wang, W.; Gu, B.; Liang, L., A Combined Physical–Chemical Polymerization Process for Fabrication of Nanoparticle–Hydrogel Sensing Materials. *Macromolecules* **2012,** *45* (20), 8382-8386.

100. Chen, X.; Chen, Z.; Fu, N.; Lu, G.; Yang, B., Versatile nanopatterned surfaces generated via three-dimensional colloidal crystals. *Advanced Materials* **2003,** *15* (17), 1413-1417.

101. Galusha, J. W.; Jorgensen, M. R.; Bartl, M. H., Diamond-Structured Titania Photonic-Bandgap Crystals from Biological Templates. *Advanced Materials* **2010,** *22* (1), 107-110.

102. Cho, Y.; Lee, S. Y.; Ellerthorpe, L.; Feng, G.; Lin, G.; Wu, G.; Yin, J.; Yang, S., Elastoplastic Inverse Opals as Power-Free Mechanochromic Sensors for Force Recording. *Advanced Functional Materials* **2015,** *25* (38), 6041-6049.

103. Yap, W. F.; Yunus, M.; Mahmood, W.; Moksin, M.; Talib, Z. A.; Yusof, N. A., Optical properies of crosslinked chitosan thin film with glutaraldehyde using surface plasmon resonance technique. *American Journal of Engineering and Applied Sciences* **2011,** *4* (1), 61-65.

104. Ligler, F. S.; Lingerfelt, B. M.; Price, R. P.; Schoen, P. E., Development of Uniform Chitosan Thin-Film Layers on Silicon Chips. *Langmuir* **2001,** *17* (16), 5082-5084.

105. Stokes, D. J., Principles of SEM. *Principles and Practice of Variable Pressure/Environmental Scanning Electron Microscopy (VP-ESEM)*, 17-62.

106. Schwalfenberg, G. K., The alkaline diet: is there evidence that an alkaline pH diet benefits health? *Journal of environmental and public health* **2012,** *2012*, 727630.

107. Azevedo, L. B.; De Schryver, A. M.; Hendriks, A. J.; Huijbregts, M. A., Calcifying species sensitivity distributions for ocean acidification. *Environmental science & technology* **2015,** *49* (3), 1495-500.

108. Rouwet, D.; Tassi, F.; Mora-Amador, R.; Sandri, L.; Chiarini, V., Past, present and future of volcanic lake monitoring. *Journal of Volcanology and Geothermal Research* **2014,** *272*, 78-97.

109. Zhang, Z.-H.; Han, Z.; Zeng, X.-A.; Xiong, X.-Y.; Liu, Y.-J., Enhancing mechanical properties of chitosan films via modification with vanillin. *International Journal of Biological Macromolecules* **2015,** *81*, 638-643.

110. Qin, Y. Y.; Zhang, Z. H.; Li, L.; Yuan, M. L.; Fan, J.; Zhao, T. R., Physio-mechanical properties of an active chitosan film incorporated with montmorillonite and natural antioxidants extracted from pomegranate rind. *Journal of food science and technology* **2015,** *52* (3), 1471-9.

111. Rong Huei, C.; Hwa, H.-D., Effect of molecular weight of chitosan with the same degree of deacetylation on the thermal, mechanical, and permeability properties of the prepared membrane. *Carbohydrate Polymers* **1996,** *29* (4), 353-358.

112. Leceta, I.; Guerrero, P.; de la Caba, K., Functional properties of chitosan-based films. *Carbohydr. Polym.* **2013,** *93* (1), 339-346.

113. Park, S. Y.; Marsh, K. S.; Rhim, J. W., Characteristics of different molecular weight chitosan films affected by the type of organic solvents. *JOURNAL OF FOOD SCIENCE-CHICAGO-* **2002,** *67* (1), 194-197.

114. Li, H.; Gao, X.; Wang, Y.; Zhang, X.; Tong, Z., Comparison of chitosan/starch composite film properties before and after cross-linking. *International Journal of Biological Macromolecules* **2013,** *52*, 275-279.

115. Nanotechnology and Food Safety. http://www.cfs.gov.hk/english/programme/programme_rafs/programme_rafs_ft_01_04_Nanotechnology.html (accessed 11th November).

116. Mathesan, S.; Rath, A.; Ghosh, P., Molecular mechanisms in deformation of cross-linked hydrogel nanocomposite. *Materials Science and Engineering: C* **2016,** *59*, 157-167.

117. Rose, S.; Prevoteau, A.; Elziere, P.; Hourdet, D.; Marcellan, A.; Leibler, L., Nanoparticle solutions as adhesives for gels and biological tissues. *Nature* **2014,** *505* (7483), 382-385.

118. Brunsveld, L.; Folmer, B. J. B.; Meijer, E. W.; Sijbesma, R. P., Supramolecular polymers. *Chemical Reviews* **2001,** *101* (12), 4071-4098.

119. Sun, Y.; Xia, Y., Shape-Controlled Synthesis of Gold and Silver Nanoparticles. *Science* **2002,** *298* (5601), 2176-2179.

120. M Ferreira, D.; Y Saga, Y.; Aluicio-Sarduy, E.; Tedesco, A. C., Chitosan nanoparticles for melanoma cancer treatment by photodynamic therapy and electrochemotherapy using aminolevulinic acid derivatives. *Current medicinal chemistry* **2013,** *20* (14), 1904-1911.

121. Zeng, R.; Tu, M.; Liu, H.; Zhao, J.; Zha, Z.; Zhou, C., Preparation, structure, drug release and bioinspired mineralization of chitosan-based nanocomplexes for bone tissue engineering. *Carbohydrate Polymers* **2009,** *78* (1), 107-111.

122. Wang, X.; Du, Y.; Liu, H., Preparation, characterization and antimicrobial activity of chitosan–Zn complex. *Carbohydrate Polymers* **2004,** *56* (1), 21-26.

123. Wang, X.; Du, Y.; Fan, L.; Liu, H.; Hu, Y., Chitosan- metal complexes as antimicrobial agent: Synthesis, characterization and Structure-activity study. *Polymer Bulletin* **2005,** *55* (1), 105-113.

124. Yang, Z.; Shu, J.; Liu, L., Enhanced phytoremediation of lead-contaminated soils by chitosan chelating agent. *Journal of Agro-Environment Science* **2006,** *25* (1), 86-89.

125. Ramesh, A.; Hasegawa, H.; Sugimoto, W.; Maki, T.; Ueda, K., Adsorption of gold(III), platinum(IV) and palladium(II) onto glycine modified crosslinked chitosan resin. *Bioresource Technology* **2008,** *99* (9), 3801-3809.

126. Kim, J. S.; Kuk, E.; Yu, K. N.; Kim, J.-H.; Park, S. J.; Lee, H. J.; Kim, S. H.; Park, Y. K.; Park, Y. H.; Hwang, C.-Y., Antimicrobial effects of silver nanoparticles. *Nanomedicine: Nanotechnology, Biology and Medicine* **2007,** *3* (1), 95-101.

127. Sharma, V. K.; Yngard, R. A.; Lin, Y., Silver nanoparticles: green synthesis and their antimicrobial activities. *Advances in colloid and interface science* **2009,** *145* (1), 83-96.

128. Rai, M.; Yadav, A.; Gade, A., Silver nanoparticles as a new generation of antimicrobials. *Biotechnology Advances* **2009,** *27* (1), 76-83.

129. Hosseinnejad, M.; Jafari, S. M., Evaluation of different factors affecting antimicrobial properties of chitosan. *International Journal of Biological Macromolecules* **2016,** *85*, 467-475.

130. Liu, H.; Du, Y.; Wang, X.; Sun, L., Chitosan kills bacteria through cell membrane damage. *International Journal of Food Microbiology* **2004,** *95* (2), 147-155.

131. Helander, I. M.; Nurmiaho-Lassila, E. L.; Ahvenainen, R.; Rhoades, J.; Roller, S., Chitosan disrupts the barrier properties of the outer membrane of Gram-negative bacteria. *International Journal of Food Microbiology* **2001,** *71* (2–3), 235-244.

132. Chung, Y. C.; Su, Y. P.; Chen, C. C.; Jia, G.; Wang, H. L.; Wu, J. C.; Lin, J. G., Relationship between antibacterial activity of chitosan and surface characteristics of cell wall. *Acta pharmacologica Sinica* **2004,** *25* (7), 932-6.

133. Liu, N.; Chen, X.-G.; Park, H.-J.; Liu, C.-G.; Liu, C.-S.; Meng, X.-H.; Yu, L.-J., Effect of MW and concentration of chitosan on antibacterial activity of Escherichia coli. *Carbohydrate Polymers* **2006,** *64* (1), 60-65.

134. Cruz-Romero, M. C.; Murphy, T.; Morris, M.; Cummins, E.; Kerry, J. P., Antimicrobial activity of chitosan, organic acids and nano-sized solubilisates for potential use in smart antimicrobially-active packaging for potential food applications. *Food Control* **2013,** *34* (2), 393-397.

135. Sudarshan, N. R.; Hoover, D. G.; Knorr, D., Antibacterial action of chitosan. *Food Biotechnology* **1992,** *6* (3), 257-272.

136. Trung, T. S.; Thein-Han, W. W.; Qui, N. T.; Ng, C.-H.; Stevens, W. F., Functional characteristics of shrimp chitosan and its membranes as affected by the degree of deacetylation. *Bioresource Technology* **2006,** *97* (4), 659-663.

137. Kong, M.; Chen, X.-g.; Xue, Y.-p.; Liu, C.-s.; Yu, L.-j.; Ji, Q.-x.; Cha, D. S.; Park, H. J., Preparation and antibacterial activity of chitosan microshperes in a solid dispersing system. *Frontiers of Materials Science in China* **2008,** *2* (2), 214-220.

138. Chung, Y.-C.; Chen, C.-Y., Antibacterial characteristics and activity of acid-soluble chitosan. *Bioresource Technology* **2008,** *99* (8), 2806-2814.

139. Takahashi, T.; Imai, M.; Suzuki, I.; Sawai, J., Growth inhibitory effect on bacteria of chitosan membranes regulated with deacetylation degree. *Biochemical Engineering Journal* **2008,** *40* (3), 485-491.

140. No, H. K.; Young Park, N.; Ho Lee, S.; Meyers, S. P., Antibacterial activity of chitosans and chitosan oligomers with different molecular weights. *International Journal of Food Microbiology* **2002,** *74* (1–2), 65-72.

141. Fernandez-Saiz, P.; Lagaron, J. M.; Ocio, M. J., Optimization of the biocide properties of chitosan for its application in the design of active films of interest in the food area. *Food Hydrocolloids* **2009,** *23* (3), 913-921.

142. Li, B.; Shan, C.-L.; Zhou, Q.; Fang, Y.; Wang, Y.-L.; Xu, F.; Han, L.-R.; Ibrahim, M.; Guo, L.-B.; Xie, G.-L.; Sun, G.-C., Synthesis, Characterization, and Antibacterial Activity of Cross-Linked Chitosan-Glutaraldehyde. *Marine drugs* **2013,** *11* (5), 1534.

143. Tripathi, S.; Mehrotra, G. K.; Dutta, P. K., Physicochemical and bioactivity of cross-linked chitosan–PVA film for food packaging applications. *International Journal of Biological Macromolecules* **2009,** *45* (4), 372-376.

144. Tan, H.; Ma, R.; Lin, C.; Liu, Z.; Tang, T., Quaternized Chitosan as an Antimicrobial Agent: Antimicrobial Activity, Mechanism of Action and Biomedical Applications in Orthopedics. *International Journal of Molecular Sciences* **2013,** *14* (1), 1854.

145. Mohamed, N. A.; Fahmy, M. M., Synthesis and Antimicrobial Activity of Some Novel Cross-Linked Chitosan Hydrogels. *International Journal of Molecular Sciences* **2012,** *13* (9), 11194.

146. Zhang, D.; Zhou, W.; Wei, B.; Wang, X.; Tang, R.; Nie, J.; Wang, J., Carboxyl-modified poly(vinyl alcohol)-crosslinked chitosan hydrogel films for potential wound dressing. *Carbohydrate Polymers* **2015,** *125*, 189-199.

147. Horikoshi, S.; Serpone, N., *Microwaves in Nanoparticle Synthesis: Fundamentals and Applications*. Wiley: 2013.

148. Srivastava, S., *Understanding bacteria*. Springer Science & Business Media: 2013.

149. Paumier, G. Comparison of various biological assemblies and technological devices. https://commons.wikimedia.org/wiki/File:Biological_and_technological_scales_compared-mk.svg (accessed 13/10/2016).

150. Prabhu, S.; Poulose, E. K., Silver nanoparticles: mechanism of antimicrobial action, synthesis, medical applications, and toxicity effects. *International Nano Letters* **2012,** *2* (1), 32.

151. Kvítek, L.; Panáček, A.; Soukupová, J.; Kolář, M.; Večeřová, R.; Prucek, R.; Holecová, M.; Zbořil, R., Effect of Surfactants and Polymers on Stability and Antibacterial Activity of Silver Nanoparticles (NPs). *The Journal of Physical Chemistry C* **2008,** *112* (15), 5825-5834.

152. Danilczuk, M.; Lund, A.; Sadlo, J.; Yamada, H.; Michalik, J., Conduction electron spin resonance of small silver particles. *Spectrochimica acta. Part A, Molecular and biomolecular spectroscopy* **2006,** *63* (1), 189-91.

153. Matsumura, Y.; Yoshikata, K.; Kunisaki, S.-i.; Tsuchido, T., Mode of Bactericidal Action of Silver Zeolite and Its Comparison with That of Silver Nitrate. *Applied and Environmental Microbiology* **2003,** *69* (7), 4278-4281.

154. Morones, J. R.; Elechiguerra, J. L.; Camacho, A.; Holt, K.; Kouri, J. B.; Ramirez, J. T.; Yacaman, M. J., The bactericidal effect of silver nanoparticles. *Nanotechnology* **2005,** *16* (10), 2346-53.

155. Jin, Y.; Zhao, X., Cytotoxicity of Photoactive Nanoparticles. In *Safety of Nanoparticles: From Manufacturing to Medical Applications*, Webster, T. J., Ed. Springer New York: New York, NY, 2009; pp 19-31.

156. Hussain, S. M.; Hess, K. L.; Gearhart, J. M.; Geiss, K. T.; Schlager, J. J., In vitro toxicity of nanoparticles in BRL 3A rat liver cells. *Toxicology in vitro : an international journal published in association with BIBRA* **2005,** *19* (7), 975-83.

157. Zhou, Y.; Kong, Y.; Kundu, S.; Cirillo, J. D.; Liang, H., Antibacterial activities of gold and silver nanoparticles against Escherichia coli and bacillus Calmette-Guerin. *Journal of nanobiotechnology* **2012,** *10*, 19.

158. Zhang, X., Gold Nanoparticles: Recent Advances in the Biomedical Applications. *Cell biochemistry and biophysics* **2015,** *72* (3), 771-5.

159. Hainfeld, J. F.; Dilmanian, F. A.; Zhong, Z.; Slatkin, D. N.; Kalef-Ezra, J. A.; Smilowitz, H. M., Gold nanoparticles enhance the radiation therapy of a murine squamous cell carcinoma. *Physics in medicine and biology* **2010,** *55* (11), 3045-59.

160. Hainfeld, J. F.; Smilowitz, H. M.; O'Connor, M. J.; Dilmanian, F. A.; Slatkin, D. N., Gold nanoparticle imaging and radiotherapy of brain tumors in mice. *Nanomedicine (London, England)* **2013,** *8* (10), 1601-9.

161. Ojeda, R.; de Paz, J. L.; Barrientos, A. G.; Martín-Lomas, M.; Penadés, S., Preparation of multifunctional glyconanoparticles as a platform for potential carbohydrate-based anticancer vaccines. *Carbohydrate Research* **2007,** *342* (3–4), 448-459.

162. Parry, A. L.; Clemson, N. A.; Ellis, J.; Bernhard, S. S. R.; Davis, B. G.; Cameron, N. R., 'Multicopy Multivalent' Glycopolymer-Stabilized Gold Nanoparticles as Potential Synthetic Cancer Vaccines. *Journal of the American Chemical Society* **2013,** *135* (25), 9362-9365.

163. Feoktistova, M.; Geserick, P.; Leverkus, M., Crystal Violet Assay for Determining Viability of Cultured Cells. *Cold Spring Harbor protocols* **2016,** *2016* (4).

164. O'Toole, G. A., Microtiter dish biofilm formation assay. *Journal of visualized experiments : JoVE* **2011,** (47).

165. Robasky, K.; Lewis, N. E.; Church, G. M., The role of replicates for error mitigation in next-generation sequencing. *Nat Rev Genet* **2014,** *15* (1), 56-62.

166. Blainey, P.; Krzywinski, M.; Altman, N., Points of Significance: Replication. *Nature Methods* **2014,** *11* (9), 879-880.

167. Anitha, A.; Sowmya, S.; Kumar, P. T. S.; Deepthi, S.; Chennazhi, K. P.; Ehrlich, H.; Tsurkan, M.; Jayakumar, R., Chitin and chitosan in selected biomedical applications. *Progress in Polymer Science* **2014,** *39* (9), 1644-1667.

168. Noel, S. P.; Courtney, H. S.; Bumgardner, J. D.; Haggard, W. O., Chitosan sponges to locally deliver amikacin and vancomycin: a pilot in vitro evaluation. *Clinical orthopaedics and related research* **2010,** *468* (8), 2074-80.

169. Lih, E.; Lee, J. S.; Park, K. M.; Park, K. D., Rapidly curable chitosan–PEG hydrogels as tissue adhesives for hemostasis and wound healing. *Acta biomaterialia* **2012,** *8* (9), 3261-3269.

170. Patrulea, V.; Ostafe, V.; Borchard, G.; Jordan, O., Chitosan as a starting material for wound healing applications. *European Journal of Pharmaceutics and Biopharmaceutics* **2015,** *97*, 417-426.

171. Pang, H. T.; Chen, X. G.; Ji, Q. X.; Zhong, D. Y., Preparation and function of composite asymmetric chitosan/CM-chitosan membrane. *Journal of Materials Science: Materials in Medicine* **2008,** *19* (3), 1413-1417.

172. Wound Dressings Market worth 8.46 Billion USD by 2021. Markets and Markets: http://www.marketsandmarkets.com/PressReleases/wound-dressings.asp, 2016

173. Obesity and overweight - Fact sheet. http://www.who.int/mediacentre/factsheets/fs311/en/ (accessed 10/4/17).

174. *Healthy Ireland Survey 2015 - Summary of Findings*; http://health.gov.ie, 2015.

175. *Health in Ireland - Key Trends 2016*; http://health.gov.ie/publications-research/statistics/, 2016.

2. Review paper- Current trends in chitosan-related research in the biomedical field: A short review

This review paper was written in Spring-Summer 2016 as a specific trend was observed when surveying the literature on the antimicrobial properties of chitin and chitosan. A significant deviation was observed with consistently growing interest in chitosan with declining interest in its predecessor, chitin, waning. The short review was written from this point of view, with the top 12 search terms with respect to chitosan on Science Direct being compared. It was accepted for publication in a special issue of Natural Products Communications in November 2016. The authors and their contributions are given below:

Catherine Ryan[1, 2] – Research, production and corrections

Martyn Pemble[1, 2] – Supervision and corrections

Maria Bardosova[1, 3] – Supervision and corrections

[1] Tyndall National Institute, University College Cork, Lee Maltings, Prospect Row, Cork, Ireland

[2]Department of Chemistry, University College Cork, Cork, Ireland

[3]Slovak Technical University in Bratislava (STUBA), Ilkovičova 3, 81219 Bratislava, Slovak Republic

Abstract

Chitosan is a derivative of the naturally-occurring polysaccharide chitin. Both have been extensively studied in the past thirty-five years with an observable increase in interest occurring since the turn of the century, reflected by the increased number of publications based on chitosan research and also the development of international bodies such as the American Journal of Chitin and Chitosan Science (2000-2016)[1] and the European Chitin Society who held their first international conference in 1996[2]. Statistical analysis carried out on the number of publications containing the word 'chitosan' on Science Direct also shows that there has been a dramatic increase in chitosan research in the past 16 years as compared to the years previous; a total of 4613 publications were published between 1940 and 2000 compared to a total of 41295 publications published since then[3]. This review article contains a statistical analysis on the principal search terms related to chitosan on Science Direct over the past ten years, with respect to both growing and declining areas. Although chitosan and its analogues have been proposed and, in some cases, accepted as a material for certain biomedical applications the question is whether there has been sufficient advances in the chemistry and materials science associated with chitosan to be able to clearly identify chitosan as an important material for future applications, from both an industrial and general public perspective. This review article surveys the literature in an attempt to provide an informed answer to this question.

Keywords: chitosan, chitin, biomedical, applications

2.1 Review

Chitin is a naturally occurring polysaccharide which serves as the structural backbone to crustacean exoskeletons and fungal cell walls. Its polysaccharide structure is analogous to the chemical structure of cellulose with the hydroxyl groups in the C2 position replaced by acetamido groups. Chitin has been greatly studied in the biomedical field due to its biocompatibility and abundance in nature. However, there are some drawbacks associated with chitin, the most prominent of which is its insolubility in most solvents. This is due to the presence of the acetamido groups which form very strong intersheet hydrogen bonds in the chitin structure[4]. Due to these solubility problems an acid-soluble derivative of chitin, known as chitosan, has come to the forefront as a valuable substitute for the insoluble polysaccharide. Chitosan is formed by the deacetylation of chitin in the presence of alkali hydroxides such as sodium hydroxide. Importantly, the conversion process doesn't lead to 100% deacetylation. Generally, once the degree of deacetylation exceeds 70% the polysaccharide structure is referred to as chitosan[5]. Following deacetylation, chitosan now contains more amino groups than acetamido groups, these amino groups are highly susceptible to protonation and so chitosan becomes acid-soluble. A very important feature of chitosan is its cationic polyelectrolyte structure. Unlike other naturally charged polysaccharides chitosan's structure contains many positive charges rather than many negative charges e.g. alginates composed of alginic acid are anionic polyelectrolytes[6]. Due to its cationic structure chitosan is a good candidate for selective complexation with negatively charged ligands and chelation to macromolecules such as proteins.

Being naturally abundant, non-toxic and biocompatible chitosan is a potentially valuable commodity in many research fields such as chemistry, biochemistry and biomedicine. Nanoparticles, microparticles, hydrogels and composites are reported in the literature[7]. Chitosan nanoparticles and microparticles are being developed for *in vivo* drug and gene delivery, the ionic gelation technique is commonly employed for both nanoparticle[8] and microparticle[9] fabrication. High surface area and increased mechanical properties are among the attributes of chitosan micro- and nanoparticles. Chitosan hydrogels are often reported in medical and biomedical journals due to their antimicrobial and antifungal activity[10]. This is largely due to the positive charge density of chitosan hydrogels which can chelate to negatively charged ligands, such

as those on the surface of bacteria[11]. Sensitivity towards pH is a feature of chitosan which is present due to the amino groups available for protonation, hence the greater the degree of deacetylation the greater the pH-sensitivity. This phenomenon has been extensively researched for nano- and microparticles along with hydrogels as part of drug-release systems[12]. Chitosan membranes, which are generally prepared by drop-casting of hydrogels, are pH-sensitive but tend to lack in mechanical strength. This can be improved upon by the introduction of cross-linking capabilities[13]. A cross-link in a polymer structure is an interaction which links one polymer chain to another. Cross-linkers such as tetraethylorthosilicate (TEOS) used by Park *et al*. and genipin used by Lien *et al.*[14], serve to enhance the mechanical stability of chitosan membranes[15]. Glutaraldehyde is also commonly used as a cross-linker in hydrogel systems. Rohindra *et al.* conducted a study on chitosan hydrogels cross-linked with glutaraldehyde and reported how the hydrogel structure becomes increasingly "compacted" with increasing cross-linker concentration; while the swelling ability, % free water and glass transition temperature (Tg) decreased[16].

The attributes listed above are among the prominent chitosan-related research topics since the relatively recent increase in interest in the area. The graph in figure 2.1 illustrates the statistic comparison of the number of publications on Science Direct (October 2016) containing the words 'chitosan' and 'chitin' in the past 16 years. The number of chitosan-related searches is growing significantly year by year with a 6-fold increase in the ten-year time frame. On the other hand, the number of chitin related searches is growing at a much slower rate with a 2-3 fold increase over the ten-year period. Results are representative of the development of ease of processing of chitosan compared to chitin; attributed to improved solubility characteristics following the deacetylation process.

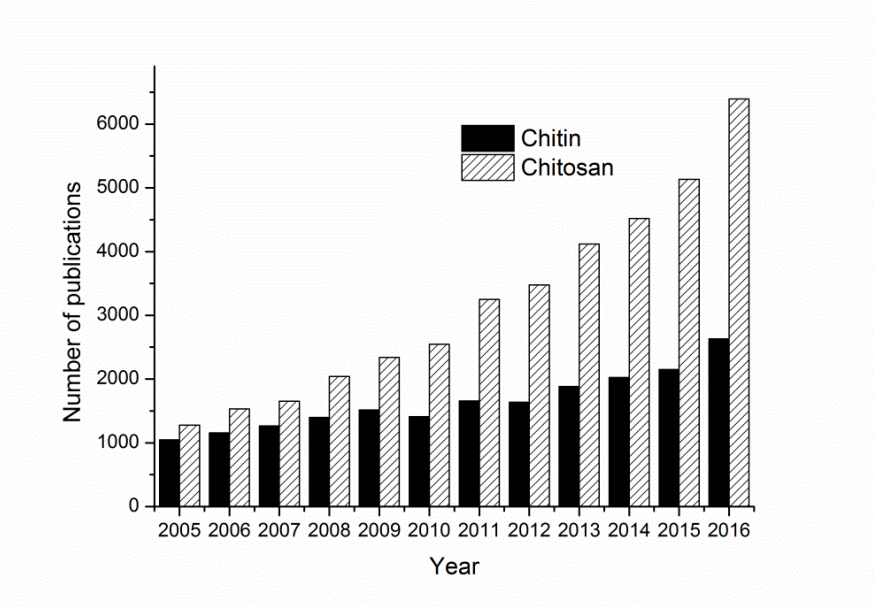

Figure 2.1. Number of publications with ‘chitin’ vs ‘chitosan’ in the title per year on Science Direct.

The top 12 topics in chitosan related searches are listed in Table 2.1 along with the average number of publications a year and the overall percentage increase in the ten-year period. The top two search terms are ‘adsorption’ and ‘cell’, both with an average of 142/ 116 papers per year. ‘Film’ and ‘chitin’ have the lowest values for average number of publications a year; this is further evidence of the decline in chitin-related research. The remaining topics lie within the 40-70 publications a year range, with keywords such as ‘drug’, ‘membrane’ and ‘food’ increasing significantly indicating increased interest in these areas. A representation of all of the data can be seen in table 2.1. The trends and deviations in recent chitosan related research will be studied by looking at some of these thriving, moderately active and currently declining topics.

Current Position	Keyword	Average no. of publications a year	% Increase over 11 year period
1	Adsorption	142	344
2	Cell	116	258
3	Polymer	61	-20
4	Drug	85	610
5	DNA	67	208
6	Membrane	55	210
7	Food	46	647
8	PVA	48	1766
9	Poly	12	-76
10	Drug Delivery	45	334
11	Film	48	975
12	Chitin	23	318

DNA: deoxyribonucleic acid; PVA: polyvinyl alcohol

Table 2.1. Top 12 topics in chitosan related searches on Science Direct.

Of the top two topics ('adsorption' and 'cell'), 'cell' is the more predominantly associated with the biomedical area. The regeneration of tissue and cells is aided by the cyto-compatibility of chitosan and its derivatives. This was demonstrated in a series of studies involving tissue engineering of highly deacetylated chitosan scaffolds with buffalo embryonic stem cells[17, 18]. An in-depth study was initially carried out on the physico-chemical properties of chitosan scaffolds prepared by the freezing and lypophillization of chitosan solution[17]. The relationship between % degree of deacetylation (%DD) and the physico-chemical properties of chitosan scaffolds were studied in-depth with both positive and negative results observed. Water uptake and retention tests showed that the scaffolds had the ability to uptake and store more water than their own weight; this is highly advantageous in the biomedical field e.g. for the transfer of nutrients and metabolites in bodily fluids. Degradation of the chitosan scaffolds in the presence of lysozyme was observed, with rapid degradation and complete loss of the sample within 7 days. However, it was observed that degradation

occurs as a function of %DD with highly deacetylated forms exhibiting lower degradation rates with the possibility of lasting up to a couple of months *in vivo.* As observed in previous studies[19-21], chitosan shows promising results as a potential scaffold for tissue engineering, this is due to large interconnecting pore sizes in the polymer structure allowing for a large volume of cells in a small volume of scaffold. The natural, biocompatible polysaccharide make-up of the scaffold provides ideal conditions for cell attachment and maintenance. The follow-up study[18], looked at the biological response of buffalo embryonic cells to chitosan-gelatin scaffolds. Here the main study was whether the incorporation of gelatin would slow down the degradation of the chitosan scaffold. Although degradation cannot be completely inhibited the lowest degradation profile was observed for the scaffold with the highest concentration of gelatin. The dimensions of the chitosan-gelatin scaffold also allowed for migration of buffalo embryonic stem cells through pores in the scaffold, this was observed by fluorescence microscopy analysis in relation to cell proliferation, penetration and viability.

In recent years, tissue engineering and rejuvenation has been a prominent area in chitosan-related research. The case study described by Thein-Han *et al.* is an example specifically related to buffalo embryonic stem cells. A more broad area is that of musculoskeletal tissue engineering which may include utilizing chitosan for bone, cartilage or muscle regeneration. The promotion of cell proliferation is reported as a characteristic method of action of chitosan in bone tissue regeneration[22-23]. Gümüsdereliog˘lu *et al.* cross-linked chitosan with heparin, which reacts with proteins for enhanced growth, in the formation of a chitosan scaffold for bone tissue engineering[24]. See figure 2.2 below.

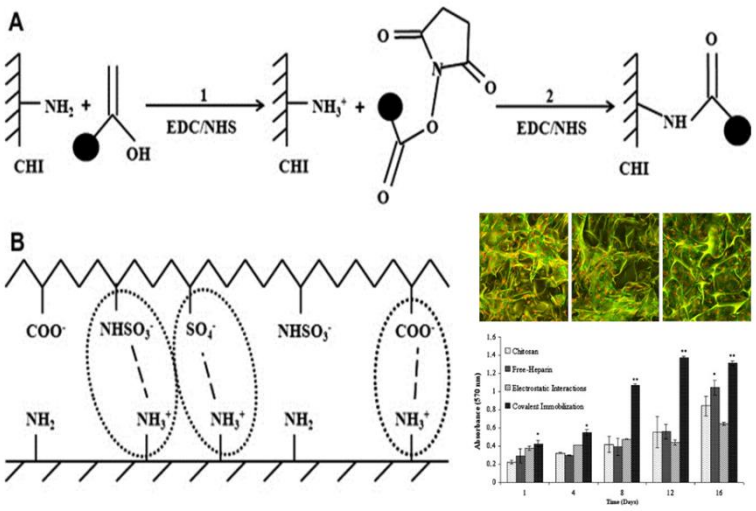

Figure 2.2. Schematic of the covalent and electrostatic immobilization of heparin on chitosan with SEM images and results from bacterial cell attachment assay [24].

Tsai *et al.* also prepared chitosan scaffolds suitable for applications in bone tissue engineering[25], the method involves UV-crosslinking with arginylglycylaspartic acid (RGD), a cell-binding peptide composed of arginine-glycine-aspartic acid. Cell proliferation was enhanced by 50% over a 10-day period with comparison to a control. Pore size and mechanical properties were also enhanced by the RGD-crosslink. In a separate study based on the topic of tissue regeneration chitosan microparticles are proposed as injectable, non-invasive biomaterials for cell immobilization[26]. This is based on previous research which proved chitosan's ability to selectively attach to cells and promote cell growth[27]. Chitosan microparticles functionalized with biotin serve as binding sites for biotinylated antibodies which are suitable as an injectable material for tissue regeneration, the number of antibodies and rate of growth is essentially sped up by chitosan's cell attachment and proliferation effects. The role of chitosan in cell-related mechanisms such as those described is facilitated by its biocompatibility and biodegradability. The amino groups present on the polymer structure serve as sites ideal for chemical bonding with functional groups such as carboxyl groups on antibodies[28].

Another thriving topic in chitosan related-research is related to the keyword 'adsorption'. This is primarily related to non-biomedical applications such as the

selective adhesion to specific molecules and subsequent removal from the associated system[29-30]. One prolific area where chitosan is utilized for its adsorption properties is the specific adsorption of metal ions in a variety of systems. Ramesh *et al.* carried out experiments on the adsorption of Au (III), Pt(IV) and Pd(III) onto a chitosan-glycine cross-linked resin via pH, contact time, concentration and ionic strength studies[31]. FTIR analysis displayed two key changes in bonding; the first was the appearance of a peak at 1601cm^{-1} which signified the cross-linking process. Following the adsorption process this peak at 1601cm^{-1} disappeared and was replaced by a new peak at 1730cm^{-1}. Maximum adsorption occurred at pH 2.0 as electrostatic interactions occur between the cationic chitosan structure and the various chloro-anionic metals, which become negatively charged in the presence of HCl. Results, were sufficient to propose the chitosan-glycine cross-linked resin as a candidate for the removal of the metal ions from aqueous systems such as wastewater. This premise has also been explored in proposed applications of chitosan in the adsorption of ions in biomedical applications[32]. For example the uptake of mercury by sulphated chitosan systems has been explored; this is biomedically relevant as mercury has poisonous and sometimes fatal effects at relatively low dosages with potential sources throughout our ecosystem including air, water, plants and animals[33]. Adsorption studies carried out by Rahbar *et al.* are based on the adsorption of ions in acidic to neutral solution[34]. In their research chitosan–coated magnetite nanoparticles were prepared by combination an aqueous-acidic chitosan solution with a basic solution of ferrous/ ferric chloride, this was followed by magnetic extraction of the chitosan-coated metal nanoparticles. It was concluded that at optimal conditions 99.91% of Hg^{2+} can be adsorbed by the chitosan-coated magnetite nanoparticles, this is supported by both Langmuir and Freundlich adsorption isotherms. In a similar study by Guibal *et al.* a sulphated chitosan network is proposed as a source for the sorption of palladium, this effectively enhances the number of electrostatic interactions as the thiolated chelating groups are available as well as amino groups[35]. This is a further example of how cross-linking and functionalization can enhance the natural attributes of chitosan. Biosorption of metals utilizing chitosan and its derivatives accounts for a significant portion of the 'adsorption' related research[36-37], although predominantly associated with environmental research there is scope for integration into the biomedical area[38-39].

Drug delivery and drug release were regularly proposed as applications of chitosan systems since the growth in research at the turn of the century reflected by highly cited articles from the time[40-41]. However, this has gradually steadied, perhaps due to a lack of potential for growth in the area. This levelling out has occurred along with the growth in research areas described in the previous paragraphs. References from the time report encapsulating drugs in various chitosan based networks with the aim of controlled release of the drug in specific areas of the body, often dependant on pH. Park *et al.* developed a pH-sensitive composite of chitosan and tetraethylorthosilcate, an in-depth study of the swelling ability was carried out with the expected swelling in acidic conditions observed[42]. It was observed that electrostatic interactions between the drug and the network played a big part in drug permeation abilities. In acidic conditions the cationic chitosan network attracted the anionic drug (sodium salicylate) and repelled the cationic drug (lidocaine-HCl), in both of these cases the permeation and diffusivity of the drug was affected by ionic interactions while there was no effect observed for the non-ionic drug (4-acetamidophenol). Steric interactions also played a part with diffusivity results increasing with decreasing molecular size of the drug; with decreasing size in order of lidocaine-HCl > 4-acetamidophenol > sodium salicylate.

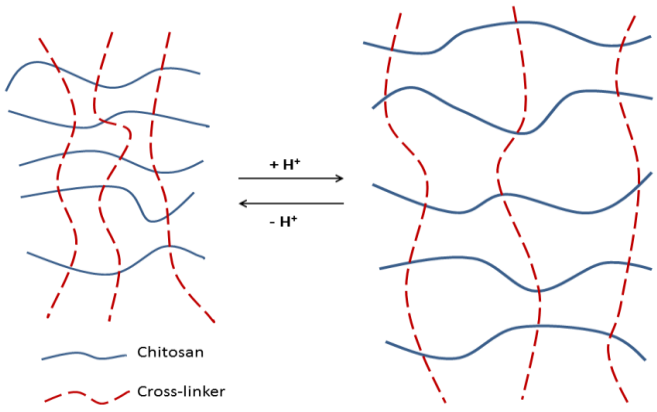

Figure 2.3: The reversible pH-sensitivity of chitosan is illustrated in the schematic. When introduced to acidic conditions the chitosan part of the cross-linked network will swell, leading to an overall swollen state.

Chitosan's pH-sensitivity is regularly taken advantage of when it comes to the topic of controlled drug release. Wu *et. al* developed a hybrid nanosystem composed of a

crosslinked chitosan-PMAA network and CdSe quantum dots[43]. Both chitosan and PMAA provide pH-sensitive functionality for specific areas of the body while the CdSe quantum dots provide bioimaging functionality due to their interesting optical properties. The bioimaging functionality of CdSe and other quantum dot entities is due to a long fluorescence lifetime and photostability, making them ideal candidates for fluorescence imaging at shorter wavelengths[44-45]. Results display the formation of a single multifunctional nanosystem with the functionality of optical pH-sensing, cellular image stability, regulated drug delivery and low cytotoxicity. pH-sensitivity in the range of pH 2-10 analysed in conjunction with photoluminescence shows that the change in pH can be monitored by the presence of fluorescent CdSe quantum nanodots. Scanning confocal fluorescence imaging of the tumour cells shows successful staining of the hybrid nanogels. Zhang *et. al* developed a Schiff-base cross-linked network of chitosan and polyethylene glycol[46]. The network is a candidate for *in vivo* controlled release as it is sensitive to biochemical stimuli and can be broken down by certain enzymes in the body providing a transport and release mechanism. This has been successfully demonstrated with molecules such as rhodamine B and lysozyme e.g. studies on the release of rhodamine B from the chitosan-PEG network show that after two and a half hours there was a 52% release of the molecule in water, 59% release of the molecule in lysozyme and 99% release of the molecule in papain, an enzyme which breaks down the chitosan network.

As seen in the previously mentioned articles the pH range for drug release is generally quite broad, in some cases the drug release mechanisms are simply carried out in neutral aqueous conditions[47]. Although this is relevant to some biological conditions there are isolated areas of the body which may have unique pH conditions[48-49], it also reduces the specificity of targeting and releasing the drug in the correct site. The ability for a chitosan network to release drugs at a specific site according to a narrow pH range was carried out by Chen *et. al*[50]. Controlled release of ibuprofen in the pH range of 6.8-7.4 was studied in order to investigate the drug release profile for tumour or inflamed conditions (pH 6.8) compared to that of normal tissue (pH 7.4). Silica nanoparticles loaded with the drug were initially investigated with release of about 90% after 24 hours in both conditions of pH 6.8 and 7.4. However, when the silica nanoparticles were encapsulated in chitosan the specificity vastly improved with 35% release at pH 7.4 and 65% release at pH 6.8. The phenomenon occurs because at pH

7.4 the chitosan chains are orientated in an orthorhombic unit-cell which has a rigid structure, while at pH 6.8 this changes to a gel-like state due to the reduced influence of hydrogen-bonding.

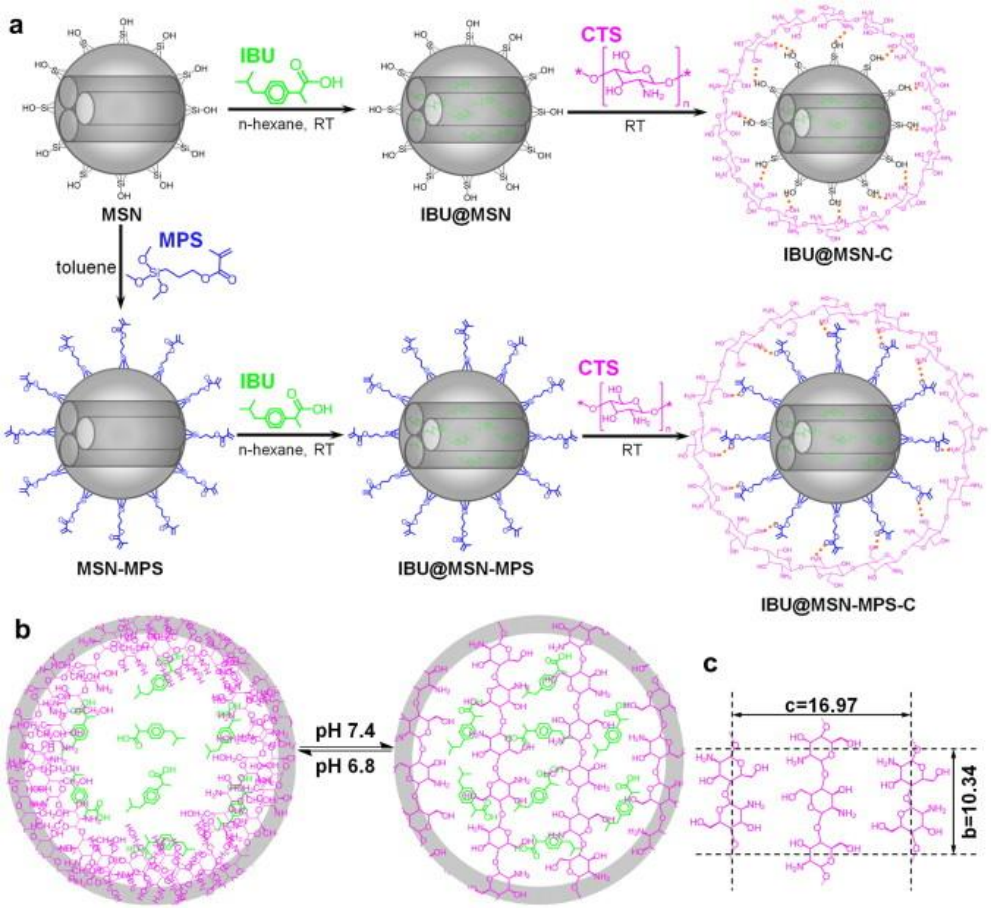

Figure 2.4. Part (a) of the schematic illustrates the fabrication route of ibuprofen loaded chitosan-mesoporous silica nanoparticles, part (b) The release mechanism of ibuprofen and part (c) the structure in hydrated form at pH 7.4[50].

In contrast to the previously mentioned highly-cited keywords which are explicitly related to the biomedical field (cell, drug, drug delivery, DNA, membrane) the keyword ‘film’ which is moderately searched for seems to have relevance in the biomedical field but more so in relation to essential analysis on the structural and chemical properties of chitosan films prior to application stage. This is an invaluable area of any research as the characterization and preparation of all materials must be studied in-depth prior to any application developments or proposals. Chitosan films are predominantly utilized for their antimicrobial properties due to their

biocompatibility and ability to form chemically cross-linked networks with other chemical entities, for improvements in either structural or antimicrobial behaviour, or both. In 2002, Tanabe *et al.* reported the synthesis of chitosan-keratin-glycerol composite films of varying concentration formed by the very common aqueous acid casting method[51]. The originally brittle keratin becomes mechanically stronger when cross-linked with chitosan with an improvement in water stability also observed. The Young's modulus is seen to increase up to 310 MPa as the chitosan content increases. However, the addition of glycerol reduces the Young's modulus while increasing the flexibility of the composite film, this was seen in the results for elongation of a composite film containing 20 weight percent glycerol which displayed 28 ± 9% elongation and reduced Young's modulus of 11 MPa. These results suggest that the mechanical properties can be tailored by varying the chitosan/ keratin/ glycerol concentrations in the films. Antibacterial activity was reduced in the presence of the films due to the formation of strong ionic bonds between cationic amino groups on the chitosan structure and anionic bacterial cell walls. Promising results display up to 82% reduction of bacteria with increasing concentration of chitosan in the films. Around the time of publication of this particular paper the chelating ability of chitosan film's cationic amino groups had been regularly taken advantage of in a range of applications including metal adsorption and antimicrobial activity[52-54].

In similar work[55] chitosan-nanocomposite films were prepared by the casting method – using two montmorillonite nano-structures and two nano-silver structures. The films are described as being 'flexible and free-standing' with the nanostructures evenly dispersed throughout all except those containing Ag ions. While the XRD patterns of all nanocomposite films showed shifts due to intercalation it was interesting to see the Ag-ion shifted from crystalline to amorphous, again indicating a disturbed chitosan polymer structure. Despite these results it is the Ag-ion loaded film which displayed the best tensile strength values of 38 MPa with lowest percentage elongation of 38.9% due to reduced flexibility, in comparison the neat chitosan film displayed a tensile strength of 32.9 MPa and 54.6% elongation. The greatest flexibility was observed with Cloisite-B loaded nanocomposite film with a percentage elongation of 66%. The Ag-ion loaded chitosan film also displayed the best antimicrobial activity, this is attributed to Ag-ion nanoparticles' ability to chelate to negatively charged bacterial cell walls and modify bacterial DNA which essentially leads to bacterial cell death[56-58]. Nguyen

et al. prepared chitosan composite films cross-linked with poly (vinyl alcohol) (PVA), the films were again prepared by the drop-casting method with subsequent UV irradiation[59]. The acrylic acid concentration and the UV-irradiation time were varied and analysed with significant differences in the results observed; the non-cross-linked chitosan structure displayed greater water adsorption with a swelling ratio of 700% in DI water, however no pH-sensitivity was observed. SEM analysis showed the chitosan films containing PVA had an interlinked porous structure which is more desirable in the fabrication of a high surface area, porous wound-dressing material. The PVA-containing film displayed the opposite effects to bare chitosan with low swelling ratio in DI water (<300%) and clear pH-dependency with greater degree of swelling in basic conditions due to repulsion between anionic carboxylate groups in the PVA structure. This is in contrast to the majority of biomedical pH-sensitive chitosan networks which generally swell in acidic conditions due to charged amino groups in the chitosan structure[60-62].

Upon study of the prolific keywords associated with chitosan and the biomedical area it appears that 'chitin' is on the decline in both the frequency of publication and novel research proposals. In fact, it most commonly appears alongside its deacetylated derivative as 'chitin and chitosan' suggesting that the research is limited in relation to chitin alone[63-64]. This is because compared to chitosan; chitin is a much more rigid, unreactive material leading to its insolubility in solvents and limited applications. While chitosan is utilized for its flexibility, ability to cross-link, porosity, pH-sensitivity and antimicrobial activity among other characteristics, chitin is more limited. One prominent area of research is linked to naturally occurring chitin structures (such as exoskeletons) and the interesting optical properties associated with these, however in relation to the biomedical field there seems to be very little that chitin can offer on its own.

The optical properties of chitin structures were studied by Azofeifa *et al.* predominantly in relation to structural colour in naturally-occurring biopolymer structures[65-66]. Previous research was centred on determining the refractive index of shrimp-shell chitin and to determine in which part of the spectrum the associated bands lie with reflections observed in the UV-VIS region between 400 and 700nm. In more recent work the optical properties of the exoskeleton of scarab beetles were analysed optically, revealing a broad band throughout the visible region from 525 to 950nm.

This is a broad area of research with the optical properties depending on the dimensionality, size and structure of the chitin network. Chitin is an important material in the area of biomimetics as it is a natural source of polysaccharide, compared to deacetylated chitin. Nanofibrous chitin/ silk blends have been prepared by self-assembly in solution in an attempt to mimic natural materials such as those found in crustacean and plant exoskeletons. The interest lies in mimicking characteristics properties such as hardness and tensile strength for mechanical applications. Jin *et al.* prepared a β-chitin/silk composite which owes its mechanical strength to strong interatomic hydrogen-bonding[67]. Varying the chitin/ silk ratio resulted in a chitin concentration-dependant elastic modulus. Park *et al.* also employed silk in the formation of a biomimetic nanofibrous blend with chitin[68]. The electrospun blends were characterized and analysed with regard to their biofunctionality as a possible candidate for tissue engineering. The aim was to mimic extra cellular protein matrices with chitin providing an ideal candidate for structural and biofunctional requirements. Water uptake, viscosity and conductivity increase with chitin content owing to the high polarity of the polysaccharide structure which is porous and hydrophilic. Cellular attachment of human epidermal keratinocytes and fibroblasts was best with a 75:25 chitin: silk composition, this composition also revealed the structure most similar to the desired extracellular matrix model explaining the good cell attachment results.

Despite the biomimetic interest and biodegradability, chitin is still limited in a processing sense due to solubility limitations and little further development has been made on the 'chitin' topics discussed. There are a significantly lower number of citations on articles such as those discussed compared to 'chitosan' related articles on the same topic. The dominating problem with chitin is its insolubility and the characteristic which separates it from chitosan is the degree of acetylation. Chitin is converted to chitosan with increasing degree of deacetylation – the greater the degree of deacetylation the purer form of chitosan and the greater processing ability [4-5, 69]. As stated by Anitha *et al.* – 'the properties of (chitosan) such as solubility, viscosity and biocompatibility are inversely proportional to degree of acetylation'[70].

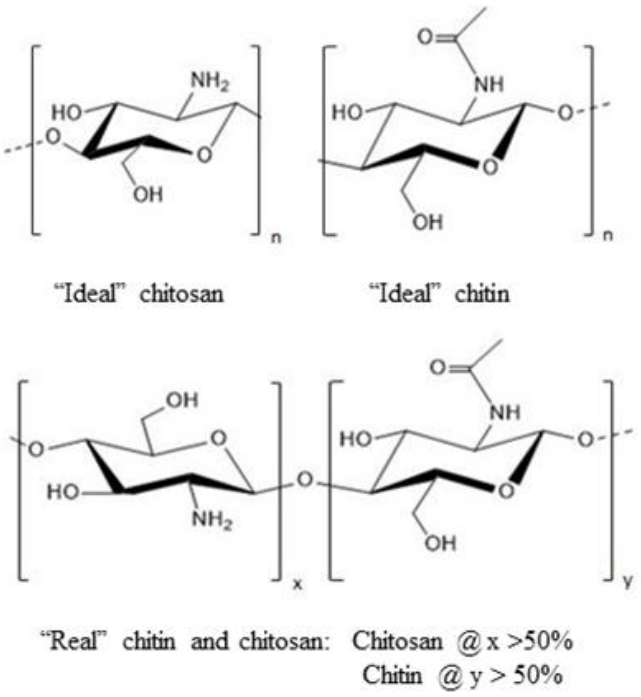

Figure 2.5. "Ideal" chitin versus "ideal chitosan" and the relative percentages in the "real" structures.

Upon consideration of the literature it appears that over the past ten years the scope of chitosan-related research has narrowed towards the biomedical field with a gradual decline of investigative research on the physical and chemical properties of the polymer structure. This biomedical lead can be attributed to the successful results and proof of concepts related to drug delivery, wound dressing and tissue engineering – it has become clear that chitosan is an ideal candidate and perhaps further investigation into the structural properties is no longer required – except for novel composite structures. Chitosan-related biomedical patents range from topics such as manufacturing and methods, water treatment, nanocomposites and a broad range of biomedically-related topics such as wound dressings and antimicrobial hydrogels. Chitin-related patents are based on the same topics as chitosan-related patents but, as expected, the overall number is lower for chitin compared to chitosan. According to freshpatents.com, at the time of writing a relatively new patents and technology website, there have been 24 new chitosan patents since the start of 2016 compared to 7 new chitin patents[71]. This indicates that chitosan is a valuable commodity not only in relation to early-stage research but also at the grand scale in terms of patent

processing and the development of commercially available biomedical products. On the other hand, the status of its predecessor, chitin, is on a gradual decline.

References

1. Journal of Chitin and Chitosan Science. http://www.aspbs.com/jcc.htm (accessed 15th of January).

2. European Chitin Society. http://www.euchis.org/ (accessed 15th of January).

3. Science Direct. http://www.sciencedirect.com/science?_ob=ArticleListURL&_method=list&_ArticleListID=-923209334&_sort=r&_st=13&view=c&md5=baae3c439502a72f82ca561ff2f2d54d&searchtype=a (accessed 15th of January).

4. Pillai, C.; Paul, W.; Sharma, C. P., Chitin and chitosan polymers: Chemistry, solubility and fiber formation. *Progress in Polymer Science* **2009,** *34* (7), 641-678.

5. Goosen, M. F., *Applications of Chitin and Chitosan*. CRC Press: 1996.

6. George, M.; Abraham, T. E., Polyionic hydrocolloids for the intestinal delivery of protein drugs: Alginate and chitosan — a review. *Journal of Controlled Release* **2006,** *114* (1), 1-14.

7. Shukla, S. K.; Mishra, A. K.; Arotiba, O. A.; Mamba, B. B., Chitosan-based nanomaterials: A state-of-the-art review. *International journal of biological macromolecules* **2013,** *59*, 46-58.

8. Fan, W.; Yan, W.; Xu, Z.; Ni, H., Formation mechanism of monodisperse, low molecular weight chitosan nanoparticles by ionic gelation technique. *Colloids and Surfaces B: Biointerfaces* **2012,** *90*, 21-27.

9. Ko, J.; Park, H.; Hwang, S.; Park, J.; Lee, J., Preparation and characterization of chitosan microparticles intended for controlled drug delivery. *International journal of pharmaceutics* **2002,** *249* (1), 165-174.

10. Qian, T. S., Haijia; Tan, Tianwei., The bactericidal and mildew-proof activity of a TiO_2-chitosan composite. *Journal of Photochemistry and Photobiology A: Chemistry* **2011,** (218), 130-136.

11. Kong, M.; Chen, X. G.; Xing, K.; Park, H. J., Antimicrobial properties of chitosan and mode of action: a state of the art review. *International journal of food microbiology* **2010,** *144* (1), 51-63.

12. Qu, X.; Wirsen, A.; Albertsson, A.-C., Novel pH-sensitive chitosan hydrogels: swelling behavior and states of water. *Polymer* **2000,** *41* (12), 4589-4598.

13. Dash, M.; Chiellini, F.; Ottenbrite, R.; Chiellini, E., Chitosan—A versatile semi-synthetic polymer in biomedical applications. *Progress in Polymer Science* **2011,** *36* (8), 981-1014.

14. Lien, S.-M.; Li, W.-T.; Huang, T.-J., Genipin-crosslinked gelatin scaffolds for articular cartilage tissue engineering with a novel crosslinking method. *Materials Science and Engineering: C* **2008,** *28* (1), 36-43.

15. Park, S.-B.; You, J.-O.; Park, H.-Y.; Haam, S. J.; Kim, W.-S., A novel pH-sensitive membrane from chitosan—TEOS IPN; preparation and its drug permeation characteristics. *Biomaterials* **2001,** *22* (4), 323-330.

16. Rohindra, D. R.; Nand, A. V.; Khurma, J. R., Swelling properties of chitosan hydrogels. *The South Pacific Journal of Natural and Applied Sciences* **2004,** *22* (1), 32-35.

17. Thein-Han, W. W.; Kitiyanant, Y., Chitosan scaffolds for in vitro buffalo embryonic stem-like cell culture: An approach to tissue engineering. *Journal of Biomedical Materials Research Part B: Applied Biomaterials* **2007,** *80B* (1), 92-101.

18. Thein-Han, W. W.; Saikhun, J.; Pholpramoo, C.; Misra, R. D. K.; Kitiyanant, Y., Chitosan–gelatin scaffolds for tissue engineering: Physico-chemical properties and biological response of buffalo embryonic stem cells and transfectant of GFP–buffalo embryonic stem cells. *Acta Biomaterialia* **2009,** *5* (9), 3453-3466.

19. Shanmugasundaram, N.; Ravichandran, P.; Neelakanta Reddy, P.; Ramamurty, N.; Pal, S.; Panduranga Rao, K., Collagen–chitosan polymeric scaffolds for the in vitro culture of human epidermoid carcinoma cells. *Biomaterials* **2001,** *22* (14), 1943-1951.

20. Li, Z.; Ramay, H. R.; Hauch, K. D.; Xiao, D.; Zhang, M., Chitosan–alginate hybrid scaffolds for bone tissue engineering. *Biomaterials* **2005,** *26* (18), 3919-3928.

21. Puppi, D.; Chiellini, F.; Piras, A.; Chiellini, E., Polymeric materials for bone and cartilage repair. *Progress in Polymer Science* **2010,** *35* (4), 403-440.

22. Mori, T.; Okumura, M.; Matsuura, M.; Ueno, K.; Tokura, S.; Okamoto, Y.; Minami, S.; Fujinaga, T., Effects of chitin and its derivatives on the proliferation and cytokine production of fibroblasts in vitro. *Biomaterials* **1997,** *18* (13), 947-951.

23. Depan, D.; Kumar, A. P.; Singh, R. P., Cell proliferation and controlled drug release studies of nanohybrids based on chitosan-g-lactic acid and montmorillonite. *Acta Biomaterialia* **2009,** *5* (1), 93-100.

24. Gümüşderelioğlu, M.; Aday, S., Heparin-functionalized chitosan scaffolds for bone tissue engineering. *Carbohydrate Research* **2011,** *346* (5), 606-613.

25. Tsai, W.-B.; Chen, Y.-R.; Liu, H.-L.; Lai, J.-Y., Fabrication of UV-crosslinked chitosan scaffolds with conjugation of RGD peptides for bone tissue engineering. *Carbohydrate Polymers* **2011,** *85* (1), 129-137.

26. Custódio, C. A.; Cerqueira, M. T.; Marques, A. P.; Reis, R. L.; Mano, J. F., Cell selective chitosan microparticles as injectable cell carriers for tissue regeneration. *Biomaterials* **2015,** *43*, 23-31.

27. Custodio, C. A.; Frias, A. M.; del Campo, A.; Reis, R. L.; Mano, J. F., Selective cell recruitment and spatially controlled cell attachment on instructive chitosan surfaces functionalized with antibodies. *Biointerphases* **2012,** *7* (1-4), 65.

28. Custódio, C. A.; Santo, V. E.; Oliveira, M. B.; Gomes, M. E.; Reis, R. L.; Mano, J. F., Functionalized Microparticles Producing Scaffolds in Combination with Cells. *Advanced Functional Materials* **2014,** *24* (10), 1391-1400.

29. Juang, R. S.; Tseng, R. L.; Wu, F. C.; Lin, S. J., Use of chitin and chitosan in lobster shell wastes for color removal from aqueous solutions. *Journal of Environmental Science & Health Part A* **1996,** *31* (2), 325-338.

30. Rangel-Mendez, J.; Monroy-Zepeda, R.; Leyva-Ramos, E.; Diaz-Flores, P.; Shirai, K., Chitosan selectivity for removing cadmium (II), copper (II), and lead (II) from aqueous phase: pH and organic matter effect. *Journal of hazardous materials* **2009,** *162* (1), 503-511.

31. Ramesh, A.; Hasegawa, H.; Sugimoto, W.; Maki, T.; Ueda, K., Adsorption of gold(III), platinum(IV) and palladium(II) onto glycine modified crosslinked chitosan resin. *Bioresource Technology* **2008,** *99* (9), 3801-3809.

32. Jayakumar, R.; Nwe, N.; Tokura, S.; Tamura, H., Sulfated chitin and chitosan as novel biomaterials. *International Journal of Biological Macromolecules* **2007,** *40* (3), 175-181.

33. Zahir, F.; Rizwi, S. J.; Haq, S. K.; Khan, R. H., Low dose mercury toxicity and human health. *Environmental Toxicology and Pharmacology* **2005,** *20* (2), 351-360.

34. Rahbar, N.; Jahangiri, A.; Boumi, S.; Khodayar, M. J., Mercury Removal From Aqueous Solutions With Chitosan-Coated Magnetite Nanoparticles Optimized Using the Box-Behnken Design. *Jundishapur Journal of Natural Pharmaceutical Products* **2014,** *9* (2), e15913.

35. Guibal, E.; Von Offenberg Sweeney, N.; Vincent, T.; Tobin, J. M., Sulfur derivatives of chitosan for palladium sorption. *Reactive and Functional Polymers* **2002,** *50* (2), 149-163.

36. Dodson, J. R.; Parker, H. L.; García, A. M.; Hicken, A.; Asemave, K.; Farmer, T. J.; He, H.; Clark, J. H.; Hunt, A. J., Bio-derived materials as a green route for precious & critical metal recovery and re-use. *Green Chemistry* **2015,** *17* (4), 1951-1965.

37. Wang, L.; Xing, R.; Liu, S.; Cai, S.; Yu, H.; Feng, J.; Li, R.; Li, P., Synthesis and evaluation of a thiourea-modified chitosan derivative applied for adsorption of Hg(II) from synthetic wastewater. *International Journal of Biological Macromolecules* **2010,** *46* (5), 524-528.

38. Alves, N. M.; Mano, J. F., Chitosan derivatives obtained by chemical modifications for biomedical and environmental applications. *International Journal of Biological Macromolecules* **2008,** *43* (5), 401-414.

39. Elkholy, S. S.; Salem, H. A.; Eweis, M.; Elsabee, M. Z., Synthesis and characterization of some acyl thiourea derivatives of chitosan and their biocidal activities. *International Journal of Biological Macromolecules* **2014,** *70*, 199-207.

40. Agnihotri, S. A.; Mallikarjuna, N. N.; Aminabhavi, T. M., Recent advances on chitosan-based micro- and nanoparticles in drug delivery. *Journal of Controlled Release* **2004,** *100* (1), 5-28.

41. Hejazi, R.; Amiji, M., Chitosan-based gastrointestinal delivery systems. *Journal of Controlled Release* **2003,** *89* (2), 151-165.

42. Park, S.-B.; You, J.-O.; Park, H.-Y.; Haam, S. J.; Kim, W.-S., A novel pH-sensitive membrane from chitosan — TEOS IPN; preparation and its drug permeation characteristics. *Biomaterials* **2001,** *22* (4), 323-330.

43. Wu, W.; Shen, J.; Banerjee, P.; Zhou, S., Chitosan-based responsive hybrid nanogels for integration of optical pH-sensing, tumor cell imaging and controlled drug delivery. *Biomaterials* **2010,** *31* (32), 8371-8381.

44. Bardelang, D.; Zaman, M.; Moudrakovski, I. L.; Pawsey, S.; Margeson, J. C.; Wang, D.; Wu, X.; Ripmeester, J. A.; Ratcliffe, C. I.; Yu, K., Interfacing supramolecular gels and quantum dots with ultrasound: smart photoluminescent dipeptide gels. *Advanced materials* **2008,** *20* (23), 4517-4520.

45. Michalet, X.; Pinaud, F. F.; Bentolila, L. A.; Tsay, J. M.; Doose, S.; Li, J. J.; Sundaresan, G.; Wu, A. M.; Gambhir, S. S.; Weiss, S., Quantum Dots for Live Cells, in Vivo Imaging, and Diagnostics. *Science (New York, N.Y.)* **2005,** *307* (5709), 538-544.

46. Zhang, Y.; Tao, L.; Li, S.; Wei, Y., Synthesis of Multiresponsive and Dynamic Chitosan-Based Hydrogels for Controlled Release of Bioactive Molecules. *Biomacromolecules* **2011,** *12* (8), 2894-2901.

47. Santos, D.; Neto, C.; Fonseca, J.; Pereira, M., Chitosan macroporous asymmetric membranes—Preparation, characterization and transport of drugs. *Journal of Membrane Science* **2008,** *325* (1), 362-370.

48. Helmlinger, G.; Yuan, F.; Dellian, M.; Jain, R. K., Interstitial pH and pO2 gradients in solid tumors in vivo: high-resolution measurements reveal a lack of correlation. *Nature medicine* **1997,** *3* (2), 177-82.

49. Yoshida, M.; Asano, M.; Suwa, T.; Katakai, R., Thermo- and pH-responsive gels for application in colon delivery systems. *Radiation Physics and Chemistry* **1999,** *55* (5–6), 677-680.

50. Chen, F.; Zhu, Y., Chitosan enclosed mesoporous silica nanoparticles as drug nano-carriers: sensitive response to the narrow pH range. *Microporous and Mesoporous Materials* **2012,** *150*, 83-89.

51. Tanabe, T.; Okitsu, N.; Tachibana, A.; Yamauchi, K., Preparation and characterization of keratin–chitosan composite film. *Biomaterials* **2002,** *23* (3), 817-825.

52. Wang, X.; Du, Y.; Liu, H., Preparation, characterization and antimicrobial activity of chitosan–Zn complex. *Carbohydrate Polymers* **2004,** *56* (1), 21-26.

53. Wang, X.; Du, Y.; Fan, L.; Liu, H.; Hu, Y., Chitosan- metal complexes as antimicrobial agent: Synthesis, characterization and Structure-activity study. *Polymer Bulletin* **2005,** *55* (1), 105-113.

54. Yang, Z.; Shu, J.; Liu, L., Enhanced phytoremediation of lead-contaminated soils by chitosan chelating agent. *Journal of Agro-Environment Science* **2006,** *25* (1), 86-89.

55. Rhim, J.-W.; Hong, S.-I.; Park, H.-M.; Ng, P. K. W., Preparation and Characterization of Chitosan-Based Nanocomposite Films with Antimicrobial Activity. *Journal of Agricultural and Food Chemistry* **2006,** *54* (16), 5814-5822.

56. Kim, J. S.; Kuk, E.; Yu, K. N.; Kim, J.-H.; Park, S. J.; Lee, H. J.; Kim, S. H.; Park, Y. K.; Park, Y. H.; Hwang, C.-Y., Antimicrobial effects of silver nanoparticles. *Nanomedicine: Nanotechnology, Biology and Medicine* **2007,** *3* (1), 95-101.

57. Sharma, V. K.; Yngard, R. A.; Lin, Y., Silver nanoparticles: green synthesis and their antimicrobial activities. *Advances in colloid and interface science* **2009,** *145* (1), 83-96.

58. Rai, M.; Yadav, A.; Gade, A., Silver nanoparticles as a new generation of antimicrobials. *Biotechnology advances* **2009,** *27* (1), 76-83.

59. Nguyen, N.-T.; Liu, J.-H., Fabrication and characterization of poly (vinyl alcohol)/chitosan hydrogel thin films via UV irradiation. *European Polymer Journal* **2013,** *49* (12), 4201-4211.

60. Chen, Y.-C.; Ho, H.-O.; Lee, T.-Y.; Sheu, M.-T., Physical characterizations and sustained release profiling of gastroretentive drug delivery systems with improved floating and swelling capabilities. *International Journal of Pharmaceutics* **2013,** *441* (1–2), 162-169.

61. Mukhopadhyay, P.; Sarkar, K.; Chakraborty, M.; Bhattacharya, S.; Mishra, R.; Kundu, P. P., Oral insulin delivery by self-assembled chitosan nanoparticles: In vitro and in vivo studies in diabetic animal model. *Materials Science and Engineering: C* **2013,** *33* (1), 376-382.

62. Barros, S.; da Silva, A.; Costa, D.; Cesarino, I.; Costa, C.; Lanceros-Méndez, S.; Pawlicka, A.; Silva, M., Thermo-sensitive chitosan–cellulose derivative hydrogels: swelling behaviour and morphologic studies. *Cellulose* **2014,** *21* (6), 4531-4544.

63. Tomihata, K.; Ikada, Y., In vitro and in vivo degradation of films of chitin and its deacetylated derivatives. *Biomaterials* **1997,** *18* (7), 567-575.

64. Khor, E.; Lim, L. Y., Implantable applications of chitin and chitosan. *Biomaterials* **2003,** *24* (13), 2339-2349.

65. Azofeifa, D. E.; Arguedas, H. J.; Vargas, W. E., Optical properties of chitin and chitosan biopolymers with application to structural color analysis. *Optical Materials* **2012,** *35* (2), 175-183.

66. Azofeifa, D. E.; Hernández-Jiménez, M.; Libby, E.; Solís, A.; Barboza-Aguilar, C.; Vargas, W. E., A quantitative assessment approach of feasible optical mechanisms contributing to structural color of golden-like Chrysina aurigans scarab beetles. *Journal of Quantitative Spectroscopy and Radiative Transfer* **2015,** *160*, 63-74.

67. Jin, J.; Hassanzadeh, P.; Perotto, G.; Sun, W.; Brenckle, M. A.; Kaplan, D.; Omenetto, F. G.; Rolandi, M., A Biomimetic Composite from Solution Self-Assembly of Chitin Nanofibers in a Silk Fibroin Matrix. *Advanced Materials* **2013,** *25* (32), 4482-4487.

68. Park, K. E.; Jung, S. Y.; Lee, S. J.; Min, B.-M.; Park, W. H., Biomimetic nanofibrous scaffolds: preparation and characterization of chitin/silk fibroin blend nanofibers. *International journal of biological macromolecules* **2006,** *38* (3), 165-173.

69. Kumirska, J.; Weinhold, M. X.; Czerwicka, M.; Kaczyński, Z.; Bychowska, A.; Brzozowski, K.; Thöming, J.; Stepnowski, P., Influence of the chemical structure and physicochemical properties of chitin-and chitosan-based materials on their biomedical activity. *Biomedical Engineering, Trends in Materials Science* **2011**, 25-64.

70. Anitha, A.; Sowmya, S.; Kumar, P. T. S.; Deepthi, S.; Chennazhi, K. P.; Ehrlich, H.; Tsurkan, M.; Jayakumar, R., Chitin and chitosan in selected biomedical applications. *Progress in Polymer Science* **2014,** *39* (9), 1644-1667.

71. FP2.0 Fresh Patents - New Patents and Technology. http://www.freshpatents.com/ (accessed 07/04/2016).

3. Materials and methods

3.1 Introduction

This chapter provides an overview of the experimental procedures carried out during the various studies outlined in this thesis. The main experimental procedures include photonic crystal synthesis, hydrogel preparation, thin film formation and immobilization of hydrogels on hydrophilic substrates. The analysis techniques employed to analyse the various samples are also described. They fall into the categories of spectroscopy, microscopy, swelling studies, mechanical studies and antimicrobial analysis. Deviations in the experimental procedures described in this chapter are described in the individual chapters concerned, which for the most part appear in scientific paper format.

3.2 Chitosan and Chi-TEOS IPN Materials

3.2.1 Chemical Properties of Chitosan Samples

Chitosan FTIR spectra were recorded with a Thermo Nicolet Nexus 470s Spectrophotometer. The ^{1}H NMR spectra were measured with a Bruker Avance III Spectrometer at 70 °C. The samples were solubilized in a D_2O/HCl solvent with a concentration of 9 mg/mL. The average degree of acetylation (DA) for chitosan was calculated from the ratio between the signal intensity for the hydrogens in CH_3 and the intensity for the hydrogens bonded to C2 of the glucopyranose ring. The viscosimetric molecular weight was calculated using the Mark-Houwink equation[1] (measured in triplicate), using α and K values taken from the literature[2-3], as they depend on the degree of acetylation of the samples. LMW- and MMWChi were purchased from Sigma-Aldrich, Ireland and HMWChi was purchased from Galena, Brazil. Analysis of chemical properties was carried out on the untreated powder samples in the Instituto de Física de São Carlos, Universidade de São Paulo, São Carlos, Brazil.

3.2.2 Synthesis of Chi-TEOS IPN Hydrogels

Both the chitosan networks and the interpenetrating polymer networks (IPNs) were formed by a cationic solution polymerization technique in mildly acidic solution, water being the primary solvent. Milli-Q water with a resistivity of 18.2 MΩcm was used throughout all experiments. Chitosan hydrogel synthesis simply involved

preparation of the first solution (see below) and allowing it to stir for 24 hours. Chi-TEOS IPN formation involved more steps - initially three separate solutions were prepared and allowed to stir at room temperature:

1) 1.04 g chitosan, 65 mL H_2O and 1 wt% CH_3COOH

2) 1.04 g TEOS and 15 mL EtOH

3) 25 mL H_2O, 10 mL EtOH and 0.1 wt% conc. HCl

Solution 3 was slowly added to solution 2 with stirring. The resulting mixture and solution 1 were left under continuous stirring at room temperature for 24 hours. After 24 hours, the aqueous chitosan solution was slowly added to the TEOS solution under continuous stirring and this final solution was left to stir for a further 48 hours.

The method described results in a 1:1 Chi-TEOS IPN. Changing the ratio to 1:2/1:3 simply involves doubling/tripling the quantity of TEOS used. For the purpose of our experiments the three following types of chitosan were used in preparing the 1:1 Chi-TEOS IPNs: low molecular weight (LMWChi), medium molecular weight (MMWChi) and high molecular weight (HMWChi). 1:1, 1:2 and 1:3 IPNs were prepared employing LMWChi.

3.2.3 Synthesis of Chi-TEOS IPN Membranes

The desired amount of Chi-TEOS IPN was carefully drop-casted onto the substrate of choice using a plastic dropper. The substrate bearing the Chi-TEOS IPN was placed on a level surface in an enclosed oven at 40 °C. Depending on the size of the membrane, formation and drying took anywhere between a couple of hours to a couple of days. Upon completion, the membrane could easily be peeled off the substrate surface. IPNs were typically prepared using round substrates such as petri dishes, because when the hydrogels are drop-cast onto a substrate they automatically form and dry in a circular shape. Small membranes were employed for swelling studies; multiple samples of 1 mL of IPN were drop-cast onto a petri dish and allowed to dry for two hours at 40 °C. For large samples, 13 mL of IPN hydrogel was drop-cast onto a 90 mm petri-dish and allowed to dry at 40 °C for 24 hours. This resulted in the formation of a membrane bearing the dimensions of the petri dish.

3.2.4 Scanning Electron Microscopy (SEM) Analysis

SEM analysis was carried out with a FEI Quanta 650 FEG High Resolution Scanning Electron Microscope. Typical beam energies were in the range of 10-20 kV and typical spot sizes in the range of 2.0-3.5 (irradiated area and beam current increase with increasing spot size which has an arbitrary range of 1 to 7). The sample was cut to size and mounted on a sample holder with conductive carbon tape. It was important to mount the sample on a sample holder which allows for tilting of the sample for thickness measurements. Thickness measurements were carried out at a tilt angle of 60°. Measurements were carried out on a variety of areas of each sample to determine the deviation in thickness across the sample.

3.2.5 Swelling Studies

Phosphate buffer solutions having pH values of 2.66 and 7.12 were freshly prepared and used for the swelling studies experiments carried out on the Chi-TEOS IPN membranes. The weight of the dried Chi-TEOS IPN membrane was determined using a pre-weighed weigh-boat. Following determination of the original, dry weight of the membrane it was then immersed in pH 2.66 solution for one minute. After one minute, the solution was carefully removed and the weigh-boat with swollen membrane was weighed. This was repeated twice and the membrane was rinsed with water.

The membrane was then immersed in a pH 7.12 solution for one minute. After one minute, the solution was removed and the weigh-boat weighed with membrane. This step was also repeated twice. Swelling studies of the various membranes were analysed and compared by determination of the swelling ratio using the following equation:

Equation 3.1: $Sw = (Wt-Wo)/ Wo$

Here Wo and Wt are the original weight of the membrane and the weight of the membrane after being immersed in solution for time, t, respectively.

The first swelling study focussed on comparing the swelling ability of 1:1LMWChi-TEOS IPN, 1:1 MMWChi-TEOS IPN and 1:1 HMWChi-TEOS IPN; essentially comparing swelling ability with increasing molecular weight. The second study aimed to determine how swelling was affected upon increasing the volume of TEOS in the IPNs. For this purpose, 1:1, 1:2 and 1:3 LMWChi-TEOS IPNs were used. A further

study was aimed at testing the reusability of the IPNs over a number of days, in this case 1:1 MMWChi-TEOS IPN was employed.

3.3 Synthesis of SiO_2-based Photonic Crystals

3.3.1 Synthesis of Silica Particles via the Stöber Process

Silica particles were prepared by the Stöber process[4], which is the base-catalysed hydrolysis and condensation of tetra alkyl silicates. The tetra alkyl silicate used was >99.0 % TEOS (tetraethyl orthosilicate) solution, purchased from Sigma Aldrich Ireland and the base used was 28.0-30.0 % ammonium hydroxide solution, also purchased from Sigma Aldrich Ireland.

A solution (solution 1) was prepared containing 60 mL 100 % EtOH and 20 mL TEOS in a 100 mL glass bottle. A stir bar was placed in the bottle and the solution was allowed to stir on a magnetic stirring plate for 3-4 hours. A second solution (solution 2) was prepared containing 52 mL H_2O and varying amounts of EtOH and NH_4OH to a total solution volume of 120 mL in a 500 mL glass bottle. This solution was also allowed to stir for up to 10 minutes. Solution 1 was poured into solution 2 and the combined solutions were allowed to stir overnight. The clear solution changed to a milky-white solution after a few minutes. After stirring overnight, the solution was washed using EtOH and H_2O. This involved centrifugation, using the Hettich Zentrifugen EBA21, and sonication of the particle solutions, using a Cole-Palmer Ultrasonic Cleaner Model 08849-00. A Stuart SA8 Vortex mixer was also used in ensuring the particles were thoroughly mixed in solution prior to centrifugation.

As mentioned previously the size and distribution of the particles were analysed using the SEM. To prepare a sample for SEM analysis a small amount of solution was placed on a piece of silicon wafer using a plastic dropper and was allowed to dry. In order to calculate an accurate standard deviation (SD) of the particle size 100 particles were measured during SEM analysis. It was established that 0-5 % is the optimum value for SD in order to prepare good quality ordered layers of the particles. The structural quality and order of the particles was also inspected using SEM.

3.3.2 Deposition Methods

The first deposition method employed was the under-oil capillary enhanced method[5, 6]. An adjustable platform was placed in an oven set to a constant temperature of 50 °C

and adjusted horizontally with a spirit level. The prepared, clean substrate was placed in a petri dish on the platform. The required volume of the aqueous SiO_2 particle solution was carefully deposited onto the substrate using a plastic dropper, in a dropwise fashion. At this point the substrate and solution were covered with 10 CST silicone oil using a pipette until the sample was just covered with oil. The sample was left in the closed oven for about three days. The high viscosity 10 CST oil was then removed with a pipette and recycled and the SiO_2 photonic crystal sample prepared was rinsed with 0.65 CST silicon oil to remove any remaining oil. Both the high and low viscosity silicone oils were supplied by Dow Corning.

The second method employed was the vertical deposition technique which also works by capillary forces and is sometimes referred to as controlled evaporation[7]. Solution preparation was the same as for the under-oil capillary enhanced method described above except that solution volume was much greater, depending on the size of the substrate. The SiO_2 particle solution was placed in a beaker. The cleaned substrate of choice was clamped using a retort stand setup and carefully lowered into the solution at an angle of 25°. The setup was left in a closed oven for a number of days at 55 °C. Generally, the EtOH: H_2O ratio employed was 3:1. Upon analysis of various concentrations ranging from 3:1, 2:1, 1:1, 1:2, 1:3 (EtOH: H_2O) it emerged that the 3: 1 was the optimum ratio in terms of evaporation rate, particle ordering, formation of even layers and quality of resulting spectra[8].

The final deposition method was a large-scale under-oil deposition method which is essentially a combination of both methods described above. It was devised by Dr Hiroshi Fudouzi and all experiments were carried out in the research labs of the Colloidal Crystals Materials Group at the National Institute of Materials Science[9]. The experiment was performed using the device developed by Fudouzi *et al.* except that colloidal silica was used instead of colloidal polystyrene. The method involved submerging a hydrophilic PET sheet with dimensions of 200 mm x 100 mm into a colloidal suspension in a large, narrow container as shown in figure 3.1. The surface of the colloidal suspension was then covered with high viscosity silicone oil. Film growth occurred as the suspended substrate was raised from the colloidal suspension at a rate of 1 μms^{-1}.

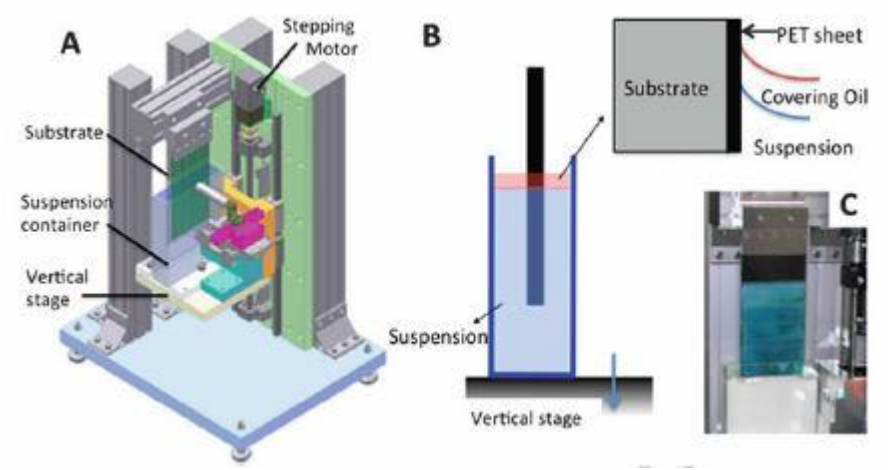

Figure 3.1. (a) Schematic of the large-scale coating equipment constructed by Fudouzi *et al.* (b) vertical coating setup with substrate suspended and silicone oil on the surface (c) 200 nm PS coated on PET, by Fudouzi *et al.* [9].

3.3.3 Substrates and Associated Cleaning Methods

Two substrate-cleaning methods were employed, depending on whether the substrate had glass or plastic-type properties. The first applied to glass and Mica and the second applied to PMMA and PET.

Generic glass slides were used for glass substrates and were cut to size using a diamond tipped pen. Mica is a rigid to flexible substrate material made from the highest-grade ruby muscovite having the chemical formula $KAl_3Si_3O_{10}(OH)_2$. Glass and Mica have very similar properties involving the silica surface chemistry and so they could be cleaned using the same method. Substrates were cleaned in a 5:1:1 solution of H_2O: H_2O_2: NH_4OH and sonicated for ten minutes, rinsed with water and dried with N_2 gas to provide an inert, hydrophilic surface.

The (plastic) polymers used, PMMA (polymethyl methacrylate) and PET (polyethylene terephthalate) were rinsed in detergent water and then treated in a basic plasma cleaner, purchased from Harrick Plasma. The plasma cleaning process involves placing samples in a high-energy plasma environment under vacuum for 5-10 minutes and results in a hydrophilic plastic surface free from any externally deposited organic matter.

3.3.4 SEM and Optical Analysis

Following deposition, the SiO_2 photonic crystal films were analysed to determine whether the technique employed had been successful. The first part of the analysis was accomplished by SEM, allowing determination of the packing quality and the number of layers in the sample. Statistical analysis on the particle dimensions was also carried out by measuring a specific number of particles using the SEM software or ImageJ software. An example of an SEM image bearing the particle size measurements is shown below in figure 3.2.

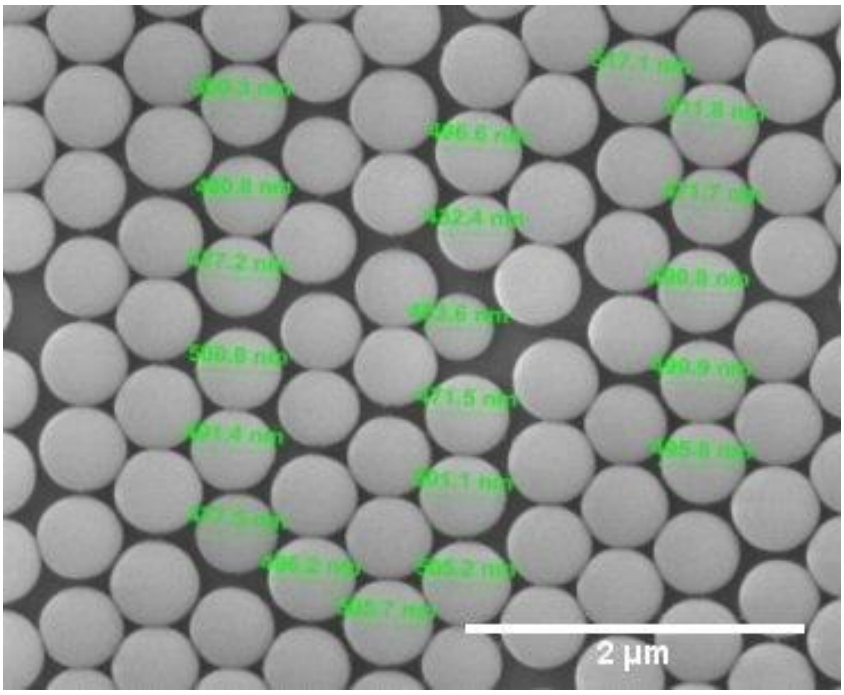

Figure 3.2. SEM image of silica particles prepared via the Stöber method and measured using SEM software. These particles correspond to a synthesis using 7 mL of catalytic NH_4OH.

Optical analysis was very useful in determining the quality of the films. Samples were analysed using an Ocean Optics spectrometer setup and Spectra Suite software. The optical setup used could be interchanged from transmittance to reflectance measurements. The spectrometer was calibrated prior to analysis. For the plastics, this involved using a plain piece of the plastic in question. Calibration allowed for the measured beam intensity to be maximized by adjusting the integration time. As such a minimum integration time of 10 seconds was always used as a starting point. This allowed for the beam intensity to be increased by increasing the integration time.

Following calibration, the sample was loaded onto the sample holder and the transmission/ reflection peak position recorded from over the angular range 0-80˚with respect to the apparent surface normal. The sample holder could be rotated manually and was equipped with an angle gauge at its base.

3.4 Determination of the Optical Properties of the Chi-TEOS-SiO_2 Composites

3.4.1 Synthesis of the Initial SiO_2 Photonic Crystal Films

SiO_2 film growth was carried out by the vertical controlled evaporation method outlined in detail in section 3.3.2. PET was employed as a substrate due to the high quality of resulting films as observed using the methods described in section 3.3. The SiO_2 nanoparticles used for film growth were synthesised via the Stöber process outlined in section 3.3.1. Particles in the range of 250-380 nm were employed as their Bragg diffracted wavelengths lie in the visible range of the spectrum and as such the resulting films were suitable for optical analysis by UV-Vis spectroscopy while the diffracted colour could also be observed by the naked eye. Optical analysis of the SiO_2 films was carried out prior to composite formation, in order to compare the optical quality before and after infilling. Analysis was carried out using an Ocean Optics spectrometer setup and Spectra Suite software.

3.4.2 Synthesis of Chi-TEOS IPN Hydrogels

The method used for Chi-TEOS IPN hydrogel formation was the same as that outlined in section 3.2.2. Following analysis of the results obtained via application of the methods outlined in section 3.3 it was decided that the 1:1 LMWChi-TEOS IPN and 1:1 MMWChi-TEOS IPN hydrogels would be used to make the Chi-TEOS-SiO_2 composite. The factors contributing to this decision were the good dispersity index of both LMW and MMW samples, the preservation of chitosan's flexibility characteristic with the 1:1 chitosan: TEOS ratio and the ideal degree of swelling of both types of IPN. The degree of swelling of both types of composites was believed to be adequate in terms of enlarging a SiO_2 photonic crystal lattice embedded in a composite membrane to such a degree that the Bragg diffracted wavelength should still be detected in the UV-Vis range of the electromagnetic spectrum. As mentioned previously the substrate selected for SiO_2 photonic crystal growth was PET and this

substrate was also suitable for deposition of the hydrogel. The hydrogel dried to form a membrane which peeled off the substrate surface easily. This was ideal in comparison to glass, which was a good candidate for SiO_2 film growth, but not for thin film formation. When the hydrogel was allowed to dry on glass it stuck to the surface preventing formation of a free-standing film.

3.4.3 Chi-TEOS-SiO_2 Composite Formation

A very straightforward method was devised for Chi-TEOS-SiO_2 composite formation. The SiO_2 photonic crystal film on PET was placed on a level horizontal platform in a vacuum oven preheated to 40 °C. The desired amount of 1:1 LMW-/MMW Chi-TEOS IPN hydrogel was then drop-casted onto the film and allowed to spread over the entire film surface. Vacuum was then applied to the closed oven. Drying time varied depending on the size of the substrate and volume of hydrogel, but generally the samples were left in an oven for a period of 24 hours. Upon formation of the composite the vacuum was released. The solid Chi-TEOS-SiO_2 composite membrane easily peeled off the PET substrate with the change in environmental pressure. This was the final step in the formation of the free-standing composite.

3.4.4 SEM Analysis of Composite Films

The sample was cut to size and mounted on a sample holder with conductive carbon tape. Both the surface and side of the films were observed and so it was important that the sample stage was suitable for tilting at an angle of 60°.

3.4.5 Swelling Studies Combined with Optical Analysis of Composite Films

Swelling analysis on the films was carried out in conjunction with optical studies in order to gain a complete understanding of their physical properties. Using the procedures outlined in section 3.3.4, samples were placed in a vertical position in the sample holder and UV-Vis spectra were recorded at a series of viewing angles. This arrangement proved to be suitable for dry samples with supporting substrates. However, the combined optical analysis and swelling studies involved the use of free-standing membranes (without substrate support), for the most part kept under aqueous conditions. For this reason, a horizontal optical analysis setup was assembled at Tyndall National Institute for Chi-TEOS-SiO_2 composite analysis. An example of the optical setup for transmission can be seen in figure 3.3. This setup involved

rearranging the previous setup via the incorporation of a horizontal stage for the sample. An enclosed optical setup for reflection analysis was utilized at NIMS. This was very important as the original setup at Tyndall National Institute only allowed for transmission analysis. Ocean Optics hardware and Spectra Suite software were employed at both locations; Tyndall National Institute and NIMS.

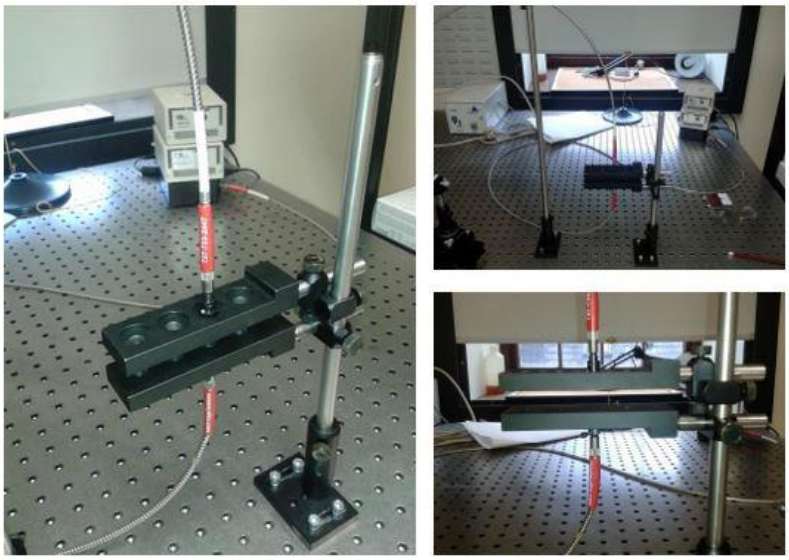

Figure 3.3. The horizontal optics setup employed for analysis of free-standing Chi-TEOS-SiO_2 composites.

Analysis with this setup was very straightforward. The free-standing Chi-TEOS-SiO_2 composite was placed in a clear dish and then onto the horizontal sample stage with the light source and detector aligned for analysis in transmission mode. It was important to carry out a background scan prior to analysis. This allowed for elimination of the surrounding light conditions and accounted for the presence of the clear dish in the final transmission spectrum. These corrections were not necessary for analysis in reflection mode as the enclosed area was completely blacked out. After preparing the setup and performing background analysis the UV-Vis spectrum of the dry composite membrane was recorded. The composite membrane was then immersed in solutions of varying pH at regular time intervals in order to observe the associated shifts in Bragg diffracted wavelength. After recording the various spectra, they were then plotted and the observed shifts in Bragg dip/ peak interpreted in terms of whether the embedded photonic crystal lattice was swelling or shrinking in the IPN as a function of applied pH.

3.5 Determination of the Mechanical Properties of Chitosan and Chi-TEOS IPN Thin Films

3.5.1 Chitosan Hydrogel and IPN Synthesis

Low molecular weight chitosan purchased from Sigma Aldrich, Ireland was used for the synthesis of the chitosan hydrogel and subsequent formation of the IPN by cross-linking with a TEOS polymeric network. A 1:1 chitosan: TEOS ratio was employed. A description of the synthesis is outlined in section 3.2. Membranes were formed by drop-casting 13 mL of the hydrogel into a standard petri dish (90 mm diameter) and allowed to dry in an enclosed oven at 40 °C for 24 hours. After drying the membranes were cut into individual 40 mm x 10 mm strips, to be used for grafting with nanoparticle solutions.

3.5.2 Synthesis of the Micro-/Nanoparticles Added to the IPNs

SiO_2 nanoparticles were prepared by the Stöber process, previously described in detail in section 3.3.1. Particles with diameters in the range of 180-450 nm were used for grafting/ embedding. Aqueous solutions of the nanoparticles were prepared, in the range of 0.5-0.8 gmL^{-1}. Polystyrene nanoparticles were prepared by the polymerisation of styrene monomers by Fudouzi *et al.* at the National Institute of Materials Science, Tsukuba, Japan. Particles in the range of 180-450 nm diameters were also used for grafting/ embedding with the concentration of the solutions falling between 0.5-0.76 gmL^{-1}. By using similar experimental parameters for both SiO_2 and PS solution preparation the results could then be compared. The dimensions of the polymer particles were measured by SEM - see section 3.3.4.

Silver and gold nanoparticles were purchased from Sigma-Aldrich, Ireland. Aqueous dispersions contained particles of 20 nm diameter at a concentration of 0.02 mg/mL. They were introduced to the hydrogel at varying concentrations of 1-10 vol%. The Ag and Au nanoparticles were analysed by UV-Vis spectroscopy to confirm the dimensions of the particles; this was carried out on a Shimadzu UV-2401PC UV-Vis spectrometer. Both Ag and Au nanoparticles absorb light in the UV-Vis region of the electromagnetic spectrum with the wavelength specific to particle diameter. They absorb and scatter visible light due to the surface plasmon resonance (SPR) phenomenon producing the yellow and red colours of the Ag and Au solutions,

respectively. The SPR phenomenon occurs when conduction electrons on the surface of metal nanoparticles are excited by incident radiation generating oscillations known as surface plasmons. This results in the absorption and reflection of certain wavelengths of visible light depending on the size, shape and agglomeration of the metal nanoparticles. In comparing the absorbance peaks due to the SPRs of Ag and Au nanoparticles of the same concentration there is generally a broader, more intense peak observed for the Ag nanoparticles. This is due to greater photoluminescence intensity or plasmon excitation efficiency[10,11]. Ag and Au nanoparticles of the same diameter exhibit different characteristic absorbance wavelengths, this is because different energies (or wavelengths) of excitation induce the surface electron oscillations.

3.5.3 Embedding the Micro/Nanoparticles into the IPNs

Embedding the micro-/nanoparticles into the IPNs involved introducing them to the Chi-TEOS IPN hydrogel prior to membrane formation at a concentration of 1-10 vol%, depending on the nanoparticle solution. All polymer particles were introduced at a concentration of 1 vol% with varying particle size and metal nanoparticles were introduced at 1-10 vol% with constant particle size, see table 3.1 for details. For one complete synthesis 13 mL of 1:1 LMWChi-TEOS IPN was placed in a beaker with a stir bar. 130-1300 µL of the desired particle solution was introduced to the hydrogel and left to stir for about an hour. The entire solution was drop-cast on to a standard petri dish and allowed to dry in an enclosed oven at 40 °C for 24 hours. The full-size membrane was cut into 40 mm x 10 mm strips suitable for tensile strength tests.

Membrane type	Cross-linker	Diameter of nanoparticles	Concentration of cross-linker	Volume of cross-linker
Chitosan	-	-	-	-
Chi-TEOS IPN	TEOS	-	1:1 (Chitosan: TEOS)	-
Chi-TEOS IPN	TEOS/ SiO_2	100 nm	0.076 gmL^{-1}	130 µL
Chi-TEOS IPN	TEOS/ SiO_2	290 nm	0.075 gmL^{-1}	130 µL
Chi-TEOS IPN	TEOS/ SiO_2	420 nm	0.066 gmL^{-1}	130 µL
Chi-TEOS IPN	TEOS/ SiO_2	516nm	0.063 gmL^{-1}	130 µL
Chi-TEOS IPN	TEOS/PS	100 nm	0.070 gmL^{-1}	130 µL
Chi-TEOS IPN	TEOS/PS	290 nm	0.061 gmL^{-1}	130 µL
Chi-TEOS IPN	TEOS/PS	420 nm	0.050gmL^{-1}	130 µL
Chi-TEOS IPN	TEOS/PS	520 nm	0.074 gmL^{-1}	130 µL
Chi-TEOS IPN	TEOS/ Ag	20 nm	<0.020 gmL^{-1}	130 µL
Chi-TEOS IPN	TEOS/ Ag	20 nm	<0.020 gmL^{-1}	650 µL
Chi-TEOS IPN	TEOS/ Ag	20 nm	<0.020 gmL^{-1}	1300 µL
Chi-TEOS IPN	TEOS/ Au	20 nm	<0.020 gmL^{-1}	130 µL
Chi-TEOS IPN	TEOS/ Au	20 nm	<0.020 gmL^{-1}	650 µL
Chi-TEOS IPN	TEOS/ Au	20 nm	<0.020 gmL^{-1}	1300 µL

Table 3.1. The various types of membranes that were prepared and tested in this work.

3.5.4 Grafting the Micro/Nanoparticles onto the IPNs

The method employed for grafting separate 1:1 LMWChi-TEOS IPNs was very straightforward as the individual 40 mm x 10 mm IPN strips were both flexible and durable. One strip was placed flat on a clean, dry surface and 100 µL of the desired nanoparticle solution was carefully deposited onto the IPN using a micropipette, covering about 30 mm x 10 mm of the surface. A second IPN was then placed over this area and spread evenly so that 30 mm x 10 mm of both IPNs have been grafted,

leaving 10 mm x 10 mm exposed at either end. This was repeated to the desired number of grafted IPNs and they were placed in an oven at 40°C to dry for a few hours. See figure 3.4 for a basic schematic on the grafting of two separate LMWChi-TEOS IPNs with nanoparticles.

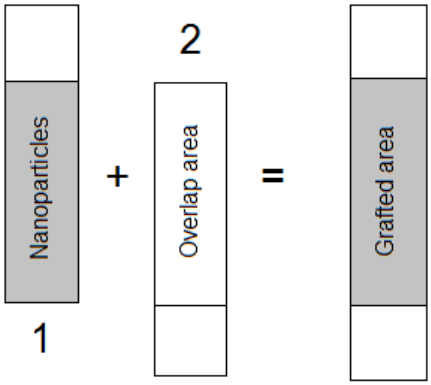

Figure 3.4. Schematic of two 40 mm x 10 mm 1:1 LMWChi-TEOS IPN strips, (1) shows the area introduced to nanoparticles and (2) shows the overlap area, these were combined for a total grafted area of 30 mm x 10 mm and overall area of 50 mm x 10 mm.

3.5.5 Tensile Strength Tests

Initial tensile strength tests were carried out on the membranes prepared by the methods described using an Imada desk-type mechanical tester at the National Institute of Materials Science, Tsukuba, Japan. Follow-up tests were carried out using an Instron 5565 Universal Testing Machine at Tyndall National Institute employing 10 mm x 40 mm thin film strips clamped with PDMS supports cut to the size of the clamp. The tensile test method involved clamping the thin film membrane, using PDMS supports, under a load of 5 kN. The thin film was then pulled at a rate of 0.5 mm/min. Depending on the flexibility of the film this may result in the film stretching to the point of fracture or a sudden fracture may be observed. The load and displacement were measured; this could then be converted to a stress vs strain graph. All tests were repeated at least ten times.

3.6 Determination of the Antimicrobial Properties of Chitosan and Chi-TEOS IPN Thin Films

3.6.1 Preparation of Thin Film Hydrogels Immobilized on Glass

The chitosan and Chi-TEOS IPN hydrogels were prepared according to the same methods outlined in section 3.2.2. Five different sample types were prepared, these were: glass, chitosan on glass, Chi-TEOS IPN on glass, Chi-TEOS IPN-Ag on glass and Chi-TEOS IPN-Au on glass. The same silver and gold nanoparticles as described in section 3.5.2 were added to the Chi-TEOS IPN hydrogel at 10 vol% concentration. Sample preparation included plasma cleaning the glass substrates to ensure clean, hydrophilic surfaces - a Harrick Plasma basic plasma cleaner was used. 250 µL of the desired hydrogel was then drop-cast onto the substrate surface with an area of 15 mm x 15 mm and allowed to dry in an enclosed oven at 40 °C.

3.6.2 Structural Analysis of the Nanoparticle-Modified IPN Films

It was necessary to gain an understanding of the structural and bonding properties of the various chitosan composite networks under investigation and as such the analysis methods described in sections 3.5 and 3.6 were used. It was believed that application of these methods would provide insight into possible contrasting results and highlight discrepancies between non-cross-linked and cross-linked chitosan networks.

Both FTIR and Raman spectroscopy were used to investigate structural differences between chitosan and the subsequently-formed cross-linked networks. These methods are spectroscopic techniques which monitor the vibrational and rotational modes of molecules via their interactions with light. The frequencies of the various vibrational/ rotational modes are specific to certain functional groups and so a vibrational/rotational spectrum provides crucial information on the types of functional groups are present in a sample. The two methods in question are complimentary to one another in that infrared spectroscopy is utilised for the detection of vibrations in which there is a change in dipole moment and Raman spectroscopy is utilised for the detection of vibrations in which there is a change in polarizability[12, 13].

Infrared analysis was carried out on free-standing thin film samples using a Bruker Alpha FTIR spectrometer in single attenuated total reflection (ATR) mode which utilizes a platinum-diamond crystal. The presence of the platinum-diamond crystal

enhances the light-sample interactions greatly by producing an evanescent wave which interacts with the compacted sample over a short path length[14]. This setup is ideal for solid and liquid samples to be analysed since it can be applied with no sample preparation, often an inconvenience which is encountered in many other infrared spectroscopy techniques. Figure 3.5 displays the ATR principle as illustrated in the instruments' application notes.

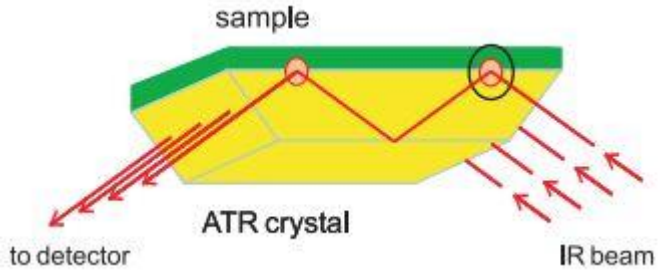

Figure 3.5. Schematic of the ATR crystal with sample compacted on the surface and the incident beam paths[14].

A Renishaw inVia confocal Raman microscope was used for Raman analysis on the thin film samples immobilized on glass slides. The sample was focussed using 50X magnification prior to laser exposure. Monochromatic light in the form of a laser beam interacts with the sample surface; the scattered light (elastically and inelastically) is detected. The initial laser power and exposure time were 1% and 10 seconds, respectively. For optimum spectral readouts of the chitosan sample these were gradually built up to 100% and 30 seconds, respectively. Samples were prepared by drying the chitosan hydrogels on glass substrates. No further treatment was required and damage to the sample was minimal.

SEM was performed as a complimentary technique. As previously described in Chapter 1 SEM is an analytical technique which reveals spatial heterogeneities of structure with dimensions of nm to mm. The sample surface is scanned with a high-energy electron beam, which results in the production of backscattered electrons and secondary electrons. It is these electrons which are detected and provide information on the composition and structural properties of the sample. Backscattered electron imaging is used to examine samples with areas of contrasting molecular weight due to the fact that heavier atomic constituents backscatter electrons more intensively than lighter atomic constituents. SEM analysis provides vital information associated with

the size of the particles, the order and uniformity of the structure, the thickness of the sample, the structure of the substrate and the presence of impurities or defects; it is an excellent 'visual' aid.

Transmission Electron Microscopy (TEM) was employed to image and measure the Ag and Au NPs in the Chi-TEOS IPN membrane; it was carried out on a JEOL 2100 High Resolution TEM, operated at 200 kV in bright field mode using a Gatan double tilt holder. TEM differs from SEM in a number of ways. Electrons are transmitted through the sample, which must be extremely thin (< 200 nm). This results in excellent resolution and provides information on advanced sample characteristics such as crystallite orientation, the chemical and electronic structure of nanocrystals as well as thermodynamic, magnetic and mechanical domains and stresses[15]. TEM provides a two-dimensional representation of a sample at a minute scale. If samples cannot be prepared < 200 nm they can be 'thinned' by a focused ion beam milling technique. This adds time and cost constraints to TEM analysis but allows for the analysis of thicker films[16, 17]. In general, better resolution is observed for thinner samples. In thicker samples, the sample often causes a buildup of electrons which induces sample charging. This significantly affects the resolution and is also observed during SEM analysis.

Surface morphology analysis was carried out using a KLA Tencor P15 Profilometer. Surface profiling is a straightforward technique which involves scanning a sample surface with a sensitive stylus in order to quantify the roughness of a surface as well as measuring step heights and surface features on a scale of nm to mm. The sample remains static on a calibrated stage while the stylus laterally scans the surface at the user's desired speed, direction and distance. It was important that sample dimensions were kept roughly constant during both mechanical and antimicrobial testing. For this reason, sample thickness was measured using both the surface profiler and SEM. The surface roughness of each sample was measured using the surface profiler. It was important that this parameter was monitored following cross-linking with TEOS and also after introducing the micro-nanoparticles.

3.6.3 Crystal violet Cell Attachment Assays

Antimicrobial tests were carried out in the UCC Microbiology Department under the supervision of Dr David Clarke and Mr Finbarr Buttimer. The crystal violet attachment

assay was used as a qualitative test for comparing the degree of attachment of bacteria to the various chitosan samples[18]. This test is designed to reveal the affinity bacteria may or may not have for the various chitosan surfaces. Initial tests were carried out utilising two biological replicates of the gram-negative bacteria *E. coli*.

Aseptic techniques were applied at all times during the antimicrobial tests. The optical density of both bacterial replicates was initially determined using a spectrophotometer; the absorbance was measured with a light source at a wavelength of 600 nm. The bacterial samples were then centrifuged and re-suspended in saline solution having an optical density of 1. The optical density was further diluted to 0.05 while immersing the samples in bacterial solution in a 6-well plate; this is a low starting optical density which increases with bacterial growth. The 6-well plates were prepared by placing a sample in each well – the first two wells were then filled with 5 mL of lysogeny broth (LB), the third and fourth wells were filled with 5 mL of bacterial replicate 1 at an optical density of 0.05, the final two wells were filled with the second bacterial sample at an optical density of 0.05. This was carried out for each sample (glass, chitosan on glass, Chi-TEOS IPN on glass, Chi-TEOS IPN-Ag on glass and Chi-TEOS IPN-Au on glass) so there was a total of five 6-well plates incubated at 37 °C for 24 hours. There were essentially two 'controls' in the form of the glass samples and the first two wells of each 6-well plate bearing LB growth medium but no bacteria. Figure 3.6 displays a schematic of the 6-well plate model described.

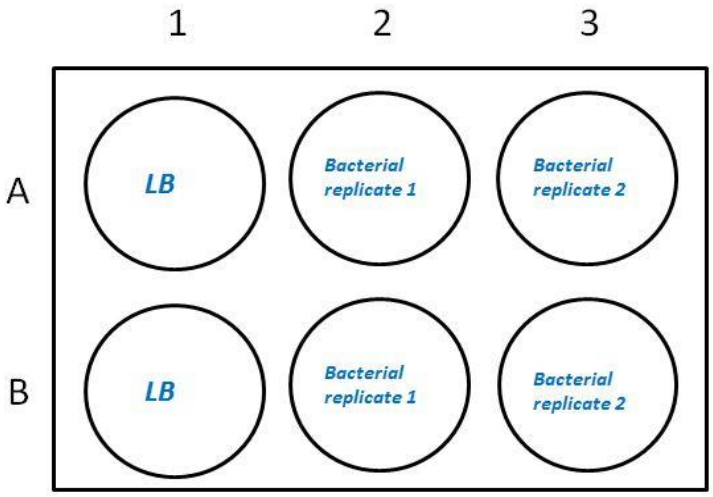

Figure 3.6. Schematic representation of the 6-well plate setup described, this setup was used for six samples of each of the five different sample types.

Following 24 hours of incubation at 37 °C the absorbance of each solution from all 6-well plates was measured. It was expected that the control samples would have significantly lower absorbance values due to minimal bacterial growth, unless contamination had occurred. The samples (still immobilized on glass) were then cleaned thoroughly using water and subsequently stained with crystal violet. They were stored in the crystal violet solution for twenty minutes and then rinsed carefully with water such that only the crystal violet which had stained the bacteria on the sample remained. Samples were then rinsed with ethanol, dissolving any crystal violet which had remained attached to the sample. 200 µL of ethanol solution was then taken from each plate and placed in order in a 96-well plate. The absorbance was measured using a Tecan Genios plate reader with X Fluor 4 software on Microsoft Excel. The absorbance values were then compared in a relative manner. Fig 3.7 shows a schematic of the first 30 occupied wells of the 96-well plate following introduction of samples from five 6-well plates.

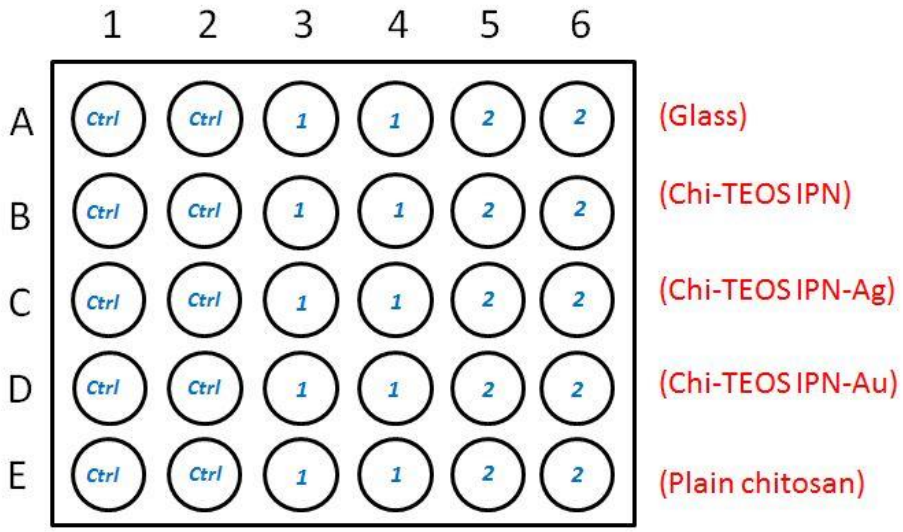

Figure 3.7. Schematic representation of the first 30 wells of the 96-well plate setup described.

3.6.4 Determination of Release Profiles

An investigation into whether the Ag/ Au NPs were being released from the Chi-TEOS IPN network under specific conditions was carried out by immersing the samples in relevant solutions and subsequent analysis of the resulting solutions using a Shimadzu UV-2401PC UV-Vis Spectrometer. The method involved immersing the cross-linked

samples (Chi-TEOS IPN, Chi-TEOS IPN-Ag and Chi-TEOS IPN-Au) in 5 mL of 0.01 M phosphate buffered saline (PBS) solution in a series of six-well plates – six of each sample per plate, therefore three plates. The plates were then stored in an enclosed oven at 37 °C to replicate the growth environments for *E. coli* as described in section 3.6.3. Transmission measurements of the PBS solutions were measured at hourly intervals over a six-hour period, using the PBS with Chi-TEOS IPN samples immersed as the background correction. Transmission measurements were also recorded after 24 hours of storage at microbiological-replicate growth conditions. A few drops of 0.1 M NaCl were added to each solution to detect whether ions were released into solution. Tests were also carried out in 0.1 M phosphate buffers at pH 2.5 and 11.5, to test whether release was dependent on the inherent pH-sensitivity of the chitosan network.

References

1. Wang, W.; Bo, S.; Li, S.; Qin, W., Determination of the Mark-Houwink equation for chitosans with different degrees of deacetylation. *International Journal of Biological Macromolecules* **1991,** *13* (5), 281-285.

2. Rinaudo, M.; Milas, M.; Dung, P. L., Characterization of chitosan. Influence of ionic strength and degree of acetylation on chain expansion. *International Journal of Biological Macromolecules* **1993,** *15* (5), 281-285.

3. Kassai, M. R., Calculation of Mark–Houwink–Sakurada equation viscosimetric constants for chitosan in any solvent-temperature system using experimental reported viscosimetric constants data. *Carbohydrate Polymers* **2007,** *68*, 447-488.

4. Stober, W., Fink, A., Bohn, E., Controlled growth of mono-disperse silica spheres in the micron size range. *Journal of Colloid and Interface Science* **1968,** *26*, 62-69.

5. Fudouzi, H., Fabricating high-quality opal films with uniform structure over a large area. *Journal of Colloid and Interface Science* **2004,** *275* (1), 277-283.

6. Fudouzi, H., Novel coating method for artificial opal films and its process analysis. *Colloids and Surfaces A: Physicochemical and Engineering Aspects* **2007,** *311* (1), 11-15.

7. Jiang, P.; Bertone, J.; Hwang, K.; Colvin, V., Single-crystal colloidal multilayers of controlled thickness. *Chemistry of Materials* **1999,** *11* (8), 2132-2140.

8. McGrath, J. Development of large-scale colloidal crystallisation methods for the production of photonic crystals. University College Cork, CORA, 2014.

9. Fudouzi, H., Colloidal Photonic Crystal Films: Fabrication and Tunable Structural Color and Applications. In *Nanomaterials and Nanoarchitectures: A Complex Review of Current Hot Topics and their Applications*, Bardosova, M.; Wagner, T., Eds. Springer Netherlands: Dordrecht, 2015; pp 1-19.

10. Eichelbaum, M.; Rademann, K., Plasmonic Enhancement or Energy Transfer? On the Luminescence of Gold-, Silver-, and Lanthanide-Doped Silicate Glasses and Its Potential for Light-Emitting Devices. *Advanced Functional Materials* **2009,** *19* (13), 2045-2052.

11. Inc., C. Silver nanoparticle properties. http://www.cytodiagnostics.com/store/pc/Silver-Nanoparticle-Properties-d11.htm (accessed 23/11/2016).

12. Aroca, R., *Surface-Enhanced Vibrational Spectroscopy*. John Wiley & Sons: 2006.

13. Tuschel, D., Practical group theory and Raman spectroscopy, Part I: Normal vibrational modes. *Spectroscopy* **2014,** *29* (2), 14.

14. Bruker *Attenuated Total Reflection (ATR) – a versatile tool for FR spectroscopy*; Application Note AN # 79; https://www.bruker.com/, 2011.

15. Wang, Z. L., Transmission Electron Microscopy of Shape-Controlled Nanocrystals and Their Assemblies. *The Journal of Physical Chemistry B* **2000,** *104* (6), 1153-1175.

16. Mayer, J.; Giannuzzi, L. A.; Kamino, T.; Michael, J., TEM sample preparation and FIB-induced damage. *MRS Bulletin* **2007,** *32* (5), 400-407.

17. Giannuzzi, L. A.; Stevie, F. A., A review of focused ion beam milling techniques for TEM specimen preparation. *Micron* **1999,** *30* (3), 197-204.

18. Feoktistova, M.; Geserick, P.; Leverkus, M., Crystal Violet Assay for Determining Viability of Cultured Cells. *Cold Spring Harbor Protocols* **2016,** *2016* (4), 343-346.

4. Preliminary Investigations into the Properties of Synthetic Colloidal Photonic Crystals and Chitosan-based IPNs

4.1 Introduction

This chapter presents preliminary results obtained for a series of colloidal photonic crystals and chitosan-based IPNs synthesised using the methods described in sections 3.2 and 3.3. In particular this chapter focuses on the structural, chemical and simple optical properties of the materials synthesised, while later chapters discuss their more advanced optical, mechanical and antimicrobial properties. Preliminary experiments were carried out on chitosan-tetraethyl orthosilicate interpenetrating polymer networks (Chi-TEOS IPNs) and SiO_2 photonic crystals, the results of which are outlined in sections 4.2 and 4.3, respectively.

4.2 Chitosan Studies and IPN formation

4.2.1 The Chemical Properties of the Chitosan Samples

The three types of chitosan were employed in these experiments. Information relating to their chemical composition is given in Table 4.1. These data were obtained from the as-received chitosan, prior to IPN formation. The average molecular weight (Mw) of the chitosan used would naturally be expected to increase accordingly from the low molecular weight samples to the high molecular weight samples. However, the results obtained for intrinsic viscosity (η), viscosimetric molecular weight (Mv) and polydispersity index (PDI) suggest that the so-called high molecular weight chitosan material was of poor quality. From the data presented in table 4.1 it is likely that the high molecular weight chitosan was actually composed of a wide range of molecular weight materials rather than primarily being a single, high molecular weight material.

Chitosan Sample	Mw ($gmol^{-1}$)	η (mLg^{-1})	Mv ($gmol^{-1}$)	% DA	PDI
LMWChi	140,300	442(±3)	89,832	8	1.9
MMWChi	312,300	586(±9)	134,841	40	2.3
HMWChi	479,000	377(±9)	75,470	22	4.2

Table 4.1. Data for LMW-, MMW- and HMWChi prior to formation of IPN.

The viscosimetric molecular weight was calculated by the intrinsic viscosity of the samples (measured in triplicate), using the Mark-Houwink Equation (Equation 4.1). The results are tabulated in table 4.1. The following α and K values were determined from the literature: α=0.76 and K=0.076 for LMWChi; α=0.76 and K=0.074 for MMWChi and HMWChi[1-3].

Equation 4.1: $Mv = \sqrt[\alpha]{\frac{[\eta]}{K}}$

FTIR analysis provided information on the functional groups present in the samples. The main bands in the chitosan FTIR spectra were assigned as follows: 3500-3000 cm^{-1} (O-H stretching overlapped with N-H stretching), 2980-2880 cm^{-1} (C-H axial stretching), 1656 cm^{-1} (amide I band, C=O axial stretching of acetyl groups), 1593 cm^{-1} (amide II band), 1382 cm^{-1} (asymmetric bending in CH_2 groups, symmetric angular deformation in CH_3 groups and axial deformation in amino groups), 1325 cm^{-1} (C-N axial stretching, amide III). See figure 4.1 for the associated FTIR spectra.

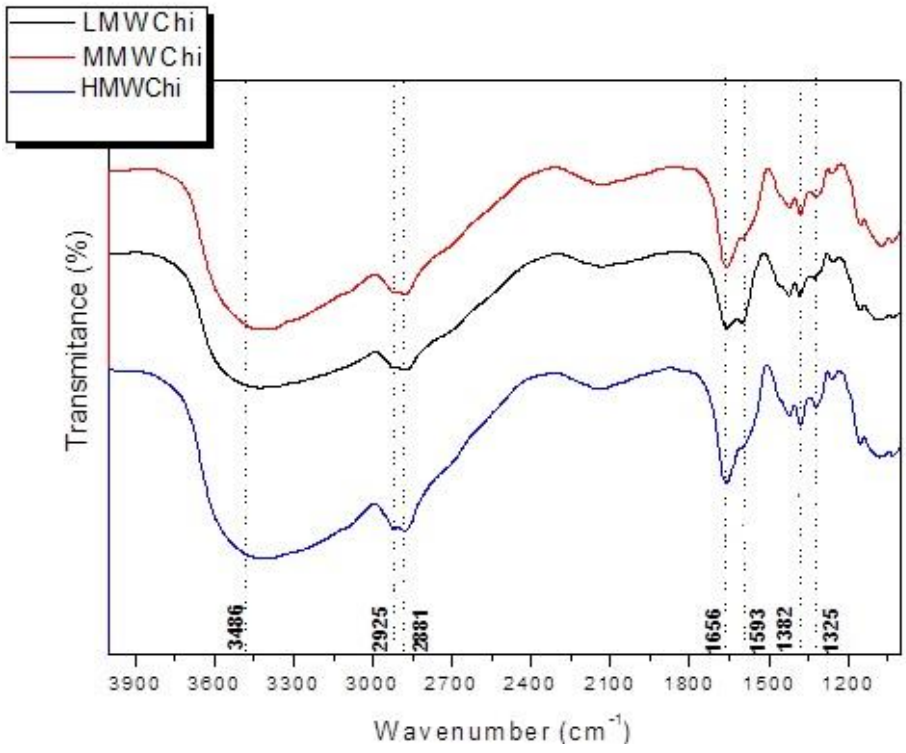

Figure 4.1. FTIR spectrum of the original LMW-, MMW- and HMWChi samples.

^{1}H NMR analysis provided information on the nature of the C-H bonds present in the sample and their positioning within the molecule. The peaks were assigned as follows: 2.0 - 2.2 ppm: methyl hydrogens, 3.1 - 3.4 ppm: hydrogen bonded to C2 of the

glucopyranose ring, 3.5- 4.1 ppm: hydrogen bonded to C3, C4, C5 and C6, 4.6 - 4.8 ppm: hydrogen bonded to C1 of the acetyl glucopyranose ring and 4.9 - 5.1 ppm: hydrogen bonded to C1 of the glucopyranose ring. The associated spectra are presented in figure 4.2.

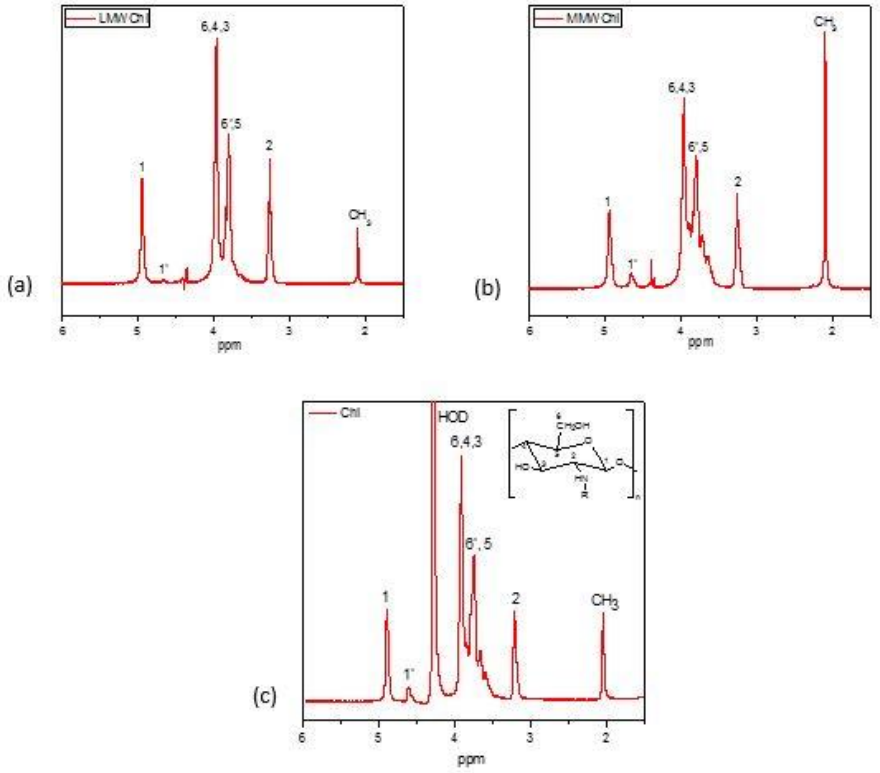

Figure 4.2. ^{1}H NMR data of (a) LMWChi, (b) MMWChi and (c) HMWChi samples.

The average degree of acetylation (DA) for chitosan was calculated from the ratio between the signal intensity for the hydrogens in CH_3 and the intensity for the hydrogen bonded to C2 of the glucopyranose ring. %DA = percentage of the degree of acetylation of the samples may be determined from equation 4.2:

Equation 4.2: $\%DA = \frac{\frac{CH_3}{3}}{HC2} * 100$

The degree of acetylation was also determined by titrimetric analysis using phenolphthalein as an indicator, as outlined by Tan *et al.*[4]. The results for degree of acetylation can be seen in table 4.2.

Sample	%DA
LMWChi	13
MMWChi	26
HMWChi	22

Table 4.2. % Degree of acetylation for LMW-, MMW- and HMWChi samples.

Thus, it may be seen that the properties presented in tables 4.1 and 4.2 highlight the anomalous behaviour noted for the HMWChi sample in that the data do not conform to the anticipated trend with varying molecular weight. As noted earlier, it is likely that the HMWChi sample consisted of a wide range of molecular weight materials rather than primarily being a single, high molecular weight material.

Based on these findings it was decided that subsequent use of HMWChi for the formation of IPNs in the work presented here would be somewhat limited.

4.2.2 Chi-TEOS IPNs

The LMW-, MMW- and HMWChi-TEOS IPN hydrogels were synthesised according to the method outlined in section 3.2.2 and membrane formation performed according to the description given in section 3.2.3. A slight difference in colour was observed with the LMW-, MMW- and HMWChi-TEOS IPNs; there was a slightly darker hue to the hydrogels with (apparent) increasing molecular weight. A more apparent difference was seen when comparing the 1:1, 1:2 and 1:3 LMWChi-TEOS IPNs (increasing the proportion of TEOS); a difference in the physical quality of the IPNs was noted by the viscosity of the hydrogel, which noticeably increased going from 1:1 to 1:2 to 1:3 LMWChi-TEOS IPN. The cloudiness of the solutions also increased in the same order. Figure 4.3 shows photographs of the three hydrogels in solution and figure 4.4 shows the resulting membranes which formed upon drying of the hydrogels. From figure 4.4 it may be seen that the membrane structure was very clearly compromised as the quantity of siloxane cross-linker in the IPN was increased- see in particular figure 4.4 (c) which shows that the membrane structure is completely disrupted for the 1:3 material. These observations are attributed to an increase in the mechanical strength and a consequent decrease in flexibility of the IPN with increasing

cross-linker concentration; these properties are discussed in more detail in section 4.2.5.

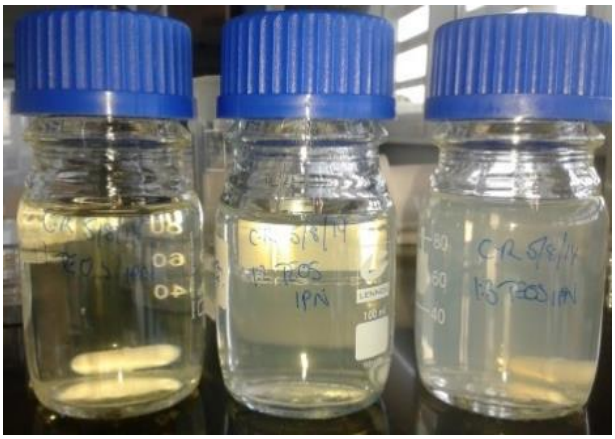

Figure 4.3. The three hydrogels in glass bottles; left to right, 1:1, 1:2 and 1:3 LMWChi-TEOS IPN respectively. Note that the cloudiness of the hydrogel increases with increasing quantity of TEOS used.

Figure 4.4. 1:1, 1:2 and 1:3 LMWChi-TEOS IPNs respectively. The images clearly show the film quality; 1:1 is fully intact and only slightly turned at the edges, 1:2 is intact but very tightly folded and broken at the edges and 1:3 is completely impaired and in separate pieces. These membranes were formed in standard 9 mm petri dishes.

4.2.3 SEM Analysis of Chi-TEOS IPNs

SEM analysis of both the 1:1 LMWChi-TEOS IPN and the 1:1 MMWChi-TEOS IPN was carried out as described in section 3.3.4; see figures 4.5 and 4.6, respectively. These images clearly reveal the smooth topology of the films while the thickness measurements suggest that the hydrogel forms membranes of uniform thickness when dried on a horizontal platform in an enclosed oven at 40 °C. These results also suggest that a slightly thicker membrane was formed with the higher molecular weight sample, figures 4.5 and 4.6.

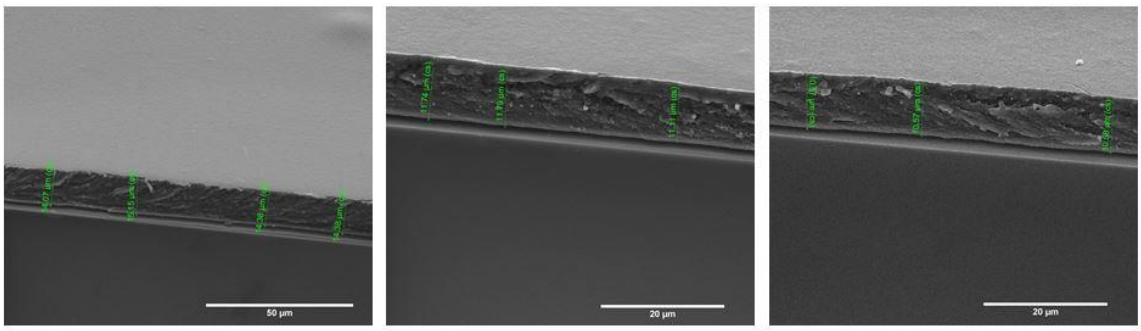

Figure 4.5. SEM images of a side view of a 1:1 LMWChi-TEOS IPN.

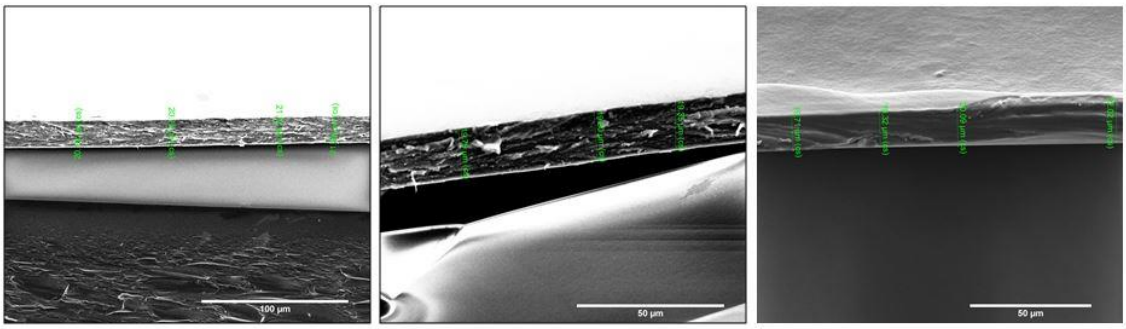

Figure 4.6. SEM images of a side view of a 1:1 MMWChi-TEOS IPN.

The thickness measurements yielded results of 12.4 µm ± 1.8 SD for LMWChi-TEOS IPN and 20.3 µm ± 0.9 SD for MMWChi-TEOS IPN. The formation of thicker film using the MMWChi material may result from the cross-linking of longer chains present in this material.

4.2.4 A Swelling Analysis for the Chi-TEOS IPNs

Three different types of swelling studies were carried out in order to compare and contrast the quality of the IPNs formed from the various types of chitosan. The first swelling study, see figure 4.7, compared the swelling ability of the LMW-, MMW- and HMWChi-TEOS IPNs directly. These measurements were carried out with phosphate buffers of pH 2.66 and 7.12. Despite the uncertainty in the structural quality of the HMWChi noted earlier, samples made with this material displayed the highest swelling ability, as determined from the so-called ‘swelling ratio’ (see section 3.2.5) upon transition from pH 2.66 to pH 7.12. This was closely followed by the medium molecular weight chitosan and then finally the low molecular weight chitosan respectively, suggesting that with the caveat regarding the HMWChi accepted, the swelling ratio increases with increasing chain length.

The second swelling study investigated how varying the amount of TEOS present in the IPN affected the swelling ability. As mentioned previously, the degree of cross-linking increases with increasing quantity of TEOS, with the chitosan contributing to the flexibility of the film and the TEOS contributing to the mechanical strength of the film. With this in mind, as expected, it was observed that the swelling ability decreased notably with increasing volume of TEOS added during IPN formation. This can be seen in figure 4.8.

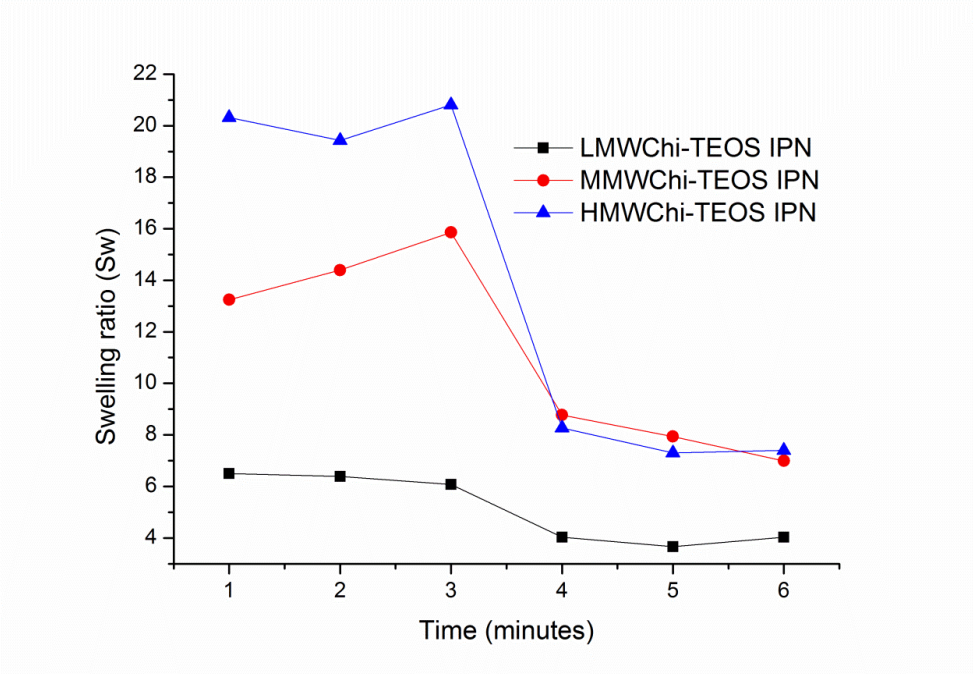

Figure 4.7. A comparison of swelling ability of LMW-, MMW- and HMWChi-TEOS IPNs. pH 2.66 phosphate buffer for minutes 0-3 and pH 7.12 phosphate buffer for minutes 3-6.

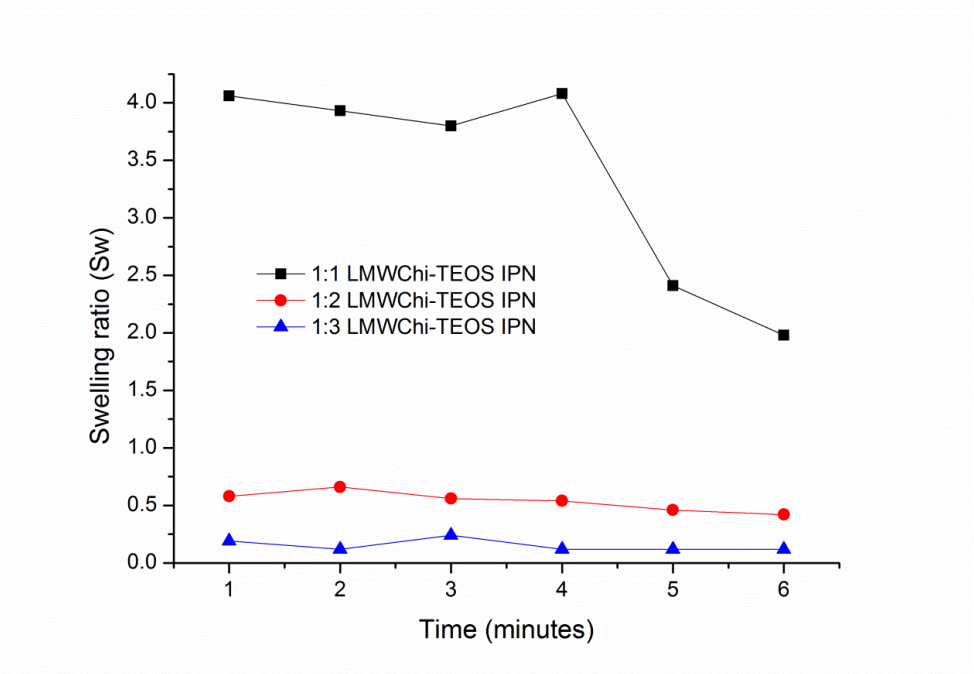

Figure 4.8. A comparison of the swelling abilities of 1:1, 1:2 and 1:3 LMWChi-TEOS IPNs. The quantity of TEOS in the IPN increases accordingly. pH 2.66 phosphate buffer for minutes 0-3 and pH 7.12 phosphate buffer for minutes 3-6.

The final swelling experiments examined the potential 'reusability' of the membranes by repeating the swelling tests on the same membrane with phosphate buffers of pH 2.66 and 7.12 over the course of seven days. The results confirmed that the membrane was reusable and the swelling characteristics remained essentially the same throughout, see figure 4.9.

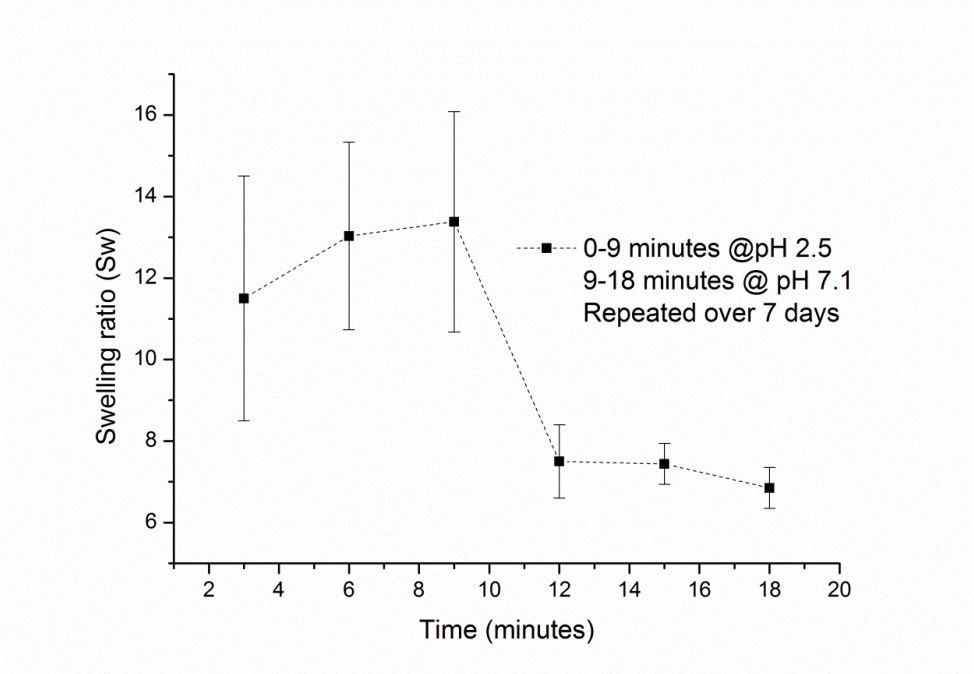

Figure 4.9. The reusability of Chi-TEOS IPN membranes in relation to pH changes made over a period of 7 days.

Based on these results, and in particular those depicted in figure 4.7, the LMW- and MMWChi-TEOS IPNs were selected as demonstrating the 'best' swelling characteristics, in terms of making hybrid photonic crystal samples since a limited degree of swelling was deemed to be more appropriate than the extensive swelling exhibited by the HMWChi-TEOS IPN. The reason for making this choice was based on the need to observe colour changes with changing pH, due to the expansion and contraction of the photonic crystal lattice. Although the degree of lattice expansion would be larger for a material based on HMWChi-TEOS, for most samples the subsequent shift in photonic band gap would move the Bragg peak into the near IR region of the spectrum. Of course, for a coloured to colourless transition such a material could be most suitable.

Other potentially useful attributes of the LMW- and MMWChi-TEOS IPNs include the low PDI and low degree of acetylation associated with them. It is for this reason that 1:1, 1:2 and 1:3 LMWChi-TEOS IPNs were utilized to compare the effect of increasing the quantity of added TEOS. A difference in the physical quality of the IPNs was observable by the viscosity of the hydrogel, which noticeably increased going from 1:1 to 1:2 to1:3 LMWChi-TEOS IPNs. As can be seen from figure 4.8, the swelling ability greatly reduced as the degree of cross-linking increased, so much so

that little difference was observed from pH 2.66 to pH 7.12. This result provides further evidence that the mechanical strength is enhanced and the flexibility is reduced as cross-linker concentration rises. The photographs of the resulting IPNs presented in figure 4.4 show the effect of increasing TEOS concentrations on film quality.

The main conclusion drawn from these preliminary results was that the LMWChi-TEOS IPN and MMWChi-TEOS IPNs were the most suitable materials for further studies and in particular those IPNs formed using a 1:1 chitosan: TEOS ratio.

4.2.5 Mechanical Tests on Chi-TEOS IPNs

Two different mechanical studies were performed on the IPNs. The first was aimed at comparing the tensile strength of the 1:1, 1:2 and 1:3 LMWChi-TEOS IPNs and the second was aimed at comparing the tensile strength of the LMWChi-TEOS IPN with that of the MMWChi-TEOS IPN. Initial tests were carried out using a tensile strength tester at the Applied Photonic Materials Unit in the National Institute of Materials Science, Tsukuba, Japan. They were performed on 10 mm x 40 mm strips clamped with silicone rubber supports. As can be seen from the results in table 4.3, as might be expected the tensile strength of the IPNs increases with increasing quantity of TEOS employed. This verifies that the siloxane network increases the mechanical tensile strength for the membranes. For the second mechanical study, an Instron mechanical tester was used. The tensile strength tests were performed on 10 mm x 40 mm strips clamped with PDMS supports cut to the size of the clamp. Figure 4.10 shows the resulting stress versus strain graph.

LMWChi-TEOS IPN	**Gauge length (mm)**	**Thickness (mm)**	**Width (mm)**	**Load (N)**	**% Deviation**	**No. of tests**	**Stress (MPa)**
1:1	2	0.02	10	7.1	35	10	35.5
1:2	2	0.02	10	8.7	22	10	43.7
1:3	2	0.02	10	18.2	25	10	91.0

Table 4.3. Data obtained from tensile strength tests carried out on 1:1, 1:2 and 1:3 LMWChi-TEOS IPNs.

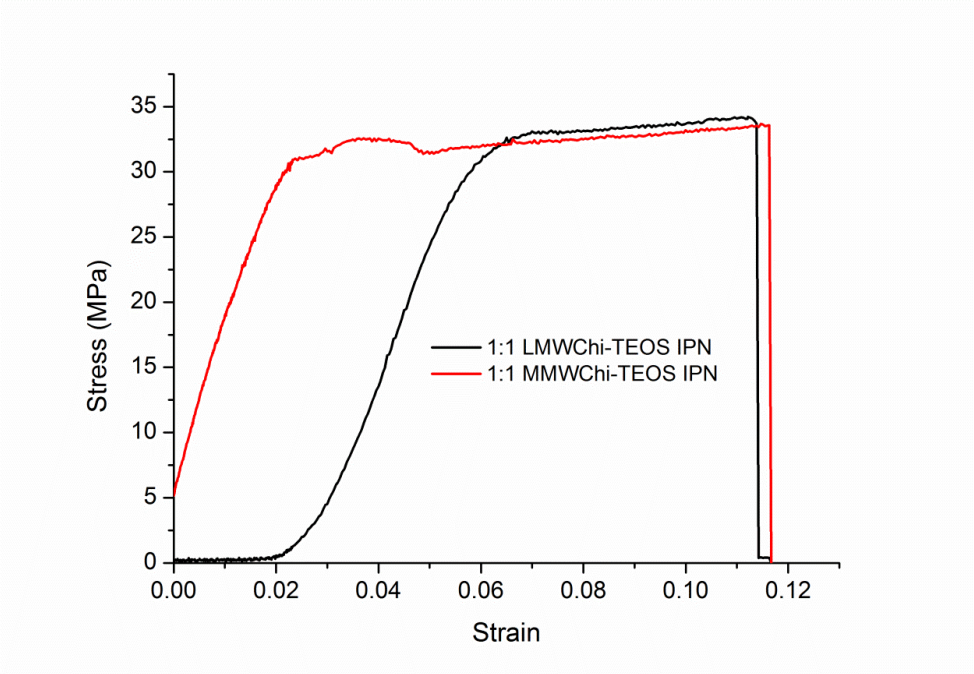

Figure 4.10. Stress vs. strain curve for 1:1 LMWChi-TEOS IPN and 1:1MMWChi-TEOS IPN.

The stress vs. strain curves for the 1:1 LMWChiTEOS IPN and the MMWChi-TEOS IPN exhibit similar properties. For both, the fracture point occurs at a stress (σ) of ca. 35.0 MPa, which was similar to the result 35.5 MPa for the 1:1 LMWChi-TEOS IPN (see table 4.3). Also, for both, the strain (ε) reached the same limit of about 0.12. For the 1:1 LMWChi-TEOS IPN the yield strength occurred at a strain of about 0.06 whereas for the 1:1 MMWChi-TEOS IPN the yield strength occurred at a strain of about 0.02. Plastic deformation of a material occurs when the yield strength has been reached; this means that a certain amount of deformation will remain even after the stress has been removed. This limit was reached at lower stress values for the MMWChi-TEOS IPN than for the LMWChi-TEOS IPN.

4.2.6 Conclusions

A variety of Chi-TEOS IPNs were fabricated and studied. There were two main variables in the synthesis of the IPNs; molecular weight (chitosan) and cross-linker (TEOS) concentration. Resulting composites were studied in terms of chemical composition, membrane quality and structure, swelling characteristics and tensile strength properties. Physical characterisation, swelling studies and tensile strength tests were carried out on the various IPNs, the results of which suggested that the

LMWChi-TEOS IPN and the MMWChi-TEOS IPN would be the best candidates for further work. Characterisation studies showed that these IPNs had higher PDIs than the high molecular weight chitosan; they also didn't swell to such a high degree as the HMWChi-TEOS IPN.

A TEOS to chitosan ratio of 1:1 was selected as the ratio to be applied in subsequent studies since it allowed for formation of a complete film, while the use of ratios of 1:2 and 1:3 resulted in the formation of incomplete films due to reduced flexibility and higher mechanical strength. Tensile strength tests showed that both the 1:1 LMWChi-TEOS IPN and the 1:1 MMWChi-TEOS IPN had similar mechanical characteristics, except that plastic deformation occurred at lower applied strain values for the 1:1 MMWChi-TEOS IPN. Thus, for certain applications the 1:1 LMWChi-TEOS IPN might have a slight advantage as it is more flexible.

4.3 Synthesis of SiO_2 Photonic Crystals

4.3.1 Silica Particle Synthesis via a Modified Stöber Method

A total of 89 Stöber syntheses were carried out with varying quantities of catalytic ammonium hydroxide used; the other experimental parameters were kept constant throughout as described in section 3.3.1. All syntheses were performed at room temperature. Figure 4.11and table 4.4 show the results of the successful syntheses including average particle diameter and SD.

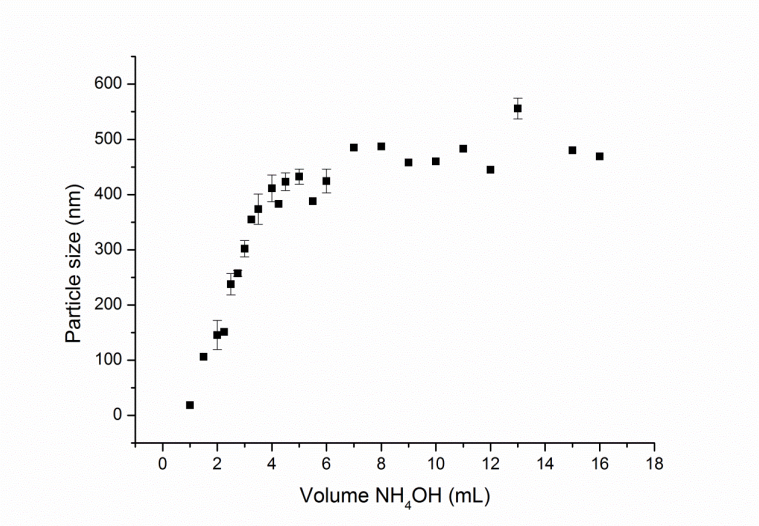

Figure 4.11. The relationship between the volume of NH_4OH used and the resulting SiO_2 particle size.

Volume NH_4OH (mL)	No. of experiments	Average particle size (nm)	Standard deviation (%)
1	1	18.5	-
1.5	1	106	-
2	5	145.5	26
2.25	1	151	-
2.5	4	237.6	19
2.75	3	257.6	5
3	15	302.2	15
3.25	1	355	-
3.5	4	373.8	27
4	10	411.5	24
4.25	1	383	-
4.5	4	423.3	16
5	4	432.5	14
5.5	1	388	-
6	2	424.5	21
7	1	485	-
8	1	487	-
9	1	458	-
10	1	460	-
11	1	483	-
12	1	445	-
13	2	556	19
15	1	480	-
16	1	469	-

Table 4.4. A summary of the results of a series of Stöber syntheses presented in order of volume NH_4OH employed.

Despite the fact that the Stöber synthesis is widely employed, figure 4.12 reveals that experience of performing such syntheses contributes towards the quality (as measured by uniformity or dispersity) of the particles produced. Figure 4.12 shows SEM images of samples made during a progressive series of experiments. For this series, a progressive improvement in sphere uniformity and dispersity is apparent as evidenced by analysis of the particle sizes and calculations of SD. Necessarily the experimental conditions employed, including the nature of the solutions used and the methods used to prepare the glassware used were kept constant throughout the series.

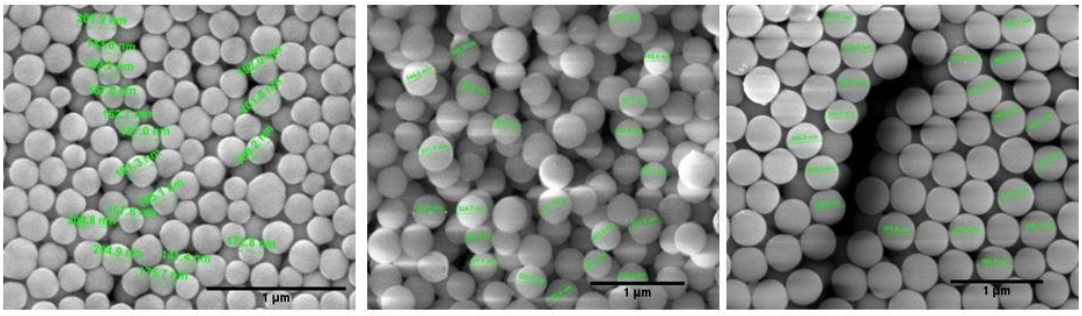

Figure 4.12. SEM images depicting particles prepared via a series of progressive Stöber syntheses. As can be seen, first efforts produced samples which were polydisperse and where the particles displayed obviously rough surfaces. However, as is also shown, subsequent experiments resulted in the production of more monodisperse assemblies of particles, possessing smoother surfaces.

4.3.2 Deposition Methods for the Production of Colloidal Photonic Crystals

Colloidal photonic crystals were deposited using the capillary enhanced under-oil method, the vertical controlled evaporation method and the large-scale vertical under-oil deposition method, see section 3.3.2.

Visually, the films formed by the vertical controlled deposition appeared both uniform and brightly coloured and also displayed structural colour variations as a function of viewing angle. The samples prepared by the vertical under-oil method also appeared visually uniform although variable structural colour was not so apparent. In contrast the visual appearance of the capillary-enhanced under-oil samples was uneven, showing only sparse regions of structural colour, indicating that not all of the sample

was suitably ordered. Figure 4.13 displays evidence of the presence of both ordered and disordered areas in the films prepared by the under-oil method, as determined using SEM. Figure 4.14 displays a series of photographs taken at different angles, from a sample prepared by the vertical controlled evaporation method, which illustrates the nature of the angle-dependent structural colour observed from this sample. Figure 4.15 displays a photograph of a large-scale, 100 mm × 200 mm sample, prepared by the vertical under-oil method.

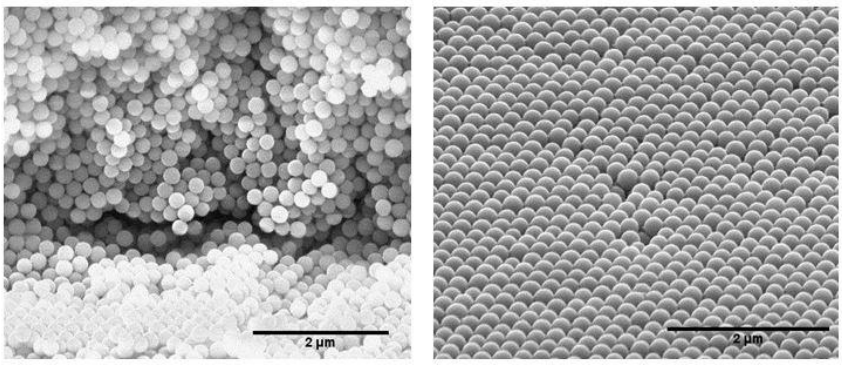

Figure 4.13. SEM images showing a disordered (100) plane and an ‘ordered’ (111) plane in a capillary-enhanced ‘under-oil’ sample.

Figure 4.14. Photographs taken from a photonic crystal sample prepared by the vertical controlled evaporation method using SiO_2 spheres of 299 nm diameter, on a 30 mm x 70 mm PET substrate as a function of angle of incidence.

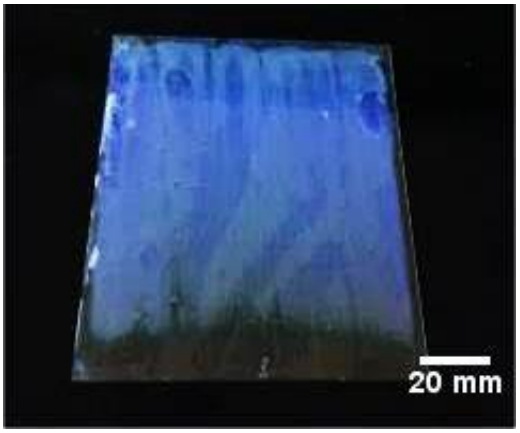

Figure 4.15. A photograph of a photonic crystal sample resulting from growth via the vertical under-oil setup; 210 nm diameter SiO_2 spheres were deposited onto a PET substrate of dimensions 100 mm × 200 mm. The device used to deposit this sample is shown in figure 3.1.

Figure 4.16 shows the transmission spectra of the three samples prepared by the three deposition methods described above. While all three display distinct Bragg transmission dips, the greatest percentage change in transmission at the wavelength associated with the Bragg dip was observed for the sample prepared by vertical controlled evaporation. From the previous discussion it is apparent that this method produced the most well-developed photonic crystal structure as evidenced by the clear changes in structural colour observed as a function of angle of viewing, see figure 4.14.

Figure 4.17 further supports this conclusion but in a more quantitative manner, showing the observed shift in the Bragg dip as a function of viewing angle. Figure 4.18 shows the linear relationship that can be generated between viewing angle and wavelength, by application of the Bragg-Snell equation, plotting $\sin^2\theta$ versus λ^2.

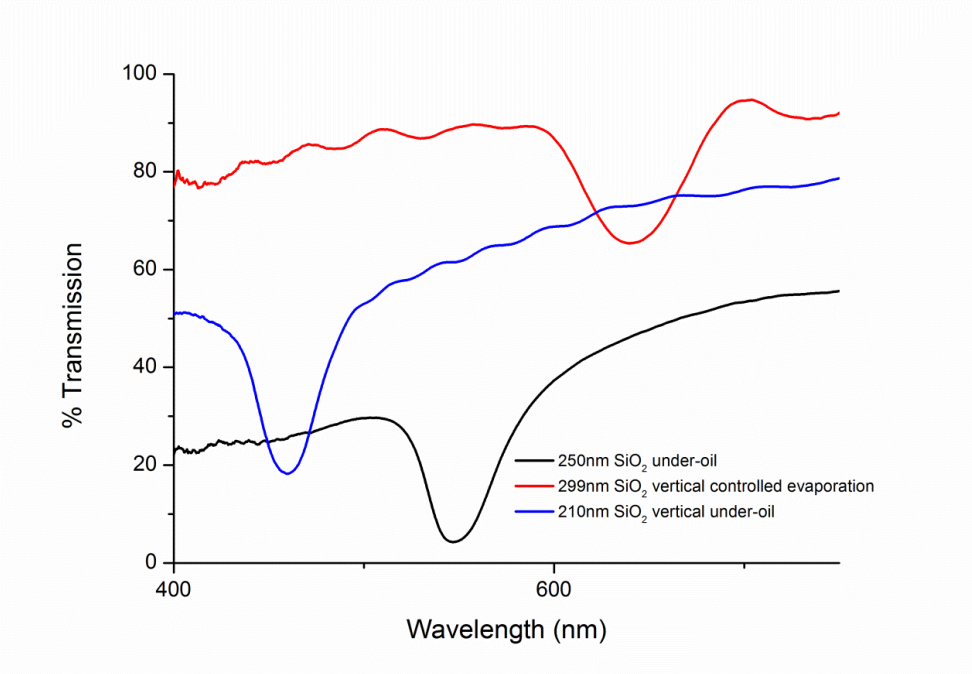

Figure 4.16. Transmission spectra of three different samples prepared using three different methods, see text and caption on the figure:

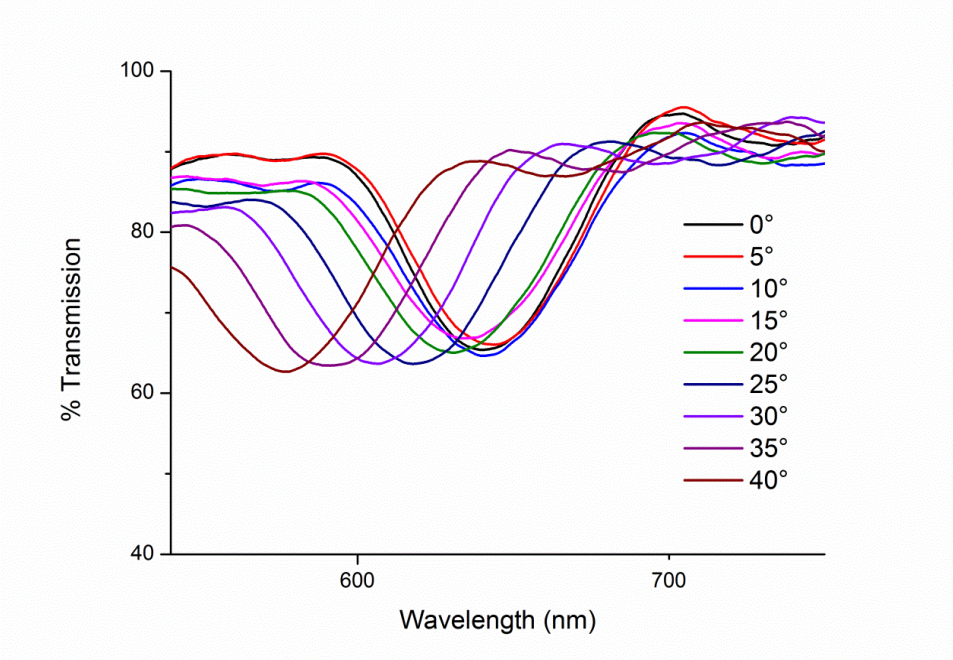

Figure 4.17. Transmission spectra obtained from a colloidal photonic crystal prepared using the vertical controlled evaporation method, using SiO_2 spheres of 299 nm diameter. This figure may be compared directly to the variations in structural colour observed for this sample, as shown in figure 4.14.

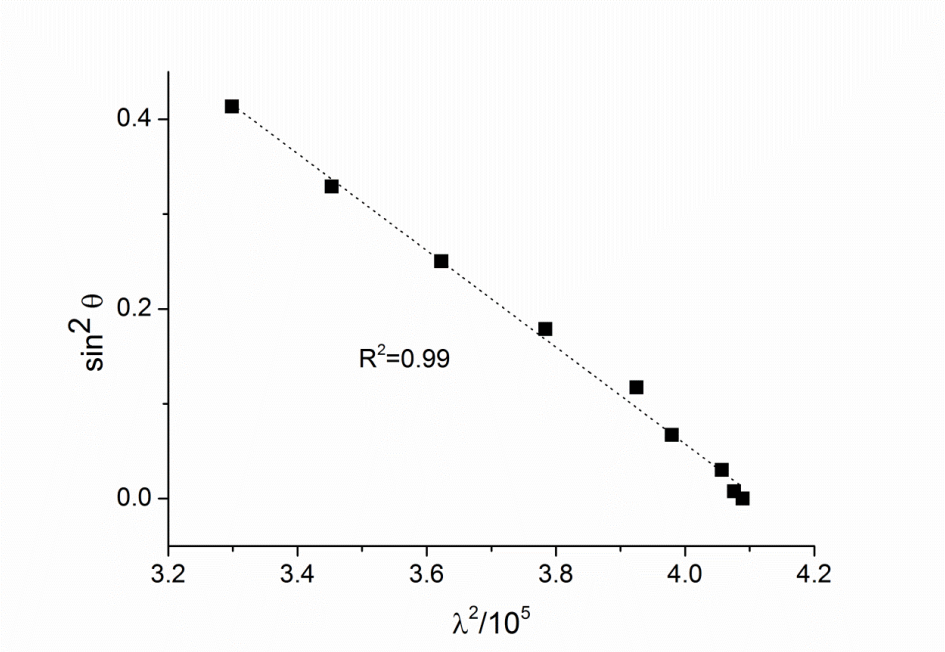

Figure 4.18. The relationship between Bragg diffracted wavelength (λ) and tilting angle (θ) for the SiO_2 colloidal photonic crystal sample described in figures 4.14 and 4.17.

The graph shown in figure 4.19 displays the relationship between periodicity (dependant on particle diameter, d) and the Bragg diffracted wavelength (λ) measured at an incident angle of 0°. A linear relationship is observed, also as expected from application of the Bragg-Snell equation. Previously it has been noted that the wavelength of diffracted electromagnetic waves should be roughly on the order of double the periodicity of the photonic crystal structure[5], so that λ/d is equal to about 2. Analysis of the results depicted in figure 4.19 showed that the average λ/d value for the photonic crystal samples prepared here was 2.24. however, the relationship between d and λ is also dependant on refractive index contrast as this may vary for differing materials of the same dimensions. This phenomenon was observed when comparing the optical results obtained for photonic crystal samples made from SiO_2 and PS spheres having the same diameter and hence also the same periodicity. Fudouzi *et al.*[6] recorded a Bragg peak wavelength of 550 nm for a PS photonic crystal made from spheres having a diameter of 202 nm, while according to the data presented in figure 4.19, by extrapolation, the Bragg peak wavelength for a SiO_2 photonic crystal made from spheres of diameter around 200 nm would occur near with the same periodicity appears at 450 nm. These values then provide different λ/ d values of 2.72

and 2.24, respectively. This phenomenon occurs due to the differing refractive indices of PS and SiO_2.

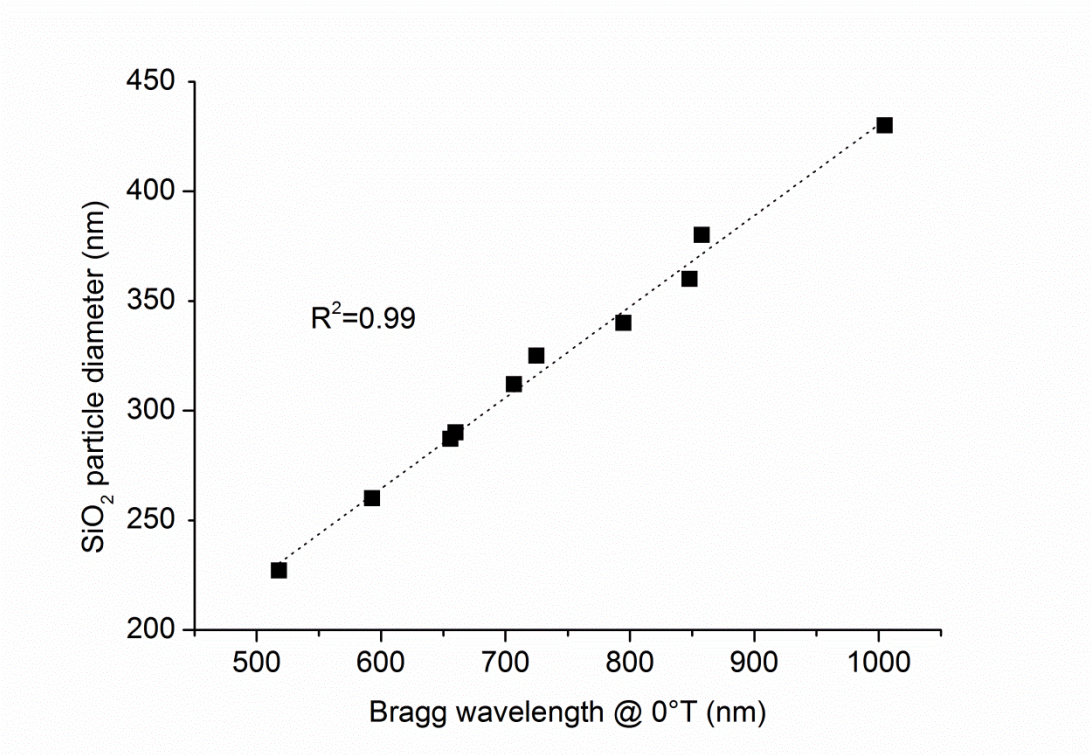

Figure 4.19. A graph showing the linear relationship between the periodicity (diameter) of the SiO_2 spheres used to make colloidal photonic crystals and the observed Bragg diffracted wavelength at an incident angle of 0°. This relationship arises directly from application of the Bragg-Snell equation.

4.3.3 Comparison of Substrates used for the Production of Colloidal Photonic Crystals

Vertical controlled evaporation was the deposition method used for the purposes of the investigations described in this section.

4.3.3.1 Glass Slides

The first substrates employed for the deposition of particles were glass slides. A 0.6 vol% solution was used. The SiO_2 particles deposited onto the surface in a uniform, ordered fashion. Visually the films appeared colourful and obvious colour changes were observed upon tilting the sample. Figure 4.20 shows a photograph of a SiO_2 colloidal photonic crystal film deposited onto a glass substrate using particles of ca. 380 nm diameter, which shows structural colour in the form of reflected green/ blue

light. SEM analysis of this film reveals an ordered fcc structure, characteristic of a SiO_2 opal.

Figure 4.21 shows the ordered fcc structure; the (100) planes and the (111) planes. Optical analysis of this sample revealed a prominent transmission dip which shifted upon rotating the sample from 0-40˚, figure 4.22. Calculation of the refractive index via application of the Bragg-Snell equation gave the result for n=1.49 and analysis of the Fabry-Pérot fringes suggested an average thickness equivalent to thirteen layers.

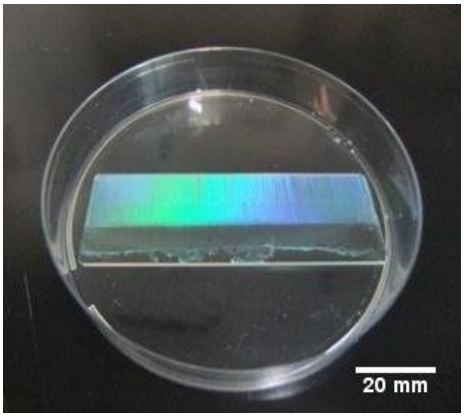

Figure 4.20. Photograph of an SiO_2 colloidal photonic crystal film on glass; the particle diameter was 380 nm. The blue-green colour observed is due to second-order diffraction.

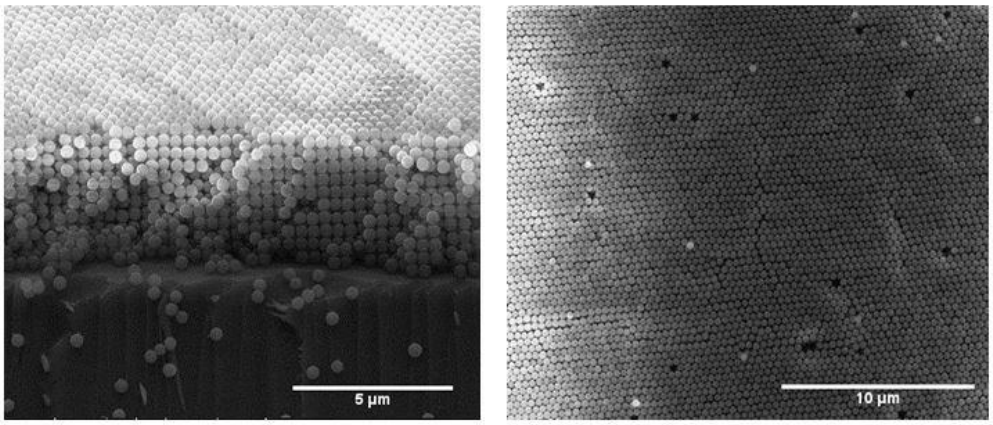

Figure 4.21. SEM images of the (100) and (111) planes of an SiO_2 colloidal photonic crystal on glass. Structural defects such as vacancies can be observed.

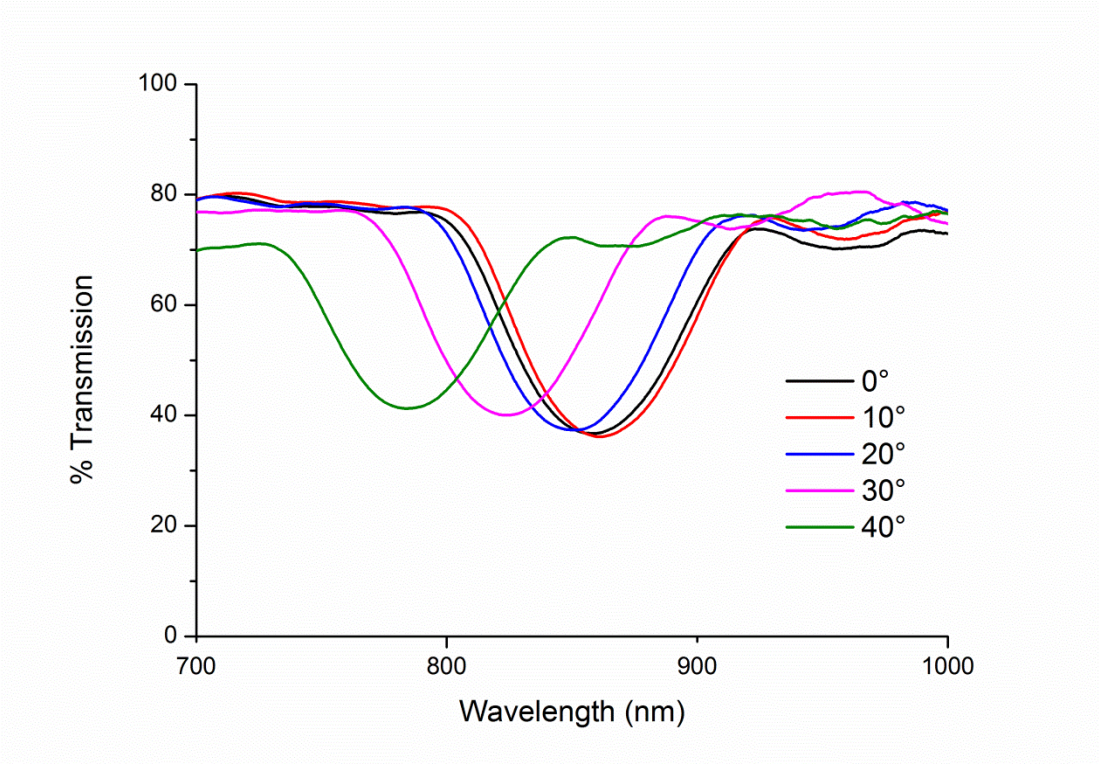

Figure 4.22. Transmission spectra from the SiO_2 colloidal photonic crystal film on glass (0-40˚). This data is a quantitative representation of the data presented in the photograph of this sample, figure 4.20.

4.3.3.2 Mica Slides

The first flexible substrate to be tested was Mica. Mica is a semi-flexible substrate with glass-like qualities. A 0.6 volume % solution with 312 nm diameter SiO_2 particles was used. The particles adhered to the surface of the Mica very well and visually the sample appeared very similar to the sample prepared on the glass slide- compare figure 4.23 with figure 4.20. The sample grown on Mica had a green/ violet appearance and colour changes were observed upon tilting the sample.

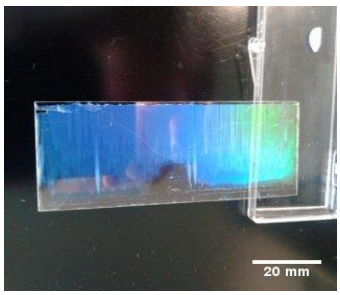

Figure 4.23. Photograph of a colloidal SiO_2 photonic crystal film on Mica; the particle diameter was 312 nm.

SEM analysis was performed after carefully cutting the sample. Mica is composed of thin layers of ruby muscovite and upon cutting the thin layers separated in certain areas. Figure 4.24 exhibits the (100) and (111) planes of the colloidal SiO_2 photonic crystal film formed on Mica respectively.

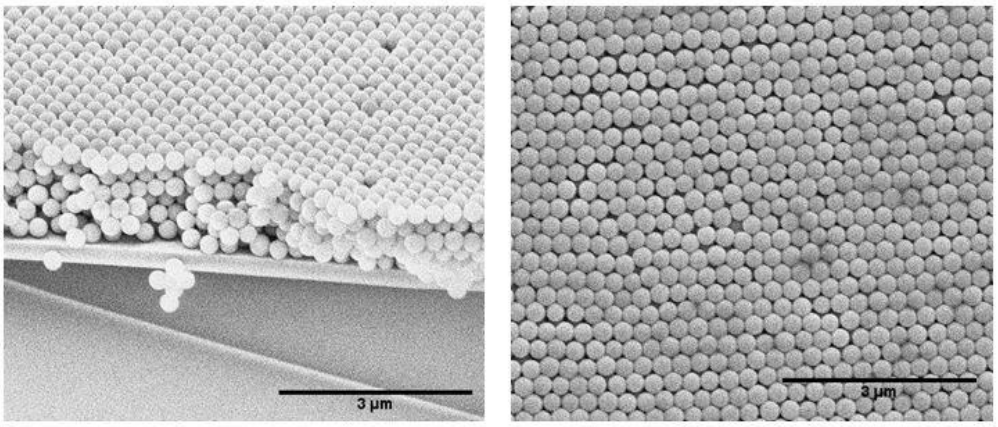

Figure 4.24. SEM images of the (100) and (111) planes of a colloidal photonic crystal film made with 312 nm diameter SiO_2 particles on Mica.

Optical analysis of this film showed the presence of clearly defined stop bands over the angular range from 0-40˚ together with somewhat indistinctive Fabry-Pérot fringes, figure 4.25. Calculations revealed the refractive index as n= 1.38, with an estimate of 24 layers in the film. These results suggest that using Mica as a substrate resulted in the formation of an ordered photonic crystal and hence also that Mica is a suitable flexible substrate for the formation of colloidal SiO_2 photonic crystals.

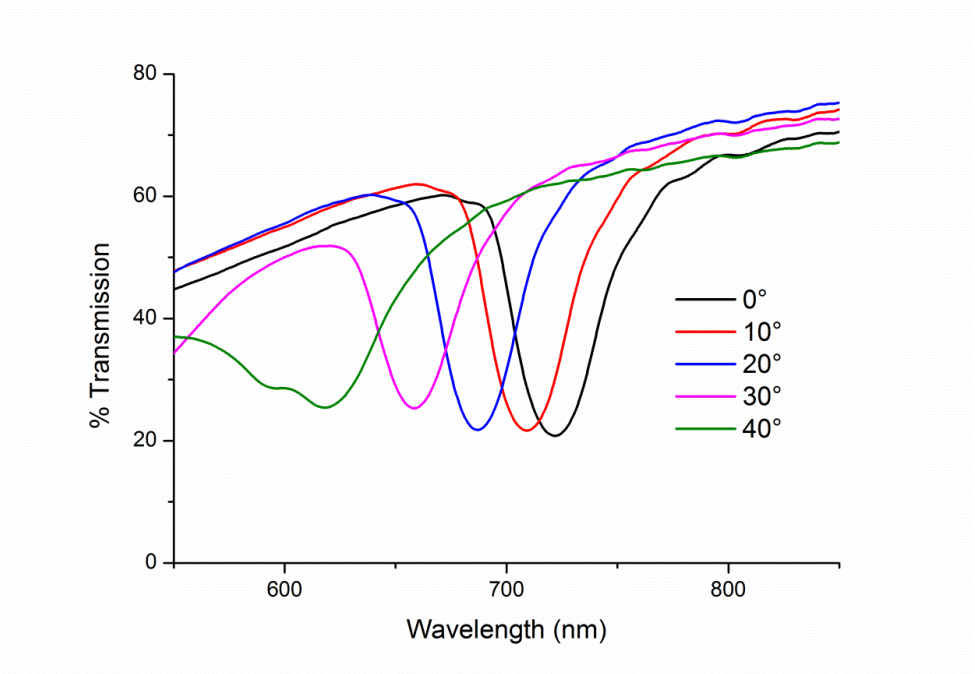

Figure 4.25. Transmission spectra from anSiO_2 colloidal photonic crystal deposited on Mica as a function of angle of incidence

4.3.3.3 Poly (methyl methacrylate) – PMMA sheets

The third substrate used was PMMA. A 0.35 volume % solution of SiO_2 particles having a diameter of 300 nm were employed. The film had a slightly pink appearance and a slight colour change was observed upon tilting the sample. Figure 4.26 displays a photograph of the resulting film.

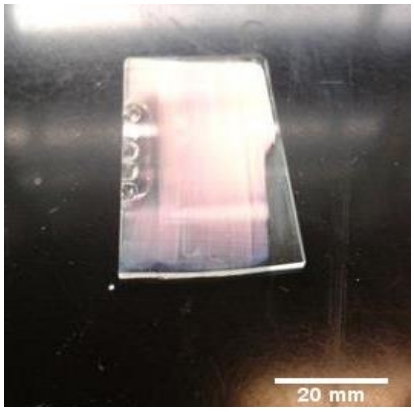

Figure 4.26. Photograph of an SiO_2 colloidal photonic crystal film deposited on PMMA; the particle diameter was 300 nm.

Due to the fragility of this specimen it was not possible to perform SEM analysis. Upon handling the samples shattered quite easily and so it wasn't possible to cut a

sample to size for SEM analysis. However, optical analysis was possible with careful handling of the sample. Figure 4.27 shows the transmission spectrum of the SiO_2 colloidal photonic crystal film deposited on PMMA. The spectrum displays quite poor transmission with no shift in stop band and a lack of Fabry-Pérot fringes. Both of these observations are strong evidence of a poorly ordered film.

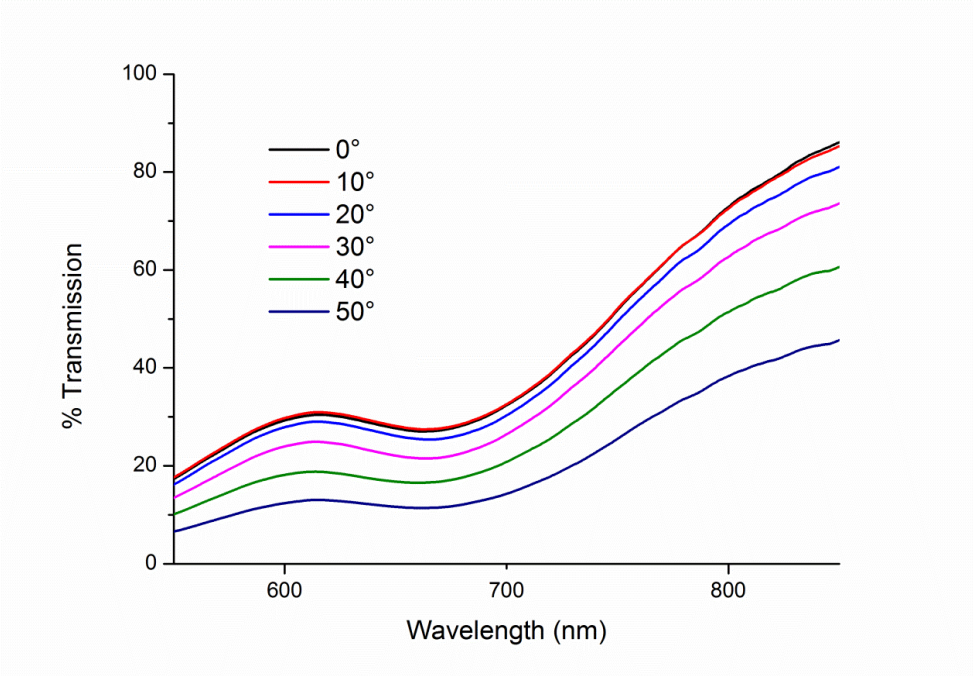

Figure 4.27. Transmission spectra from an SiO_2 colloidal photonic crystal film deposited on PMMA, as a function of angle of incidence

4.3.3.4 Polyethylene terephthalate – PET sheets?

The fourth substrate employed was PET (polyethylene terephthalate). A 0.65 volume % SiO_2 solution was used. The resulting photonic crystal film had a blue appearance and colour change to green was observed upon tilting the sample, as can be seen in figure 4.28. It was observed that the SiO_2 particles adhered to the surface of the PET more strongly than for PMMA and as a consequence the sample could be handled without signs of obvious damage. It is possible to speculate as to why PET appeared to be more suitable than PMMA as a substrate: this observation may be due to the 'moth-eye' surface effect of the PET substrate, shown in figure 4.28. The naturally rough surface shown may have provided anchor points to which particles could easily attach.

Optical analysis of this sample revealed prominent transmission dips at various wavelengths which varied with angle of incidence, as would be expected from application of the Bragg-Snell equation, figure 4.30.

This shift in the position of the stop band allowed for an estimate of the refractive index of the sample at n = 1.36 while the Fabry-Pérot fringes allowed for an estimate of the number of layers, at ca. 26.

These results suggest that the film formed on PET was well-ordered. Figure 4.31 reveals that application of the Bragg-Snell equation generated a linear relationship between viewing angle and Bragg diffracted wavelength for the sample described.

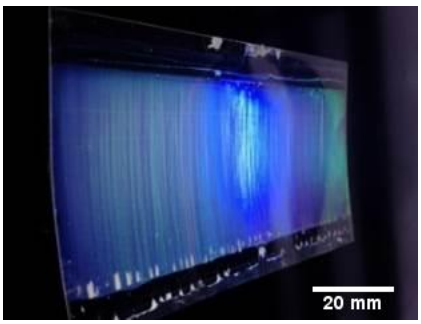

Figure 4.28. Photograph of an SiO_2 colloidal photonic crystal film on PET; the particle diameter was 312 nm.

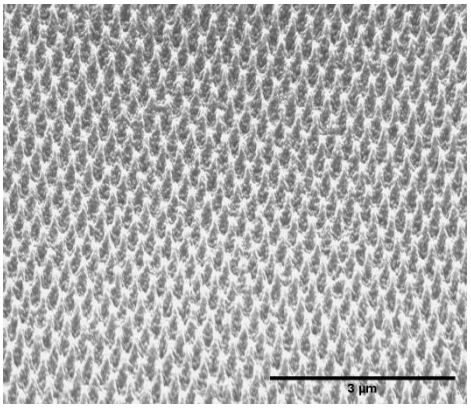

Figure 4.29. SEM image of a PET surface showing the ‘moth-eye’ morphology which may have influenced the adhesion of the SiO_2 spheres.

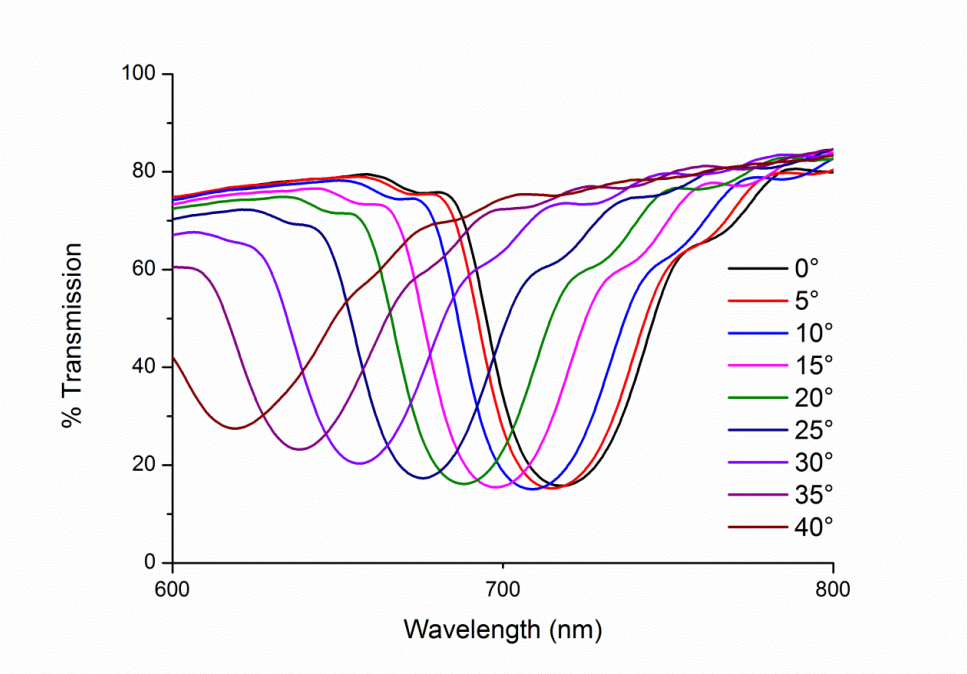

Figure 4.30. Transmission spectra of an SiO_2 colloidal photonic crystal deposited onto PET as a function of angle of incidence.

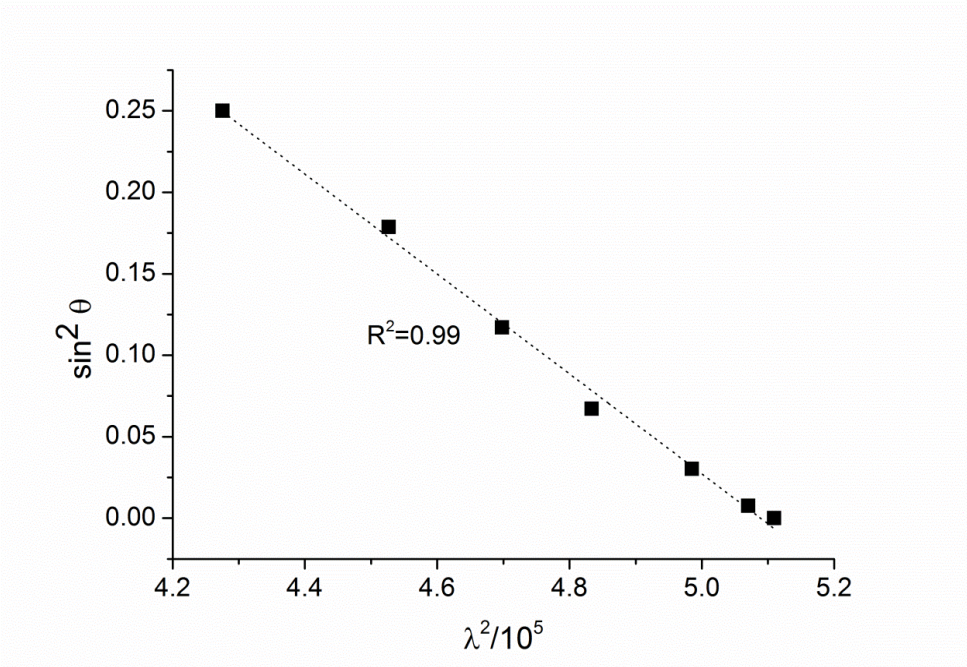

Figure 4.31. The relationship between Bragg diffracted wavelength (λ) and angle of incidence (Θ) for the spectra shown in figure 4.30, recorded from an SiO_2 photonic crystal sample prepared on PET using spheres of diameter 312 nm

4.3.4 Discussion

The results of the Stöber synthesis experiments show a clear correlation between the volume of ammonium hydroxide used and the diameter of the SiO_2 particles obtained. Upon analysing the samples after SiO_2 deposition it was evident that the most effective deposition method was the vertical controlled evaporation technique. This method produced the most uniform, ordered films. It has been observed that SiO_2 particles in the diameter range between 300-380 nm diluted in a 0.6-0.7 volume % solution produce good films on hydrophilic substrates via the vertical controlled evaporation technique. SiO_2 films containing about 20-30 layers assembled into fcc structures were fabricated. The optimum solution conditions identified were 3: 1 EtOH: H_2O. In terms of the substrates employed, it was observed that glass, PET and Mica were all suitable for particle deposition, whereas PMMA was not

4.4 Discussion and Conclusions

In section 4.2, the results presented suggest that the 1:1 LMWChi-TEOS IPN displayed the optimum properties in relation to the potential applications of chitosan-based IPNs of interest here.

For this reason, the 1:1 LMWChi-TEOS IPN was used in the subsequent experiments involving composite formation presented elsewhere in this thesis, combining the 1:1 LMWChi-TEOS IPN with a range of micro-/ nanoparticles and studying them with respect to their optical, mechanical and antimicrobial properties.

From section 4.3 it may be concluded that SiO_2 particles prepared by the modified Stöber method with diameters in the range of 300-380 nm were satisfactory for photonic crystal film growth by the vertical controlled evaporation method. Glass, MICA and PET are all suitable substrates for film growth, following pre-treatment to ensure the surface is hydrophilic. In contrast, PMMA does not appear to be a suitable substrate material.

The thesis now continues with the first of a series of more in-depth studies (Chapter 5), focusing on the study of a so-called Chi-TEOS-SiO_2 nanocomposite which was formed by combining the Chi-TEOS IPN hydrogel with a SiO_2 photonic crystal. This novel composite was studied as a possible material for sensing, taking advantage of

the interesting optical properties of the SiO_2 photonic crystal and the pH-sensitivity of the Chi-TEOS IPN.

The second more in-depth study (Chapter 6) is directed at the study of the mechanical properties of the chitosan composite materials, which were introduced in section 4.2.5, extending the list of compounds by adding further micro-/nanoparticle cross-linkers (as before). The aim here was to see if the tensile strength could be improved without jeopardising the structural integrity of the Chi-TEOS IPN.

The final more in-depth study (Chapter 7) presents a detailed analysis of the structural properties of the Chi-TEOS IPN, with a view to throwing some light on the nature of the chemical processes that occur upon cross-linking. It is in this study that the antimicrobial properties of the Chi-TEOS IPN are investigated, with the addition of metal nanoparticles which should have their own inherent antimicrobial properties.

References

1. Rinaudo, M.; Milas, M.; Dung, P. L., Characterization of chitosan. Influence of ionic strength and degree of acetylation on chain expansion. *International Journal of Biological Macromolecules* **1993,** *15* (5), 281-285.

2. Kasaai, M. R., Calculation of Mark–Houwink–Sakurada (MHS) equation viscometric constants for chitosan in any solvent–temperature system using experimental reported viscometric constants data. *Carbohydrate Polymers* **2007,** *68* (3), 477-488.

3. Ge, H.-C.; Luo, D.-K., Preparation of carboxymethyl chitosan in aqueous solution under microwave irradiation. *Carbohydrate Research* **2005,** *340* (7), 1351-1356.

4. Tan, S. C.; Khor, E.; Tan, T. K.; Wong, S. M., The degree of deacetylation of chitosan: advocating the first derivative UV-spectrophotometry method of determination. *Talanta* **1998,** *45* (4), 713-719.

5. Foteinopoulou, S., Viewpoint: Photonic Crystals "Go Hyper". *Physics* **2014,** *7*, 110.

6. Fudouzi, H., Fabricating high-quality opal films with uniform structure over a large area. *Journal of Colloid and Interface Science* **2004,** *275* (1), 277-283.

5. Journal Article - "Silica-based photonic crystals embedded in a chitosan-TEOS matrix: preparation, properties and proposed applications"

This paper was written in Autumn-Winter 2015 and was accepted for publication by the Springer Journal of Materials Science in February 2016. It is a combination of properties of the Chi-TEOS IPN in combination with SiO_2 photonic crystals, the final composite structure is proposed as a pH-sensitive optical sensor for aqueous systems. The research was carried out in a variety of labs in Tyndall National Institute in Cork, the Institute of Physics (USP) in Sao Carlõs and the National Institute of Materials Science in Tsukuba. The authors and their contributions are given below:

C. C. Ryan[1, 2] – SiO_2 photonic crystal synthesis, chitosan thin film formation, composite formation, all analysis, production and corrections to paper

J. A. M. Delezuk[3] – Composite formation, initial composite analysis, corrections

A. Pavinatto[3] – Chitosan characterisation and corrections

O. N. Oliveira Jr.[3] – Supervision and corrections

H. Fudouzi[4] - Supervision and corrections

M. E. Pemble[1, 2] - Supervision and corrections

M. Bardosova[1] - Supervision and corrections

[1]Tyndall National Institute, University College Cork, Lee Maltings, Prospect Row, Cork, Ireland

[2]Department of Chemistry, University College Cork, Cork, Ireland

[3] Institute of Physics São Carlos, University of São Paulo, CP369, São Carlos, SP, Brazil

[4] National Institute of Materials Science, 1 Chome-2-1 Sengen, Tsukuba, Ibaraki Prefecture 305-0047, Japan

Abstract

Our research involves the development of a pH-sensitive chitosan – tetraethyl orthosilicate interpenetrating polymer network (Chi-TEOS IPN) suitable for the introduction of ordered silica nanoparticles. The pH-sensitive properties of the IPN provide an innovative framework for ordered colloidal silica (SiO_2) films known as photonic crystals. The pH-sensitive properties of chitosan occur naturally due to its cationic polyelectrolyte structure; cross-linking with TEOS provides mechanical strength and incorporation of the silica photonic crystal provides a means of optical detection for a pH-driven expansion mechanism. Chi-TEOS-SiO_2 composites are formed through a three-step mechanism in which the silica photonic crystal and Chi-TEOS IPN hydrogel are synthesised separately and then combined to form the Chi-TEOS-SiO_2 composite. The silica photonic crystals, IPN membranes and final composite structures were analysed separately through optical, mechanical and swelling studies. Through the successful fabrication of a chitosan-tetraethylorthosilicate-silica (Chi-TEOS-SiO_2) composite we propose a membrane suitable for applications in environmental, chemical and biological sensing of pH.

Keywords

Silica, photonic crystal, chitosan, interpenetrating polymer network, composite, pH-sensitive

5.1 Introduction

Photonic crystals are materials constructed of nanoscale colloidal particles which self-assemble to form an ordered crystal lattice structure. Being on the order of the wavelength of visible light means that various light interactions occur, resulting in the observation of visible colour from the photonic crystal, with the colour observed depending on the diameter of the colloidal particles which form the crystal lattice structure. A key characteristic of a photonic crystal is refractive index (or dielectric constant) contrast[1, 2]. Synthetic opals are constructed by the bottom-up self-assembly of uniform colloidal particles; such as SiO_2, PS (polystyrene) or PMMA (polymethyl methacrylate), and the inverse of their structures are fabricated through the top-down approach. The primary approaches include controlled evaporation and layer-by-layer assembly. Photonic crystals composed of colloidal SiO_2 particles, as well as other materials are utilized for their interesting optical properties as the regularly repeating crystal lattice interacts with light of different wavelengths depending on the dimensions of the crystal lattice[3].

Chitosan is formed by the deacetylation of chitin in the presence of alkali hydroxides such as sodium hydroxide. The conversion process doesn't lead to 100% deacetylation. Generally, once the average degree of deacetylation exceeds 50% the polysaccharide structure is referred to as chitosan[4]. With the majority of acetamido groups replaced by amino groups, chitosan, with less hydrogen-bonding sites available, becomes more susceptible to protonation and so it becomes acid-soluble.

The formation of a composite membrane consisting of chitosan and SiO_2 particles is the principal investigation of the current study. In order to exploit the pH-sensitive characteristics of chitosan the membrane must be stable in solution, for this reason an interpenetrating polymer network (IPN) comprised of chitosan and tetraethylorthosilicate (TEOS) was researched. Synthesis of such IPN was first described by Park *et al.*[5]. The experimental method involves the preparation of a hydrogel comprised of chitosan in aqueous acid solution and TEOS in the presence of concentrated acid. Chitosan dissolves in aqueous acid and TEOS forms so-called 'strands' of linear molecules in the presence of acid[6, 7]. When combined the IPN has two distinct characteristic; flexibility due to the presence of chitosan and mechanical strength due to the presence of TEOS. The main study conducted by Park *et al.*

involved swelling studies on IPNs of varying chitosan: TEOS ratio, namely 1:1, 1:2 and 1:3. It was observed that the degree of swelling decreased with increasing TEOS concentration. Similar results were obtained in a study on chitosan hydrogels cross-linked with glutaraldehyde[8] with swelling ability decreasing with increasing cross-linker concentration; here the reduction in swelling is attributed to the structure being more compact.

Successfully introducing colloidal particles into a stimuli-sensitive framework, such as a chitosan-TEOS interpenetrating polymer network (Chi-TEOS IPN), allows for manipulation of the lattice structure as the crystal lattice would be expected to swell and shrink as the framework reacts to external stimulus. As the crystal lattice swells/ shrinks a shift in the Bragg diffracted wavelength of visible light reacting with the lattice should be observed. In order to exploit the optical properties of a photonic crystal embedded in an IPN the colloidal silica particles which make up the photonic crystal must be ordered in an fcc orientation, chitin/chitosan-silica composites have been reported in the past but without an ordered crystal structure[9, 10]. There are three key variables in the formation and study of composite membranes such as described above; hydrogel material, colloidal suspension and external stimulus. For example Asher *et al.* prepared their polymerized crystalline colloidal arrays (PCCA's) employing acrylamide as hydrogel material, polystyrene as colloidal material and pH and ionic strength as external stimuli[11]. Wu *et al.* prepared a chitosan composite with polystyrene nanoparticles incorporated, in this case water as external stimulus and varying particle size allow for a tunable stop band and observable colour[12]. Our aim involves preparing Chi-TEOS IPNs using chitosan sources of varying molecular weight. Analysis of these membranes should allow us to decipher which type of chitosan gives the best results as a candidate for the incorporation of an ordered silica photonic crystal and hence the formation of a pH-sensitive Chi-TEOS-SiO_2 composite.

Applications of an inorganic-organic composite such as the Chi-TEOS-SiO_2 composite described above would be in the areas of environmental, chemical and biological sensing. Due to the pH-sensitivity of the IPN the composite would be an ideal proton detection system in aqueous conditions, the SiO_2 photonic crystal lattice would then be expected to swell and shrink with the IPN providing a colour change or shift in Bragg wavelength as an indicator for particular pH conditions. The pH range of aqueous, biological and environmental systems is quite broad depending on the

function of the pH, with functions ranging from neutralization and protection in the body[13] to animal or plant growth and survival in bodies of water[14, 15]. The composites under development are proposed as a functional material for quick pH testing of such environments.

5.2 Materials and methods

5.2.1 SiO_2 photonic crystal synthesis, film growth and analysis

The procedure for the modified Stöber method involves a standard recipe in which the volume of ammonium hydroxide is the key variable. >99.0% TEOS and 28-30% NH_4OH were purchased from Sigma-Aldrich, Ireland. A solution containing 60 mL EtOH and 20 mL TEOS is prepared in a 100 mL glass bottle and allowed to stir at moderate speed for 2-3 hours. After 2-3 hours a second solution containing 52 mL H_2O and 68 mL EtOH/ NH_4OH is prepared and allowed to stir for 10 minutes. After 10 minutes solution 1 is poured into solution 2 and this mixture is allowed to stir for >12 hours. It can be observed that the solution turns white after a few minutes, indicating the formation of a colloidal suspension. After allowing the colloidal suspension to stir for >12 hours it must be put through a series of washes with EtOH and H_2O with intermittent centrifugation and sonication.

The substrate employed for film growth is PET (polyethylene terephthalate). This is rinsed with EtOH and Millipore H_2O and dried with N_2 gas prior to deposition. The deposition technique employed is vertical controlled evaporation and is carried out in an enclosed oven at 55-60°C. It is adapted from a method by Jiang *et al.*[16]. A SiO_2 solution of desired concentration and volume is prepared by diluting the SiO_2 suspension in 3:1 EtOH: H_2O. The SiO_2 solution of desired concentration and volume is prepared in a suitable beaker; the PET substrate is then carefully submerged into the SiO_2 solution and kept at a fixed angle of about 25°. The solution and substrate are left undisturbed in the enclosed oven for a fixed time depending on solution volume and substrate dimensions.

Analysis of the SiO_2 film must be carried out to determine the quality of the crystal structure; scanning electron microscopy (SEM) and optical analysis are the two essential methods. Upon analysing the results of these methods, it is possible to compare quality on the microscopic structural scale versus the optical scale. SEM

analysis provides vital information associated with the size of the particles, the order and uniformity of the structure, the thickness of the sample, the structure of the substrate and the presence of impurities or defects; it is an excellent visual aid. SEM analysis is carried out using an FEI Quanta 650 FEG High Resolution Scanning Electron Microscope. Optical analysis of the photonic crystal film is very important in revealing information associated with the quality and structure. Transmission and reflection analysis are carried out using Ocean Optics hardware and Spectra Suite software.

5.2.2 Chi-TEOS IPN formation and analysis

The IPN hydrogel is formed by a cationic solution polymerization technique in mildly acidic solution. The method is based on experimental work carried out by Park *et al.*[5]. Water is the primary solvent. Initially three separate solutions are prepared and allowed to stir at room temperature: (1) 1.04 g chitosan in 65 mL H_2O with 1 wt% CH_3COOH, (2) 1.04 g TEOS in 15 mL EtOH and (3) 25 mL H_2O and 10 mL EtOH with 0.1 wt% conc. HCl. Solution 3 is slowly added to solution 2 with stirring. The resulting mixture and solution 1 are left under continuous stirring at room temperature for 24 hours. After 24 hours the aqueous chitosan solution is slowly added to the TEOS solution under continuous stirring, this final solution is then left to stir for a further 48 hours.

This method results in a 1:1 Chi-TEOS IPN. Changing the ratio to 1:2/1:3 simply involves doubling/tripling the quantity of TEOS used. For the purpose of our experiments the three following types of chitosan were used in preparing the 1:1 Chi-TEOS IPNs: low molecular weight (LMWChi), medium molecular weight (MMWChi) and high molecular weight (HMWChi). LMW- and MMWChi were purchased from Sigma-Aldrich, Ireland and HMWChi was purchased from Galena, Brazil. 1:1, 1:2 and 1:3 IPNs were prepared employing LMWChi.

For membrane formation the desired amount of Chi-TEOS IPN is carefully drop-cast on to the substrate of choice using a plastic dropper. The substrate bearing the Chi-TEOS IPN is placed in an oven at 40°C. Depending on the size of the membrane, formation and drying may take a couple of hours to a couple of days. Upon completion the membrane can easily be peeled off the substrate surface.

Swelling studies and tensile strength tests are the methods utilized for analysis of the membranes. Phosphate buffers of pH 2.66 and 7.12 were freshly prepared and used for the swelling studies experiments carried out on the Chi-TEOS IPN membranes. $S_w = (W_t - W_o)/ W_o$, where W_o and W_t are the membrane's original weight and the weight after being immersed in solution for time, t.

Tensile strength tests were carried out using a desk-type Imada Mechanical Tester. Membranes are cut to dimensions of 40 mm x 10 mm and clamped using silicone rubber supports cut to the size of the clamps. This allows for sufficient gripping without interfering with the physical quality of the membrane. Tests are carried out on multiples of the same membranes e.g. 10 repeats. Experimental parameters are all kept constant to ensure results are obtained within a strict standard.

5.2.3 Fabrication of Chi-TEOS-SiO_2 composite

The sample is placed on a horizontal platform under vacuum at 40˚C with the desired amount of IPN hydrogel drop-cast onto the surface. When the SiO_2 film is first covered with the Chi-TEOS IPN colour is no longer observed however upon drying the color is observed again.

SEM analysis was employed to analyze the SiO_2 films both before and after infilling in order to provide a direct observation of the film and infilling quality. Optical analysis of the Chi-TEOS-SiO_2 composite membranes was also carried out both before and after infilling the SiO_2 film with Chi-TEOS IPN. This allowed for direct comparison of the film quality from the resultant transmission spectra.

5.3 Results and Discussion

5.3.2 SiO_2 photonic crystal synthesis, film growth and analysis

Results obtained from the modified Stöber method apply to a broad range of NH_4OH volumes and repetition of synthesis at each volume to ensure the reliability of results. Measuring the particles using the SEM is a reliable method as it gives valuable insight into the morphology of the particles and allows measurement of many particles. Photonic crystal films composed of SiO_2 nanoparticles were successfully grown on PET utilizing the vertical controlled evaporation technique. The high quality of the SiO_2 film is evident from the photo in figure 5.1(a) which displays the bright iridescent colours; characteristic of structural colour. Figure 5.1(b) displays the linear

relationship between Bragg wavelength and tilting angle, extracted from figure 5.1(c). The 0° transmission dip in figure 5.1(c) displays a narrow Bragg dip with high percentage transmission; this along with the presence of Fabry-Pérot fringes gives evidence of the ordered internal structure[17, 18].

(a)

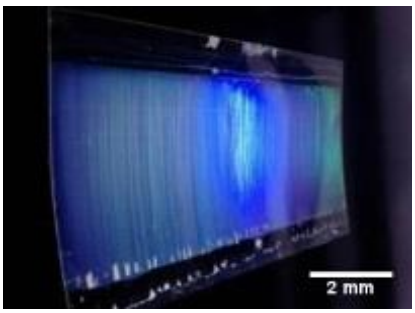

(b)

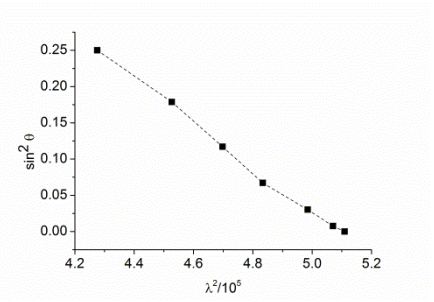

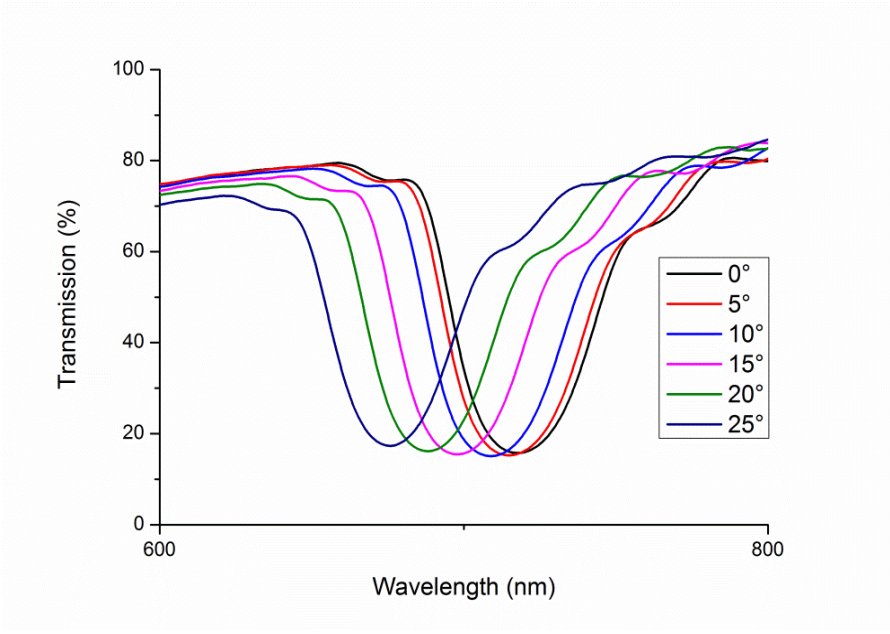

(c)

Figure 5.1. (a) Photonic crystal obtained by vertical controlled evaporation of 0.65 volume % 312nm SiO_2 on 4cm x 7cm PET substrate. (b) Relationship between Bragg diffracted wavelength (λ) and tilting angle (ϴ). (c) Transmission spectrum of SiO2 photonic crystal film on PET, photo in figure 5.1(a).

5.3.3 Chi-TEOS IPN formation and analysis

As expected the weight average molecular weight (Mw) increases accordingly from low to high molecular weight chitosan. However, the results for intrinsic viscosity (η), viscosity average molecular weight (Mv) and polydispersity index (PDI) suggest a broad distribution of molecular weights for the high molecular weight chitosan. It is likely that the high molecular weight chitosan is composed of quite a variance of

molecular weights rather than primarily high molecular weight. Due to the fact that there is still a certain average degree of acetylation (DA) in each chitosan sample all the resulting membranes will have an atactic structure. This analysis was carried out prior to formation of IPN. Data can be observed in table 5.1.

Sample	**Mw($gmol^{-1}$)**	**η(mLg^{-1})**	**Mv($gmol^{-1}$)**	**DA(%)**	**PDI**
LMWChi	140,300	442(±3)	89,832	13	1.9
MMWChi	312,300	586(±9)	134,841	26	2.3
HMWChi	479,000	377(±9)	75,470	22	4.2

Table 5.1. Data corresponding to LMW-, MMW- and HMWChi samples.

Two different types of swelling studies were carried out in order to compare and contrast the quality of the IPNs formed from the various types of chitosan. The first swelling study, see figure 5.2, compares the swelling ability of the LMW-, MMW- and HMWChi-TEOS IPNs directly (low, medium and high molecular weight chitosan-TEOS interpenetrating networks, respectively). These were carried out with 20 mM phosphate buffers of pH 2.66 and 7.12. HMWChi displays the greatest swelling ability upon transition from pH 2.66 to pH 7.12, probably due to the broad distribution of molecular weights. This is closely followed by the medium molecular weight chitosan and low molecular weight chitosan respectively in order of decreasing chain length. The second swelling study conducted was looking at how varying the amount of TEOS present in the IPN affected the swelling ability. The degree of cross-linking increases with increasing quantity of TEOS, with chitosan contributing to the flexibility of the film and TEOS contributing to the mechanical strength of the film it was observed that the swelling ability decreased notably with increasing volume of TEOS. This can be seen in figure 5.3

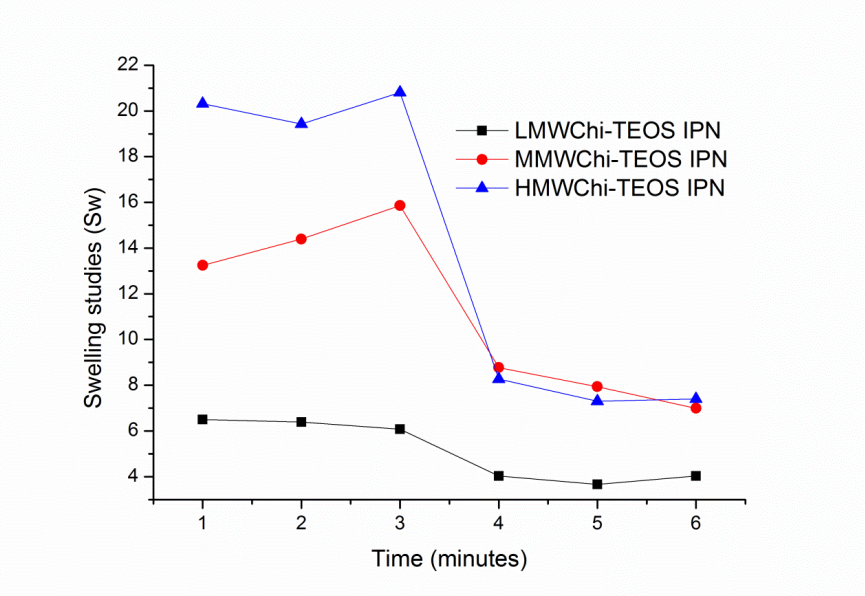

Figure 5.2. Comparison of swelling ability of LMW-, MMW- and HMWChi-TEOS IPNs. 1-3 minutes at pH 2.66 and 4-6 minutes at pH 7.12.

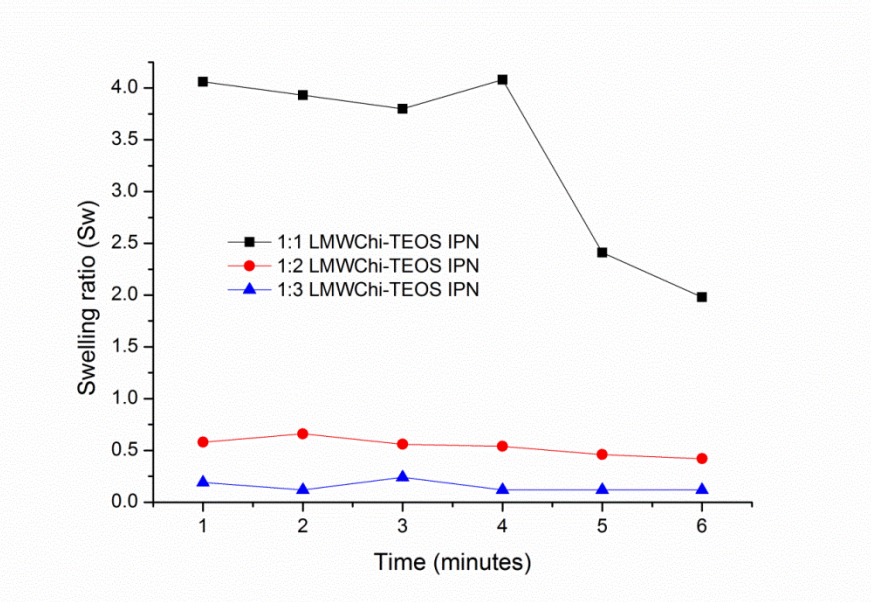

Figure 5.3. Comparison of swelling abilities of 1:1, 1:2 and 1:3 LMWChi-TEOS IPNs. Quantity of TEOS in the IPN increases accordingly. 1-3 minutes at pH 2.66 and 4-6 minutes at pH 7.12.

The LMW- and MMWChiTEOS IPNs were considered to exhibit the most suitable swelling properties, because although swelling is desired it is not desired to the extent of which the HMWChi-TEOS IPN swells. It is expected that this high degree of swelling would swell an embedded crystal lattice to an extent to which the diffracted

colour is no longer visible and so it would no longer be detectable by UV-Vis optical analysis. Other attributes of the LMW- and MMWChi-TEOS IPNs were the low PDI and high average degree of deacetylation associated with them. It is for this reason that 1:1, 1:2 and 1:3 LMWChi-TEOS IPNs were utilized to compare the effect of increasing quantity of TEOS. A difference in the physical quality of the IPNs was observable by the viscosity of the hydrogel, it noticeably increased going from 1:1 to 1:2 to 1:3 LMWChi-TEOS IPN. As can be seen in figure 5.3 the swelling ability is greatly reduced as the degree of cross-linking is increased, so much so that little difference is observed from pH 2.66 to pH 7.12. This result provides substance to the concept of mechanical strength increasing and flexibility decreasing with increasing quantity of TEOS present. The images in figure 5.4 show the significant difference in film quality. From looking at the various results it was concluded that the LMWChi-TEOS IPN or MMWChi-TEOS IPNs are the most suitable for further studies, with a 1:1 chitosan: TEOS ratio to be employed.

The mechanical tests performed on the IPNs were aimed at comparing the tensile strength of 1:1, 1:2 and 1:3 LMWChi-TEOS IPNS. Initial tests were carried out on 20 mm x 10 mm strips clamped with silicone rubber supports and a gauge length of 2 mm. A multiple of ten tests was carried out for each type of sample. The results can be seen in table 5.2, where the tensile strength of the IPNs does increase with increasing quantity of TEOS. This provides further evidence that TEOS provides mechanical strength for the membranes while chitosan provides flexibility. This result along with the swelling studies results points towards the 1:1 ratio the best for further tests prior to formation of a composite.

5.3.4 Chi-TEOS-SiO_2 composites

Chi-TEOS-SiO_2 composites were successfully fabricated using the method described in the experimental section. This was because upon completion of drying when the vacuum is released and the door of the oven is opened it can be observed that the Chi-TEOS-SiO_2 composite will peel off the PET substrate automatically with the change of environmental pressure. Photos of a resulting free-standing Chi-TEOS-SiO_2 composite can be seen in figure 5.5.

Figure 5.4. 1:1, 1:2 and 1:3 LMWChi-TEOS IPNs respectively. The images clearly show the film quality; 1:1 is fully intact, 1:2 is intact but very tightly folded and broken at the edges and 1:3 is completely impaired and in separate pieces.

Chi-TEOS IPN	Force (N)	% Deviation	Stress (MPa)
1:1	7.1	35	35.5
1:2	8.7	22	43.7
1:3	18.2	25	91

Table 5.2. Data obtained from tensile strength tests carried out on 1:1, 1:2 and 1:3 LMWChi-TEOS IPNs.

Initial swelling studies on a Chi-TEOS-SiO_2 composite were carried out on the sample displayed in figure 5.5(a) (original SiO_2 film and optical analysis in figure 5.1). Phosphate buffers of pH 2.66 and pH 7.12 were used in a certain sequence which can be seen in table 5.3. The data from table 5.3 corresponds to the swelling studies on a 1:1 MMWChi-TEOS-SiO_2 composite with 312nm SiO_2 spheres. When initially infilled with the IPN the crystal lattice expanded, this correlates with a shift of ca. 31 nm in the Bragg dip. When immersed in pH 2.66 phosphate buffer the crystal lattice swells again with a shift of the Bragg dip to 790 nm. When allowed to dry the film is more constricted than the original and the Bragg dip is observed at 736 nm. Then when immersed in pH 7.12 the crystal lattice swells to a lesser extent than with pH 2.66, here the Bragg dip shifts to 782 nm. Photos of the free-standing composite as well as a surface SEM image of a composite prepared with 290 nm spheres and 1:1 MMWChi-TEOS IPN can be seen in figure 5.5.

(a) 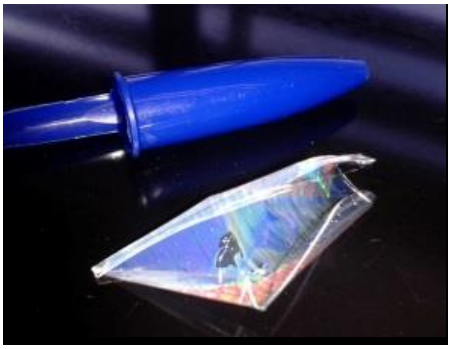 (b) 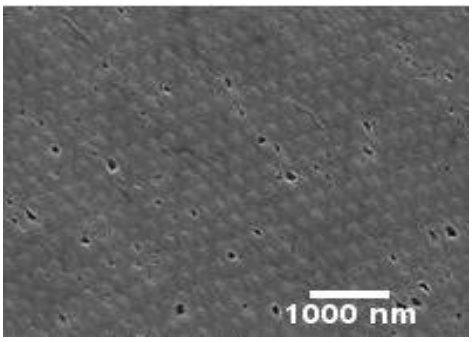

Figure 5.5. (a) MMWChi-TEOS-SiO_2 composite constructed with particles of 312nm diameter (b) SEM image of 290nm SiO_2 film infilled with 1:1 MMWChi-TEOS IPN.

Step	**1**	**2**	**3**	**4**	**5**
State of composite	Original	+ IPN	+ pH 2.66	+ allowed to dry	+ pH 7.12
Observed Bragg λ (nm)	718	749	790	736	782

Table 5.3. Data corresponding to various steps of swelling studies on 1:1 MMWChi-TEOS IPN with 312nm SiO_2 spheres. Composite can be seen in figure 5.5(a).

5.3.5 pH-sensitivity of Chi-TEOS-SiO_2 composite

Further tests were carried out in order to gain a full understanding on the swelling ability of the Chi-TEOS-SiO_2 composites. In this case a photonic crystal was prepared with SiO_2 spheres of 287nm diameter. The original optical data can be seen in figure 5.6, along with the shift in stop band upon infilling with 1:1 LMWChi-TEOS IPN. These are all characteristics which were observed for previous composites, however here in-depth swelling analysis in a closed Spectra Suite reflection setup allowed for tracking of the stop-band shift as the composite was exposed to various pH environments. After testing the composites in solutions of 0.1M HCl, H_2O and 0.1M NaOH it can be seen that the swelling ability increases as the pH of the solution decreases, in other words as the concentration of H^+ in solution increases. In 0.1M HCl the Bragg peak shifted to 703 nm and returned to the original wavelength within 8 minutes as the composite dried. For H_2O the Bragg peak shifts to 694 nm and with 0.1M NaOH it shifts to 685 nm, with both returning to the original wavelength within 9 minutes. See figure 5.7.

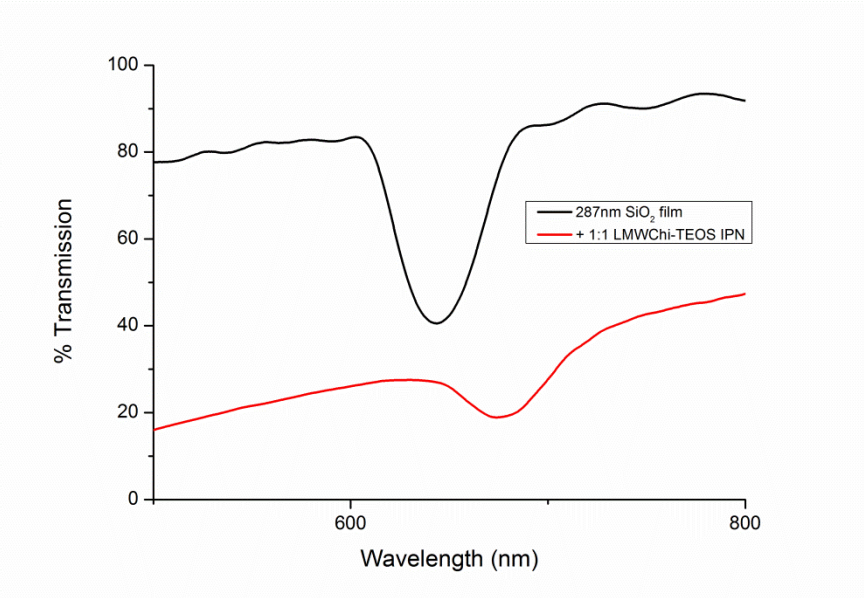

Figure 5.6. Transmission spectrum of SiO_2 photonic crystal film before and after infilling with 1:1 LMWChi-TEOS IPN.

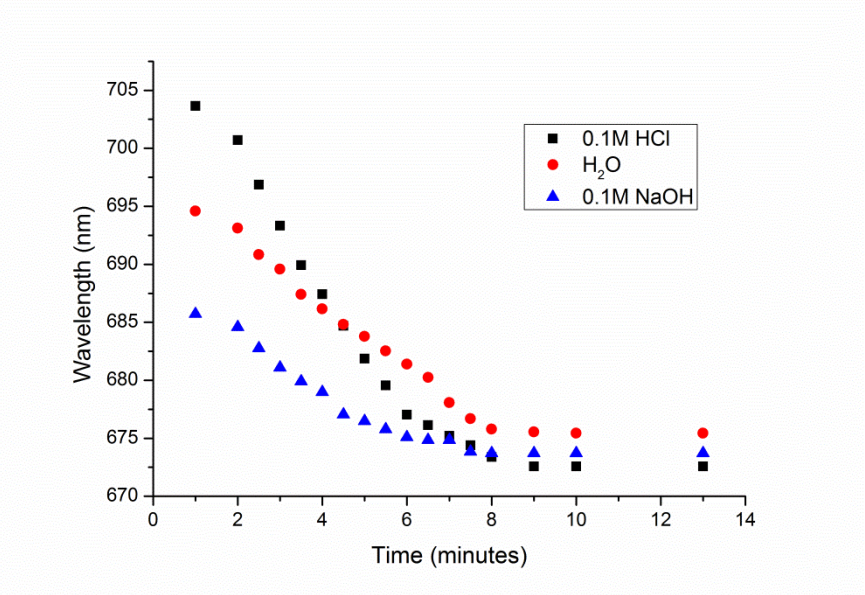

Figure 5.7. The shift in wavelength with respect to time as a Chi-TEOS-SiO_2 composite is exposed to different pH conditions. The max shift in wavelength is representative of greatest H+ concentration. As composites dry the wavelength returns to normal.

It is also interesting to note that a greater shift in Bragg diffracted wavelength was observed for the composite prepared with 1:1 MMWChi-TEOS IPN than that prepared with 1:1 LMWChi-TEOS IPN – when immersed in acidic solution the Bragg dip of

the MMWChi-TEOS-SiO_2 composites red-shifts about 40nm whereas that of the 1:1 LMWChi-TEOS IPN red-shifts about 20nm. This result was expected following the results from original swelling studies in figure 5.2. These results back up our theory that the crystal lattice swells with the IPN membrane as a function of pH. These tests were carried out in triplicate. Membranes were allowed to dry fully between tests.

5.4 Conclusions

Following the successful fabrication of colloidal photonic crystals composed of SiO_2 spheres and the formation of a range of Chi-TEOS IPNs the best experimental parameters for the combination of both to form a Chi-TEOS-SiO_2 composite were decided. Formation of the Chi-TEOS-SiO_2 composite was successful and by using PET as a substrate and forming the composite in a vacuum oven allowed for the composite to be completely free-standing.

It was required that the SiO_2 photonic crystals fabricated display structural colour in the visible range, therefore the modified-Stöber SiO_2 particles prepared in the 250-350nm range were employed for film growth. This ensured the colour would be visible to the naked eye and optical analysis could be carried out utilizing the UV-Vis spectrometer. Quite a range of substrates can be used for SiO_2 film growth e.g. glass, plastics, silicon wafers and metal-coated substrates. It was decided that PET plastic would be the ideal substrate for film growth as with subsequent deposition of IPN and drying of the film it can be easily removed from the substrate. It was observed with glass and silicon wafers that the IPN adhered to the surface of the substrate, not allowing the formation of a free-standing membrane. The PET substrate can be cut to size, allowing vertical controlled evaporation over a broad range of SiO_2 solution volumes and substrate dimensions.

Physical characterisation, swelling studies and tensile strength tests that were carried out on the various IPNs pointed towards the 1:1 LMWChi-TEOS IPN/ 1:1 MMWChi-TEOS IPN being the best candidates for formation of a Chi-TEOS-SiO_2 composite. Characterisation showed that they both had a lower PDI than the high molecular weight chitosan; they also didn't swell to such a high degree as the HMWChi-TEOS IPN. 1:1 was decided as the best chitosan: TEOS ratio as this allowed for formation of a complete film, 1:2 and 1:3 resulted in incomplete films due to reduced flexibility and higher mechanical strength.

When forming the Chi-TEOS-SiO_2 composite the best conditions were in a vacuum oven at 40°C with drying time depending on the size of the substrate. As can be seen by the SEM images and photographs, composites were successfully produced and suitable for swelling studies with optical analysis.

Swelling studies on Chi-TEOS-SiO_2 composites were combined with optical analysis to demonstrate the pH-driven expansion of the photonic crystal lattice when embedded in the IPN. This is portrayed visually by the change in colour of the composite upon swelling. This was also represented in optical analysis by the shift in stop band as the crystal lattice swells; the shift in the stop band increases with increasing H^+ concentration (decreasing pH). Upon drying the stop band returns to the original wavelength. Here, the proposed pH-driven expansion mechanism of a Chi-TEOS-SiO_2 composite in aqueous conditions of varying pH is successfully demonstrated.

References

1. Zhang, J.; Sun, Z.; Yang, B., Self-assembly of photonic crystals from polymer colloids. *Current Opinion in Colloid and Interface Science* **2009,** *14* (2), 103-114.

2. Fudouzi, H., Optical properties caused by periodical array structure with colloidal particles and their applications. *Advanced Powder Technology* **2009,** *20* (5), 502-508.

3. Joannopoulos, J. D.; Johnson, S. G.; Winn, J. N.; Meade, R. D., *Photonic Crystals: Molding the Flow of Light*. Princeton University Press: Princeton, 2011.

4. Rinaudo, M., Chitin and chitosan: Properties and applications. *Progress in Polymer Science* **2006,** *31* (7), 603-632.

5. Park, S.-B.; You, J.-O.; Park, H.-Y.; Haam, S. J.; Kim, W.-S., A novel pH-sensitive membrane from chitosan — TEOS IPN; preparation and its drug permeation characteristics. *Biomaterials* **2001,** *22* (4), 323-330.

6. Buckley, A. M.; Greenblatt, M., The Sol-Gel Preparation of Silica Gels. *Journal of Chemical Education* **1994,** *71* (7), 599.

7. Frances, N.; Nikolay, A. P.; Michael, J. F. B.; Tim, G.; Paul, A. M., Novel one-pot synthesis and characterization of bioactive thiol-silicate nanoparticles for biocatalytic and biosensor applications. *Nanotechnology* **2009,** *20* (5), 055612.

8. Rohindra, D. R.; Nand, A. V.; Khurma, J. R., Swelling properties of chitosan hydrogels. *The South Pacific Journal of Natural and Applied Sciences* **2004,** *22* (1), 32-35.

9. Wysokowski, M.; Behm, T.; Born, R.; Bazhenov, V. V.; Meissner, H.; Richter, G.; Szwarc-Rzepka, K.; Makarova, A.; Vyalikh, D.; Schupp, P.; Jesionowski, T.;

Ehrlich, H., Preparation of chitin-silica composites by in vitro silicification of two-dimensional Ianthella basta demosponge chitinous scaffolds under modified Stober conditions. *Materials Science and Engineering: C* **2013,** *33* (7), 3935-41.

10. Oliveira, F. C.; Barros-Timmons, A.; Lopes-da-Silva, J. A., Preparation and characterization of chitosan/SiO2 composite films. *Journal of nanoscience and nanotechnology* **2010,** *10* (4), 2816-25.

11. Lee, K.; Asher, S. A., Photonic crystal chemical sensors: pH and ionic strength. *Journal of the American Chemical Society* **2000,** *122* (39), 9534-9537.

12. Du, X.; Li, T.; Li, L.; Zhang, Z.; Wu, T., Water as a colorful ink: transparent, rewritable photonic coatings based on colloidal crystals embedded in chitosan hydrogel. *Journal of Materials Chemistry C* **2015,** *3* (15), 3542-3546.

13. Schwalfenberg, G. K., The alkaline diet: is there evidence that an alkaline pH diet benefits health? *Journal of environmental and public health* **2012,** *2012*, 727630.

14. Azevedo, L. B.; De Schryver, A. M.; Hendriks, A. J.; Huijbregts, M. A., Calcifying species sensitivity distributions for ocean acidification. *Environmental Science and Technology* **2015,** *49* (3), 1495-1500.

15. Rouwet, D.; Tassi, F.; Mora-Amador, R.; Sandri, L.; Chiarini, V., Past, present and future of volcanic lake monitoring. *Journal of Volcanology and Geothermal Research* **2014,** *272*, 78-97.

16. Jiang, P.; Bertone, J.; Hwang, K.; Colvin, V., Single-crystal colloidal multilayers of controlled thickness. *Chemistry of Materials* **1999,** *11* (8), 2132-2140.

17. Romanov, S.; Maka, T.; Torres, C. S.; Müller, M.; Zentel, R.; Cassagne, D.; Manzanares-Martinez, J.; Jouanin, C., Diffraction of light from thin-film polymethylmethacrylate opaline photonic crystals. *Physical Review E* **2001,** *63* (5), 056603.

18. Chaouachi, A.; Chtourou, R.; M'nif, A.; Hamzaoui, A. H., Optical characterization of colloidal silica crystals with controlled size microspheres. *Mater Lett* **2014,** *116*, 420-424.

6. Journal Article – "Structural and mechanical properties of a range of chitosan-based hybrid networks loaded with colloidal silica and polystyrene particles"

This paper was written in Autumn-Winter 2016 and was accepted for publication by the Springer Journal of Materials Science in March 2017. It is a follow-up study to the mechanical tests which were carried out in the previous paper which exhibited interesting results. The authors and their contributions are given below:

Catherine Ryan[1, 2] – All experiments and analysis, production and corrections to paper

Martyn Pemble[1, 2] – Supervision and corrections

Maria Bardosova[1, 3] – Supervision and corrections

[1] Tyndall National Institute, University College Cork, Lee Maltings, Prospect Row, Cork, Ireland

[2]Department of Chemistry, University College Cork, Cork, Ireland

[3]Slovak Technical University in Bratislava (STUBA), Ilkovičova 3, 81219 Bratislava, Slovak Republic

Abstract

We have prepared a range of chitosan-based interpenetrating network (IPN) materials in thin film form and analyzed these with respect to their mechanical and structural properties. The structures were analyzed before and after modification with a tetraethylorthosilicate (TEOS) cross-linker and various-sized silica and polystyrene particles - which were added to determine the influence of such particles on the mechanical properties of the resulting IPNs. The method of incorporation of particles was also investigated. All films were prepared by drop-casting with experimental conditions such as temperature, substrate and time kept constant throughout. Results from the mechanical tests show a decrease in flexibility of the chitosan network upon cross-linking with TEOS. However, a significant increase in the tensile strength was observed when the TEOS-modified chitosan network was combined with colloidal silica and polystyrene particles; interestingly this increase in tensile strength appears to correlate with increasing surface area of the particles, suggestive of a further cross-linking action. Results from the structural analysis show that there was little or no change to the chitosan chain network after cross-linking; this suggests that upon cross-linking a weakly-bonded IPN is being formed which may then be further modified by the inclusion of the particles studied. These findings are discussed in terms of the potential use of such hybrid materials as wound dressings or drug-release patches.

Keywords

Chitosan; interpenetrating polymer network; hybrid organic/inorganic materials; cross-link; composite; tensile strength; structure; bonding

6.1 Introduction

Chitosan is a polymer derived from chitin, a naturally-occurring polysaccharide extracted from crustacean and fungi exoskeletons. While chitin is made up of a chain of acetyl glucosamine units, its derivative is made up of acetyl glucosamine and glucosamine units, generally once the degree of deacetylation exceeds 50% it is considered as chitosan[1]. Chitosan has its advantages over chitin, including increased solubility and flexibility, and therefore it is more prevalently used. Chitosan thin film membranes, which are generally prepared by drop-casting of hydrogels, are pH-sensitive but tend to lack mechanical strength - this can be improved upon by the introduction of cross-linking capabilities[2]. A cross-link is formed by a chemical reaction with any species which successfully bonds two polymer chains together, either covalently or ionically or by weaker bonding interactions[3]. Cross-linkers such as tetraethyl orthosilicate (TEOS) used by Park *et al*. and genipin used by Lien *et al.*[4], served to enhance the mechanical stability of chitosan membranes[5]. The mechanical properties of chitosan vary depending on whether or not the system is cross-linked with a separate system. Studies on various systems have been carried out e.g. Wang *et al*. incorporated montmorillonite particles in a chitosan structure to improve its mechanical properties[6]. The aim of cross-linking is to provide further structural support for chitosan's flexible structure. Aryaei *et al*. applied a modified method of determining the elastic modulus to show that films of chitosan cross-linked with tripolyphosphate have improved hardness and mechanical properties. They also report that cross-linked films are more brittle than chitosan films[7].

The cross-linking phenomenon is also applied to the formation of so-called interpenetrating polymer networks (IPNs) which are described as a 'combination of two polymers in network form, at least one of which is synthesized and /or cross-linked in the immediate presence of the other'[8]. IPN synthesis is basically a reaction between a monomer and a cross-linker to form a polymer network. The monomer could be a polysaccharide, a protein or a synthetic monomer. According to the IUPAC definition an IPN is 'a polymer comprising of two or more networks which are at least partially interlaced on a molecular scale but not covalently bonded to each other and cannot be broken unless chemical bonds are broken'[9], indicating weaker interactions such as hydrogen-bonding and van der Waals' interactions are occurring.

The properties of chitosan which contribute most to the mechanical properties are polydispersity index (PDI) and average molecular weight. A lower PDI value will result in a lower distribution in molecular weight i.e. indicative of greater uniformity of the polysaccharide structure. It is then expected that the mechanical properties should be enhanced with increasing average molecular weight. Huei *et al.* conducted a study on how varying molecular weight affects the tensile strength, tensile elongation and enthalpy of formation of high purity chitosan samples with degree of deacetylation of 90%[10]. Results show that the mechanical properties and enthalpy increase with increasing molecular weight of chitosan. The results are attributed to two factors; more molecular entanglement with longer chain length and a higher degree of crystallinity in the higher molecular weight samples, which is suggested by the increase in enthalpy values. A study on the effects of solvent acid and molecular weight of chitosan on the barrier and mechanical properties of chitosan films was carried out by Park *et al.*[11]. Tensile strength tests reveal that acetic acid is the best solvent acid for the preparation of mechanically strong films with tensile strength results increasing accordingly from low to medium to high molecular weight chitosan. The lowest tensile strength results were obtained from chitosan films prepared with citric acid as solvent. Interestingly the opposite was seen in the percentage elongation tests, in that chitosan films prepared with acetic acid showed the lowest results while those prepared with citric acid showed the greatest percentage elongation in accordance with increasing molecular weight. These results are a good reflection on the influence of chain length and chain overlap on mechanical properties.

The mechanical properties of polymer membranes are altered when cross-linking occurs in the formation of an IPN; this is mainly due to the reduced flexibility of the polymer. Aryaei *et al.* carried out a study on the mechanical properties of both uncross-linked and cross-linked chitosan films, with the aim of enhancing the mechanical properties of chitosan for applications in the biomedical field[7]. Results from both elastic modulus and hardness tests showed that the cross-linked chitosan sample had enhanced properties; however the cross-linked chitosan was described as brittle in comparison to the uncross-linked chitosan which was described as ductile. This provides evidence for modification of surface properties due to cross-linking and although the cross-linked sample is stronger the brittle characteristic may not be desirable. The changes in physical properties of chitosan cross-linked with starch and

varying glutaraldehyde concentration were studied by Li *et al.*[12], in an extensive study with analysis methods ranging from thickness measurements, FTIR, SEM, light transmission, mechanical, swelling studies, moisture uptake and water vapour transmission rate. Spectroscopic methods provided evidence for the reaction of glutaraldehyde with the polymer composite due to the loss of the characteristic aldehyde peak in the FTIR spectrum and a decrease in light transmittance in the UV-Vis spectrum with increasing glutaraldehyde concentration. This was attributed to phase separation within the composite as the glutaraldehyde was interfering with the integrity of the composite structure. Evidence of phase separation with increasing glutaraldehyde concentration was also seen in the results from the mechanical studies. The tensile strength and elongation at break values decrease with increasing glutaraldehyde concentration. According to the authors this is a contradiction to the many studies which show that tensile strength increases with cross-linker concentration, however it could be suggested that glutaraldehyde was not acting as a cross-linker as such but rather it was interfering with the chitosan-starch composite, inducing phase separation and weakening cross-links between the chitosan and starch entities.

To date there has been an abundance of research carried out on chitosan-cross-linker networks with respect to their mechanical properties[7,13,14]. Typically, the same general trends are described and it can be concluded that the mechanical properties of chitosan are enhanced with increasing cross-linker concentration, as the cross-linker acts as a so-called 'backbone', when introduced to the chitosan polymer structure. The increase in mechanical strength generally causes a reduction in swelling ability as the flexibility and freedom of movement of polymer chains is inhibited by the presence of a cross-linker backbone.

A recent study by Mathesan *et al.* on the mechanical properties of modified chitosan samples included the effect of incorporating into the chitosan network[15]. The stress-strain behaviour of three different chitosan networks was analysed; chitosan polymer, a chitosan-hydroxyapatite (HAP) network and chitosan cross-linked with glutaraldehyde. It was found that the Young's modulus and maximum stress increased in both the presence of HAP and glutaraldehyde; with the latter showing the greater increase. Radial distribution function analysis, a method which essentially provides information on the probability of finding certain atomic species at a given distance

from a specific central carbon atom, was carried out and provided evidence that hydrogen bonding and electrostatic interactions were the primary bonding interactions leading to the enhanced mechanical properties. In the described study it was executed by interpretation of uniaxial deformation processes in the modified chitosan networks.

It is of interest to consider the role of particle diameter in such experiments since it might be expected that as the size of the particles vary the bond strength between the polymer and the particles would also vary. For a constant concentration of particles, the smaller the particle diameter the more exposed particle surface area will be available for coordination to the chitosan, which hence will facilitate more particle-chitosan interactions leading to an increase in mechanical strength. Interestingly, the opposite result was observed by Rose *et al.* as they performed tensile strength tests on various materials, including animal tissue grafted with various nanoparticles of varying size[16], including SiO_2 nanoparticles. It was suggested that this observation was due to a matching of the size of the particles to the active portions of the network where they were grafted. Their results were important from a biomedical viewpoint as the nanoparticles are proposed as wound-healing entities due to their ability to graft human tissue.

Building on a previous study performed in our laboratories in which we examined how optically active silica particle assemblies behaved in pH-sensitive chitosan matrices[17] this present study focuses on the mechanical properties of these hybrid films and examines the effects of cross-linking with TEOS together with the possibility of further enhancing the mechanical properties by introducing particles as a third cross-linking entity. We have performed these studies because cross-linked chitosan networks have a vast number of proposed applications in the biomedical industry. One proposed application which would benefit from increased cross-linker density and tensile strength is the use of chitosan membranes as wound-healing networks. Chitosan provides a biocompatible layer which is breathable and moisture permeable, therefore perfect for biomedical applications such as wound-healing[2]. However, the lifetime of such wound-healing dressings is questionable; this may be improved upon by an increase in cross-linker density and tensile strength. Surface wound-healing membranes as described are ideal candidates for the controlled release of drugs at the epidermis[18] or at surface bone tissue[19]. Electrospun chitosan networks have been proposed in the literature as candidates for wound-dressing applications, the

nanofibrous membranes can be combined with other polymer networks, a concept similar to cross-linking. Chen *et al.* prepared electrospun chitosan/ collagen fibers and studied them with respect to their mechanical properties[20] with a view towards producing electrospun wound-dressing materials[21]. An impressive average ultimate strength of about 60 MPa was reached when the chitosan: collagen ratio in the electrospun fibers was about 1:1, due to intermolecular interactions between the chitosan and collagen networks – the same interaction as occurs in cross-linked polymer networks. Other applications of such a material in the biomedical/ pharmaceutical industry include utilising chitosan networks for the controlled release of drugs at different sites in the body depending on pH[22],[23],[24]. The controlled release phenomenon is made possible due to the pH-sensitivity of the chitosan network. The polymer structure is sensitive to acidic conditions due to the protonatable amino groups throughout the structure, resulting in a swollen cationic polyelectrolyte structure. Drugs or other entities encapsulated in the membrane are released upon swelling. This is particularly applicable in the biomedical field due to varying pH throughout the body. The swelling phenomenon can also be applied for pH-sensing applications in non-biological chemical environments and enhanced mechanical strength is also desirable in this regard.

6.2 Materials and methods

6.2.1 Materials

Low molecular weight chitosan was purchased from Sigma Aldrich, Ireland (Mw 50,000-190,000 $gmol^{-1}$, 75-85% deacetylated). Silica (SiO_2) particles were prepared by a modified Stöber method[25] and polystyrene (PS) particles were supplied by the Colloidal Crystal Materials group from the National Institute of Materials Science in Tsukuba, Japan. Both the chitosan hydrogel and TEOS cross-linked interpenetrating polymer network (Chi-TEOS IPN) were prepared by a cationic polymerization technique adapted from[26] and as described in[27]. Thin film membranes of each type were formed by drop-casting 13 mL of hydrogel in a 90 mm petri dish and allowed to dry at 40°C. Colloidal particles were introduced to the IPN hydrogel and allowed to stir prior to thin film formation so they were essentially embedded in the membrane. 130 µL of SiO_2 and PS polymer particle solutions in the size range of 100-500 nm and a concentration of 0.05-0.08 gmL^{-1} were employed, see figure 6.1 for

all details. All types of thin films were formed by the drop-casting technique at 40°C. The full-sized membranes were then cut into individual 10 mm x 40 mm strips, suitable for analysis and mechanical tests. For comparison purposes a range of grafted samples were prepared and tested, this was done by grafting two 10 mm x 40 mm strips with silica and polystyrene solutions – this allows for comparison between surface grafting and embedding particles. The table below displays the details of the various types of membranes that were prepared and tested. All analysis was carried out at the Tyndall National Institute, University College Cork, Cork, Ireland.

Membrane type	**Cross-linker**	**Diameter of particles**	**Concentration of cross-linker**	**Volume of cross-linker**
Chitosan	-	-	-	-
Chi-TEOS IPN	TEOS	-	1:1 (Chitosan: TEOS)	-
Chi-TEOS IPN	TEOS/ SiO_2	100 nm	0.076 gmL^{-1}	130 µL
Chi-TEOS IPN	TEOS/ SiO_2	290 nm	0.075 gmL^{-1}	130 µL
Chi-TEOS IPN	TEOS/ SiO_2	516nm	0.063 gmL^{-1}	130 µL
Chi-TEOS IPN	TEOS/PS	100 nm	0.070 gmL^{-1}	130 µL
Chi-TEOS IPN	TEOS/PS	290 nm	0.061 gmL^{-1}	130 µL
Chi-TEOS IPN	TEOS/PS	520 nm	0.074 gmL^{-1}	130 µL

Table 6.1. Various types of membranes that were prepared and tested with associated variables.

6.2.2 Spectroscopic analysis

Infrared analysis was carried out on free-standing thin film samples using a Bruker Alpha FT-IR spectrometer in single reflection ATR mode which utilizes a platinum-diamond crystal. A Renishaw inVia confocal Raman microscope was used for Raman

analysis on thin film samples immobilized on glass slides. Both techniques investigated any structural differences between chitosan and the subsequent cross-linked networks.

6.2.3 Surface analysis

Surface thickness and roughness analysis were carried out using a KLA Tencor P15 profilometer with a scan rate of 20 µm/s and a scanning distance of 1000 µm. Scanning electron microscopy was performed using a FEI Quanta 650 FEG High Resolution Scanning Electron Microscope, typical beam energies were in the range of 10-20 kV.

6.2.4 Mechanical testing

An Instron 5565 Universal Testing Machine was used to carry out tensile strength tests on the thin film membranes with rectangular geometry of 10 mm x 40 mm. Test conditions at room temperature included a load of 5 kN, clamp speed of 0.5 mm/min and data rate of 10 pts/sec. The thin film strips were clamped with PDMS supports.

6.3 Results and Discussion

6.3.1 Chitosan-based hybrid composites

Hydrogels outlined in table 6.1 were prepared, dried to form thin film membranes and cut up into suitable 10 mm x 40 mm strips.

The spherical SiO_2 and polystyrene particles with their sizes, concentrations and their estimated surface areas are displayed in figure 6.1; the SEM images clearly show the monodispersity of the particles.

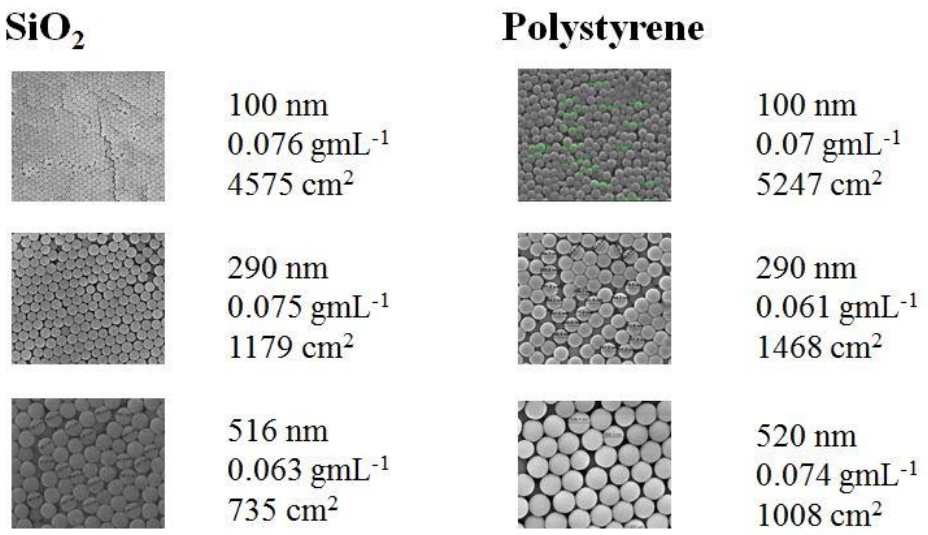

Figure 6.1. SEM images displaying the various SiO_2 and polystyrene particles showing their monodispersity, narrow concentration range and estimated surface area.

The appearance of the Chi-TEOS IPN solution changed upon addition of the micro-/ nanoparticle solutions. The originally clear hydrogel turned white upon addition of the colloidal SiO_2 and also the colloidal PS, more so for PS due to the greater refractive index contrast.

6.3.2 Spectroscopic analysis

Initial characterization was directed at comparing the chitosan sample to the Chi-TEOS IPN which was subsequently formed by cross-linking with TEOS. In comparing both the IR and Raman spectra it appears that there is no difference in the bonding and structural properties of the chitosan chain. This supports the hypothesis that there is no covalent bonding occurring during IPN formation- rather the polymer chains are interlaced and interacting by weaker interactions which do not dramatically affect the chitosan structure. The spectra can be seen in figures 6.2 and 6.3.

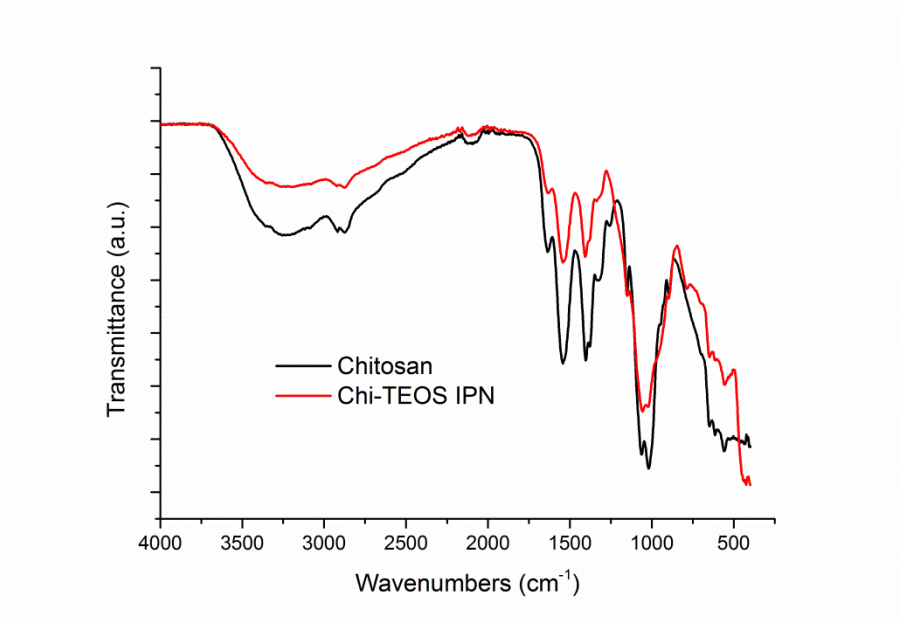

Figure 6.2. IR spectra comparing the structural properties and presence of functional groups before and after cross-linking chitosan with TEOS.

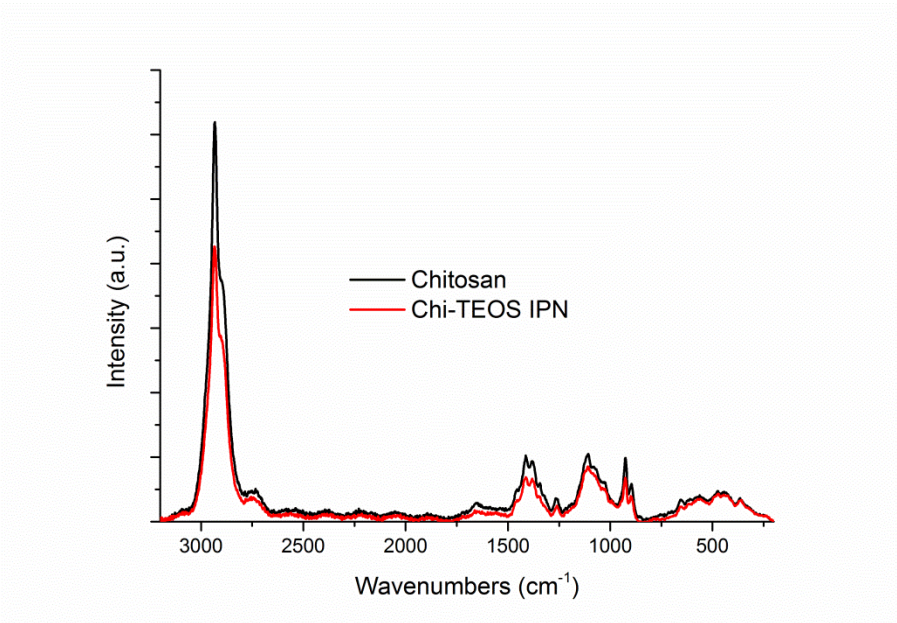

Figure 6.3. Raman spectra comparing the structural properties and presence of functional groups before and after cross-linking chitosan with TEOS.

The IR spectrum was assigned as follows: 3500-3000 cm^{-1} (broad peak) is attributed to an overlap of the O-H of the alcohol and primary and secondary amide, 1500-1600 cm^{-1} N-H of primary amine, 1000-1200 cm^{-1} C-N stretch of aliphatic amine, 800 cm^{-1} N-H wag of primary and secondary amine[28]. Analysis of the IR spectra reveals minute discrepancies in the frequencies of a range of key functional groups. A small peak

appears at 785 cm^{-1} for the chitosan samples following cross-linking with the siloxane network. Vibrations in this region correspond to deformations in N-H groups of primary and secondary amines. The presence of bend deformation vibrations indicates that there is distortion of the functional group side chains of the chitosan polymer network, in this case functional groups which would be expected to be involved in weak interactions such as H-bonding. There is a peak observed at 1250 cm^{-1} for the chitosan sample but not for the cross-linked samples, this region corresponds to stretches of methyl groups, the disappearance of the peak may be due to disturbance to the methyl stretch by an induced dipole upon cross-linking. A peak also appears at 440 cm^{-1} upon transition from chitosan to Chi-TEOS IPN, this frequency corresponds to a Si-O-Si group which is present as a bridging group in the siloxane polymer network.

The Raman spectrum was assigned as follows: 2885 cm^{-1} C-H stretching vibration of methane and methylene groups of the pyranoid ring; 1600-1680 cm^{-1} scissoring NH_2 motion; 1380-1470 cm^{-1} methine/methylene bending and C-O-H in-plane bending; 1000-1200 cm^{-1} alicyclic chain stretches, C-O stretches; 800-970 cm^{-1} C-O-C stretch; 450-550 cm^{-1} heavy atom bonding such as Si-O-Si[29]. According to the Raman spectra there appears to be very little disruption to the chitosan sample after cross-linking with the siloxane network. The fact that there are no new functional group interactions within the chitosan structure suggests that non-covalent, physical cross-linked linkages are being formed. This technique and its results are complimentary to infrared spectroscopy.

6.3.3 Surface analysis

The average thickness and surface roughness of the films were determined. The thicknesses of all membranes were in the range of 15–20 μm. Variance in the sample thickness was measured over a range of points per sample, a satisfactory percentage variance of <10 % meant the samples were suitable for mechanical testing. As can be seen in table 6.2, the surface roughness measurements revealed a smooth surface for the chitosan with a slight increase in roughness observed upon introducing the various cross-linkers. However, here the variance values were quite high suggesting a very rough surface profile.

Sample	Average step height	Average surface roughness
Chitosan	17.26 µm ± 4.9%	0.13 µm ± 33.3%
Chi-TEOS IPN	18.32 µm ± 18.6%	0.05 µm ± 85.9%
IPN + 100 nm SiO_2	17.71 µm ± 1.6%	0.34 µm ± 94.6%
IPN + 290 nm SiO_2	19.46 µm ± 7.5%	0.05 µm ± 175.8%
IPN + 516 nm SiO_2	18.11 µm ± 2.3%	0.02 µm ± 107.8%
IPN + 100 nm PS	14.44 µm ± 5.0%	0.36 µm ± 100.0%
IPN + 290 nm PS	15.97 µm ± 7.1%	0.17 µm ± 208.7%
IPN + 520 nm PS	18.34 µm ± 3.3%	1.02m ± 167.3%

Table 6.2. Table of data displaying results from surface profile analysis.

6.3.4 Mechanical Testing

(a) Chitosan and Chi-TEOS IPN

The expected decrease in flexibility was observed in comparing the tensile strength of the chitosan thin film to the chitosan cross-linked with TEOS (Chi-TEOS IPN). It is proposed that these observations can be accounted for by invoking the fact that the TEOS network adds a mechanically strong backbone to the IPN. The stress-strain curve for chitosan in figure 6.4 displays a slight linear, elastic character with a yield point comparable to literature values[28, 30]. However as can be seen in figure 5 it tears slowly and continuously. On the other hand, the Chi-TEOS IPN sample displays a linear, elastic behavior with a significantly higher yield point of 61 MPa, reached with a sudden fracture. The Chi-TEOS IPN sample in figure 6.4 is one of five measurements which yielded results of 75 MPa ± 29%. These results support the proposal that the TEOS provides enhanced mechanical strength to the chitosan network. Results are on par with those observed by Chen *et al.* in analysis of their electrospun chitosan/ collagen fibers[20], yet our cross-linked chitosan films are prepared by a simpler, more reproducible method.

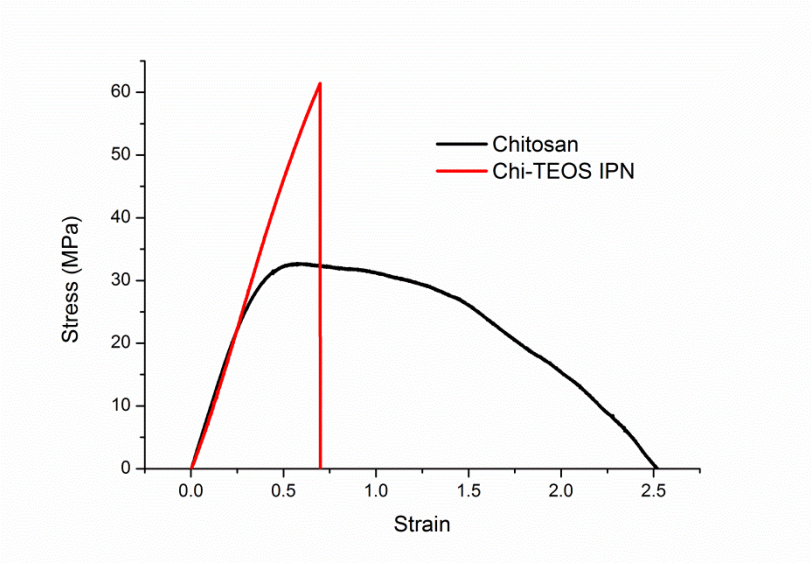

Figure 6.4. Stress-strain curves of chitosan and Chi-TEOS IPN. A greater tensile strength value is observed following cross-linking with TEOS with a significant reduction in flexibility.

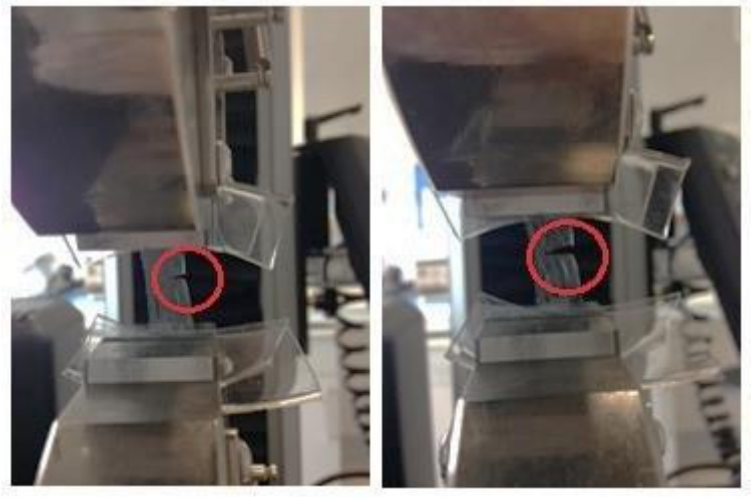

Figure 6.5 Photograph displaying the chitosan thin film during tensile testing, the gradual tear displays evidence of the flexibility of the membrane; this is also reflected in the stress-strain curve in figure 6.4.

(b) IPN with polymer particles embedded

The results obtained from the mechanical tests carried out on the Chi-TEOS IPN samples with polystyrene or silica particles embedded show that the tensile strength generally increases as more particles are introduced, presumably due to weak bonding interactions such as H-bonding and van der Waals interactions. This increase in tensile strength occurs as a function of decreasing particle diameter and therefore as a function

of increased total surface area for a given concentration of particles. This can be said for both SiO_2 and PS particles - see figure 6.6. Once again structural analysis carried out by Raman and infrared spectroscopy suggests that particle incorporation results in no significant chemical changes taking place, suggesting the presence of weak interactions with the particles embedded in the IPN.

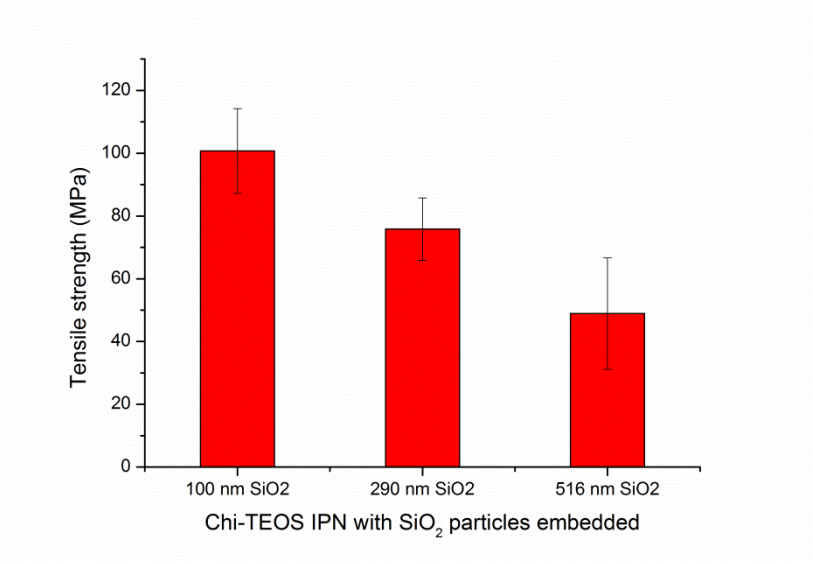

(a)

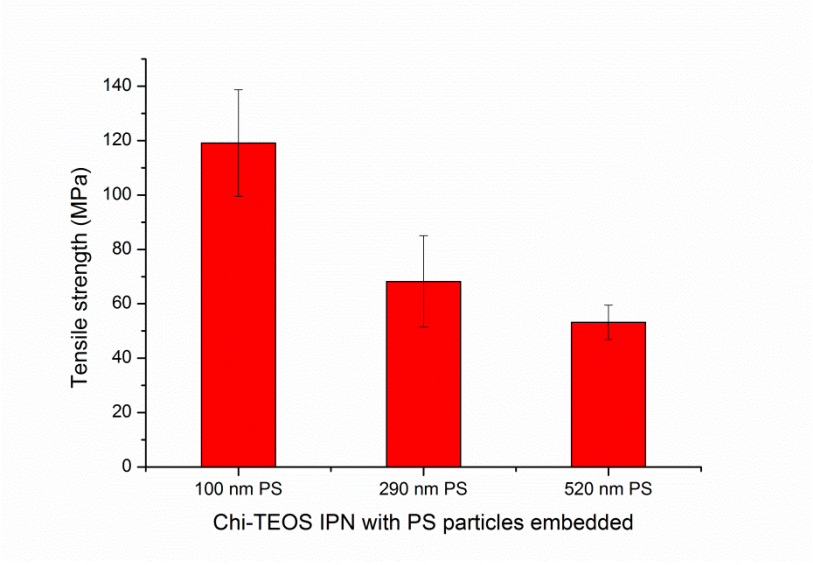

(b)

Figure 6.6. Graphs (a) and (b) display how the tensile strength of the Chi-TEOS IPN is improved upon with the presence of (a) SiO_2 and (b) PS particles, both as a function of decreasing particle size.

A range of grafted samples were prepared using the same SiO_2 and PS polymer particles and these samples were subjected to the same type of analysis as that presented above. The resulting membranes did not have the same smooth, uniform

appearance as the membranes with embedded particles. We propose that this is due to the fact that the Chi-TEOS IPN was already dry prior to exposure to the particle suspension in contrast to the method deployed to make the embedded particle membranes where in the embedding process the particles are added at the hydrogel stage and drying takes place with the particles already embedded in the hydrogel.

As a result, the mechanical integrity of the grafted membranes was degraded by the grafting process, to the point where it was on par with that of the original chitosan membranes. Addition of particles in this manner resulted in a decrease in mechanical strength as compared to the result for a sample treated only with water, where some degree of hydrogen bonding resulted in a tensile strength of 36.56 MPa.

Necessarily for the grafted samples, the particle diameter-dependent trend observed for the embedded samples was not observed. These observations together with the finding of a greater variance in the standard deviation in tensile strength indicates that that not so surprisingly, surface grafting is not a suitable method for incorporating particles into the Chi-TEOS IPN structure, see figure 6.7.

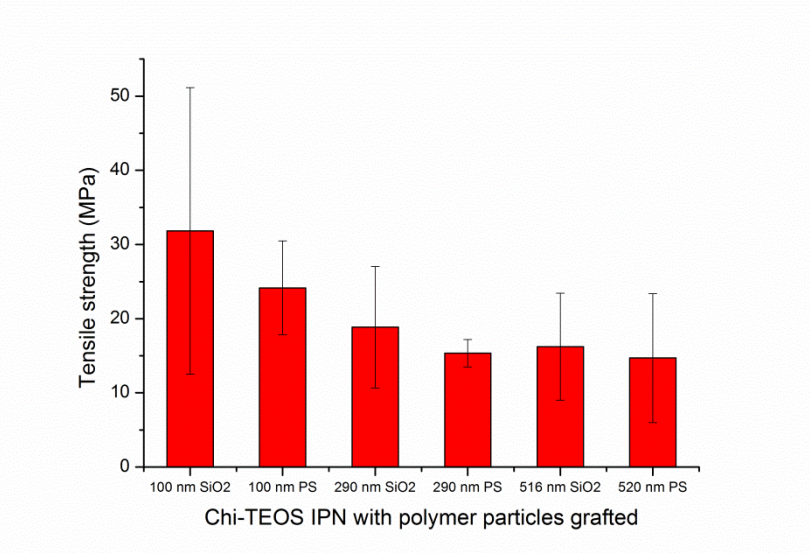

Figure 6.7. The graph displays tensile strength values obtained for Chi-TEOS IPN samples grafted with SiO_2 and PS particles. The results are indicative of a reduction in the maximum tensile strength in comparison to the Chi-TEOS IPN and Chi-TEOS IPN with polymer particles embedded.

6.4 Conclusions

Structural and mechanical analyses were carried out on chitosan membranes, Chi-TEOS IPNs and a range of cross-linked chitosan networks, all prepared by the same method and of uniform dimensions. Initial results showed a decrease in flexibility and increase in mechanical strength in progressing from the chitosan membrane to the Chi-TEOS IPN, 32 MPa to 61 MPa. Structural analysis carried out by IR and Raman spectroscopy showed little or no difference in the structural properties, proving that the networks are interlacing and bonding by weak interactions, as expected to occur in an interpenetrating polymer network.

Further tests were carried out in the same manner while investigating the effect of cross-linking with various sizes of colloidal SiO_2 and PS particles. The tensile strength increased as a function of increased total particle surface area (decreasing particle diameter for a given concentration), to almost greater than double the value of the Chi-TEOS IPN employing polymer spheres with a diameter of 100 nm (SiO_2 – 100.72 MPa, PS – 119.17 MPa). This result is very promising in relation to the overall aims of controlling the mechanical properties of chitosan-based membranes. It is suggested that the effects observed arise from weak interactions such as hydrogen-bonding between amino, hydroxyl, acetamido, siloxane and styrene groups of all the cross-linked entities.

The method of 'embedding' particles into the IPN structure demonstrated here was compared to a different method- that of surface grafting of particles to preformed Chi-TEOS IPNs. Results from samples grafted with the same polymer particles (SiO_2 and PS) displayed considerably lower tensile strength values, lower even that those from chitosan. There was also a high degree of variance in the results suggesting that there might be some issues associated with the reproducibility of the grafting process.

Overall, results from the study show that the mechanical properties of chitosan thin films can be controlled and adjusted by cross-linking with TEOS and also by cross-linking with SiO_2 and PS particles by 'embedding' the particles in the chitosan network. It was revealed that tensile strength increases as a function of decreasing particle diameter; this can be attributed to increasing overall particle surface area due to the fact that particle sample concentration was kept constant.

References

1. Rinaudo, M., Chitin and chitosan: Properties and applications. *Progress in Polymer Science* **2006,** *31* (7), 603-632.

2. Dash, M.; Chiellini, F.; Ottenbrite, R.; Chiellini, E., Chitosan—A versatile semi-synthetic polymer in biomedical applications. *Progress in Polymer Science* **2011,** *36* (8), 981-1014.

3. Ahmed, E. M., Hydrogel: Preparation, characterization, and applications: A review. *Journal of Advanced Research* **2015,** *6* (2), 105-121.

4. Lien, S.-M.; Li, W.-T.; Huang, T.-J., Genipin-crosslinked gelatin scaffolds for articular cartilage tissue engineering with a novel crosslinking method. *Materials Science and Engineering: C* **2008,** *28* (1), 36-43.

5. Park, S.-B.; You, J.-O.; Park, H.-Y.; Haam, S. J.; Kim, W.-S., A novel pH-sensitive membrane from chitosan—TEOS IPN; preparation and its drug permeation characteristics. *Biomaterials* **2001,** *22* (4), 323-330.

6. Wang, S.; Shen, L.; Tong, Y.; Chen, L.; Phang, I.; Lim, P.; Liu, T., Biopolymer chitosan/montmorillonite nanocomposites: preparation and characterization. *Polymer Degradation and Stability* **2005,** *90* (1), 123-131.

7. Aryaei, A.; Jayatissa, A. H.; Jayasuriya, A. C., Nano and micro mechanical properties of uncross-linked and cross-linked chitosan films. *Journal of the Mechanical Behavior of Biomedical Materials* **2012,** *5* (1), 82-89.

8. Sperling, L. H., *Interpenetrating Polymer Networks and Related Materials*. Springer Science & Business Media: 2012.

9. Jenkins, A.; Kratochvil, P.; Stepto, R.; Suter, U., Glossary of basic terms in polymer science (IUPAC Recommendations 1996). *Pure and Applied Chemistry* **1996,** *68* (12), 2287-2311.

10. Rong Huei, C.; Hwa, H.-D., Effect of molecular weight of chitosan with the same degree of deacetylation on the thermal, mechanical, and permeability properties of the prepared membrane. *Carbohydrate Polymers* **1996,** *29* (4), 353-358.

11. Park, S. Y.; Marsh, K. S.; Rhim, J. W., Characteristics of different molecular weight chitosan films affected by the type of organic solvents. *JOURNAL OF FOOD SCIENCE-CHICAGO-* **2002,** *67* (1), 194-197.

12. Li, H.; Gao, X.; Wang, Y.; Zhang, X.; Tong, Z., Comparison of chitosan/starch composite film properties before and after cross-linking. *International Journal of Biological Macromolecules* **2013,** *52*, 275-279.

13. Aryaei, A.; Liu, J.; Jayatissa, A. H.; Champa Jayasuriya, A., Cross-linked chitosan improves the mechanical properties of calcium phosphate–chitosan cement. *Materials Science and Engineering: C* **2015,** *54*, 14-19.

14. Berger, J.; Reist, M.; Mayer, J. M.; Felt, O.; Peppas, N.; Gurny, R., Structure and interactions in covalently and ionically crosslinked chitosan hydrogels for biomedical applications. *European Journal of Pharmaceutics and Biopharmaceutics* **2004,** *57* (1), 19-34.

15. Mathesan, S.; Rath, A.; Ghosh, P., Molecular mechanisms in deformation of cross-linked hydrogel nanocomposite. *Materials Science and Engineering: C* **2016,** *59*, 157-167.

16. Rose, S.; Prevoteau, A.; Elziere, P.; Hourdet, D.; Marcellan, A.; Leibler, L., Nanoparticle solutions as adhesives for gels and biological tissues. *Nature* **2014,** *505* (7483), 382-385.

17. Robasky, K.; Lewis, N. E.; Church, G. M., The role of replicates for error mitigation in next-generation sequencing. *Nature Reviews Genetics* **2014,** *15* (1), 56-62.

18. M Ferreira, D.; Y Saga, Y.; Aluicio-Sarduy, E.; Tedesco, A. C., Chitosan nanoparticles for melanoma cancer treatment by photodynamic therapy and electrochemotherapy using aminolevulinic acid derivatives. *Current Medicinal Chemistry* **2013,** *20* (14), 1904-1911.

19. Zeng, R.; Tu, M.; Liu, H.; Zhao, J.; Zha, Z.; Zhou, C., Preparation, structure, drug release and bioinspired mineralization of chitosan-based nanocomplexes for bone tissue engineering. *Carbohydrate Polymers* **2009,** *78* (1), 107-111.

20. Chen, Z.; Wei, B.; Mo, X.; Lim, C. T.; Ramakrishna, S.; Cui, F., Mechanical properties of electrospun collagen–chitosan complex single fibers and membrane. *Materials Science and Engineering: C* **2009,** *29* (8), 2428-2435.

21. Chen, J.-P.; Chang, G.-Y.; Chen, J.-K., Electrospun collagen/chitosan nanofibrous membrane as wound dressing. *Colloids and Surfaces A: Physicochemical and Engineering Aspects* **2008,** *313–314*, 183-188.

22. Bardelang, D.; Zaman, M.; Moudrakovski, I. L.; Pawsey, S.; Margeson, J. C.; Wang, D.; Wu, X.; Ripmeester, J. A.; Ratcliffe, C. I.; Yu, K., Interfacing supramolecular gels and quantum dots with ultrasound: smart photoluminescent dipeptide gels. *Advanced Materials* **2008,** *20* (23), 4517-4520.

23. Zhang, Y.; Tao, L.; Li, S.; Wei, Y., Synthesis of Multiresponsive and Dynamic Chitosan-Based Hydrogels for Controlled Release of Bioactive Molecules. *Biomacromolecules* **2011,** *12* (8), 2894-2901.

24. Chen, F.; Zhu, Y., Chitosan enclosed mesoporous silica nanoparticles as drug nano-carriers: sensitive response to the narrow pH range. *Microporous and Mesoporous Materials* **2012,** *150*, 83-89.

25. Wang, X.-D.; Shen, Z.-X.; Sang, T.; Cheng, X.-B.; Li, M.-F.; Chen, L.-Y.; Wang, Z.-S., Preparation of spherical silica particles by Stöber process with high concentration of tetra-ethyl-orthosilicate. *Journal of Colloid and Interface Science* **2010,** *341* (1), 23-29.

26. Park, S.-B.; You, J.-O.; Park, H.-Y.; Haam, S. J.; Kim, W.-S., A novel pH-sensitive membrane from chitosan — TEOS IPN; preparation and its drug permeation characteristics. *Biomaterials* **2001,** *22* (4), 323-330.

27. Ryan, C.; Delezuk, J.; Pavinatto, A.; Oliveira Jr, O.; Fudouzi, H.; Pemble, M.; Bardosova, M., Silica-based photonic crystals embedded in a chitosan-TEOS matrix: preparation, properties and proposed applications. *Journal of Materials Science* **2016,** *51* (11), 5388-5396.

28. Nunthanid, J.; Puttipipatkhachorn, S.; Yamamoto, K.; Peck, G. E., Physical properties and molecular behavior of chitosan films. *Drug development and industrial pharmacy* **2001,** *27* (2), 143-57.

29. Adar, F., Interpreting Raman Spectra of Functionalized Polymers: Applying the Tricks of the Trade. In *Spectroscopy*, 2012; Vol. 27.

30. Bonilla, J.; Fortunati, E.; Atarés, L.; Chiralt, A.; Kenny, J. M., Physical, structural and antimicrobial properties of poly vinyl alcohol–chitosan biodegradable films. *Food Hydrocolloids* **2014,** *35*, 463-470.

7. Journal Article – "Synthesis and characterization of cross-linked chitosan composites functionalised with silver and gold nanoparticles for antimicrobial applications"

This paper was written following a successful collaborative project with Dr David Clarke and Finbarr Buttimer of the Microbiology Department in UCC. It was published in STAM (Science and Technology of Advanced Materials in July 2017).

Catherine Ryan [1, 2] - All experiments and analysis, production and corrections to paper

Emma Alcock [2] – All experiments and production of paper

Finbarr Buttimer [3] – Advice and supervision during antimicrobial tests

Michael Schmidt [1] – TEM analysis

David Clarke [3] Supervision and corrections

Martyn Pemble [1, 2] Supervision and corrections

Maria Bardosova [1,4] – Supervision and corrections

[1]Tyndall National Institute, University College Cork, Cork, Ireland;

[2]Department of Chemistry, University College Cork, Cork, Ireland;

[3]Department of Microbiology & Alimentary Pharmabiotic Centre, University College Cork, Cork, Ireland

[4]Slovak Technical University in Bratislava (STUBA), Ilkovičova 3, 81219 Bratislava, Slovak Republic

Abstract

We present an in-depth study on the development of a range of cross-linked chitosan composites which have potential antimicrobial applications. The composites were formed by cross-linking chitosan and siloxane networks and additionally by introducing silver and gold nanoparticles (NPs). Since chitosan, silver and gold NPs possess inherent antimicrobial properties; the aim of this study was to investigate whether adding the metal NPs to the chitosan-siloxane composite would lead to a material with enhanced antimicrobial ability as compared to chitosan itself. In addition, we wished to examine whether the new composite materials formed possessed any interesting mechanical or structural properties. The composites were synthesised in hydrogel form with the silver and gold NPs introduced by embedding them in the cross-linked chitosan network. Spectroscopic and microscopic techniques were employed to investigate the structural properties of the composite. In terms of mechanical properties, the tensile strength of the various composite structures was measured. It was found that the addition of metal NPs at a range of concentrations did not influence the mechanical strength of the composite. A crystal violet attachment assay provided insight into the degree of bacterial attachment on the various composites; results, which displayed a significant reduction in the attachment of *E. coli* to the cross-linked chitosan surfaces. Release profile tests suggest that the silver or gold NPs are not released under neutral conditions and as such may not contribute to the overall antimicrobial activity. It is concluded that, the contribution to the mechanical and antimicrobial properties from cross-linking with siloxane alone is significant, giving rise to a versatile, durable, antimicrobial material suitable for thin film formation, possible wound dressing fabrication or the coating of various surfaces where robustness and a degree of antimicrobial control are required.

Keywords: chitosan, cross-linked, interpenetrating polymer network, composite, silver nanoparticle, gold nanoparticle, antimicrobial

7.1 Introduction

7.1.1 Chitosan

Chitosan has many uses in a variety of industries, specifically in the biomedical field. It has significantly surpassed the usage limits of its predecessor, chitin [1]. Chitin's disadvantages stem from its distinct lack of ease of processing, due to its insolubility in most common solvents. This has been attributed to the strong intra- and inter-polymer hydrogen bonds formed by the acetamido functionality; these strong bonds contribute greatly to the insolubility of the molecule. Although soluble in harsh solvents such as hexafluoroisopropyl alcohol, common practise is to avoid use of these solvents due to their associated hazards, especially at batch-scale in industry [2]. The conversion to chitosan is a relatively simple one, involving the deacetylation of the acetamido group to yield an amino group. This functional group interconversion confers more favourable physical properties, for example it becomes soluble in acidic solution due to the presence of proton-sensitive amino groups, allowing dissolution in media of pH less than 6 [3]. Within this process, a factor to be considered is the threshold of deacetylation required to distinguish chitin from chitosan. In general, chitin is said to have a degree of acetylation of approximately 90%, meaning the presence of some acetyl groups within the polymer is unavoidable [4]. When deacetylation reaches approximately 50%, the polymer is regarded as chitosan [5]. Therefore, chitosan is essentially a copolymer composed of randomly distributed repeating units of both *N*-acetyl-D-glucosamine and *N*-D-glucosamine, linked through β-(1-4)-glycosidic bonds [6]. Advantageously, the desirable attributes of chitin, such as its biological and ecological compatibility, are unaffected by the conversion to chitosan. It is the innate physical and chemical properties possessed by chitosan which contribute to the vast array of potential applications within the biomedical field for this material that are currently under investigation [7].

Varying molecular weight and degree of deacetylation are the two key characteristics which influence the properties and functionality of chitosan. Properties such as mechanical strength, thermal stability, permeability [6, 8], swelling ability [9] and pH-sensitivity [10] are greatly affected by variations in the two key characteristics. Biological applications of chitosan rely on manipulation of some of these key reactivity and structural features [11]. Drug delivery is a prominent area in chitosan

research - an application which exploits the biocompatibility and pH-sensitivity of the polymer [12]. Chitosan has also been proven to demonstrate diverse antimicrobial capabilities, acting as a biocidal agent against fungi [13] and both Gram-positive and Gram-negative bacteria [14]. The presence of both a primary and secondary alcohol at the C-2 and C-6 positions of each monomeric unit, coupled with a reactive amine at C-3 in the deacetylated monomers, show a key structure activity relationship [3]. In an era of extensive concern regarding antibiotic resistance, the emergence of chitosan's antimicrobial potential is one of considerable interest. At the interface of materials and biomedical science, the precise mechanism of action of chitosan as an effective antimicrobial agent is unknown, but studies have suggested various explanations. One rationale, suggested by Li *et al.*, attributes antimicrobial activity to the amine functional group [15]. At low pH, it has the potential to become ionised to NH_3^+, introducing the possibility of electrostatic interactions with negatively charged microbial cell walls. It is thought this alters permeability and strength of the cell wall, allowing for weakening and eventual rupture, thus killing the organism [15]. This activity is seen to cease at pH values greater than 6, as chitosan loses its charge, and oftentimes, can be seen precipitating from solution [16]. The molecular weight of chitosan is also shown to influence antibacterial activity. High molecular weight chitosan is regarded as too large to permeate cell walls of bacteria. It is thought to cluster on bacterial cell walls, inhibiting entry of essential nutrients and oxygen, inevitably resulting in cell death [17]. In contrast, low molecular weight chitosan possesses the ability to penetrate cells, where it is suspected of binding to cell DNA, prohibiting mRNA synthesis and resulting in termination of cell multiplication [18]. A study conducted by Liu *et al.* described the influence of chitosan concentration and molecular weight on its effectiveness as an antimicrobial agent against *Escherichia coli* (*E. coli*). At low concentration, it was concluded that chitosan displayed no biocidal effect – indeed was sometimes seen to promote bacterial growth - but at higher concentrations it acted as an effective agent, resulting in cell death [14]. Agglutination of cells resulting in cell death is the mechanism of action proposed. For this to occur, a threshold concentration of chitosan is required. Below this, bacteria continue to multiply and thrive [14]. The degree of deacetylation must also be considered when discussing the antimicrobial activity of chitosan. Chitosan with a high degree of deacetylation (HDD) shows a higher antimicrobial efficacy. HDD chitosan shows a higher acid solubility and so is expected to demonstrate better antimicrobial potential

than chitosan with a low degree deacetylation (LDD). Lysozyme, a biological enzyme responsible for cell lysis demonstrates degradative action towards chitosan. Lysozyme is far more efficient at cleaving the bond in *N*-acetyl glucosamine, which is more abundant in LDD chitosan, than the corresponding bond in N-glucosamine. For this reason, HDD chitosan is seen as a more robust polymer [9].

7.1.2 Cross-linking

Although regarded as a highly applicable polymer, chitosan does possess some drawbacks, mainly due to its high aqueous solubility - a property which proves problematical in applications involving aqueous biological media. This issue can be overcome by the introduction of a cross-linker. A cross-link is formed through a chemical reaction, which links two polymers together, either through covalent/ionic bonds or weaker bonding interactions, for example, Van der Waals forces [19]. The individual polymers within the cross-linked composite may together show new properties, whilst still maintaining their own critical features. One type of cross-link, which has undergone significant studies, is the formation of an interpenetrating polymer network (IPN). According to the International Union of Pure and Applied Chemistry, an IPN can be defined as "a polymer comprising of two or more networks which are at least partially interlaced on a molecular scale but not covalently bonded to each other and so cannot be broken unless chemical bonds are broken" [20]. Cross-linkers come in the form of polymers [21], oxides [22], metals [23] and amino acids [24], among other chemical entities. For the purpose of our research we synthesised and investigated a physically cross-linked network of two polymers, chitosan and siloxane, as well as incorporating metal nanoparticles (NPs) as further structure enhancers. There are many possible polymers which could successfully form an IPN with chitosan, especially due to the availability of chitosan's functional groups for interaction. These include polymers containing carboxylic acids, epoxides and alcohols. However the use of some of these polymers can be unfavourable as they may disrupt membrane formation [25]. One IPN that has been established as non-problematic in this regard is the IPN formed between chitosan and tetraethyl orthosilicate (TEOS) [26]. The chitosan-TEOS IPN (Chi-TEOS IPN) contains two main components; chitosan, which forms individual polymer chains and TEOS which undergoes hydrolysis followed by condensation to generate a siloxane polymer chain. These two chains subsequently cross-link to form a so-called Chi-TEOS IPN. Physical cross-linking

takes place resulting in the individual polymer chains entangling and interlacing, held together by hydrogen bonds and Van der Waals forces [27]. This combination results in the formation of an IPN which is flexible, due to the presence of chitosan while also being mechanically strong and insoluble in common aqueous systems, attributed to the siloxane cross-linker providing a structural backbone to the IPN [10]. This phenomenon was examined in a previous study from our laboratories in which tensile strength tests were carried out before and after cross-linking [28]. Chitosan exhibited elastic behaviour, tearing continuously under much less strain in comparison to the cross-linked Chi-TEOS IPN which demonstrated better mechanical strength, with sudden fracture of the membrane occurring at a much higher stress levels. The reduced solubility and improvement in mechanical strength induced by cross-linking with TEOS is desirable in developing chitosan membranes for targeted applications, such as wound dressings. . The effect of introducing colloidal particles (silica and polystyrene particles at a constant concentration and particle diameter in the range of 200-400 nm) was also examined in our previous study with results displaying a significant increase in tensile strength as a function of decreasing particle diameter, effectively increasing surface area. In this present study, the effect of incorporating metal NPs will be investigated in order to determine whether the tensile strength of the Chi-TEOS IPN is enhanced or degraded by the presence of metal NPs.

7.1.3 Silver nanoparticles

Accounting for approximately 25% of papers devoted to metal applications within biomedicine [29], silver is known to possess both anti-inflammatory and antimicrobial capabilities [30]. Seen as the most effective metallic antibacterial agent [31], with a higher potency than metals such as lead, tin, copper and chromium [32], silver has a diverse range of applications. These include medical implants, wound dressings, biosensors and emerging applications within the field of cancer therapeutics [33]. Recently, the use of silver nanoparticles (Ag NPs) has been seen to be more beneficial than the use of bulk silver within devices [32]. This has been attributed to the larger surface area and reduced mass of silver necessary to elicit an antimicrobial response. Because of this, Ag NPs are seen to possess a lower toxicity, making them a more favourable option. Recent studies have concluded that Ag NPs are more potent antibacterial agents than certain commercially available antibiotics [30].

An emerging explanation of the mechanism of bacterial resistance to these various agents involves the formation of biofilms. Biofilms can be defined as "microbial consortia embedded in self-produced exopolymer matrices composed of mainly exopolysaccharides" [34]. A medical nuisance, biofilms are resistant to many known antibiotics, detergents and disinfectants. Usually, treatment of biofilms involves their physical removal, which is traumatic for patients [35]. Advantageously, Ag NPs have been seen to be capable of inhibiting biofilm formation, making them a potential alternative to commercial antibiotics in the treatment of biofilms [34]. The mechanism of antibacterial action of Ag NPs is thought to rely on surface interactions between silver and the bacterial cell wall. Due to the large surface area of Ag NPs, they are capable of anchoring to bacterial cell walls where they can stimulate changes in the strength and permeability of the cell. These changes can ultimately lead to cell lysis and extrusion of cell contents, resulting in bacterial cell death [36]. This mechanism of action was seen to be dependent on the type of bacterial cell being targeted. For example, according to Kim *et al.*, Gram-negative *E. coli* shows a higher sensitivity to Ag NPs than Gram-positive *Staphylococcus aureus (S. aureus)* strains [37]. This difference can be rationalised by considering the structural differences between both bacteria. Gram-positive bacteria have much thicker cell walls made up of multiple peptidoglycan layers compared to a single peptidoglycan layer in the cell wall of Gram-negative bacteria [38]. The additional teichoic acid and peptidoglycan layers give extra protection to Gram-positive bacteria [33]. It has also been speculated that interactions between silver and lipid molecules in the cell membrane contribute to antibacterial activity. Silver is assumed to alter the fluidity of cell membranes through alterations in fatty acid composition. This can result in the loss of membrane integrity, allowing for easier penetration of Ag^+ ions to the intercellular bacterial environment [39]. Thiol functional groups are present in many bacterial enzymes necessary for cell function. Ag^+ ions can interact with sulfur atoms within the bacterial enzymes, disrupting their activity, with cell death an eventuality [40]. The extent of this interaction is also seen to rely on the composition of the bacterial cell wall. In order to cause an antibacterial effect, Ag^+ ions must penetrate the cell wall and enter the cell cytoplasm. This has been shown to be more difficult in Gram-positive bacteria [33]. Durán *et al.* concluded that thiol-silver complexation resulted in the disruption of oxidative phosphorylation, a key step in metabolism, eventually leading to bacterial mortality [41]. Conflicting theories exist as to which form of silver is responsible for its

antimicrobial potency. There is considerable evidence that ionic silver, Ag^+, is responsible for the major antibacterial pathways, with many researchers believing that the silver cation has a high affinity for negatively charged DNA and thiol groups within bacteria. A study conducted by Xiu *et al.* found that under anaerobic conditions Ag NPs displayed no antibacterial activity [42]. This would suggest that antibacterial activity is solely due to Ag^+. Many suggest the role of Ag NPs is simply to generate a continuous flow of Ag^+ through oxidation of Ag^0. It is believed these ions are then transported to their biological targets, where they elicit an antibacterial response [43].

7.1.4 Gold nanoparticles

In comparison to silver, gold is a metal which is not so commonly sought after for its antimicrobial abilities. In a review by Zhang *et al.* [44] it was proposed that gold, in both NP and ionic form, does not exhibit antimicrobial properties unless found at very high concentrations or in ionic complexes. Gold NPs (Au NPs) are generally stabilised by coating with surfactant molecules such as polyvinylpyrrolidone (PVP) or sodium dodecyl sulfate (SDS) or ions such as citrate, which prevents agglomeration of the NPs in solution. In a study by Mukha *et al.* surfactant-stabilised Au NPs in the diameter range of 20-30 nm showed no antimicrobial activity against either *S. aureus* or *E. coli* [45]. In a similar test by Hernandez-Sierra *et al.* positive results were observed as the concentration of Au NPs in solution increased [46]. Interestingly, with the development of a "green" synthesis approach to Au NPs there has been an improvement in results relating to bactericidal studies. "Green" synthesis is essentially the name given to an eco-friendly approach to the chemical processing of Au NPs, which can be carried out using naturally-occurring substances as reducing agents, such as flower extracts [47] or fungi [48]. Mishra *et al.* synthesised gold and silver NPs by a "green" method with high antimicrobial efficiency observed against *S. aureus* [49]. The exact reasoning as to why there is such a marked improvement in results when synthesising Au NPs using the "green" approach is thus far unknown but it is proposed it may be a synergistic effect enhanced by inherent bactericidal activity of the natural sources [50]. A similar dilemma arises in investigating the bactericidal properties of gold as does with silver – namely, is the antibacterial activity observed due to the presence of the metal NPs or ions released from the NPs? The general consensus is that the mechanism of action is due to gold ions but in this case as part of an ionic complex, due to the fact that ionic gold is not as stable as ionic silver. It has been proposed that Au^+ and Au^{3+} are the ionic

forms predominantly responsible, with Au^{+} studied more extensively than Au^{3+}. Au^{+} complexed with phosphine and n-heterocyclic carbenes has shown antimicrobial and antifungal activity. Au^{3+} organometallic complexes co-ordinated through Au-C or Au-N bonds interact with biological thiol groups found in bacterial enzymes which are essential for cell function [51]. Bacterial growth inhibition tests carried out by Dasari *et al.* revealed that both Au^{+} and Au^{3+} inhibit bacterial growth as a function of concentration. Further tests revealed that Au^{3+} is the more dominant ion as the bacterial inhibition significantly reduced with gradual removal of Au^{3+} ions. The cytotoxicity of Au^{3+} increases with concentration, posing possible problems *in vivo* [52].

7.1.5 Applications

Blaser likens the use of antibiotics to a 'four-edged sword' [53]. The initial use of antibiotics benefited both individuals and communities by fighting and preventing the spread of infection. The other two 'edges' transpired as antibiotic resistance became apparent in communities as well as the emergence that antibiotic use, can alter 'good' bacteria which is essential to an individual's microbiome. Van Boeckel *et al.* conducted a study on global antibiotic consumption in the time period from 2000 to 2010 [54]. Their results revealed a 36% global increase in the use of antibiotics in the ten-year time period. An increasing global trend has been noted in the use of 'last-resort' polymixin antibiotics. This is believed to reflect the growth-rate of drug-resistant bacteria [55]. Bacterial evolution and inappropriate use of drugs contribute greatly to the development of said drug-resistant bacteria.

Cross-linked chitosan membranes with antimicrobial properties are possible candidates in the development of simple, low-cost, antimicrobial wound-dressings. Previous studies have reported the development of chitosan wound-dressings which especially show promise when reinforced by other natural materials [56, 57]. For example Zhao *et al.* found that electrospun chitosan/sericin composites effectively inhibit the growth of Gram-positive and Gram-negative bacteria by means of a simple colony-counting technique [58]. There is an urgent need for the development of such materials in our modern, antibiotic-dependant society which has arisen as a result of the emergence of drug-resistant bacteria. The aim of this present study is to investigate the structural changes induced on a chitosan network upon cross-linking with a siloxane network along with the inclusion of Ag and Au NPs and to look at the

influence cross-linking may have on the antimicrobial properties of these composite materials.

7.2 Materials and methods

7.2.1 Synthesis of hydrogels and thin films

All chemicals were supplied by Sigma Aldrich, Ireland. The chitosan hydrogel and siloxane cross-linked interpenetrating polymer network (Chi-TEOS IPN) were synthesised by a cationic polymerization technique adapted from [10] and as described in [4] utilising low molecular weight chitosan. Chi-TEOS IPNs containing Ag and Au NPs were prepared at a 0.02% concentration (0.02 $mgmL^{-1}$ at 10 vol%). All samples were formed by a drop casting technique which involved drop casting a volume of 250 µL onto a hydrophilic glass surface with a surface area of 15 mm x 15 mm and allowing the sample to dry at 40 °C. Corning® plain microscope slides were employed in all experiments. This method could be easily modified according to the requirements for specific sample preparation.

7.2.2 Spectroscopic analysis

The Ag and Au NPs were analysed by UV-vis spectroscopy to confirm the dimensions of the particles; this was carried out on a Shimadzu UV-2401PC UV-vis spectrometer. Infrared analysis was carried out on free-standing thin film samples using a Bruker Alpha Fourier transform infrared spectrometer in attenuated total reflection mode which utilises a platinum-diamond crystal. A Renishaw inVia confocal Raman microscope was used for Raman analysis on thin film samples immobilised on glass slides. The structural differences between the chitosan and the hybrid cross-linked networks were investigated.

7.2.3 Microscopy

Scanning electron microscopy (SEM) analysis was performed using a FEI Quanta 650 FEG High Resolution scanning electron microscope. Typical beam energies were in the range of 10-20 kV. SEM analysis allowed for membrane thickness measurements and topological investigation. Transmission electron microscopy (TEM) was employed to image and measure Ag and Au NPs in the Chi-TEOS IPN membrane; these measurements were carried out on a JEOL 2100 High Resolution TEM, operated at 200 kV in bright field mode using a Gatan double tilt holder.

7.2.4 Surface and mechanical analysis

Surface roughness analysis was carried out using a KLA Tencor P15 profilometer, for further investigation into topological quality; this was done at a scanning rate of 20 μms^{-1} and a scanning distance of 1000 µm. The same test conditions were employed as in the preceding study [28] - an Instron 5565 universal testing machine was used to carry out tensile strength tests on the thin film membranes with rectangular geometry of 10 mm x 40 mm. Test conditions at room temperature included a load of 5 kN, clamp speed of 0.5 mm/min and data rate of 10 pts/sec. The thin film strips were clamped with polydimethylsiloxane (PDMS) supports.

7.2.5 Antimicrobial tests

A crystal violet (CV) attachment assay [59] was carried out using Gram-negative bacteria – *E. coli*. The aim was to assess the affinity of bacterial samples for the various chitosan samples. Glass, chitosan, Chi-TEOS IPN, Chi-TEOS IPN-Ag and Chi-TEOS IPN-Au samples were all tested under aseptic conditions. Six slides of each sample were immersed in a six-well plate containing 2 x lysogeny broth (LB) growth medium, 2 x biological replicate 1 of bacterial sample in LB and 2 x biological replicate 2 of the same bacterial sample in LB. These were prepared at an initial optical density (OD) of 0.05 and stored at 37 °C for 24 hours, ideal growth conditions for *E. coli*. There were two controls in the form of the glass samples and the first two wells of each 6-well plate bearing the LB growth medium but no bacteria. After 24 hours, the samples were thoroughly rinsed and stained with CV solution followed by rinsing in ethanol. The relative absorbance of all samples was measured allowing for a qualitative comparison. The absorbance was measured using a Tecan Genios plate reader with X Fluor 4 software on Microsoft Excel.

7.2.6 Release profile

An investigation into whether the Ag/ Au NPs were capable of being released from the Chi-TEOS IPN network was carried out by immersing samples in relevant solutions and subsequently analysing the solutions using a Shimadzu UV-2401PC UV-vis spectrometer. The method involved immersing the cross-linked samples (Chi-TEOS IPN, Chi-TEOS IPN-Ag and Chi-TEOS IPN-Au) in 5 mL of 0.01 M phosphate buffered saline (PBS) solution in a series of six-well plates – six of each sample per plate, therefore three plates. The plates were then stored in an enclosed oven at 37 °C

to replicate the growth environment for *E. coli* as described in section 2.4. Transmission spectra of the PBS solutions were measured at hourly intervals over a six-hour period, using the PBS with Chi-TEOS IPN samples immersed as the background correction. Transmission spectra were also recorded after 24 hours of storage at microbiological-replicate growth conditions. A few drops of 0.1 M NaCl were subsequently added to each solution to detect whether ions, rather than NPs, were released into solution. Tests were also carried out in 0.1 M phosphate buffers at pH 2.5 and 11.5, to determine test whether the release (if any) was pH-dependant due to the inherent pH-sensitivity of the chitosan network.

7.3 Results and Discussion

7.3.1 Synthesis of hydrogels and thin films

The chitosan hydrogels described in section 7.2.1 were prepared and deposited onto glass surfaces. It was important that the thin films were immobilised on a substrate in order to be able to perform the microbiological testing, because such samples need a solid support due to the rigorous washing and staining during the procedure for the CV attachment assay. This method was kept standard during other tests. Figure 7.1 displays the hydrogels; the yellow and pink appearance of the Chi-TEOS IPN-Ag/Au samples, respectively, is due to the surface plasmon resonance phenomenon which is characteristic of Ag and Au NPs.

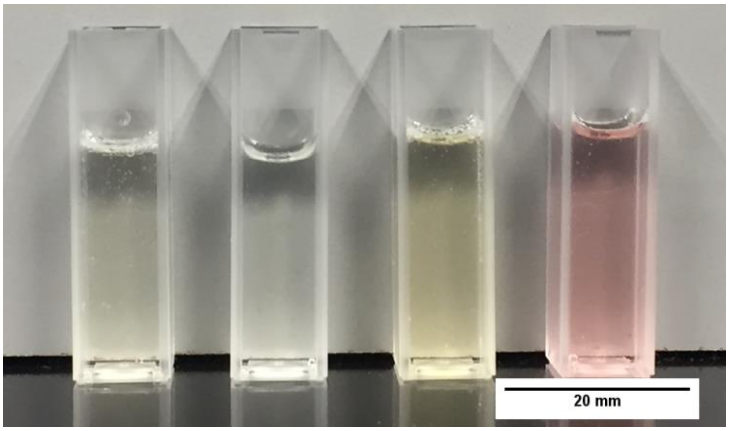

Figure 7.1. Chitosan composite hydrogels (L-R); chitosan, Chi-TEOS IPN, Chi-TEOS IPN-Ag and Chi-TEOS IPN-Au.

7.3.2 Spectroscopic analysis

7.3.2.1 UV-vis spectroscopy

Transmission measurements carried out on the metal NP dispersions by UV-vis spectroscopy revealed that the diameter of the Ag and Au NPs were 20 nm as the transmission wavelength corresponds with the literature values for the associated particle diameters. See figure 7.2.

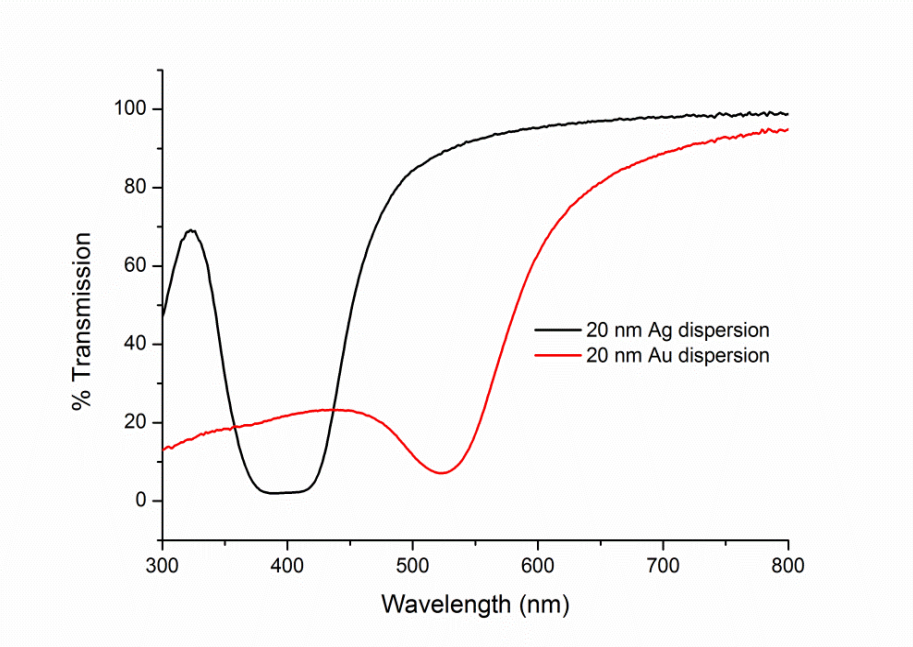

Figure 7.2. Transmittance spectra of Ag and Au dispersions.

7.3.2.2 Infrared (IR) spectroscopy

The IR spectra for Chi-TEOS IPN-Ag and Chi-TEOS IPN-Au reveal that the same functional groups are present as in the Chi-TEOS IPN. The peak at 785 cm^{-1}, which is not present for chitosan, is representative of deformations in amino (N-H) groups – occurring as weak H-bonds that distort the chitosan structure. A chitosan peak at 1250 cm^{-1} is lost at a frequency where methyl group stretches are usually found. This is probably due to an induced dipole disturbance to the structure caused by the presence of the cross-linked siloxane network. See figure 7.3 for the associated IR spectrum. Full assignment of the IR spectra is available in [28].

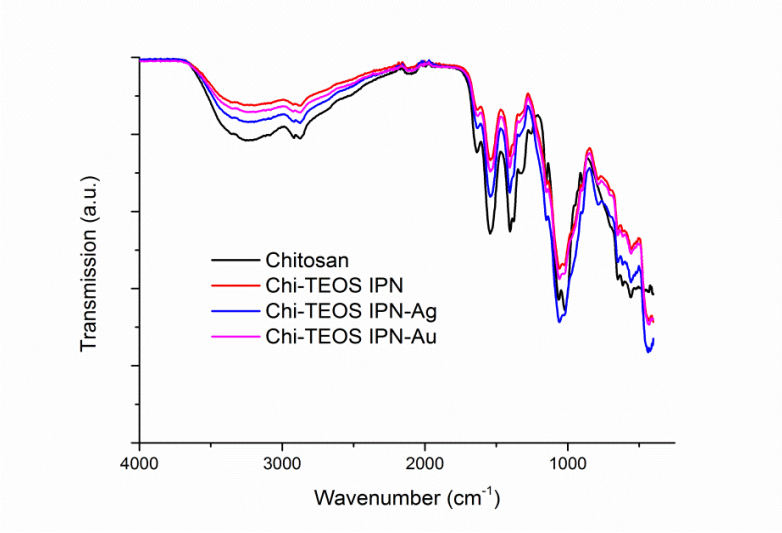

Figure 7.3. Infrared spectra of chitosan samples before and after cross-linking with siloxane polymer network and metal NPs.

7.3.2.3 Raman spectroscopy

There appears to be very little disruption to the chitosan sample after cross-linking with the siloxane network and the metal NPs, according to the Raman data obtained, figure 7.4. Again, this suggests that non-covalent, physically cross-linked linkages are being formed. The fact that no new peaks appear upon inclusion of the metal NPs highlights the lack of influence that the Ag/ Au NPs have on the structure of the Chi-TEOS IPN, a trait which was also suggested from the IR spectra in figure 7.3.

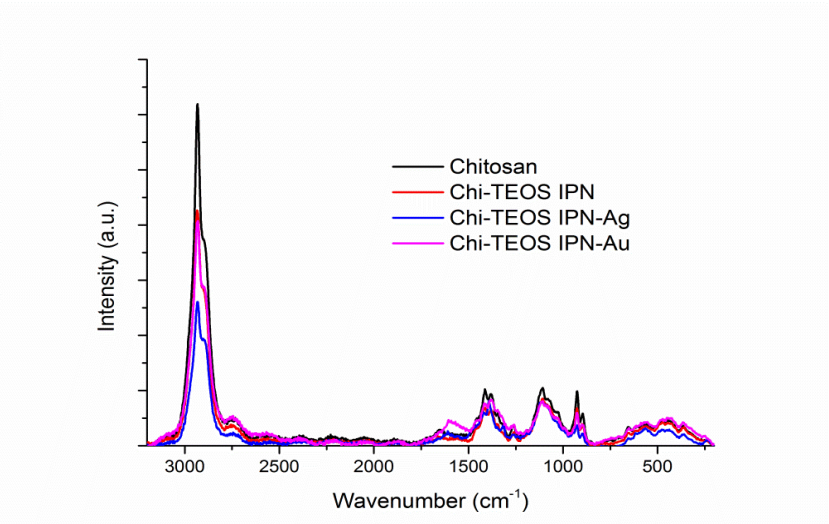

Figure 7.4. Raman spectra of chitosan samples before and after cross-linking with siloxane polymer network and metal NPs.

7.3.3 Microscopy

7.3.3.1 SEM

SEM analysis revealed that the samples have a uniform thickness of 8-10 µm when prepared according to the method described in section 7.2.1. Thickness measurements yielded 8.58 µm, 10.04 µm, 9.31 µm and 8.30 µm for the chitosan, Chi-TEOS IPN, Chi-TEOS IPN-Ag and Chi-TEOS IPN-Au samples, respectively. Increased surface porosity was observed in the cross-linked samples; however, this is somewhat ambiguous due to the difficulties which arise in achieving contrast when imaging polymer samples. During these measurements it also became apparent that the thin film samples were not completely bound to the glass surface, but were perhaps remaining in place due to electrostatic interactions, possibly induced by the electron beam. The associated images can be seen in figure 7.5.

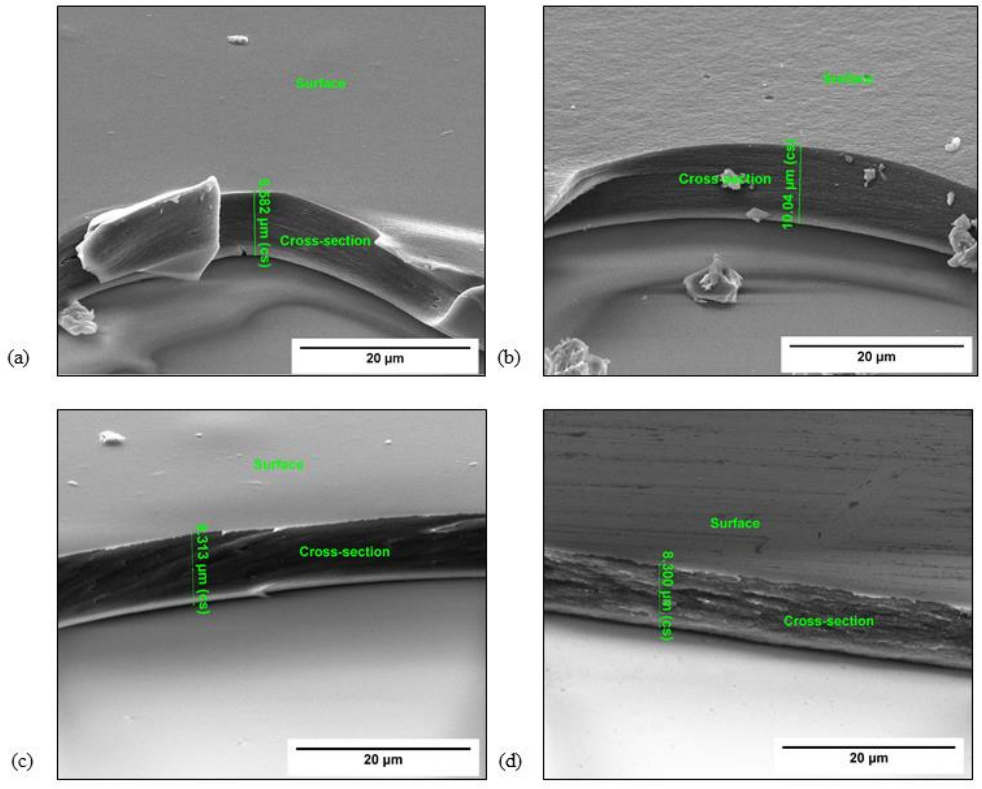

Figure 7.5. SEM images displaying the thickness and apparent surface roughness of the various chitosan samples; (a) chitosan, (b) Chi-TEOS IPN, (c), Chi-TEOS IPN-Ag and (d) Chi-TEOS IPN-Au.

7.3.3.2 TEM

TEM analysis was chosen as a method for imaging the metal NPs in the IPN due to its high resolution as well as the fact that less charging occurs in comparison to SEM. The sample was prepared at a thickness of 200 nm by dropping <0.3 µL of the 10 vol% Chi-TEOS IPN-Ag/Au hydrogel onto a lacy carbon TEM grid. Imaging was successful for both samples – see figure 7.6. It became apparent that the Ag dispersion 7.6(a) is not as concentrated as the Au dispersion 7.6(c) by the number of particles counted per image; 38 Ag NPs were counted over ten images with an average particle size of 16 nm ± 25%, while for the Au dispersion 107 NPs were counted over 10 images and the average particle size was 19 nm ± 18%. A single Ag NP can be seen in figure 7.6(b). The darker area shows the atomic scale crystal lattice, suggesting that the Ag NP is monocrystalline. Figure 7.6(d) shows an Au NP which seems to be polycrystalline due to the appearance of two dark areas, possibly representing two different crystal facets.

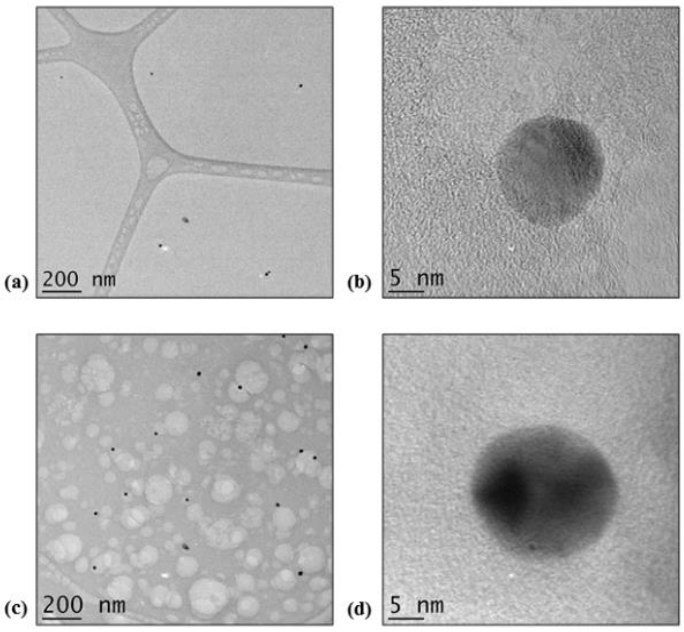

Figure 7.6. TEM images of (a) Ag NPs embedded in the Chi-TEOS IPN (b) single Ag NP with one crystal facet observed (c) Au NPs embedded in the Chi-TEOS IPN (d) single multifaceted Au NP.

7.3.4 Surface and mechanical analysis

7.3.4.1 Surface roughness measurements

Surface profiling was carried out in order to determine the roughness of the various samples, following the SEM observation that samples become more porous upon crosslinking. Scans were set at a speed of 20 μms^{-1} over a scanning distance of 1000 µm, with ten scans per sample. The results are outlined in table 7.1. The surface roughness increases as the cross-linker density increases - a characteristic which was also suggested from analysis of the SEM images. Comparable results were seen between the membranes with NPs embedded, suggesting both the Ag and Au NPs act similarly within the membranes, causing the same subtle structural alterations. The greater percentage dispersity of the chitosan sample was due to a bubble on the sample surface which came in contact with the stylus.

Sample	**Average surface roughness (Å)**	**Dispersity (±%)**
Chitosan	4588	250
Chi-TEOS IPN	6347	200
Chi-TEOS IPN-Ag	9174	209
Chi-TEOS IPN-Au	9722	196

Table 7.1. Surface roughness measurements of the various samples, showing an increased average surface roughness with increasing cross-linker density.

7.3.4.2 Tensile strength tests

The tests carried out investigated the effect of the presence of Ag and Au NPs with a diameter of 20 nm. Results showed that both NP types produced hybrid membranes capable of reaching mechanical stresses of up to 74 MPa, compared to 75 MPa ± 29% for the Chi-TEOS IPN [28]. This value was reached with the lowest concentration of metal NPs used and increasing this concentration made little or no change to the mechanical stress reached by the membranes. These results displayed low variance values, a favourable trait in terms of reproducibility of the samples. See figure 7.7 for a graphical representation of the results as a function of increasing Ag/ Au NP concentration; 130/ 650/ 1300 µL corresponding to 1/ 5/ 10 vol%, respectively.

Due to the dilute nature of the metal NP dispersions the Ag/ Au NPs are present at a very low concentration. This may be the reason why the NPs do not appear to act as structure enhancers. The low concentration was also apparent in the TEM analysis. However, the low concentration of Ag/ Au may still contribute towards enhancing the antimicrobial properties of a cross-linked chitosan membrane without causing appreciable degradation in mechanical strength - a property which would be highly desirable for certain types of anti-microbial membranes or drug delivery systems.

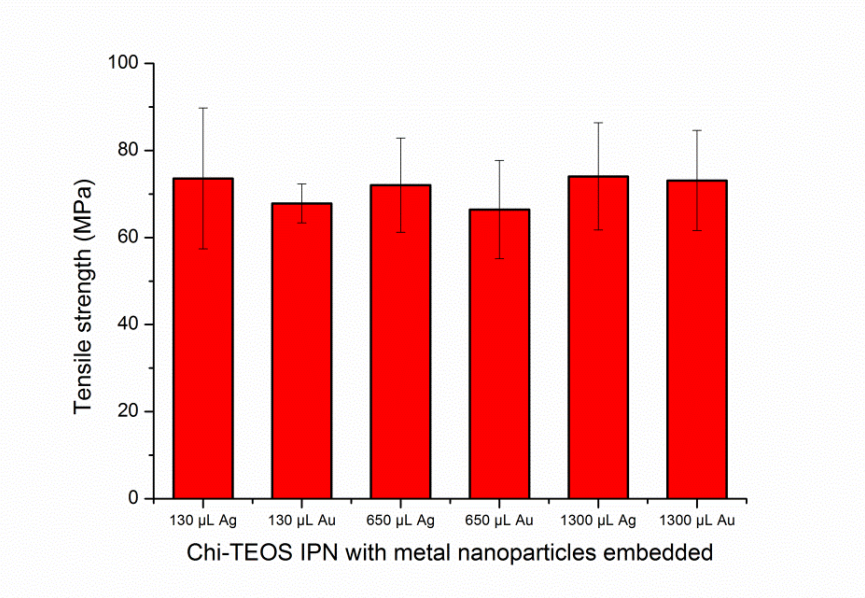

Figure 7.7. Tensile strength results with metal NPs embedded as a function of increasing concentration. Results are on par with stresses reached by the Chi-TEOS IPN prior to addition of NPs. No concentration dependence was observed.

7.3.5 Crystal violet attachment assay

Results from the CV attachment assay with *E. coli* show that cross-linking contributes to the antimicrobial activity by reducing the attachment of bacteria to the surface by up to 80%. It is not known whether the siloxane cross-linker itself demonstrates antibacterial activity but, due to observations made throughout the tests, we suggest that the improved antibacterial activity of the Chi-TEOS IPN is due to the enhanced structural strength it imparts on the membranes. During the tests, the chitosan membranes were seen to completely detach from the glass substrate and disintegrate in the bacterial solution. Conversely, the cross-linked membranes, including those with embedded NPs, maintained their structural integrity and appeared to be almost

unchanged after the tests were conducted. This again suggests that the cross-linkers enhance the strength of the membranes.

It appears that the addition of Ag and Au NPs has no effect on the degree of bacterial attachment, indicating that the metal NPs do not contribute to the antimicrobial activity, perhaps because they are not being released from the membrane in neutral conditions. See figure 7.8.

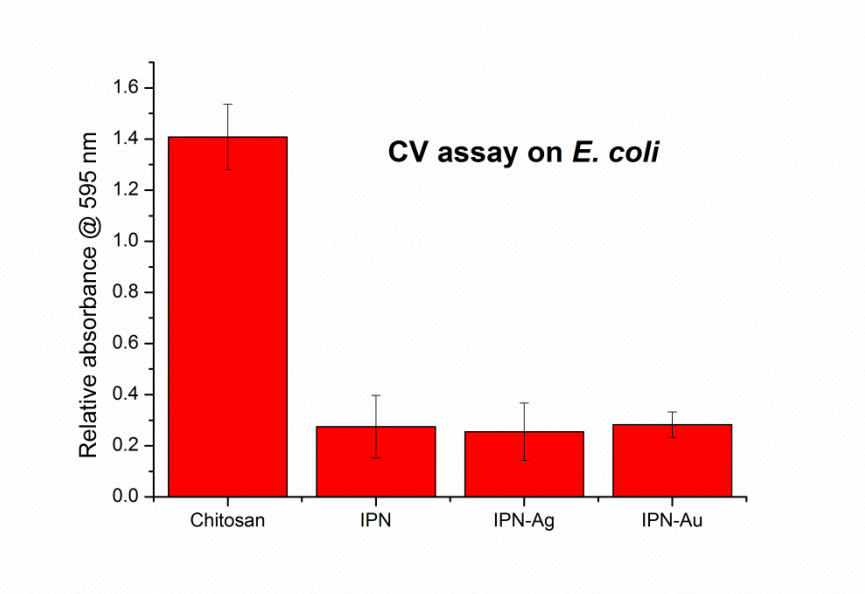

Figure 7.8. Relative absorbance values of chitosan, cross-linked Chi-TEOS IPN and Chi-TEOS IPN with Ag/ Au NPs. The absorbance corresponds to the degree of bacterial attachment during the CV assay with *E. coli*. There is a significant reduction in attachment upon cross-linking with TEOS, while the addition of Ag/ Au NPs does not contribute to antimicrobial activity.

7.3.6 Release of Ag/ Au NPs

Our measurements indicate that the metal NPs are not released in either NP or ionic form. If correct, this would indicate that their inclusion provides no additional contribution towards the antimicrobial activity, other than that which may arise from the enhanced mechanical properties alone. Figure 7.9 displays the UV-vis spectra of both Ag and Au NPs at a range of concentrations. The initial concentration of NPs employed was 2.5% and we estimate that the lower limit of detection of NPs from the UV-vis measurement was 0.25%, figure 7.11. However, when the PBS test solution

was measured there was no peak observed, meaning that within experimental error there was no release of NPs into the solution, over the time allowed.

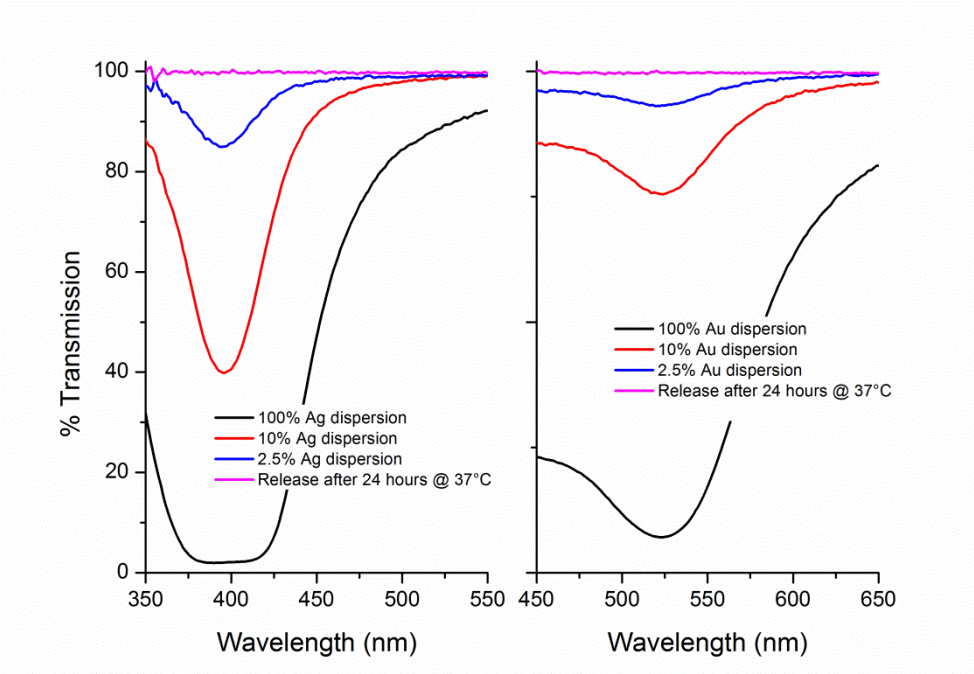

Figure 7.9. UV-vis spectra of Ag/ Au NPs at a series of concentrations. 2.5% is the concentration of Ag/Au NPs present in each sample. This peak is not observed during the release tests meaning NPs are not being released.

As noted above the possibility of ion release was investigated by adding a few drops of 0.1 M NaCl to the tests PBS solution. If there were an appreciable number of ions present the solution would turn cloudy due to the formation of AgCl/ AuCl salts, which may be observable by eye or by a possible reduction in transmission. Neither of these changes were observed, suggesting that again, within the constraints of our measurements, no Ag/ Au ion release was taking place, see figure 7.10. Upon drying the samples, the yellow/ pink hue of the Ag/ Au NPs was still observed, providing evidence that the NPs were still present in the Chi-TEOS IPN structure.

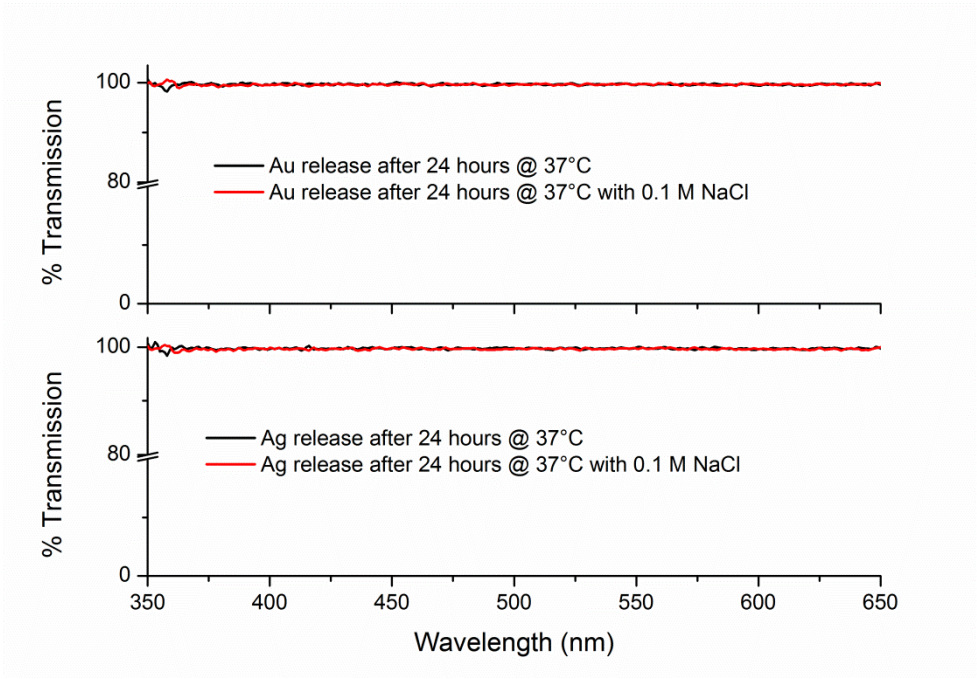

Figure 7.10. UV-vis spectra of the PBS solutions in combination with 0.1 M NaCl, results indicate that Ag/Au ions are not being released as there is no change to the transmission spectrum.

The release tests were carried out in phosphate buffers of pH 2.5 and 11.5 in order to investigate whether the Ag/Au NPs were being released in acidic/ basic conditions. The IPNs might be expected to release the NPs at low pH as the chitosan network swells in acidic conditions due to the protonation of amino groups. The results of these release studies are shown in figure 7.11.

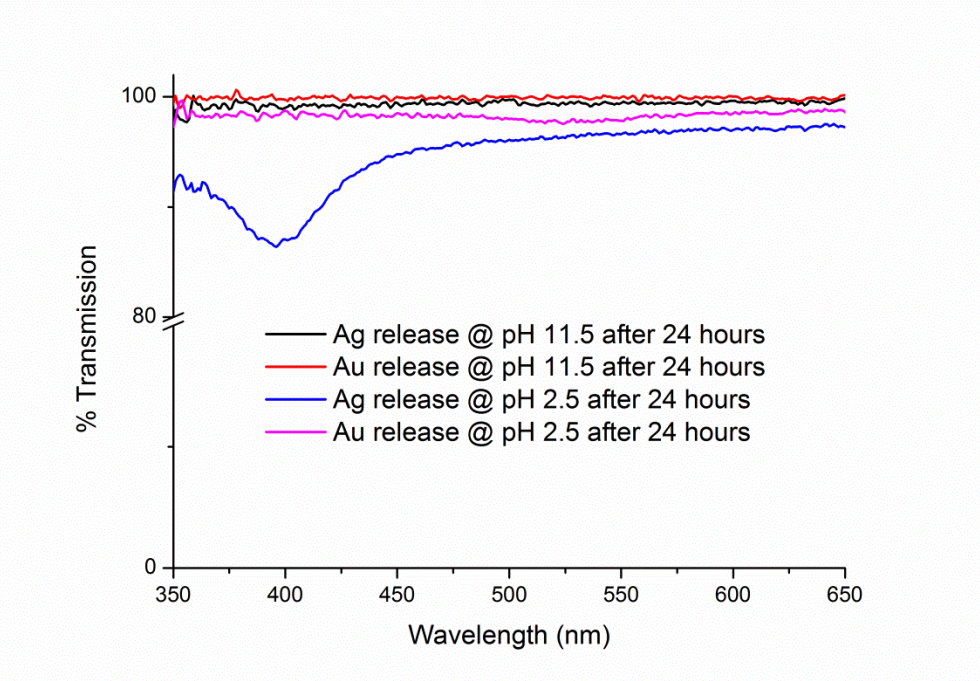

Figure 7.11. UV-vis spectra of Chi-TEOS IPN-Ag/Au samples being tested for release in basic and acidic conditions. The dips at about 395 and 525 nm indicate that the Ag and Au NPs are being released from the membrane in acidic conditions, respectively.

From figure 7.11, it is apparent that the Ag/ Au NPs were released in acidic conditions, as expected. Thus, we conclude that the Ag/ Au NPs can indeed be released from the membrane but the membrane must swell to allow for release. So, although not suitable for NP release under neutral conditions the cross-linked Chi-TEOS IPN with NPs embedded may be suitable for release in gastric conditions which are acidic in nature or in surface wounds which are often treated to deliberately create an acidic environment [60, 61].

7.4 Conclusions

Chitosan along with silver and gold NPs are well-known individually for their inherent antimicrobial properties [15, 30, 62]. The aim of this study was to investigate whether combining these materials would lead to any enhanced antimicrobial effects, induced by any structural or mechanical changes to the composite.

Our results demonstrate that the IPNs synthesised here show little evidence of any major chemical changes, although the inclusion of the metal NPs was found to influence the overall porosity of the IPN formed.

Under neutral conditions no evidence was found to support the hypothesis that the IPN could release either the metal NPs themselves, or ions derived from them- rather that the NPs were released under acidic conditions that would be more aligned to the conditions found in the digestive system, which would facilitate swelling of the chitosan part of the IPN. These observations account for the lack of additional antimicrobial activity arising from the presence of the metal NPs under the neutral conditions employed for the microbiological assay. It is therefore concluded that the metal NPs are simply physically confined within the IPN. With this in mind it is perhaps not so surprising that we found that the inclusion of the metal NPs did also not appreciably alter the mechanical properties of the films. What is perhaps surprising is that we have clearly identified additional mechanical strength and additional antimicrobial activity arising from the presence of the siloxane cross linker. In terms of the enhanced mechanical properties we clearly observe an increase in the robustness of the films in the bacteria solutions deployed in the assay, for those films containing the siloxane cross linker. In terms of the degree of attachment of *E. coli* to the cross-linked IPN, we found that this was some ~80% less than the attachment of the same bacteria to the non-cross-linked chitosan.

This is a very positive result. Chitosan has been known to have antimicrobial effects on Gram-negative bacteria however our results show that providing additional mechanical strength to the chitosan network enhances this effect, in that the cross-linked membranes are much more stable in bacterial solution than the non-cross-linked chitosan membranes.

We suggest that our findings may stimulate the production of a range of chitosan/siloxane IPNs for a variety of biomedical applications such as wound dressings. In addition, we suggest that the release of metal NPs from these IPNs under acidic conditions may find application is the treatment of a range of disorders of the digestive system.

References

1. Ryan, C. C.; Pemble, M. E.; Bardosova, M., Current trends in chitosan-related research in the biomedical field: A short review. *Natural Product Communications* **2017,** *12*.

2. Mourya, V.; Inamdar, N. N., Chitosan-modifications and applications: opportunities galore. *Reactive and Functional Polymers* **2008,** *68* (6), 1013-1051.

3. Kumar, M. N. R., A review of chitin and chitosan applications. *Reactive and Functional Polymers* **2000,** *46* (1), 1-27.

4. Ryan, C.; Delezuk, J.; Pavinatto, A.; Oliveira Jr, O.; Fudouzi, H.; Pemble, M.; Bardosova, M., Silica-based photonic crystals embedded in a chitosan-TEOS matrix: preparation, properties and proposed applications. *Journal of Materials Science* **2016,** *51* (11), 5388-5396.

5. Dash, M.; Chiellini, F.; Ottenbrite, R.; Chiellini, E., Chitosan—A versatile semi-synthetic polymer in biomedical applications. *Progress in Polymer Science* **2011,** *36* (8), 981-1014.

6. Rong Huei, C.; Hwa, H.-D., Effect of molecular weight of chitosan with the same degree of deacetylation on the thermal, mechanical, and permeability properties of the prepared membrane. *Carbohydrate Polymers* **1996,** *29* (4), 353-358.

7. Iosody Silva-Castro, P. M.-R., Patruta Mihaela Matei, Marciabela Fernandes-Correa, Salvador Hernandez-Navarro, Jesús Martín-Gil, Eco-Friendly Nanocomposites of Chitosan with Natural Extracts, Antimicrobial Agents, and Nanometals. In *Handbook of Composites from Renewable Materials* Vijay Kumar Thakur, M. K. T., Michael R. Kessler, Ed. Wiley: 2017; Vol. Volume 8, Nanocomposites: Advanced Applications, pp 35-60.

8. Jabeen, S.; Kausar, A.; Saeed, S.; Muhammad, B.; Gul, S., Poly(vinyl alcohol) and chitosan blend cross-linked with bis phenol-F-diglycidyl ether: mechanical, thermal and water absorption investigation. *Journal of the Chinese Advanced Materials Society* **2016,** *4* (3), 211-227.

9. Trung, T. S.; Thein-Han, W. W.; Qui, N. T.; Ng, C.-H.; Stevens, W. F., Functional characteristics of shrimp chitosan and its membranes as affected by the degree of deacetylation. *Bioresource Technology* **2006,** *97* (4), 659-663.

10. Park, S.-B.; You, J.-O.; Park, H.-Y.; Haam, S. J.; Kim, W.-S., A novel pH-sensitive membrane from chitosan — TEOS IPN; preparation and its drug permeation characteristics. *Biomaterials* **2001,** *22* (4), 323-330.

11. Xia, W.; Liu, P.; Zhang, J.; Chen, J., Biological activities of chitosan and chitooligosaccharides. *Food Hydrocolloids* **2011,** *25* (2), 170-179.

12. Liu, J.; Huang, Y.; Kumar, A.; Tan, A.; Jin, S.; Mozhi, A.; Liang, X.-J., pH-Sensitive nano-systems for drug delivery in cancer therapy. *Biotechnology Advances* **2014,** *32* (4), 693-710.

13. Matei, P. M.; Martín-Ramos, P.; Sánchez-Báscones, M.; Hernández-Navarro, S.; Correa-Guimaraes, A.; Navas-Gracia, L. M.; Rufino, C. A.; Ramos-Sánchez, M. C.; Martín-Gil, J., Synthesis of chitosan oligomers/propolis/silver nanoparticles composite systems and study of their activity against *Diplodia seriata*. *International Journal of Polymer Science* **2015,** *2015*, 1-11.

14. Liu, N.; Chen, X.-G.; Park, H.-J.; Liu, C.-G.; Liu, C.-S.; Meng, X.-H.; Yu, L.-J., Effect of MW and concentration of chitosan on antibacterial activity of *Escherichia coli*. *Carbohydrate Polymers* **2006,** *64* (1), 60-65.

15. Li, Z.; Yang, F.; Yang, R., Synthesis and characterization of chitosan derivatives with dual-antibacterial functional groups. *International journal of biological macromolecules* **2015,** *75*, 378-387.

16. Liu, H.; Du, Y.; Wang, X.; Sun, L., Chitosan kills bacteria through cell membrane damage. *International Journal of Food Microbiology* **2004,** *95* (2), 147-155.

17. Devlieghere, F.; Vermeulen, A.; Debevere, J., Chitosan: antimicrobial activity, interactions with food components and applicability as a coating on fruit and vegetables. *Food Microbiology* **2004,** *21* (6), 703-714.

18. Hosseinnejad, M.; Jafari, S. M., Evaluation of different factors affecting antimicrobial properties of chitosan. *International Journal of Biological Macromolecules* **2016,** *85*, 467-475.

19. Ahmed, E. M., Hydrogel: Preparation, characterization, and applications: A review. *Journal of Advanced Research* **2015,** *6* (2), 105-121.

20. Jenkins, A.; Kratochvil, P.; Stepto, R.; Suter, U., Glossary of basic terms in polymer science (IUPAC Recommendations 1996). *Pure and Applied Chemistry* **1996,** *68* (12), 2287-2311.

21. Li, B.; Shan, C.-L.; Zhou, Q.; Fang, Y.; Wang, Y.-L.; Xu, F.; Han, L.-R.; Ibrahim, M.; Guo, L.-B.; Xie, G.-L.; Sun, G.-C., Synthesis, Characterization, and Antibacterial Activity of Cross-Linked Chitosan-Glutaraldehyde. *Marine drugs* **2013,** *11* (5), 1534.

22. Salehi, R.; Arami, M.; Mahmoodi, N. M.; Bahrami, H.; Khorramfar, S., Novel biocompatible composite (Chitosan–zinc oxide nanoparticle): Preparation, characterization and dye adsorption properties. *Colloids and Surfaces B: Biointerfaces* **2010,** *80* (1), 86-93.

23. Vasconcelos, H. L.; Camargo, T. P.; Gonçalves, N. S.; Neves, A.; Laranjeira, M. C. M.; Fávere, V. T., Chitosan crosslinked with a metal complexing agent: Synthesis, characterization and copper(II) ions adsorption. *Reactive and Functional Polymers* **2008,** *68* (2), 572-579.

24. Tsai, W.-B.; Chen, Y.-R.; Liu, H.-L.; Lai, J.-Y., Fabrication of UV-crosslinked chitosan scaffolds with conjugation of RGD peptides for bone tissue engineering. *Carbohydrate Polymers* **2011,** *85* (1), 129-137.

25. Yeh, J.-T.; Chen, C.-L.; Huang, K.-S., Synthesis and properties of chitosan/SiO2 hybrid materials. *Materials Letters* **2007,** *61* (6), 1292-1295.

26. Tsai, G. J.; Wu, Z. Y.; Su, W. H., Antibacterial activity of a chitooligosaccharide mixture prepared by cellulase digestion of shrimp chitosan and its application to milk preservation. *Journal of food protection* **2000,** *63* (6), 747-52.

27. Sperling, L. H., *Interpenetrating Polymer Networks and Related Materials*. Springer Science & Business Media: 2012.

28. Ryan, C. C.; Bardosova, M.; Pemble, M. E., Structural and mechanical properties of a range of chitosan-based hybrid networks loaded with colloidal silica and polystyrene particles. *Journal of Materials Science* **2017,** *52* (13), 8338-8347.

29. Liu, J.; Hurt, R. H., Ion Release Kinetics and Particle Persistence in Aqueous Nano-Silver Colloids. *Environmental Science & Technology* **2010,** *44* (6), 2169-2175.

30. Martínez-Gutierrez, F.; Thi, E. P.; Silverman, J. M.; de Oliveira, C. C.; Svensson, S. L.; Hoek, A. V.; Sánchez, E. M.; Reiner, N. E.; Gaynor, E. C.; Pryzdial, E. L. G.; Conway, E. M.; Orrantia, E.; Ruiz, F.; Av-Gay, Y.; Bach, H., Antibacterial activity, inflammatory response, coagulation and cytotoxicity effects of silver nanoparticles. *Nanomedicine: Nanotechnology, Biology and Medicine* **2012,** *8* (3), 328-336.

31. González-Campos, J. B.; Mota-Morales, J. D.; Kumar, S.; Zárate-Triviño, D.; Hernández-Iturriaga, M.; Prokhorov, Y.; Lepe, M. V.; García-Carvajal, Z. Y.; Sanchez, I. C.; Luna-Bárcenas, G., New insights into the bactericidal activity of chitosan-Ag bionanocomposite: The role of the electrical conductivity. *Colloids and Surfaces B: Biointerfaces* **2013,** *111*, 741-746.

32. Vimala, K.; Mohan, Y. M.; Sivudu, K. S.; Varaprasad, K.; Ravindra, S.; Reddy, N. N.; Padma, Y.; Sreedhar, B.; MohanaRaju, K., Fabrication of porous chitosan films impregnated with silver nanoparticles: A facile approach for superior antibacterial application. *Colloids and Surfaces B: Biointerfaces* **2010,** *76* (1), 248-258.

33. Kumar-Krishnan, S.; Prokhorov, E.; Hernández-Iturriaga, M.; Mota-Morales, J. D.; Vázquez-Lepe, M.; Kovalenko, Y.; Sanchez, I. C.; Luna-Bárcenas, G., Chitosan/silver nanocomposites: Synergistic antibacterial action of silver nanoparticles and silver ions. *European Polymer Journal* **2015,** *67*, 242-251.

34. Pérez-Díaz, M. A.; Boegli, L.; James, G.; Velasquillo, C.; Sánchez-Sánchez, R.; Martínez-Martínez, R.-E.; Martínez-Castañón, G. A.; Martinez-Gutierrez, F., Silver nanoparticles with antimicrobial activities against Streptococcus mutans and their cytotoxic effect. *Materials Science and Engineering: C* **2015,** *55*, 360-366.

35. Lynch, A. S.; Robertson, G. T., Bacterial and fungal biofilm infections. *Annu Rev Med* **2008,** *59*, 415-28.

36. Prabhu, S.; Poulose, E. K., Silver nanoparticles: mechanism of antimicrobial action, synthesis, medical applications, and toxicity effects. *International Nano Letters* **2012,** *2* (1), 1-10.

37. Kim, J. S.; Kuk, E.; Yu, K. N.; Kim, J. H.; Park, S. J.; Lee, H. J.; Kim, S. H.; Park, Y. K.; Park, Y. H.; Hwang, C. Y.; Kim, Y. K.; Lee, Y. S.; Jeong, D. H.; Cho, M. H., Antimicrobial effects of silver nanoparticles. *Nanomedicine: Nanotechnology, Biology, and Medicine* **2007,** *3* (1), 95-101.

38. Umadevi, M.; Rani, T.; Balakrishnan, T.; Ramanibai, R., Antimicrobial activity of silver nanoparticles prepared under an ultrasonic field. *International Journal of Pharmaceutical Sciences and Nanotechnology* **2011,** *4* (3), 1491-1496.

39. Ansari, M. A.; Khan, H. M.; Khan, A. A.; Ahmad, M. K.; Mahdi, A. A.; Pal, R.; Cameotra, S. S., Interaction of silver nanoparticles with Escherichia coli and their cell envelope biomolecules. *Journal of Basic Microbiology* **2014,** *54* (9), 905-915.

40. Matsumura, Y.; Yoshikata, K.; Kunisaki, S.-i.; Tsuchido, T.

41. Durán, N.; Marcato, P. D.; De Conti, R.; Alves, O. L.; Costa, F. T. M.; Brocchi, M., Potential use of silver nanoparticles on pathogenic bacteria, their toxicity and possible mechanisms of action. *Journal of the Brazilian Chemical Society* **2010,** *21* (6), 949-959.

42. Xiu, Z. M.; Zhang, Q. B.; Puppala, H. L.; Colvin, V. L.; Alvarez, P. J. J., Negligible particle-specific antibacterial activity of silver nanoparticles. *Nano Letters* **2012,** *12* (8), 4271-4275.

43. Lok, C.-N.; Ho, C.-M.; Chen, R.; He, Q.-Y.; Yu, W.-Y.; Sun, H.; Tam, P. K.-H.; Chiu, J.-F.; Che, C.-M., Silver nanoparticles: partial oxidation and antibacterial activities. *JBIC Journal of Biological Inorganic Chemistry* **2007,** *12* (4), 527-534.

44. Zhang, Y.; Shareena Dasari, T. P.; Deng, H.; Yu, H., Antimicrobial Activity of Gold Nanoparticles and Ionic Gold. *Journal of Environmental Science and Health, Part C* **2015,** *33* (3), 286-327.

45. Mukha, I.; Eremenko, A.; Korchak, G.; Michienkova, A., Antibacterial action and physicochemical properties of stabilized silver and gold nanostructures on the surface of disperse silica. *Journal of Water Resource and Protection* **2010,** *2010*.

46. Hernández-Sierra, J. F.; Ruiz, F.; Pena, D. C. C.; Martínez-Gutiérrez, F.; Martínez, A. E.; Guillén, A. d. J. P.; Tapia-Pérez, H.; Castañón, G. M., The antimicrobial sensitivity of *Streptococcus mutans* to nanoparticles of silver, zinc oxide, and gold. *Nanomedicine: Nanotechnology, Biology and Medicine* **2008,** *4* (3), 237-240.

47. Nagaraj, B.; Divya, T.; Malakar, B.; Krishnamurthy, N.; Dinesh, R.; Negrila, C.; Ciobanu, C.; Iconaru, S., Phytosynthesis of gold nanoparticles using *Caesalpinia pulcherrima* (peacock flower) flower extract and evaluation of their antimicrobial activities. *Digest Journal of Nanomaterials and Biostrustures* **2012,** *7* (3), 899-905.

48. Das, S. K.; Das, A. R.; Guha, A. K., Gold nanoparticles: microbial synthesis and application in water hygiene management. *Langmuir* **2009,** *25* (14), 8192-8199.

49. Mishra, A.; Tripathy, S. K.; Yun, S.-I., Bio-synthesis of gold and silver nanoparticles from *Candida guilliermondii* and their antimicrobial effect against pathogenic bacteria. *Journal of nanoscience and nanotechnology* **2011,** *11* (1), 243-248.

50. Annamalai, A.; Christina, V.; Sudha, D.; Kalpana, M.; Lakshmi, P., Green synthesis, characterization and antimicrobial activity of Au NPs using *Euphorbia hirta* L. leaf extract. *Colloids and Surfaces B: Biointerfaces* **2013,** *108*, 60-65.

51. Glisic, B. D.; Djuran, M. I., Gold complexes as antimicrobial agents: an overview of different biological activities in relation to the oxidation state of the gold ion and the ligand structure. *Dalton Transactions* **2014,** *43* (16), 5950-5969.

52. Shareena Dasari, T. P.; Zhang, Y.; Yu, H., Antibacterial Activity and Cytotoxicity of Gold (I) and (III) Ions and Gold Nanoparticles. *Biochemistry & Pharmacology* **2015,** *4* (6), 199.

53. Blaser, M. J., Antibiotic use and its consequences for the normal microbiome. *Science* **2016,** *352* (6285), 544-545.

54. Van Boeckel, T. P.; Gandra, S.; Ashok, A.; Caudron, Q.; Grenfell, B. T.; Levin, S. A.; Laxminarayan, R., Global antibiotic consumption 2000 to 2010: an analysis of national pharmaceutical sales data. *The Lancet Infectious Diseases* **2014,** *14* (8), 742-750.

55. Nordmann, P., Global Spread of Carbapenemase-producing Enterobacteriaceae-Volume 17, Number 10—October 2011-Emerging Infectious Disease journal-CDC. **2011**.

56. Sweeney, I. R.; Miraftab, M.; Collyer, G., Absorbent alginate fibres modified with hydrolysed chitosan for wound care dressings – II. Pilot scale development. *Carbohydrate Polymers* **2014,** *102*, 920-927.

57. Santos, T. C.; Höring, B.; Reise, K.; Marques, A. P.; Silva, S. S.; Oliveira, J. M.; Mano, J. F.; Castro, A. G.; Reis, R. L.; van Griensven, M., *In vivo* performance of chitosan/soy-based membranes as wound-dressing devices for acute skin wounds. *Tissue Engineering Part A* **2013,** *19* (7-8), 860-869.

58. Zhao, R.; Li, X.; Sun, B.; Zhang, Y.; Zhang, D.; Tang, Z.; Chen, X.; Wang, C., Electrospun chitosan/sericin composite nanofibers with antibacterial property as potential wound dressings. *International Journal of Biological Macromolecules* **2014,** *68*, 92-97.

59. Feoktistova, M.; Geserick, P.; Leverkus, M., Crystal Violet Assay for Determining Viability of Cultured Cells. *Cold Spring Harbor protocols* **2016,** *2016* (4), pdb.prot087379.

60. Nagoba, B.; Gandhi, R.; Wadher, B.; Potekar, R.; Kolhe, S., Microbiological, histopathological and clinical changes in chronic infected wounds after citric acid treatment. *Journal of Medical Microbiology* **2008,** *57* (5), 681-682.

61. Nagoba, B.; Wadher, B.; Kulkarni, P.; Kolhe, S., Acetic acid treatment of pseudomonal wound infections. **2008**.

62. Zhang, X., Gold Nanoparticles: Recent Advances in the Biomedical Applications. *Cell biochemistry and biophysics* **2015,** *72* (3), 771-5.

8. Conclusions and Future Work

8.1 Introduction

As described in chapter one the progression from chitosan to cross-linked chitosan is a logical one, when the enhancement of properties is considered. Three important features which have been considered are chitosan's variable molecular weight and degree of deacetylation as well as its cationic polyelectrolyte structure which is the main contributor to chitosan's pH-sensitivity, biocompatibility and antibacterial properties[1, 2]. Chitosan sources are naturally abundant in the form of its source material, chitin, and the processing of chitin to chitosan is straightforward and inexpensive. One major drawback associated with chitosan is its high aqueous solubility which is a prominent feature associated with the flexible nature of the polymeric structure[3]. Cross-linking is a potential solution to the high aqueous solubility but depending on the nature of the cross-linker it may help or hinder the natural properties of chitosan. The cross-linker employed here was a siloxane network sourced from TEOS. The effects of cross-linking with the associated siloxane units as well as the effects of adding polymer and metal nanoparticles were studied with respect to the physical, optical, mechanical and antimicrobial properties. It was found that in general these additives or structure enhancers resulted in positive changes to the properties investigated.

8.2 Chitosan and Chi-TEOS IPN Characterisation

Molecular weight and degree of deacetylation of the three chitosan sources were determined during an initial investigation. LMWChi and MMWChi had satisfactory results with average molecular weight of 89,832 $gmol^{-1}$ and 134, 841 $gmol^{-1}$ and percentage degree of acetylation of 13% and 26%, respectively. The HMWChi wasn't so satisfactory with an average molecular weight of 75,740 $gmol^{-1}$ and polydispersity index of 4.2; these results suggest that the HMWChi polymer is made up of polydisperse monomers. Despite this, all chitosan sources were employed for cross-linking experiments. Results from swelling studies in acidic phosphate buffer showed a logical increase in swelling ability as chain length increased from low to medium to high molecular weight. The effect of cross-linking was analysed on LMWChi-TEOS IPN samples, with chitosan: siloxane ratios of 1:1, 1:2 and 1:3. As was expected the samples become more brittle upon cross-linking, due to changes in the mechanical

properties. This was observed visually as the samples failed to remain intact with increasing cross-linker concentration; swelling ability was greatly reduced upon transition from 1:1 to 1:2 to 1:3 to such an extent that little or no swelling was observed for the latter two ratios. A combination of all results pointed towards the 1:1 LMWChi-TEOS IPN and 1:1 MMWChi-TEOS IPN as the best candidates for further tests and composite formation. SEM analysis on the samples revealed a smooth surface with average sample thicknesses of 12.4 μm ± 14% and 20.3 μm ± 4% for the 1:1 LMWChi-TEOS IPN and 1:1 MMWChi-TEOS IPN samples, respectively. A slightly thicker membrane forms with greater viscosity-average molecular weight. This is supported by a hypothesis by Spangler et al which states that viscosity is the dominant molecular weight parameter influencing film thickness[4].

The true effect of cross-linking was revealed during tensile strength tests. Both 1:1 LMWChi-TEOS IPN and 1:1 MMWChi-TEOS IPN reach similar stresses with plastic deformation occurring for the MMW sample, meaning it is a less elastic or flexible structure. The tensile strength increases with increasing cross-linker density for stresses of up to 91 MPa reached by 1:3 LMWChi-TEOS IPN. This is slightly greater than Kapton polyimide films of the same dimensions[5], however the brittle character is a major drawback. SiO_2 photonic crystal synthesis

SiO_2 particles with a narrow dispersity were prepared by the modified Stöber method and used for photonic crystal growth. A series of syntheses were carried out and revealed a linear relationship between volume of catalytic NH_4OH and resultant particle size up to about 7/8 mL NH_4OH at which point the particle growth was limited to about 500 nm. It is proposed that at this point the volume of TEOS is used up, meaning there is no Si source remaining for particle growth. Vertical controlled evaporation was found to be the best deposition method. The resulting films were of very high quality in terms of ordering of particles and adhering to the substrate. Both the horizontal and vertical under-oil methods were also studied and found to be satisfactory, however the quality of particle packing achievable using these methods is not of the highest order and close-packing is limited to individual domains in the sample rather than long-range order. It was also found that for the under oil approaches, removal of oil from the samples can cause problems, in that this process can be destructive causing samples to shatter and peel off the substrate.

All substrates employed (glass, MICA, PMMA and PET) were suitable for film growth, with the best results observed for glass and PET. Treating the sample to make the surface hydrophilic ensured that the particles were attracted to and adhered to the sample surface. The PET surface was found to have a slight edge over glass, perhaps due to the moth-eye surface of the plastic[6] which ensured high-quality ordering of the initial monolayer of particles leading to long-range order growth of subsequent layers[7]. The PET surface was also very suitable since the Chi-TEOS IPN hydrogel deposited and formed a thin film which could subsequently be peeled off the surface. This is essential for the formation of a free-standing composite[8].

8.3 Silica-based photonic crystals embedded in a chitosan-TEOS matrix

The first study carried out aimed at producing a composite structure made up of a SiO_2 photonic crystal and Chi-TEOS IPN to form a free-standing, pH-sensitive, optically active composite. The two separate entities were combined in a simple manner with the hydrogel infilling a PET-immobilized SiO_2 photonic crystal in regular film-forming conditions under vacuum. When the vacuum was released the Chi-TEOS-SiO_2 composite peeled off the PET substrate, resulting in a free-standing thin film.

The first swelling study examined the optical response to pH utilised neutral and acidic phosphate buffers. Results were promising despite the crude analysis setup. A red-shift of Bragg diffracted wavelength was observed suggesting that the fcc crystal lattice had swollen and a reduction in percentage transmission was noted due to changes in refractive index contrast that result as air is replaced with Chi-TEOS IPN, MMWChi in this case. When immersed in acidic/ neutral conditions - a greater red-shift occurs in acidic conditions as the Chi-TEOS IPN was found to swell more in the presence of H^+. This phenomenon was studied further, allowing for improved optical analysis, with 0.1 M HCl and 0.1 M NaOH. A Chi-TEOS-SiO_2 composite prepared with LMWChi was tested in acidic, neutral and basic conditions as a function of time with results showing that a greater red-shift in wavelength is observed as a function of H^+ in solution. The composite dried at the same rate no matter which conditions, returning to the original Bragg diffracted wavelength each time. This feature is highly desirable in shape memory polymer composites[9]. A red-shift of about 20 nm was observed for the LMWChi sample in acidic conditions while a greater red-shift of

about 40 nm was observed for the composite prepared with MMWChi. This result is reminiscent of earlier results which showed swelling increased as a function of increasing molecular weight (see section 8.2).

The Chi-TEOS-SiO_2 composite is a potentially novel material for use in the area of stimuli-sensitive composite structures, such as those provided by Ward et al in the detection of glucose[10]. Advantages associated with the composite lie in the fact that it is made up of environmentally-friendly materials, which are abundantly found in nature. Production is very straight-forward compared to methods used in more complicated studies[11,12] and most importantly the proof of concept was successful. In conclusion, the pH-sensitivity of chitosan does carry forward to the Chi-TEOS IPN and when combined with a SiO_2 photonic crystal it produces an optically-active pH-sensor with detection occurring in the visible region of the electromagnetic spectrum.

8.4 Structural and mechanical properties of a range of chitosan-based hybrid networks loaded with colloidal silica and polystyrene particles

The mechanical properties of the Chi-TEOS IPN samples were briefly investigated in the previous study with an increase in tensile strength with increasing cross-linker concentration. The results were interesting in terms of the observed increase in mechanical strength, but there were drawbacks in that the samples greatly reduced in flexibility and it became difficult to form robust, good quality films. PLMW chitosan samples reached stresses of 32 MPa. This increased to 61 MPa upon cross-linking to form the 1:1 LMWChi-TEOS IPN – producing results which are on a par with literature values[13,14,15]. The aim of this study was to see if the stresses reached could be increased without increasing the concentration of cross-linker by adding colloidal SiO_2 and PS particles as a structure enhancer.

The polymer particles were introduced to the IPN by two methods – embedding and grafting. Embedding the particles involved introducing them to the hydrogel prior to thin film formation. Both SiO_2 and PS particles were introduced at the same concentration range but with varying particle diameter (100-520 nm). Results were again positive in the sense that an increase in tensile strength was observed as a function of decreasing particle diameter (or increasing surface area). The resulting extra bonding interactions, proposed to be due mainly to weak, non-covalent type

bonding, increased the stress reached to 120 MPa for a sample with 100 nm PS particles embedded. This stress is greater than that of Kapton imide films[5] as well as typical polyester, vinyl ester and epoxy resin polymers[16,17]. The samples prepared by grafting with polymer particles were tested in the same manner but exhibited lower mechanical strength results in comparison to the samples with particles embedded. The best stress value achieved for such samples was ca. 32 MPa and it was noted that there was a significant standard deviation in the results. These results indicated a reduction in tensile strength as compared to chitosan and Chi-TEOS IPN and therefore the method of grafting samples (adapted from a method by Rose *et al.*[18]) is not recommended as a means to enhance the mechanical properties of the Chi-TEOS IPN or thin films of the same ilk.

Structural analysis on the chitosan-based hybrid composites was predominantly carried out by spectroscopic means. The hypothesis that the physically cross-linked IPN is formed by weak bonding interactions is supported by the fact that no new peaks or dramatic changes to either the IR or Raman spectra were observed when comparing the chitosan and Chi-TEOS IPN spectra. This was particularly true for the Raman spectra which displayed no difference in either spectrum. The IR spectra, on the other hand, displayed some minute discrepancies; a peak appeared at 785 cm^{-1} for the Chi-TEOS IPN samples which was not observed for chitosan. Vibrations in this region correspond to deformations in N-H groups of primary and secondary amines and also to bend deformations of alkenes. These vibrations are hypothesised to occur due to the distortion of functional groups of chitosan side chains- the functional groups expected to be involved in H-bonding. Another peak at 1250 cm^{-1} was observed for chitosan but not Chi-TEOS IPN. This corresponds to a methyl stretch which has been disturbed upon cross-linking. Finally, a new peak was observed at 440 cm^{-1} for the Chi-TEOS IPN. This is a characteristic Si-O-Si peak, appearing following the introduction of the siloxane network. The same phenomenon was observed by Mitra *et al.* in a study of chitosan and succinic acid cross-linked chitosan; FTIR analysis on both materials had few significant changes with the authors stating that "no change in the main backbone" of chitosan was observed[19], with non-covalent interactions such as ionic and intermolecular hydrogen-bonding proposed to be occurring.

8.5 Synthesis and characterization of cross-linked chitosan composites functionalized with silver and gold nanoparticles for antimicrobial applications

The flexible Chi-TEOS IPN films are ideal candidates for wound-dressings as they may be formed as mechanically strong, transparent, solution stable thin films. This final study was aimed at investigating the antimicrobial abilities of the chitosan composite thin films. Chitosan is known to have inherent antimicrobial properties; the addition of Ag and Au NPS was also investigated.

The Chi-TEOS IPN hydrogels were prepared by the standard method with Ag and Au NPs introduced at a concentration of 0.02% by the 'embedding' procedure. Spectroscopic analysis confirmed that there were no changes to the Chi-TEOS IPN after introducing Ag/ Au NPs. While the NPs weren't observable by SEM analysis, TEM analysis showed that they were dispersed throughout the IPN with average particle diameters of 16 nm ± 25% and 19 nm ± 18% for the Ag and Au dispersions, respectively. Although SEM and surface analysis showed that the surface of the chitosan composites became rougher with cross-linking it was found that this had no influence over the mechanical properties - the presence of the NPs did not affect the tensile strength at a range of concentrations up to 0.02%. The maximum stress reached for such films was 74 MPa which is comparable with the result achieved by the Chi-TEOS IPN without Ag/ Au NPs (75 MPa)

The antimicrobial ability of the chitosan composite samples was investigated by studying the attachment of *E. coli* to the sample surface by a method known as a crystal violet attachment assay. Results revealed that a significant (80%) reduction in the degree of bacterial attachment was observed in progressing from chitosan to the cross-linked Chi-TEOS IPN. However, the presence of Ag/ Au NPs provided no additional observable contribution. It is proposed that his may be due to the fact that the NPs were not being released from the IPN in neutral conditions. Despite the lack of particle release under neutral conditions it was established that by cross-linking with a siloxane polymer network to form a Chi-TEOS IPN, bacterial attachment to the chitosan surface was reduced by 80% - this shows that improved strength in the chitosan network is a factor in improving antimicrobial abilities. This may be a result of the improved stability of chitosan in aqueous conditions due to its enhanced mechanical

properties upon cross-linking. Normally under aqueous conditions the chitosan polymer would break down, meaning its efficiency is reduced, however when cross-linked it no longer breaks down meaning its antimicrobial action is more long-lasting. In a study by Mohamed *et al.* inhibition zone tests on *E. coli* with cross-linked chitosan films showed better antimicrobial activity than 'parent' chitosan[20]. The authors stipulate that swelling ability plays a factor in antimicrobial ability as antimicrobial ability was seen to decrease with increasing cross-linker concentration, this suggests that the chitosan chain requires a certain degree of freedom in order to be able to interact with bacteria while still being attached and stabilised by the cross-linker network.

A study on the release of Ag/ Au NPs was conducted in order to investigate this phenomenon further. The Chi-TEOS IPN samples with Ag/ Au embedded were stored in phosphate buffer solutions of varying pH and UV-Vis analysis was then subsequently deployed in order to detect whether the NPs had been released into solution. Following on from these tests it was concluded that within the limits of the experiment concerned, the Ag/ Au NPs were not being released from the IPN under neutral pH conditions. Interestingly this approach revealed that NPs were being released from the same membranes under acidic conditions (stored in 0.1 M phosphate buffer of pH 2.5 for 24 hours). This result proved that the particles were being released as the membranes swelled.

This finding is of considerable significance in terms of in-vivo drug release type applications of chitosan-based films. While no release occurs at neutral-basic conditions, which are pH conditions for *E. coli* in LB broth[21], it has been proven that release occurs in acidic conditions. This is important with regards to surface wound-healing as it has been demonstrated that wound-healing efficiency improves from neutral-acidic conditions[22,23], with 'chronic' wounds occurring in alkaline conditions[24,25]. Acidic conditions provide ideal conditions for oxygen release to damaged tissues, as well as protease activity and bacterial toxicity. Surface wounds can be topically treated to induce acidic conditions e.g. by application of dilute acetic acid[26] or citric acid[27]. This, coupled with application of an antimicrobial wound dressing which could release further antimicrobial agents in acidic conditions (such as Chi-TEOS IPN with Ag/ Au NPs embedded) may provide the perfect conditions for wound-healing, eliminating the requirement of antibiotic use.

8.6 Overall Conclusion and Future work

The main study over the course of this research has been to examine the progression from chitosan to cross-linked Chi-TEOS IPN to films containing structural enhancers and how the various processing steps deployed influence the mechanical and optical properties of the materials synthesized. It can be concluded that the pH-sensitivity of chitosan carries forward to the Chi-TEOS IPN and that by combining this feature with the optical properties of a SiO_2 photonic crystal provides a pH-sensitive composite which elicits an optical response as an indicator of pH conditions. The mechanical properties of chitosan are found to be enhanced by cross-linking, even though it is occurring by weak bonding interactions. The ideal chitosan: TEOS ratio was determined as 1:1 as this ratio results in a mechanically strong thin film which retains chitosan's inherent flexibility. This is then further enhanced by the addition of polymer particle structure enhancers in the form of colloidal silica and polystyrene particles. While the addition of Ag and Au NPs did not contribute towards enhanced tensile strength these films were also investigated with respect to their antimicrobial abilities. Here it was concluded that the NPs weren't being released when pH is neutral and so they effectively couldn't contribute towards antimicrobial activities. In contrast the metal NPs were released under more acidic conditions, potentially providing some possibilities in terms of their use in *in-vivo* drug release materials. While embedding particles/ drugs for release in neutral conditions isn't suitable, the Chi-TEOS IPN is an ideal candidate as a stand-alone antimicrobial wound-dressing or for drug release in acidic conditions. Future work may be dedicated towards this area of research with a variety of studies already available in the literature[28,29,30,31,32].

References

1. Mourya, V.; Inamdar, N. N., Chitosan-modifications and applications: opportunities galore. *Reactive and Functional polymers* **2008,** *68* (6), 1013-1051.

2. Younes, I.; Sellimi, S.; Rinaudo, M.; Jellouli, K.; Nasri, M., Influence of acetylation degree and molecular weight of homogeneous chitosans on antibacterial and antifungal activities. *International Journal of Food Microbiology* **2014,** *185*, 57-63.

3. Qin, C.; Li, H.; Xiao, Q.; Liu, Y.; Zhu, J.; Du, Y., Water-solubility of chitosan and its antimicrobial activity. *Carbohydrate Polymers* **2006,** *63* (3), 367-374.

4. Spangler, L. L.; Torkelson, J. M.; Royal, J. S., Influence of solvent and molecular weight on thickness and surface topography of spin-coated polymer films. *Polymer Engineering & Science* **1990,** *30* (11), 644-653.

5. Yu, D. Y.; Spaepen, F., The yield strength of thin copper films on Kapton. *Journal of Applied Physics* **2004,** *95* (6), 2991-2997.

6. Nakata, K.; Sakai, M.; Ochiai, T.; Murakami, T.; Takagi, K.; Fujishima, A., Antireflection and self-cleaning properties of a moth-eye-like surface coated with TiO2 particles. *Langmuir* **2011,** *27* (7), 3275-3278.

7. Parchine, M.; McGrath, J.; Bardosova, M.; Pemble, M. E., Large area 2D and 3D colloidal photonic crystals fabricated by a roll-to-roll Langmuir–Blodgett method. *Langmuir* **2016,** *32* (23), 5862-5869.

8. Barney, N. A.; Weinberg, M. G.; Sauer, B. B., Chitosan films with reduced shrinkage and laminates made therefrom. Google Patents: 2013.

9. Meng, H.; Li, G., A review of stimuli-responsive shape memory polymer composites. *Polymer* **2013,** *54* (9), 2199-2221.

10. Ward Muscatello, M. M.; Stunja, L. E.; Asher, S. A., Polymerized crystalline colloidal array sensing of high glucose concentrations. *Analytical chemistry* **2009,** *81* (12), 4978-4986.

11. Ruan, C.; Zeng, K.; Grimes, C. A., A mass-sensitive pH sensor based on a stimuli-responsive polymer. *Analytica Chimica Acta* **2003,** *497* (1–2), 123-131.

12. Paek, K.; Yang, H.; Lee, J.; Park, J.; Kim, B. J., Efficient Colorimetric pH Sensor Based on Responsive Polymer–Quantum Dot Integrated Graphene Oxide. *ACS Nano* **2014,** *8* (3), 2848-2856.

13. Kim, K. M.; Son, J. H.; Kim, S.-K.; Weller, C. L.; Hanna, M. A., Properties of Chitosan Films as a Function of pH and Solvent Type. *Journal of Food Science* **2006,** *71* (3), E119-E124.

14. Chen, J. L.; Zhao, Y., Effect of Molecular Weight, Acid, and Plasticizer on the Physicochemical and Antibacterial Properties of β-Chitosan Based Films. *Journal of Food Science* **2012,** *77* (5), E127-E136.

15. Nunthanid, J.; Puttipipatkhachorn, S.; Yamamoto, K.; Peck, G. E., Physical properties and molecular behavior of chitosan films. *Drug development and industrial pharmacy* **2001,** *27* (2), 143-57.

16. Holbery, J.; Houston, D., Natural-fiber-reinforced polymer composites in automotive applications. *JOM Journal of the Minerals, Metals and Materials Society* **2006,** *58* (11), 80-86.

17. Malkapuram, R.; Kumar, V.; Negi, Y. S., Recent development in natural fiber reinforced polypropylene composites. *Journal of Reinforced Plastics and Composites* **2009,** *28* (10), 1169-1189.

18. Rose, S.; Prevoteau, A.; Elziere, P.; Hourdet, D.; Marcellan, A.; Leibler, L., Nanoparticle solutions as adhesives for gels and biological tissues. *Nature* **2014,** *505* (7483), 382-385.

19. Mitra, T.; Sailakshmi, G.; Gnanamani, A.; Mandal, A. B., Studies on Cross-linking of succinic acid with chitosan/collagen. *Materials Research* **2013,** *16*, 755-765.

20. Mohamed, N. A.; Fahmy, M. M., Synthesis and Antimicrobial Activity of Some Novel Cross-Linked Chitosan Hydrogels. *International Journal of Molecular Sciences* **2012,** *13* (9), 11194.

21. Sezonov, G.; Joseleau-Petit, D.; D'Ari, R., Escherichia coli physiology in Luria-Bertani broth. *Journal of bacteriology* **2007,** *189* (23), 8746-8749.

22. Stewart, C. M.; Cole, M. B.; Legan, J. D.; Slade, L.; Vandeven, M. H.; Schaffner, D. W., Staphylococcus aureus growth boundaries: moving towards mechanistic predictive models based on solute-specific effects. *Applied and environmental microbiology* **2002,** *68* (4), 1864-1871.

23. Thomas, L. V.; Wimpenny, J. W.; Davis, J. G., Effect of three preservatives on the growth of Bacillus cereus, Vero cytotoxigenic Escherichia coli and Staphylococcus aureus, on plates with gradients of pH and sodium chloride concentration. *Int J Food Microbiol* **1993,** *17* (4), 289-301.

24. Greener, B.; Hughes, A.; Bannister, N.; Douglass, J., Proteases and pH in chronic wounds. *Journal of wound care* **2005,** *14* (2), 59-61.

25. Gethin, G., The significance of surface pH in chronic wounds. *Wounds uk* **2007,** *3* (3), 52.

26. Nagoba, B.; Wadher, B.; Kulkarni, P.; Kolhe, S., Acetic acid treatment of pseudomonal wound infections. **2008**.

27. Nagoba, B.; Gandhi, R.; Wadher, B.; Potekar, R.; Kolhe, S., Microbiological, histopathological and clinical changes in chronic infected wounds after citric acid treatment. *Journal of medical microbiology* **2008,** *57* (5), 681-682.

28. Shu, X.; Zhu, K.; Song, W., Novel pH-sensitive citrate cross-linked chitosan film for drug controlled release. *International journal of pharmaceutics* **2001,** *212* (1), 19-28.

29. Park, J. H.; Saravanakumar, G.; Kim, K.; Kwon, I. C., Targeted delivery of low molecular drugs using chitosan and its derivatives. *Advanced drug delivery reviews* **2010,** *62* (1), 28-41.

30. Arora, S.; Budhiraja, R. D., Chitosan-alginate microcapsules of amoxicillin for gastric stability and mucoadhesion. *Journal of Advanced Pharmaceutical Technology & Research* **2012,** *3* (1), 68-74.

31. Argin, S.; Kofinas, P.; Lo, Y. M., The cell release kinetics and the swelling behavior of physically crosslinked xanthan–chitosan hydrogels in simulated gastrointestinal conditions. *Food Hydrocolloids* **2014,** *40*, 138-144.

32. Li, L.; Jiang, G.; Yu, W.; Liu, D.; Chen, H.; Liu, Y.; Tong, Z.; Kong, X.; Yao, J., Preparation of chitosan-based multifunctional nanocarriers overcoming multiple barriers for oral delivery of insulin. *Materials Science and Engineering: C* **2017,** *70*, 278-286.